An Analysis of Fretting Fatigue

by

David Nowell

A thesis submitted for the degree

of Doctor of Philosophy

at

The University of Oxford

Lincoln College

Trinity Term 1988

Abstract

David Nowell

Lincoln College

D.Phil. Thesis

Trinity Term 1988

An Analysis of Fretting Fatigue

This thesis describes a series of fretting fatigue experiments carried out under closely controlled conditions of partial slip. These experiments confirm the existence of a size effect whereby the fretting fatigue life of an aluminium alloy is shown to vary with contact size.

The configuration chosen, of cylindrical fretting pads contacting a plane specimen is amenable to classical stress analysis and the surface tractions between the contacting bodies are derived. The effects of tension in the specimen, finite specimen thickness, differing elastic constants, and surface roughness are all investigated and incorporated into the analysis where appropriate. A technique is then developed to calculate stress intensity factors for plane cracks growing under the contact load at an arbitrary angle to the free surface.

The analysis is then applied to the experimental results and three possible explanations for the size effect are proposed, based on statistical effects, crack arrest, and crack initiation. These are examined in the light of the experimental evidence and it is proposed that the variation of fatigue life with contact size is due to an increase in the amount of fretting damage above a threshold level for crack initiation.

A composite parameter is chosen to characterise the severity of fretting conditions and this is shown to describe the experimental results accurately. Finally, the use of this parameter in design calculations is discussed.

Acknowledgements

The work described in this thesis was carried out in the Department of Engineering Science at the University of Oxford. My foremost thanks must go to Dr David Hills, who supervised me during the project and to whom I am deeply grateful for advice, guidance and encouragement. I am also grateful to Dr. John O'Connor, who was always ready to offer helpful advice based on his wide knowledge of the subject. Messrs. Philip Webb and Roger Stone provided extremely valuable help with the experimental side of the work.

The project was supported financially by the Science and Engineering Research Council and, in the latter stages of the work I was fortunate to hold a Junior Research Fellowship at Lincoln College.

The fear of the Lord is the beginning of all Knowledge

Proverbs 2:7

Contents

Notation

a	Contact semi-width
a_∞	Contact semi-width (Hertz theory)
A	$(1 - \nu_1)/\mu_1 + (1 - \nu_2)/\mu_2$
b	Crack length
b_x	Burger's vector in x-direction
b_y	Burger's vector in y-direction
B_x, B_y	Burgers vector densities
c	Stick zone boundary
d	Rigid body normal approach
D	d/a
e	Eccentricity of stick zone
$\tilde{e}$	Eccentricity of contact patch
E	Young's Modulus
E^*	$\{ (1 - \nu_1^2)/E_1 + (1 - \nu_2^2)/E_2 \}^{-1}$
f	Coefficient of friction
h	Specimen semi-width
$h(x)$	$\partial u_1/\partial x - \partial u_2/\partial x$
H	h/a
k	Relative curvature of cylinders
K_I, K_{II}	Mode I and II stress intensity factors
N	Number of cycles to failure
$N(x)$	Unsatisfied direct traction on crack face
$p(x)$	Normal traction under contact
$\bar{p}$	Mean normal traction
p_o	Peak normal traction

P	Normal force per unit length
$\bar{P}(x)$	$p(x)/\bar{p}$
$q(x)$	Shear traction under contact
$q'(x)$	Perturbation on $q(x)$ in stick zone
Q	Tangential force per unit length
$\bar{Q}(x)$	$q(x)/\bar{p}$
r	x/a
R	Relative radius of curvature of cylinders
R_1, R_2	Radii of curvature of cylinders
s	Probability of failure
S	Order of refinement in linear approximation of surface traction
$S(x)$	Unsatisfied shear traction on crack face
u	Displacement in x-direction
v	Displacement in y-direction
x	Tangential co-ordinate
x'', y''	Co-ordinates relative to crack
y	Normal co-ordinate
Y	Amplitude of surface roughness
α	a/a_∞
β	Dundurs' constant $((1 - 2\nu_1)/\mu_1) - ((1 - 2\nu_2)/\mu_2)/2A$
τ	c/a
δ_t	Rigid body tangential displacement
ΔK_I, ΔK_{II}	Stress intensity factor ranges in fatigue
ΔK_{th}	Threshold mode I stress intensity factor range in fatigue
ϵ	Linear strain
η	$\tilde{e}/a$
θ	Crack angle
λ	Wavelength of surface roughness

μ	Modulus of rigidity
υ	Poisson's ratio
ρ	Radius of curvature of asperities
σ	Direct stress
τ	Shear stress
ϕ	Bounded function used in solution of integral equations
χ	$3 - 4\upsilon$ in plane strain

Chapter 1

Introduction and literature survey

1.1 Introduction

When two contacting surfaces are subjected to oscillating tangential forces, zones of microslip develop in which the two surfaces slide over each other. This action often leads to considerable surface damage and is referred to as fretting. Two important effects can arise as a result. First, wear of the surfaces may take place in a process known as fretting wear. Secondly, and perhaps more important from an engineering point of view, if the fretting takes place in an environment where fatigue crack growth is possible, the fatigue life of the components is considerably reduced. This second effect is known as fretting fatigue and it has been responsible for many service failures of components . Several typical service failures are reported by Forsythe (1981). Fretting fatigue is of major concern in the aerospace and nuclear industries, where assemblies are subjected to vibration and the consequences of failure are serious. The prediction of the fatigue life of materials under fretting conditions has proved an elusive goal since many parameters appear to be involved.

A series of experiments undertaken by Bramhall (1973) demonstrated the existence of a critical contact size, below which fretting had no effect on fatigue life. Subsequent analysis by O'Connor and Hills (1986) suggested that fracture mechanics could provide a partial explanation of this phenomenon. The object of the current research is two-fold: first, to confirm the existence of a size effect as observed by Bramhall, using a series of experiments designed to measure all the relevant parameters,

and secondly to use the techniques of elastic stress analysis and fracture mechanics to attempt to explain the observations. The ultimate goal is to provide design criteria which will assist in avoiding fretting fatigue failures.

1.2 History

The first documentation of fretting in the scientific literature was produced by Eden, Rose, and Cunningham (1911). They report the presence of iron oxide on the surface of a fatigue specimen where it was gripped by the jaws of a testing machine. Since then there have been many further reports of fretting occurring in practical situations. Almen (1937) held fretting responsible for the failure of car wheel bearings transported by railway. Fenner, Wright, and Mann (1956) describe many service failures due to fretting and highlight the reduction in fatigue life which is brought about. Reduction factors of between 2.5 and 20 are recorded although the geometric stress concentrations existing in many of these cases are also likely to be contributory factors. Maxwell et al (1967) were among several authors to describe the fatigue failure of railway axles in which fretting between the axle and wheel plays a significant role.

More recently, further occurrences have come to light. Forsyth (1981) describes fretting in steel ropes in addition to more common types of failure such as fatigue at bolted or rivetted joints. Antler (1985) documents fretting in electrical contacts as a source of increased resistance, whereas Waterhouse and Lamb (1980) describe fretting between artificial joint replacements and the surrounding bone cement.

1.3 Experimental investigations

The first systematic study of the phenomenon of fretting was carried out by Tomlinson (1927). He concluded that fretting was associated with tangential motion between the surfaces. This work was continued by several other investigators in subsequent years so that Tomlinson, Thorpe, and Gough (1939) were able to conclude that fretting was a purely mechanical process associated with micro-slip. They were, however, unable to reach any firm conclusion on whether there was an associated strength reduction. Although a reduction in fatigue strength was observed they were unable to attribute this to fretting since the unknown stress concentration at the contact could also have played a part. The problem was first resolved by Warlow-Davies (1941). He separated the two effects by carrying out fretting in the absence of a propagating bulk stress and comparing results of subsequent fatigue tests to those for unfretted specimens. Reductions of fatigue strength of up to 18% were recorded.

Investigations continued after the war, and two distinct areas of research, viz. fretting wear, and fretting fatigue began to emerge. Uhlig and Ming Feng (1954) carried out a fundamental investigation of the process of fretting wear which enabled Uhlig (1954) to discuss a proposed mechanism in which the wear was attributed to a combination of mechanical and chemical factors. Fenner and Field (1960) carried out a basic investigation of fatigue damage due to fretting. They were among the first to use a 'bridge' type of fretting pad with two flat surfaces which was to become popular with several researchers (e.g. Doeser (1981), Edwards (1981)). Milestone (1970), however, chose to employ cylindrical fretting pads which have the advantage that the stress field developed

may be calculated analytically. Indeed, this paper is among the first recorded attempts to calculate the stresses in fretting contact and to compare the results with experimental observations. His main conclusion is that the reduction in fatigue life can be explained purely by the high local stresses involved. A comprehensive series of tests was undertaken in the late 1960s by Nishioka and Hirakawa (1968),(1969 a-d),(1972) using cylindrical steel pads and steel specimens. In Nishioka and Hirakawa (1969a) they report the existence of non-propagating fretting fatigue cracks, suggesting that, although fretting may assist the initiation and initial growth of cracks, there may be combinations of parameters under which these cracks self-arrest. Another conclusion reached is that the amount of relative slip between the surfaces has an effect on the fatigue life. Below 5μm of slip there appeared to be little reduction in life in the presence of fretting. Between 5μm and 50μm the fatigue strength was reduced to as little as 1/8 of the value in the absence of fretting. Above 50μm of slip significant wear took place and fatigue cracks were not observed, probably because they were worn away before they could start to propagate.

Further investigations by Nishioka and Hirakawa (1969b) highlight the initiation site and direction of initial propagation. Cracks were found to start in a region of high stress near to the edge of the contact and to propagate obliquely under the contact during the initial phase of growth. Another interesting observation was the increase in the coefficient of friction f during the experiment. It was found to grow from 0.2 at the begining of the test to a limiting value of 0.67 reached after 100 cycles. A similar effect was later observed by Milestone and Janeczo (1971) and by Endo, Goto, and Fukunaga (1974).

Nishioka and Hirakawa (1969c) also investigated the effect of the mean value of the alternating stress applied to the specimen on the fatigue life in fretting. They found that it had little effect on the initiation of cracks, but that a higher mean stress in the specimen reduced the fatigue life. Hence fretting is seen to be important in the formation of micro-cracks and the independence of this process from the alternating bulk stress within the specimen suggests that it is controlled by local stresses at the contact. The bulk stress plays a significant role in later stages of propagation just as in normal fatigue.

The effect of slip amplitude was further investigated by the same authors (Nishioka and Hirakawa (1969d)). They first demonstrated that, if a tangential force less than that necessary to cause sliding was applied, zones of micro-slip developed at both edges of the contact. Furthermore, in this regime of partial slip, the tangential force and the amount of slip are dependent variables, so that a greater tangential force causes larger amounts of slip. The fatigue life is dependent on slip but this effect can be explained purely in terms of the higher tangential force required and the consequent increase in local stresses. At very large values of slip, where full sliding took place significant wear was again reported. These observations are confirmed by Bryggman and Söderberg (1986), who highlight the existence of three distinct slip regimes; elastic slip, plastic slip, and gross sliding. They conclude that fretting fatigue is to be expected under conditions of partial slip, whereas wear takes place under gross sliding.

In the last paper of the series Nishioka and Hirakawa (1972) investigated the effect of material hardness and of contact pressure. Hardness was found to have little effect on the fretting fatigue life.

Increased contact pressure resulted in reduced life but, since their experiments were run at constant slip amplitude, the increase in contact pressure simply allowed a higher tangential force to be sustained in full sliding and this was thought to be responsible for the reduction in life.

In the last 15 years many investigators have addressed the problem of fretting fatigue, investigating the effects of varying the numerous parameters involved. Kantimathi and Alic (1981) examine the effects of periodic high loads on fretting of an aluminium alloy. Poon and Hoeppner (1981) apply statistical methods to establish that both environment and the level of oscillating bulk stress affect the fretting fatigue life. Chivers and Gordelier (1984) examine the effect of various palliatives, only to conclude that the only successful approach is to attenuate the local stress concentration. The number of dependent variables is so large that the work of different investigators can sometimes appear contradictory. Hoeppner and Gates (1981) highlight this problem and are led to conclude that each example of fretting occurring in practice should be treated as a separate problem.

However, several theories to explain the reduction in fatigue strength have been advanced. Wright (1970) examined the proposition that the geometric stress concentration is responsible for the reduction. By comparing tests of assemblies and geometrically similar solid components he was able to show that the effect of fretting was greater than could be explained by the geometric stress concentration alone. He concluded that high local stresses caused by contact of surface asperities may play a role. Further work by Bramhall (1973) investigated the effect of varying the size of contact while keeping the local stress concentration constant. The results revealed that there was a critical contact size below which the fretting had no detrimental effect on fatigue

performance. It was postulated that the local stress field produced by the contact needed to be of sufficient size to propagate cracks to a critical length from which they could grow in normal fatigue under the bulk stress alone. It is this phenomenon which the current work hopes to explain.

In plain fatigue cracks exhibit two distinct phases in their life; initiation and subsequent growth, as discussed by Frost, Marsh, and Pook (1974). The basic question which needs to be answered is whether fretting reduces fatigue life by accelerating crack initiation, crack growth, or both of these. Hoeppner and Goss (1974) carried out experiments in which fretting was only applied for the first portion of a test. They demonstrate the existence of a damage threshold, ie. that a certain amount of fretting must take place before the fatigue life is affected. They also show that fretting is only effective in the first 25% of the life of their specimens since samples where fretting was removed after 25% of their life exhibited the same fatigue life as those which were fretted throughout. From these results they conclude that fretting accelerates the initiation of fatigue cracks.

More recently Endo and Goto (1976) carried out experiments on the fretting of 0.34% carbon steel using cylindrical fretting pads under conditions of full slip. By measuring the crack growth rate they were able to demonstrate that the initial propagation of fretting cracks was faster than that for cracks in plain fatigue. This initial rate of growth is dependent on the fretting conditions. At a certain critical crack length, however, the growth rate dropped to that of cracks in normal fatigue under the same bulk stress and was independent of fretting conditions. This critical length was of the order of 70μm in their experiments and appeared to coincide with a change in the direction of

propagation from being obliquely under the contact to a final direction normal to the bulk stress. The accelerated period of growth corresponded to the first 25% of fatigue life. Similar results were obtained by Sato, Fujii, and Kodama (1986) who employed flat fretting pads. From these results it seems clear that fretting does accelerate the initial growth of the cracks. However, the effect of fretting on crack initiation should not be discounted. Several authors report the existence of non-propagating cracks (e.g. Bramhall (1973), Nishioka and Hirakawa (1969a,1972)) and these suggest that fretting has aided initiation but that the local stress field has not been sufficient to propagate the cracks to a stage where the bulk stress alone is sufficient to produce growth.

The available evidence suggests, therefore, that fretting accelerates both crack initiation and the initial growth rate. To produce a significant reduction in fatigue life the following effects must both be present; (i) The surface damage must be sufficiently severe to initiate a crack, and (ii) the local stress field due to the contact must be capable of propagating the crack to a critical length from which it can grow under the bulk stress alone. If (i) is not present, no fretting cracks will form. If (ii) is absent, cracks formed will self-arrest.

1.4 Analysis

Several workers have proposed that the phenomenon of fretting fatigue can be explained purely on the basis of the increased local stresses due to the contact (e.g. Milestone (1970), Nishioka and Hirakawa (1969b), and Wright (1970)). An important pre-requisite for any analysis

of fretting fatigue is, therefore, a knowledge of the surface tractions present at the contact and the corresponding stress field within the material. It is at this point that the advantage of employing cylindrical fretting pads on a plane specimen becomes apparent. If conforming surfaces are used, as is the case with plane pads, the theoretical pressure distribution is difficult to determine as the simpler analyses give rise to singularities at the edge of the contact. Such configurations also present experimental difficulties since a small change in the alignment of the pads can have a large effect on the distribution of surface tractions. Under these circumstances a traction distribution has to be assumed for subsequent calculations. This approach was adopted by Edwards, Ryman and Cook (1977),who analysed several possible configurations. Cylindrical pads are therefore to be preferred if any analysis of experimental results is contemplated.

The first analysis of the problem of contact between non-conforming elastic bodies under the action of a normal force was performed by Hertz (1882). He assumed that both bodies could be represented as semi-infinite and that the stresses and associated deformations due to the contact were confined to a small region adjacent to the surfaces. For axi-symmetric contact the relative curvature of the surfaces was approximated by a rotated parabola (or paraboloid). The results of his calculations showed that the contact pressure distribution required to cause the correct displacements within the bodies was of the form $p_o\sqrt{1 - (r/a)^2}$, where p_o is the peak contact pressure, r the radial co-ordinate from the centre of the contact, and a the radius of the contact patch. Similarly, surfaces having different reletive radii of curvature R_1 and R_2 in perpendicular directions were found to give an elliptical contact patch. The conditions for contact between cylinders

with parallel axes may be revealed by taking the limit $R_2 \rightarrow \infty$, or by carrying out a similar two-dimensional analysis. Hertz considered the case where the bodies were frictionless and hence no shear tractions arose. More generally, when the elastic constants of the two bodies are identical, relative tangential displacement between any pair of contacting points is found to be zero and no shear tractions are generated.

Fuchs (1913) calculated the stresses resulting from a Hertzian distribution of surface tractions numerically and Morton and Close (1922) extended this work for the special case of contact between spherical surfaces and used recurrence formulae to calculate the displacements and hence the stresses in the neighbourhood of the contact. In fretting fatigue a tangential force is present at the contact as well as the normal force considered by Hertz. This problem was first addressed by Cattaneo (1938) and independently by Mindlin (1949). Mindlin initially assumed that the two bodies remained adhered at all points in the contact patch under the influence of a tangential force Q less than that neccessary to cause gross sliding. This assumption was shown to require infinite values of the coefficient of friction at the edges of contact. Mindlin therefore postulated that slip took place in the outer region of contact and that adhesion was confined to a central stick zone. This assumption was shown to give consistent results. For contact between cylinders the width of the stick zone (2c) is given by $c/a = \sqrt{1 - Q/fP}$, where a is the contact semi width, P the normal force, and f the coefficient of friction. Mindlin's results have been verified experimentally for contact between spheres by Johnson (1955) and for contact between cylinders by Nishioka and Hirakawa (1969d).

The stress field beneath a contact in the presence of a tangential force was first calculated by Poritsky (1950) and independently by Smith and Liu (1953) using a different method. The results have recently been presented in a more convenient form by Sackfield and Hills (1983). These solutions are, however, limited to the application of a monotonically increasing tangential force, whereas in fretting fatigue an oscillating force is applied. The problem of unloading was first dealt with by Mindlin and Deresiewicz (1953). From their results it can be shown that, after the first quarter cycle, the surface tractions are cyclic between the limits found by Mindlin. The oscillating tangential force causes oscillating tangential motion within the slip zones and hence fretting.

These results were first applied to fretting fatigue by Nishioka and Hirakawa (1969c) and also by Milestone (1970). Both investigations showed that fretting fatigue cracks initiate at the edge of the contact, in the region of highest predicted tensile stress. Unfortunately, the experiments of Nishioka and Hirakawa were carried out under full slip conditions and considerable wear of the pads took place such that the distribution of surface tractions could not be calculated with any accuracy during the later stages of each experiment. Doeser (1981) employed plane fretting pads in his experiments and was thus required to calculate the surface tractions using the technique of finite element analysis. This method was not without problems since the contact boundary conditions proved difficult to incorporate. An iterative technique was eventually adopted and the surface tractions determined. It should be pointed out, however, that any slight inaccuracies in the machining or alignment of the pads would alter the actual distributions considerably from those calculated.

Once the surface tractions have been determined the techniques of fracture mechanics can be employed to calculate the stress intensity factors (SIFs) at the tip of any crack growing under the contact stress field. A common assumption is that the surface tractions are unaffected by the presence of the crack (ie. that there is negligible change in the compliance of the specimen). This has been verified by Bryant, Miller, and Keer (1984). Rooke and Jones (1977) have provided the basic Green's function for this calculation by deriving stress intensity factors for a normal crack in a half-plane under the action of point normal and tangential forces at the surface. Integration of this solution can be performed to derive SIFs for normal cracks under any contact loading and these calculations were first performed by Edwards, Ryman, and Cook (1977). They wished to compare their calculations with results from experiments carried out with plane fretting pads and hence produced solutions for seven different assumed distributions of surface tractions. Similar methods were employed by Nix and Lindley (1984) who calculated critical defect sizes, from which cracks would grow in fretting conditions under the regime explained by linear-elastic fracture mechanics.

O'Connor and Hills (1986) used a similar Green's function method to analyse the results of Bramhall (1973) and again calculated critical defect sizes. All these methods assume that the crack propagates in a direction normal to the surface, whereas actual cracks are found to propagate obliquely during the first phase of growth (e.g. Nishioka and Hirakawa (1969c), Endo and Goto (1976)). Green's functions for oblique cracks have been calculated by Hills, Sackfield and Uzel (1984), but the authors now feel that the results are not completely reliable, particularly for shallow crack angles.

A technique for calculating stress intensity factors for cracks growing at the practically observed orientations would clearly be useful in modelling crack behaviour and this is one of the objectives of the current work.

Chapter 2

Experimental work

2.1 Background

In Hertzian contact of cylinders, the peak normal pressure p_o is proportional to $\sqrt{P/R}$, where P is the applied normal force and R the reletive radius of curvature of the contacting surfaces. The semi-width of the contact patch, a, is proportional to $\sqrt{P\,R}$. Bramhall (1973) exploited this in his experiments by noting that it is possible to vary the contact size, whilst maintaining a constant peak pressure. This varies the extent of the stress field induced by the contact but keeps its magnitude constant. This was done in Bramhall's experiments and the results showed that fretting substantially reduced fatigue life for contact widths above a critical value. Below this, fretting did not seem to impair fatigue performance. Bramhall postulates that this effect is because the stress field induced at smaller contact widths is insufficiently extensive to propagate cracks to a length where growth could take place under the bulk stress alone.

In analysing the results of these experiments O'Connor and Hills (1986) identify the salient parameters which quantify the stress field. These are; the contact semi-width a, the peak normal pressure p_o, The ratio of normal to tangential force Q/P, the coefficient of friction f, and the bulk stress in the specimen σ. Although Bramhall maintained a constant value of Q/P in each series of his experiments the value of this parameter does not appear to have been measured and is not recorded. The coefficient of friction is extremely difficult to determine in tests run

under partial slip and Bramhall had only limited success in measuring it. Other experimenters (e.g. Nishioka and Hirakawa (1969c), Sato, Fujii and Kodama (1986)) report a characteristic oblique phase of crack growth under fretting conditions. This important feature should be incorporated in any subsequent fracture mechanics analysis of experimental results. Bramhall, however, does not record crack trajectories. It was therefore necessary to carry out a further set of experiments similar to Bramhall's, but recording all the salient parameters, before any thorough analysis could be attempted.

2.2 Apparatus design

Fatigue experiments are lengthy and so the first task of the project was to design and manufacture the test equipment. Experiments were to be carried out using the Dartec servo-hydraulic fatigue testing machine in the Engineering Department. The material chosen for both specimens and pads was HE15-TF, an Al/4%Cu alloy similar to the L65 Aluminium alloy used by Bramhall, which is no longer available. This material had two advantages: it would enable comparisons with Bramhall's experiments to be made, and it is commonly used in the aerospace industry, where fretting is of particular importance. Relevant material properties are; 0.2% proof stress = 465 N/mm^2 , tensile strength = 500 N/mm^2, fatigue strength = 124 N/mm^2 at 5×10^8 cycles, Young's modulus = 74×10^3 N/mm^2. The material was polished and etched in 5% HF and the microstructure revealed is shown in Fig.2.1. The grains are highly elongated along the specimen axis, as might be expected for an extruded material.

Experiments were to be carried out in push-pull fatigue and the design of specimen chosen is shown in Fig.2.2. The design is that of a

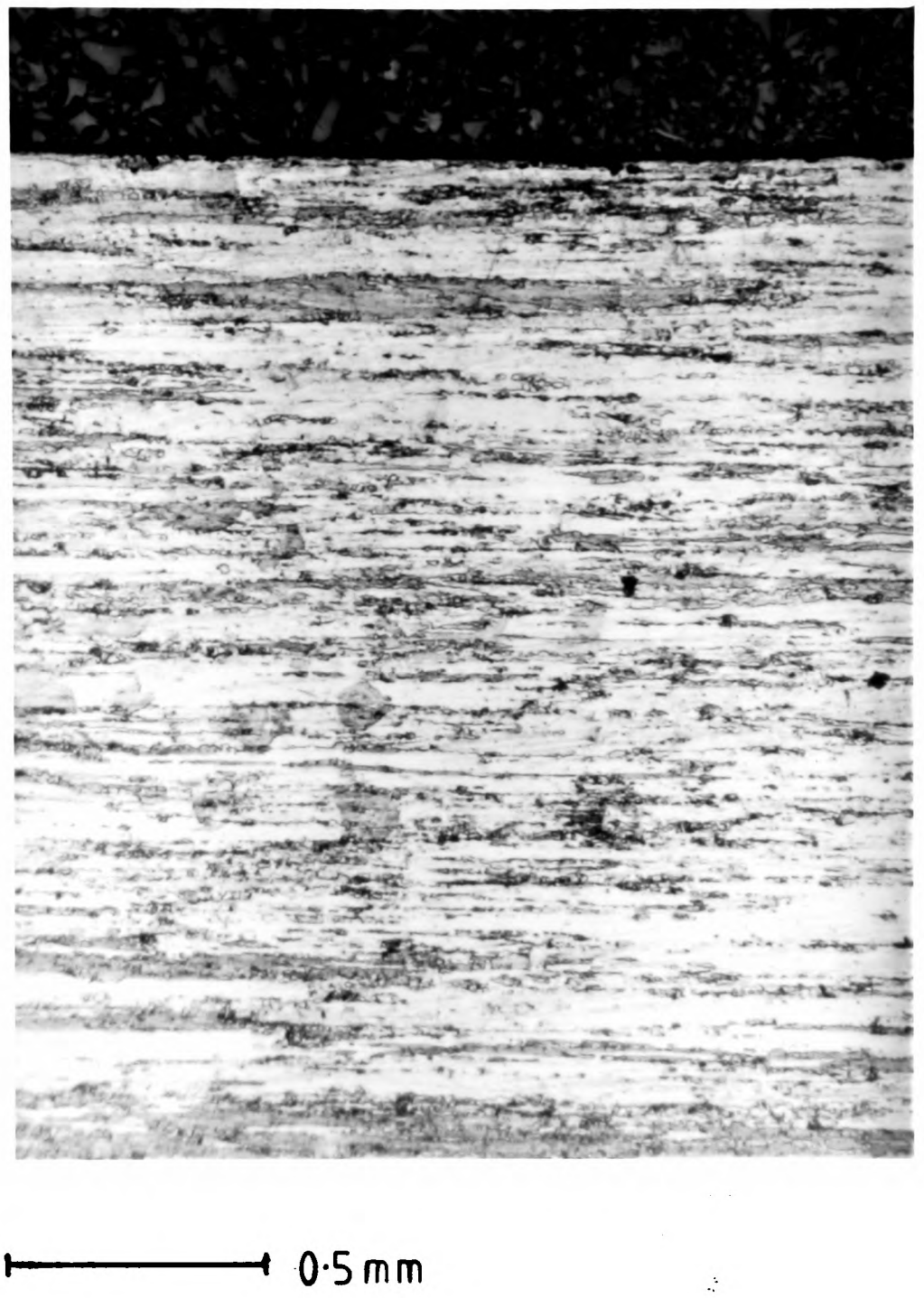

Fig. 2.1 Specimen micro-structure, axial section

standard tensile specimen with ground flats on opposite sides. A surface roughness of 0.4 μm r.m.s. was specified for the ground surfaces and for the cylindrical fretting pads The specimen has to be sufficiently large for plane strain and half-plane assumptions to be valid at the contact. However increased size entails larger loads and consequently lower frequencies from the test machine.

Figure 2.3 is a schematic representation of the configuration adopted for the apparatus. The specimen is mounted between a fixed and a movable jaw so that an alternating bulk stress $\sigma \sin \omega t$ can be applied by the fatigue machine. Cylindrical fretting pads are clamped against the specimen by a normal force P. The pads are attached to the rigid base by springs. As the specimen extends under the action of the bulk stress the point of contact is displaced and the springs apply a tangential force $Q \sin \omega t$ to the specimen through the pads. This force is in phase with the applied bulk stress.

A diagram of the actual design is shown in Fig.2.4. The fretting pads (1) consist of blocks with one face machined to part of a cylinder and are clamped to separate bases (2). Each set of clamping bolts consists of two with left- and two with right-handed threads. This ensures that no net torque is applied to the pads during clamping which might disturb their alignment. The bases are mounted on pairs of flexible plates (3). This arrangement restrains the pads vertically so that the tangential force can be applied but allows a small amount of horizontal movement so that any wear of the pads can be taken up. This is an improvement on Bramhall's apparatus, where the pads were clamped to a single base and no provision was made for wear. Bramhall was also unable to monitor the normal force applied once the pads had been clamped. The normal force is applied by two coil springs (4) acting on

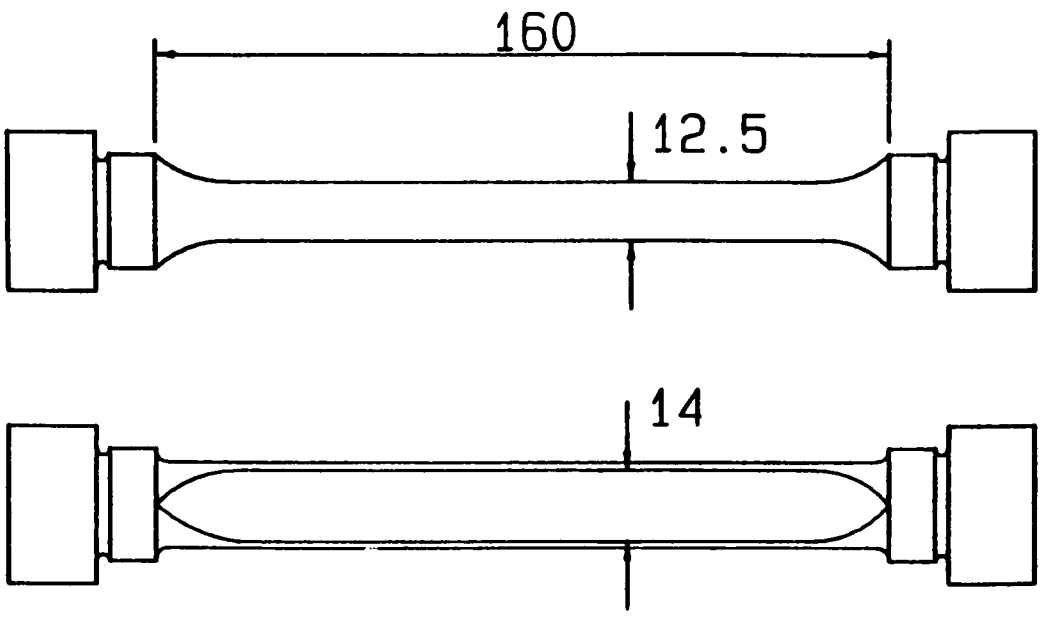

Fig.2.2 Fretting fatigue specimen

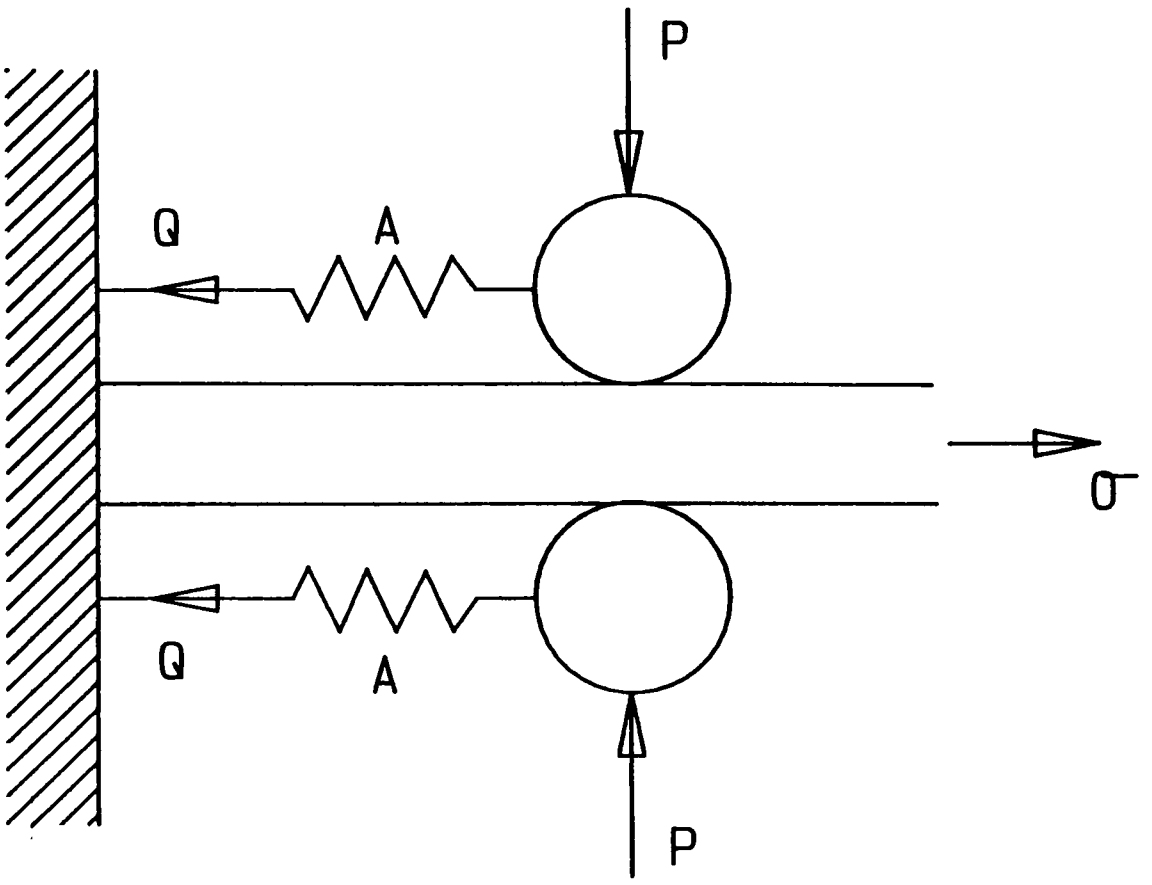

Fig. 2.3 Schematic experimental configuration

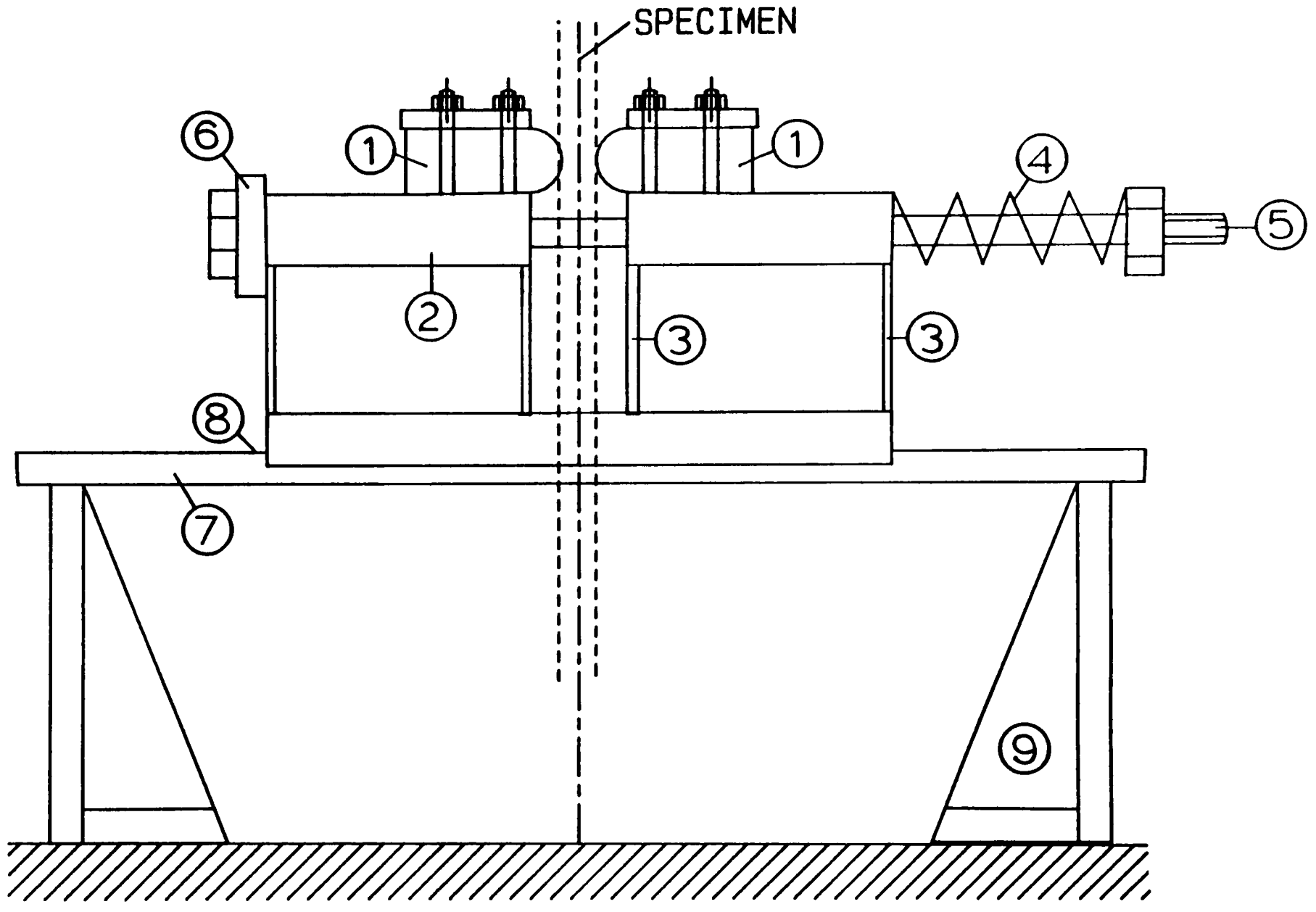

Fig. 2.4 Diagram of apparatus

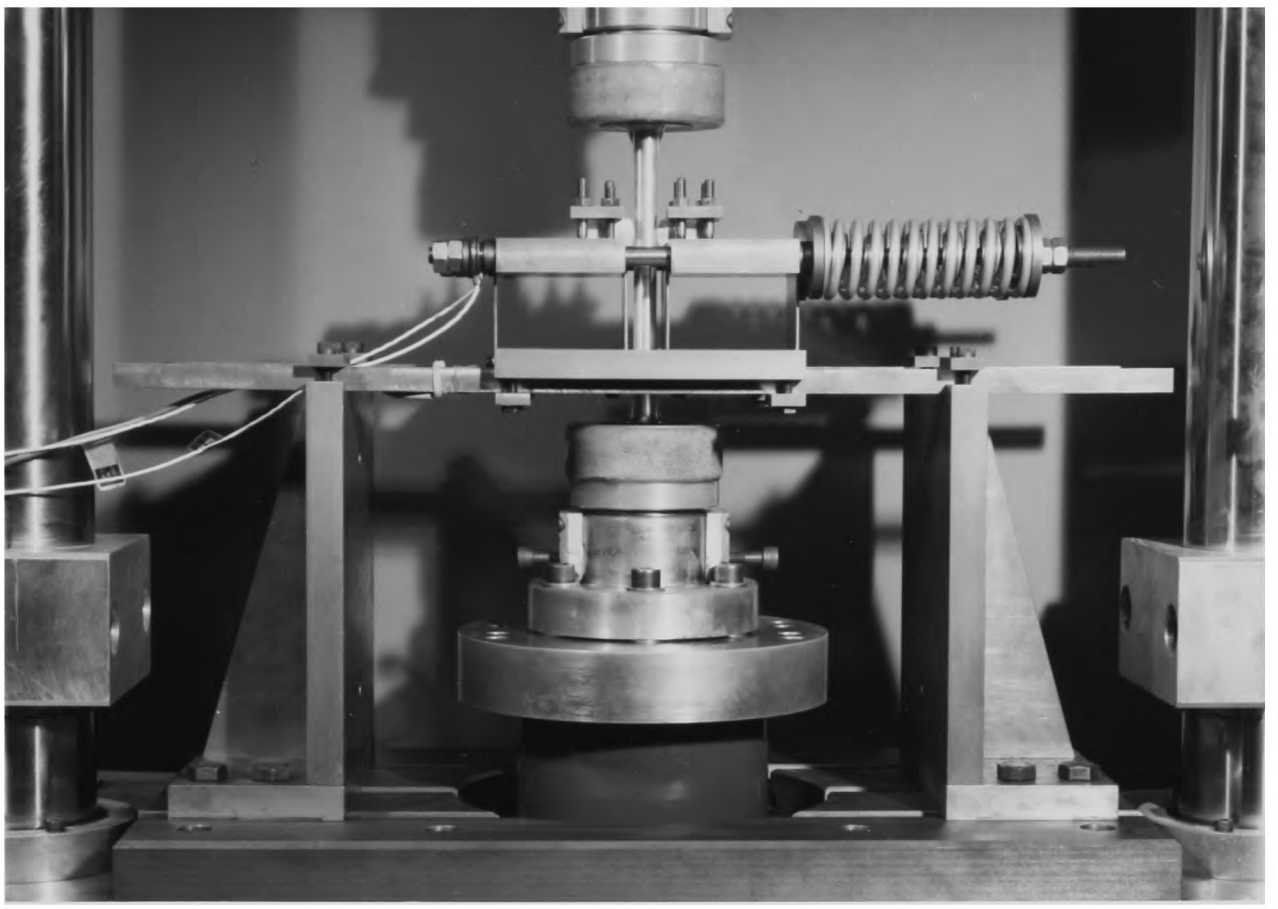

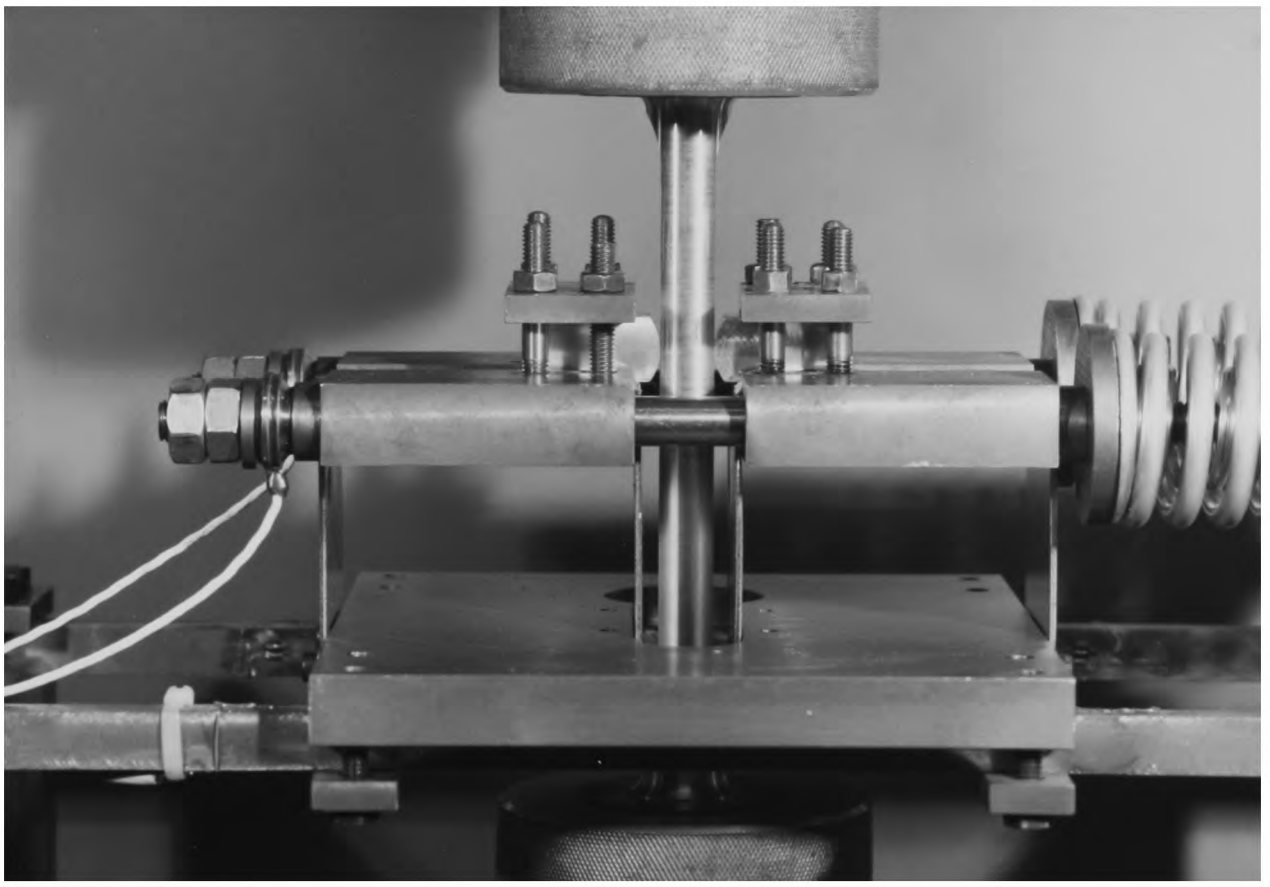

Fig. 2.5 Experimental apparatus (a) Overall view
(b) Detail

bolts (5) connecting the two bases. These bolts are a close sliding fit within the bases, helping to ensure that they remain perpendicular to the specimen during loading and do not allow the pads to roll. The applied load is monitored by a pair of commercial force transducers (6) mounted under the bolt heads.

A pair of cantilever springs (7) provides the means of applying a tangential force to the contact. The length of these can be adjusted to maintain a constant ratio of tangential to normal force (Q/P) between tests of the same series. The tangential force is monitored by strain gauges mounted near the root of the cantilevers (8) so as to record strain in bending. This position provides a variation in sensitivity with cantilever length and enables a wide range of Q values to be measured accurately. A strain gauge bridge on the Dartec machine is used to monitor the output of these gauges, enabling maximum, minimum, and mean values to be displayed. The cantilevers are supported by movable columns (9), thus providing the required length adjustment. A static calibration was carried out to establish the relationship between applied tangential force Q and recorded cantilever strain at several different lengths. Figure 2.5a gives an overall view of the apparatus in position on the Dartec machine and a more detailed view of the central portion is shown in Fig. 2.5b.

2.3 Experimental procedure

As discussed above, Bramhall's experiments suggested the existence of a critical contact width below which fretting had no effect on the fatigue life of the specimen. The main set of experiments carried out in the current study attempted to determine this critical width for several

different combinations of loading parameters. In all, five series of tests were carried out to investigate the variation of critical contact width with peak contact pressure p_o, tangential force Q, and bulk stress σ. In order to provide a range of contact sizes, eight pairs of fretting pads were chosen for each series of tests, with radii of curvature ranging from 12.5mm to 125mm. A given series of eight tests was run at constant values of peak contact pressure p_o, tangential force Q, and bulk stress σ. For each test a pair of pads was selected, cleaned with 'Genklene' and clamped against a pre-cleaned specimen. The contact pressure distribution was examined with 'Prescale' pressure-sensitive film in order to ensure even contact across the face of the specimen. Any misalignment could therefore be detected and corrected before the test commenced. The normal force P was now applied by compressing the loading springs and the experiment started. A check was made on the measured value of Q and the cantilever length adjusted, if necessary, to give the correct ratio Q/P.

The purpose of the experiments was to demonstrate that fretting has no effect on the fatigue strength of the specimen when the contact size is below a critical value. Since the tests were carried out at bulk stress levels below the unnotched fatigue strength of the material, testing to a large number of cycles was required to demonstrate that fretting has no effect. It was decided, therefore, to test each specimen to 10^7 cycles unless failure occurred first. At the required loads, the maximum operating frequency of the Dartec machine is about 22 Hz. Thus, each experiment could take up to 5 days to complete and a series of eight about eight weeks, allowing for setting-up time. Fortunately, failed specimens broke after about 2×10^6 cycles and thus the overall time was somewhat reduced. A micro-switch was fitted to the machine, which was

activated when a specimen broke and the range of actuator movement increased. The number of cycles to failure was then recorded by the controlling computer.

2.4 Estimation of coefficient of friction

Of the salient parameters identified by Hills and O'Connor (1986), p_o, Q, and σ could all be readily determined from measurements made during the course of the experiments. In order to eliminate significant wear all series of experiments were carried out in partial slip (i.e. $Q < fP$). This renders determination of the coefficient of friction impossible from the experimentally measured quantities. Furthermore, a variation of coefficient of friction with the number of fretting cycles has been reported by several authors, including Milestone and Janeczo (1971) and Endo, Goto, and Fukunaga (1974).

In order to establish whether such an effect was present in the current experiments several friction tests were carried out in the fully sliding regime. The cantilever beams were set to maximum stiffness and the machine set running at 0.1 Hz to allow recording of tangential force and contact displacement (proportional to the measured tension in the specimen) on an x-y plotter. A typical trace is shown in Fig.2.6 and the existence of sliding can be seen by the saturation of the tangential force at a nearly constant value. Under such sliding conditions, the coefficient of friction, f, may be taken as the ratio of tangential to normal force Q/P. The results of three such tests are recorded in Fig.2.7. Tests 1 and 2 were conducted with 50mm pads and p_o = 157 N/mm^2. There is a rapid rise in the coefficient of friction from an initial value of 0.2 until, after about 100 cycles, the tangential force could be

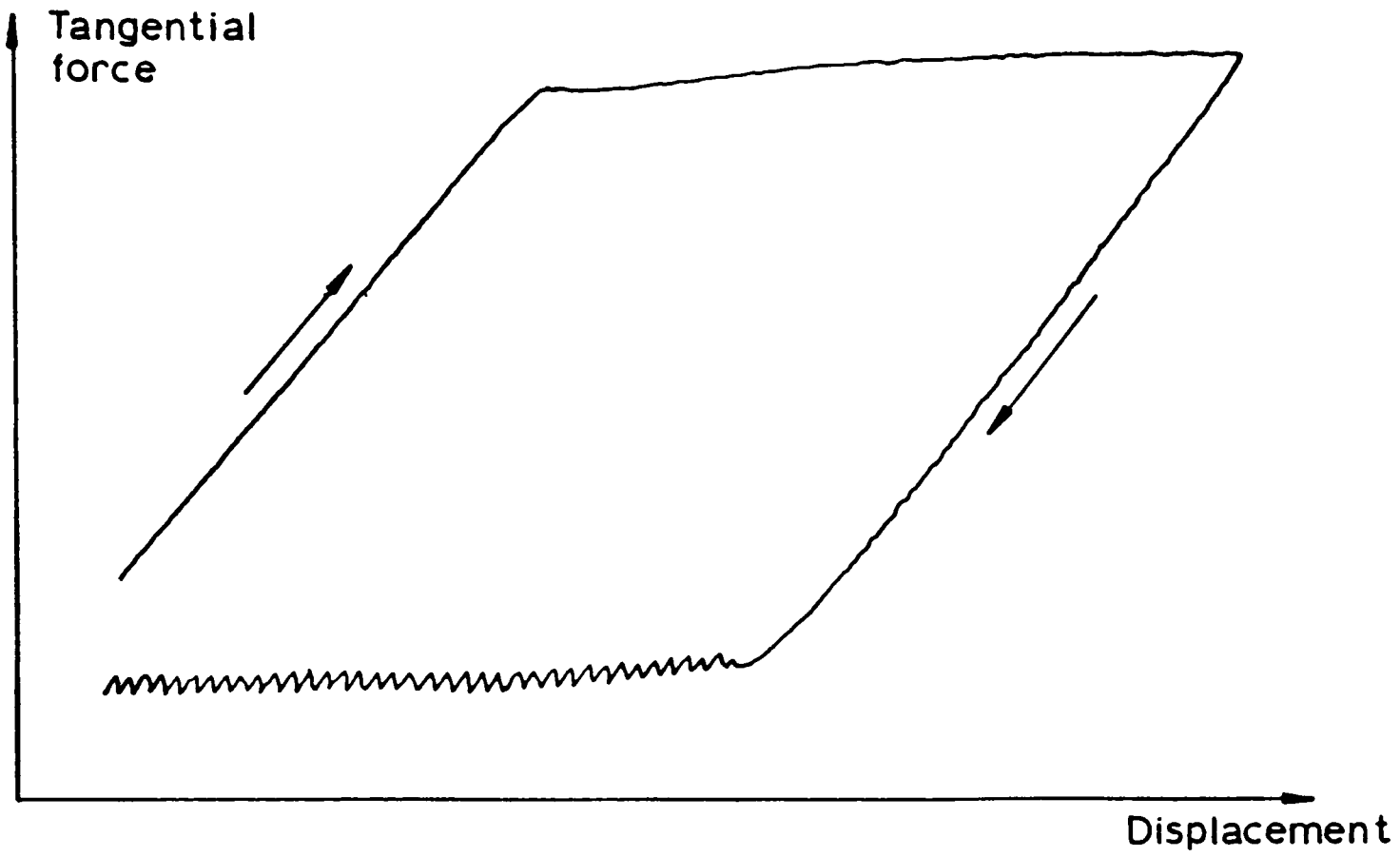

Fig. 2.6 Cyclic variation of frictional force (full slip)

f

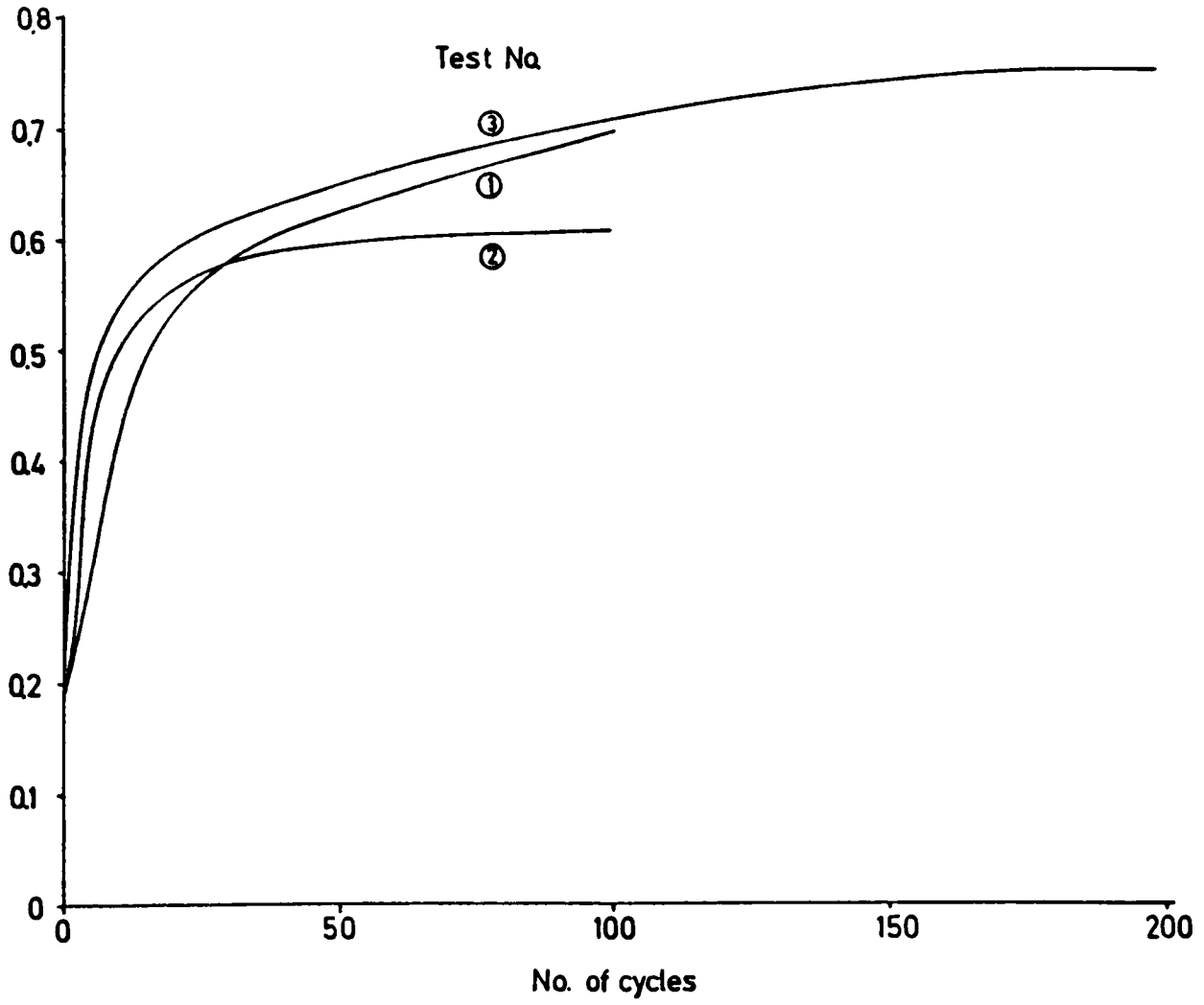

Fig. 2.7 Variation in coefficient of friction with number of fretting cycles

sustained without gross sliding. This was indicated by a change in the form of the force/displacement plot (Fig.2.8) and prevented further measurement of f. In test 3, carried out at the lower peak contact pressure of 73 N/mm^2, sliding persisted until a limiting value of f = 0.75 was reached.

It is clear from the foregoing that a substantial increase in the coefficient of friction takes place when the contact is fully sliding. This increase may be due to a self-cleaning process or to surface degradation brought about by the relative motion of the surfaces. When the applied tangential force is insufficient to cause sliding ($Q < fP$) Mindlin (1949) predicts the existence of a central stick zone bordered by two slip zones where reletive motion occurs between the surfaces. Surface degradation might be expected to take place in these regions just as in the fully sliding case with a consequent increase in the local coefficient of friction. In the central stick zone, no microslip will occur and the local value of f should remain unchanged. Thus f will vary with position as well as time.

It is possible to measure the mean coefficient of friction $\overline{f}$ at any time simply by increasing the tangential force Q until the onset of sliding. This average value may then be defined as:

$$\overline{f} = \frac{Q_{slip}}{P} = \frac{\int_{-a}^{a} q(x)\, dx}{\int_{-a}^{a} p(x)\, dx} \qquad (2.1)$$

where Q_{slip} is the tangential force measured at the onset of sliding and q(x) and p(x) are the local values of the shear and normal surface tractions respectively. The value f at a particular sliding point may be defined as:

$$f(x) = \frac{q(x)}{p(x)} \qquad (2.2)$$

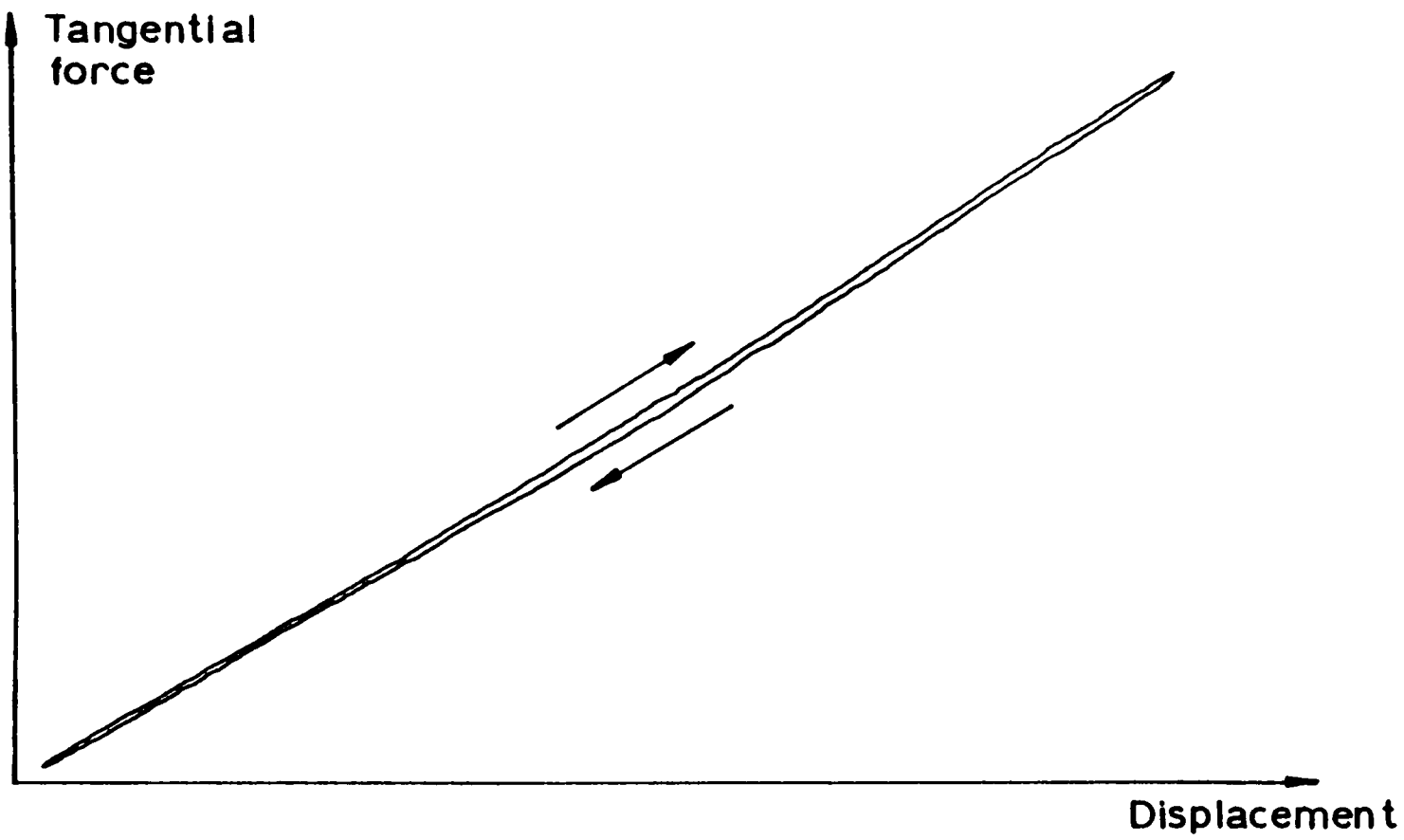

Fig. 2.8 Cyclic variation of frictional force (partial slip)

By making certain assumptions it is possible to estimate this local value from the measured average value $\bar{f}$ and the applied tangential force Q.

Figure 2.9a shows two elastically similar cylinders, loaded in the classic Mindlin configuration, with a central stick zone $|x| \leq c_o$ obtaining during the first loading cycle, when the coefficient of friction is f_o. After n cycles, the coefficient of friction in the slip zones has risen to f_n due to the surface modification process outlined above. The stick zone has concomitently increased to $|x| \leq c_n > c_o$, Fig.2.9b. Within the original stick zone the coefficient of friction will remain unchanged at f_o since no microslip has taken place. For $c_n < |x| < c_o$, f will lie between these two values. It will be appreciated that a key assumption is that the coefficient of friction is <u>constant</u> throughout the slip zone, i.e. surface modification of f is <u>independent</u> of contact pressure.

Using the result of Mindlin (1949) for the stick zone size gives:

$$(c_n/a)^2 = 1 - Q/f_n P \qquad (2.3)$$

If, at this stage, the average coefficient of friction, $\bar{f}$ is measured, by sliding the cylinders a minute distance, so as to maintain the same surfaces in registration, we obtain a measure of $\bar{f}$. From (2.1):

$$\frac{\pi a \bar{f}}{4} = \int_0^{co} f_o \sqrt{1 - (x/a)^2}\, dx + \int_{c_n}^{a} f_n \sqrt{1 - (x/a)^2}\, dx + \int_{co}^{c_n} f(x) \sqrt{1 - (x/a)^2}\, dx \qquad (2.4)$$

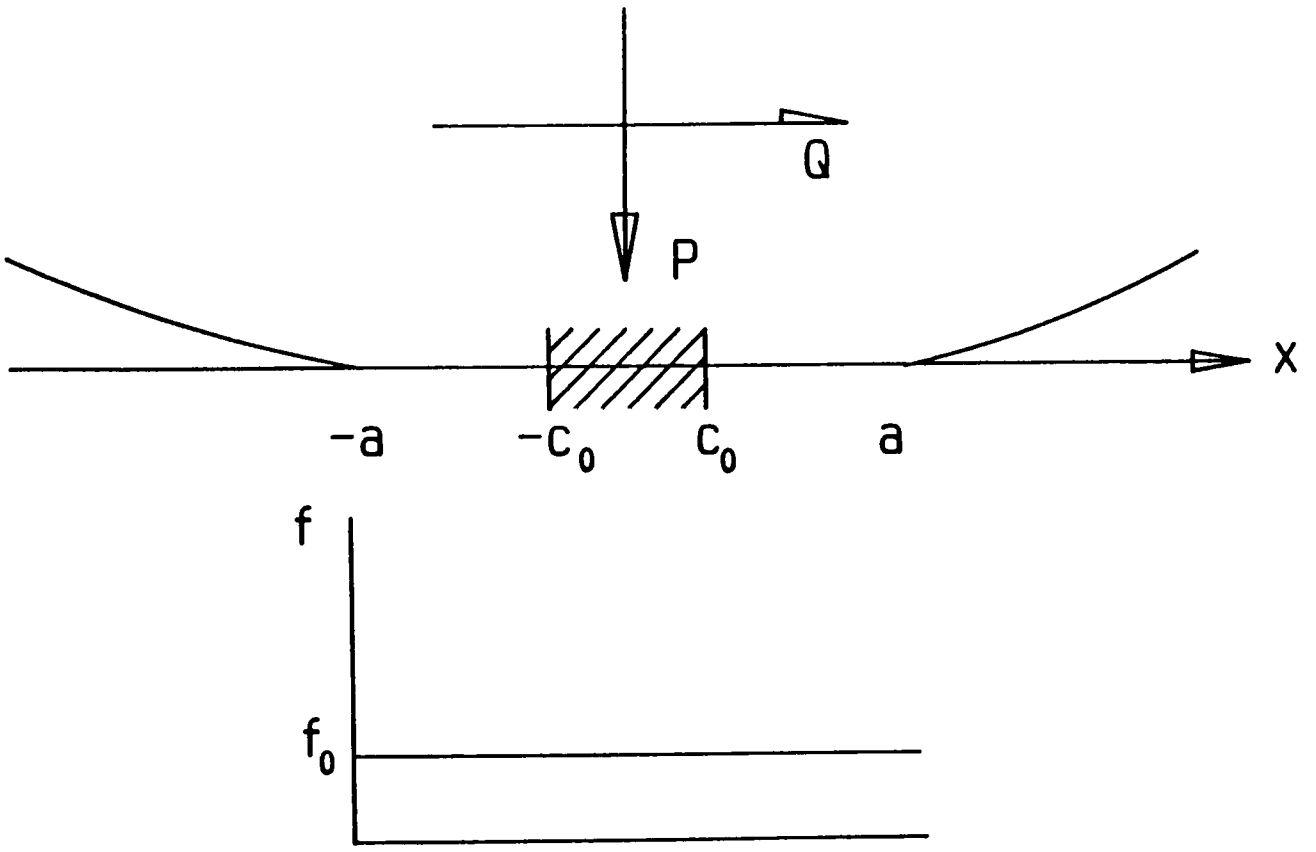

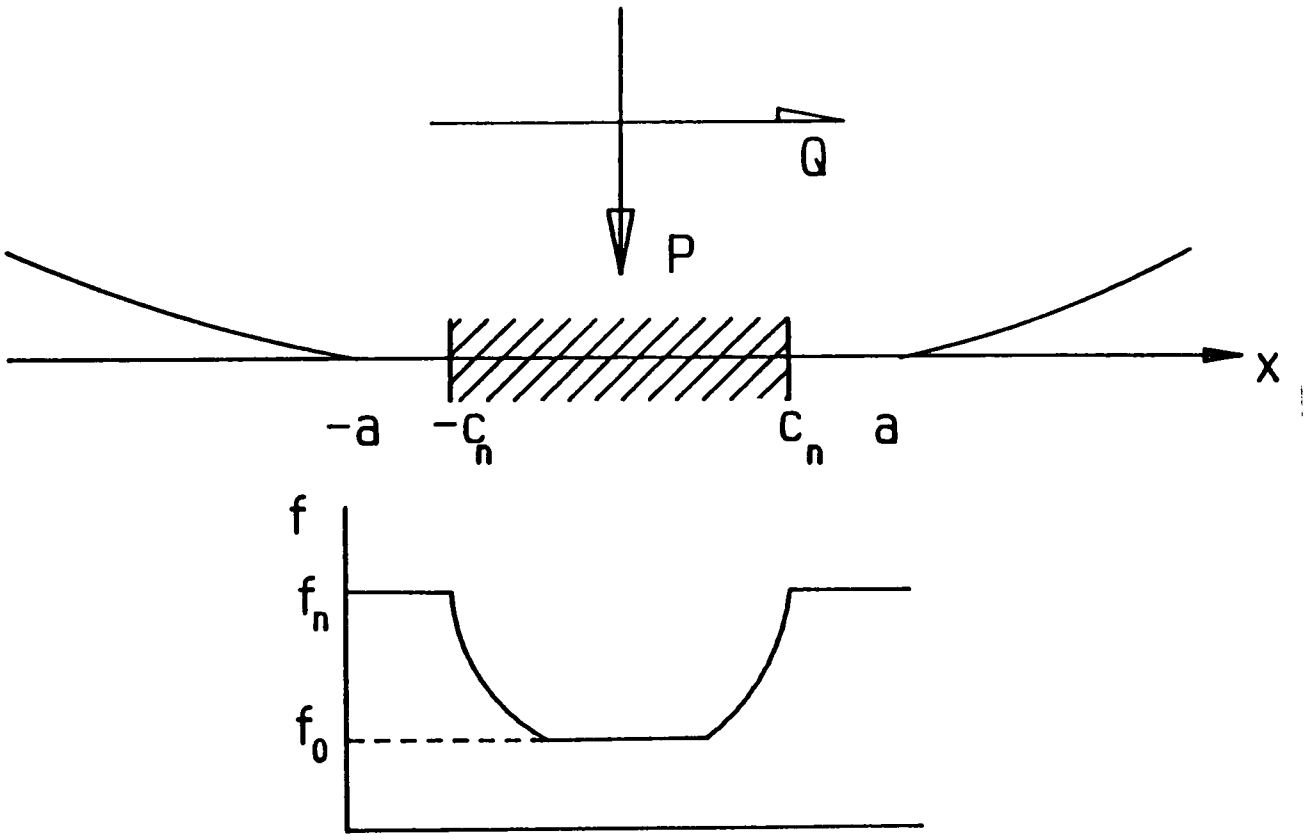

Fig. 2.9 Model of variation of coefficient of friction across contact
(a) Initially
(b) After n cycles

Differentiating (2.4) with respect to the number of cycles n yields:

$$\frac{\pi a}{4}\frac{\partial \bar{f}}{\partial n} = \frac{\partial f}{\partial n}n\left[\frac{\pi}{4} - \frac{c}{2}n\sqrt{1-(x/a)^2} + \frac{1}{2}\sin^{-1}(c_n/a)\right] \qquad (2.5)$$

Combining (2.3) and (2.5) gives:

$$\bar{f} = f_n - \frac{2}{\pi}\int_{f_o}^{f_n}\left[\frac{Q}{f_n P}\sqrt{1-\frac{Q}{f_n P}} + \sin^{-1}\sqrt{1-\frac{Q}{f_n P}}\right]df_n \qquad (2.6)$$

The friction tests conducted under full sliding suggest that the initial coefficient of friction is about 0.2. In the fretting tests carried out the steady state ratio Q/P was between 0.24 and 0.45. Hence, in these tests, sliding took place initially over the whole contact area and $f_o = Q/P$. Evaluation of the integral under these conditions gives:

$$\bar{f} = f_n - \frac{2Q}{\pi P}\left[-2\sin\alpha + 2\ln\left[\tan\left[\frac{\alpha}{2}+\frac{\pi}{4}\right]\right] + \frac{Pf}{Q}n\,\alpha - \tan\alpha\right] \qquad (2.7)$$

where $\alpha = \cos^{-1}\sqrt{\frac{Q}{f_n P}}$

Thus if a measurement of the average coefficient of friction, $\bar{f}$, is taken after n fretting cycles it is possible to predict the slip zone value, f_n. Figure 2.10 shows the relationship between these two quantities for various tangential force ratios Q/P. Values of the average coefficient of friction $\bar{f}$ were measured in two series of fretting tests after 10^4 cycles, when steady state conditions may be assumed to have developed. The results, together with the predicted value of friction coefficient in the slip zones (f_n), are tabulated overleaf.

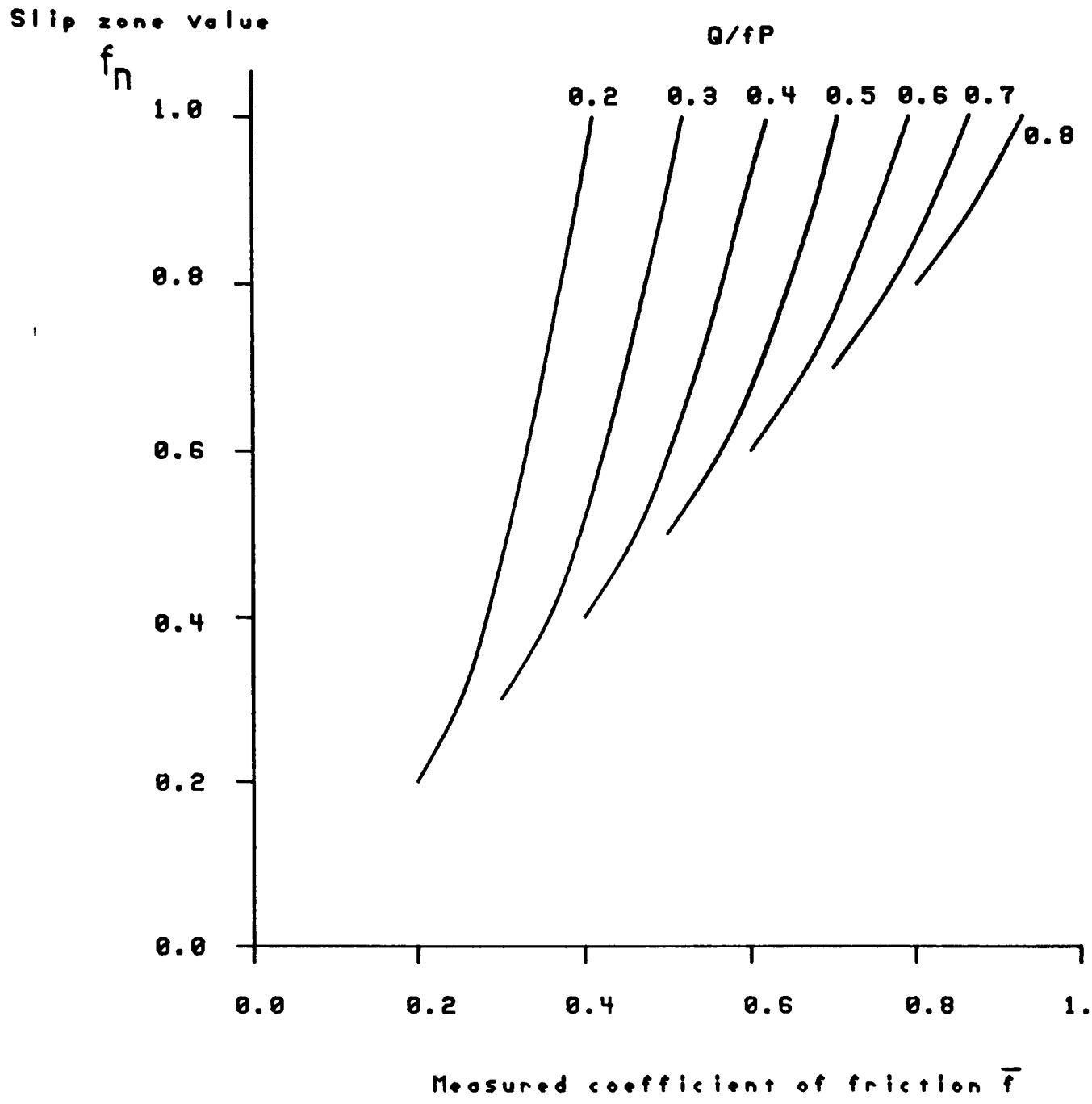

Fig. 2.10 Prediction of coefficient of friction in slip zones from measured average value

Series	Q/P	$\bar{f}$	f_n
2	0.24	0.39	0.70
3	0.45	0.61	0.80

The results of these investigations therefore confirm indications of the sliding tests and suggest that the coefficient of friction reaches a high steady-state value of about 0.75 in the slip zones. Investigations of increase in friction coefficient for fretting of steel have been carried out by Endo, Goto, and Fukunaga (1974) and Milestone and Janeczko (1971). They too report high steady-state coefficients of friction in the range 0.6 - 0.8. The rapid rise during the first 10 to 20 cycles is particularly highlighted by the latter authors.

The estimate derived here for the coefficient of friction in the slip zones (0.75) is used in all subsequent analysis. It will be shown in section 4.5 that the state of stress where fretting fatigue cracks initiate is not very sensitive to f and so the use of this estimated value is felt to be justified, particularly since no direct measurements of f can easily be made.

Chapter 3

Experimental results

3.1 Introduction

The main fretting tests were carried out until either the specimen failed or 10^7 cycles were reached, as described in the previous chapter. Nearly all of the failures which did occur took place below 2×10^6 cycles, and therefore tests in which the specimen survived demonstrated a substantially improved fatigue life, and may be regarded as having been carried out at conditions below the fretting fatigue limit of the material. The results of individual experiments in the 5 main series of tests are tabulated in Appendix A and presented graphically in Figs. 3.1a-c.

Before discussing these results in detail it is helpful to highlight some of the features observed in a typical failed specimen. Figure 3.2a shows a failed specimen in the testing machine, and Fig 3.2b shows, diagramatically, a typical section through a failed specimen. In all cases, cracks initiated close to the trailing edge of the contact (i.e. where the effect of the bulk tension in the specimen, combined with the tension caused by the tangential force Q, is a maximum). Cracks were generally found to propagate for a short distance obliquely under the contact before turning to a direction nearly normal to the free surface. This phenomenon has been observed by several other authors (e.g. Sato, Fujii, and Kodama (1986)). Usually, cracks initiated near the central plane of the specimen (Fig. 3.3a.) but occasionally the crack was found to start from near the edge of the ground flat (Fig. 3.3b). Such "corner

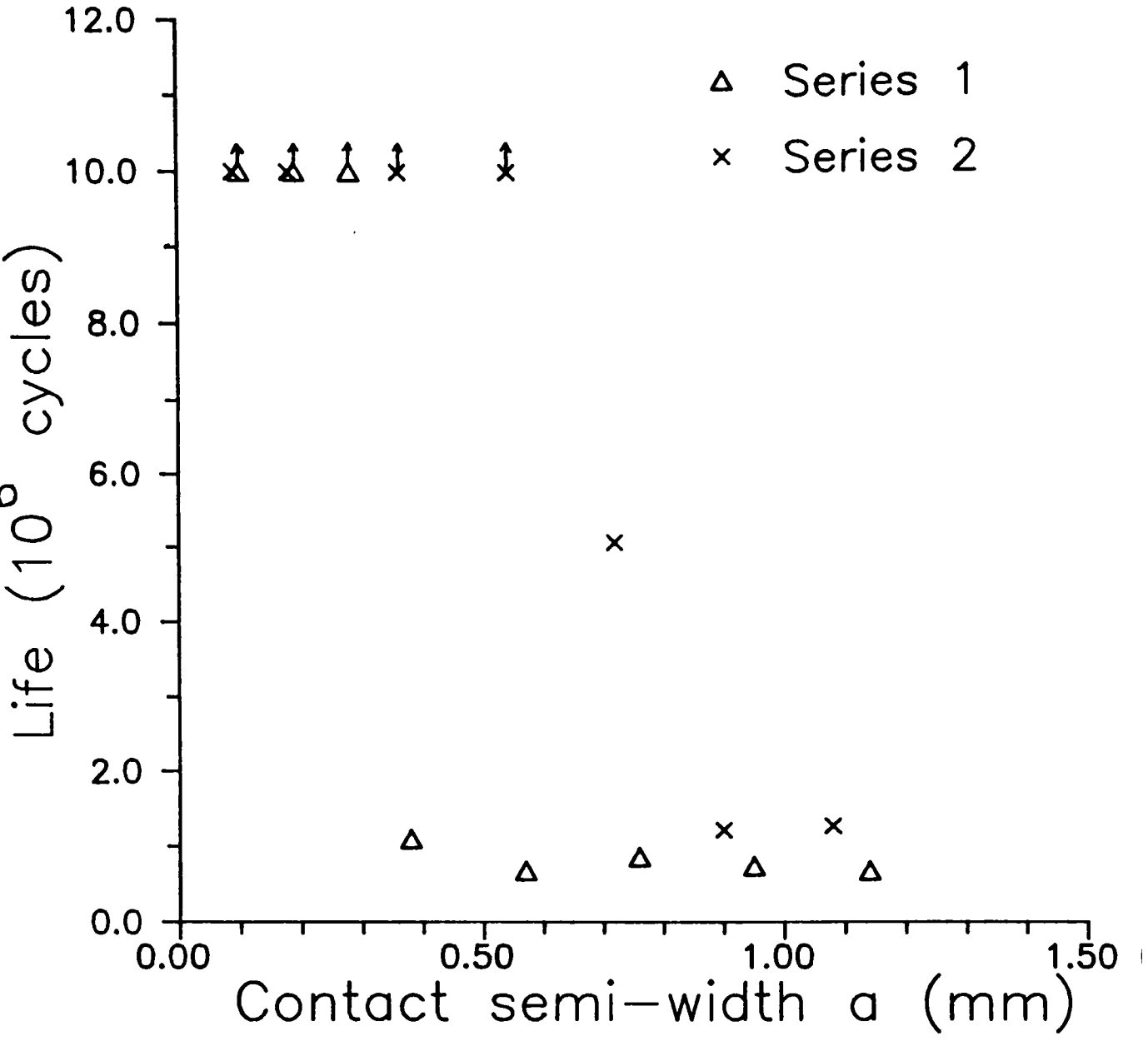

Fig. 3.1 Variation of fatigue life with contact width
(a) Series 1 and 2

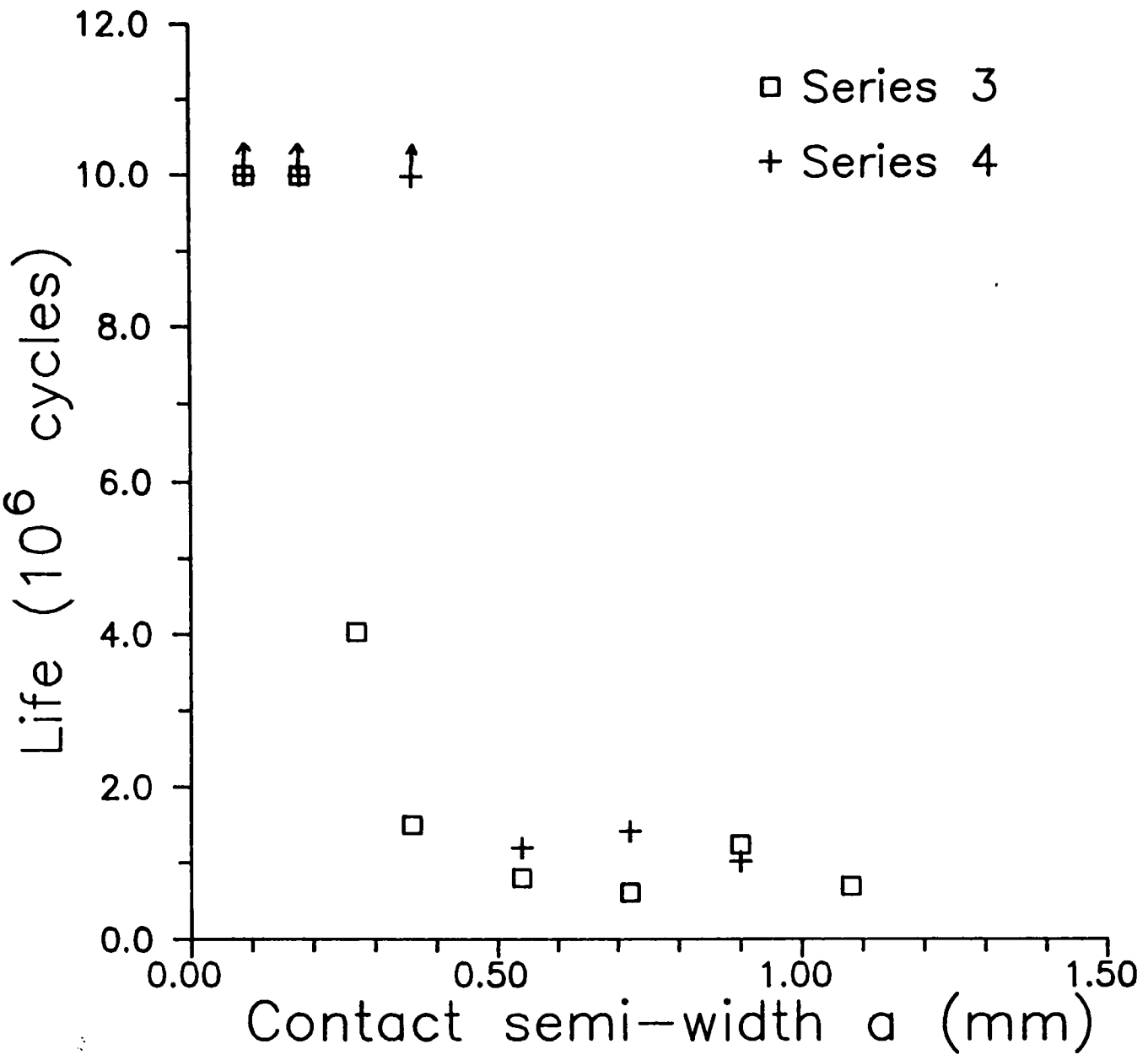

Fig. 3.1 Variation of fatigue life with contact width (b) Series 3 and 4

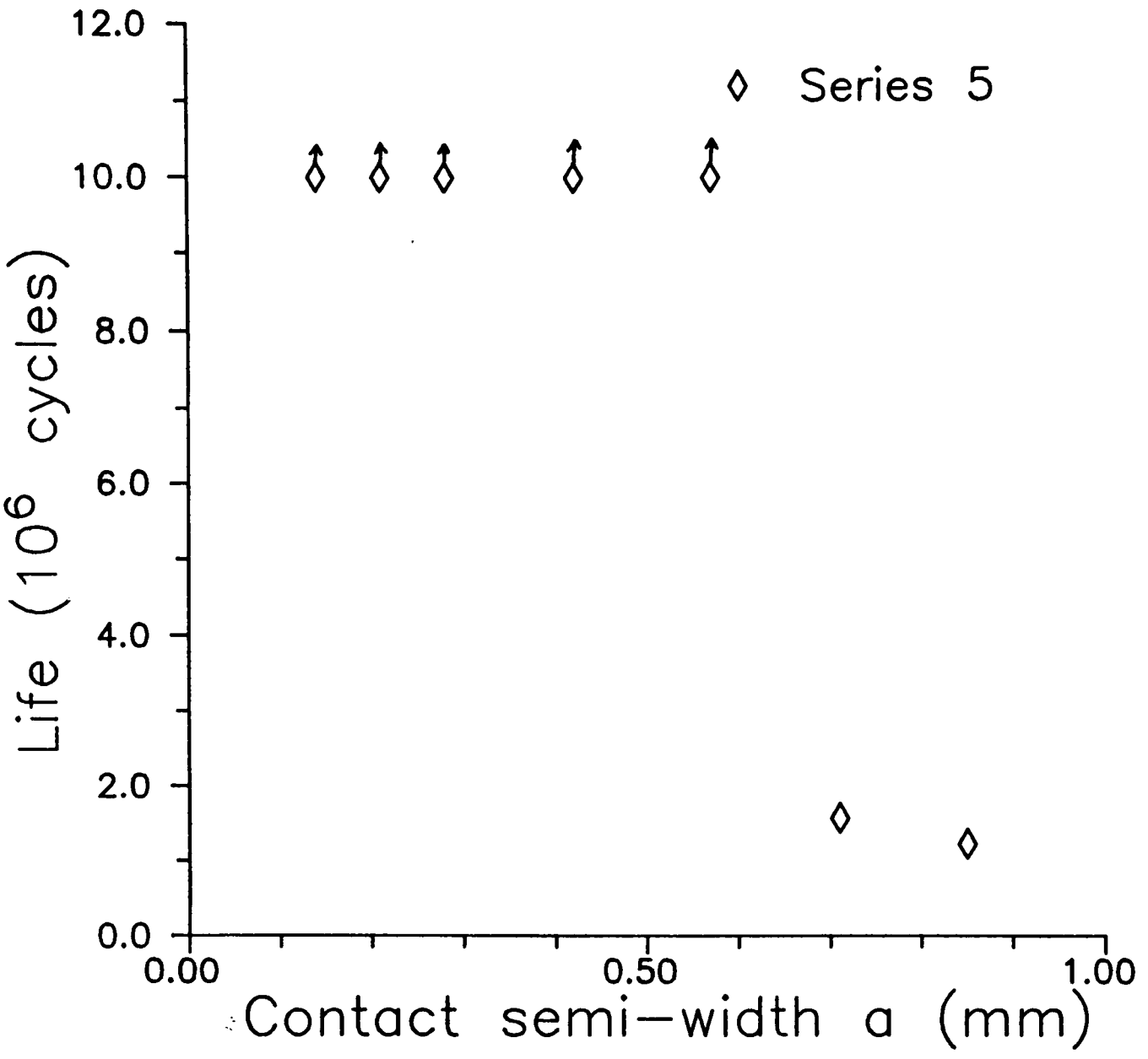

Fig. 3.1 Variation of fatigue life with contact width (c) Series 5

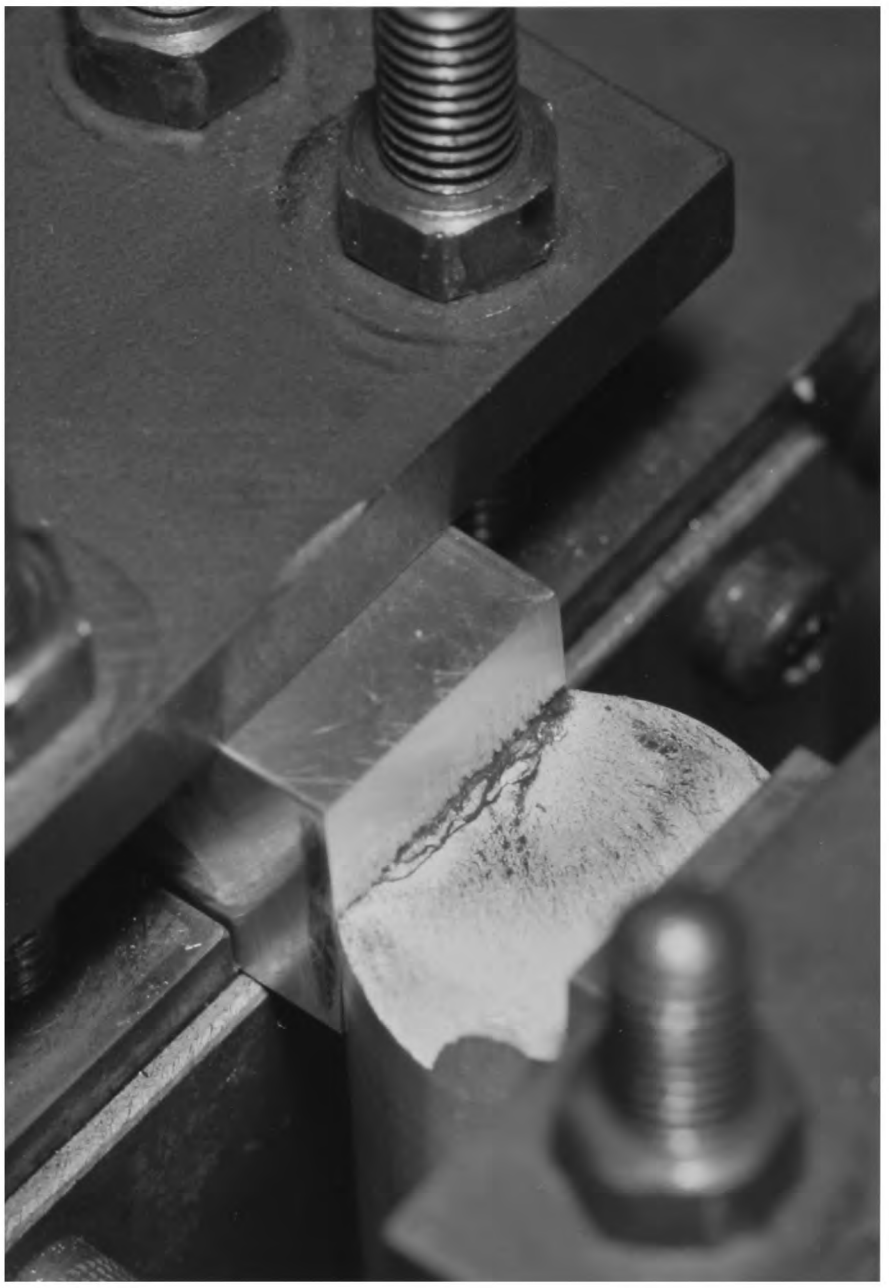

Fig. 3.2a Failed specimen in the fatigue machine

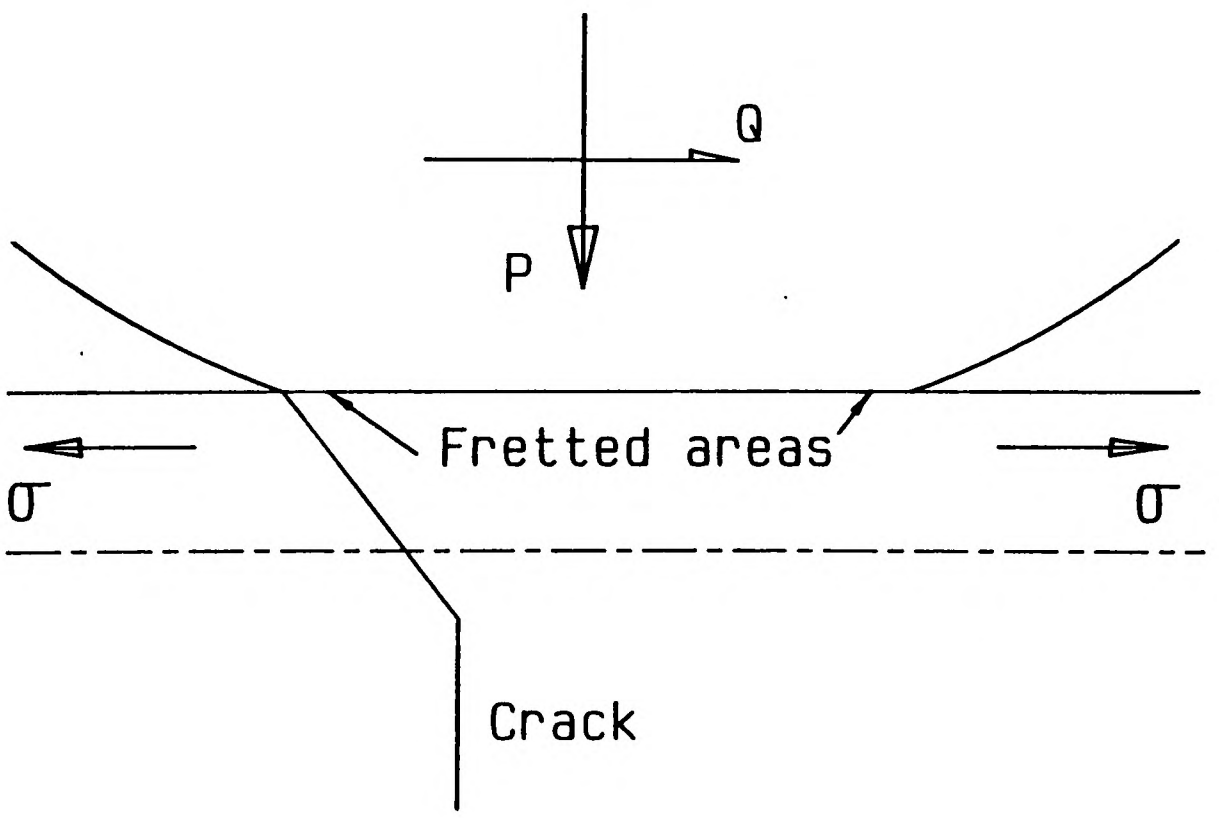

Fig. 3.2b Diagrammatic section showing typical features of a failed specimen

Fig. 3.3 Crack initiation sites: (a) central failure
(b) corner failure

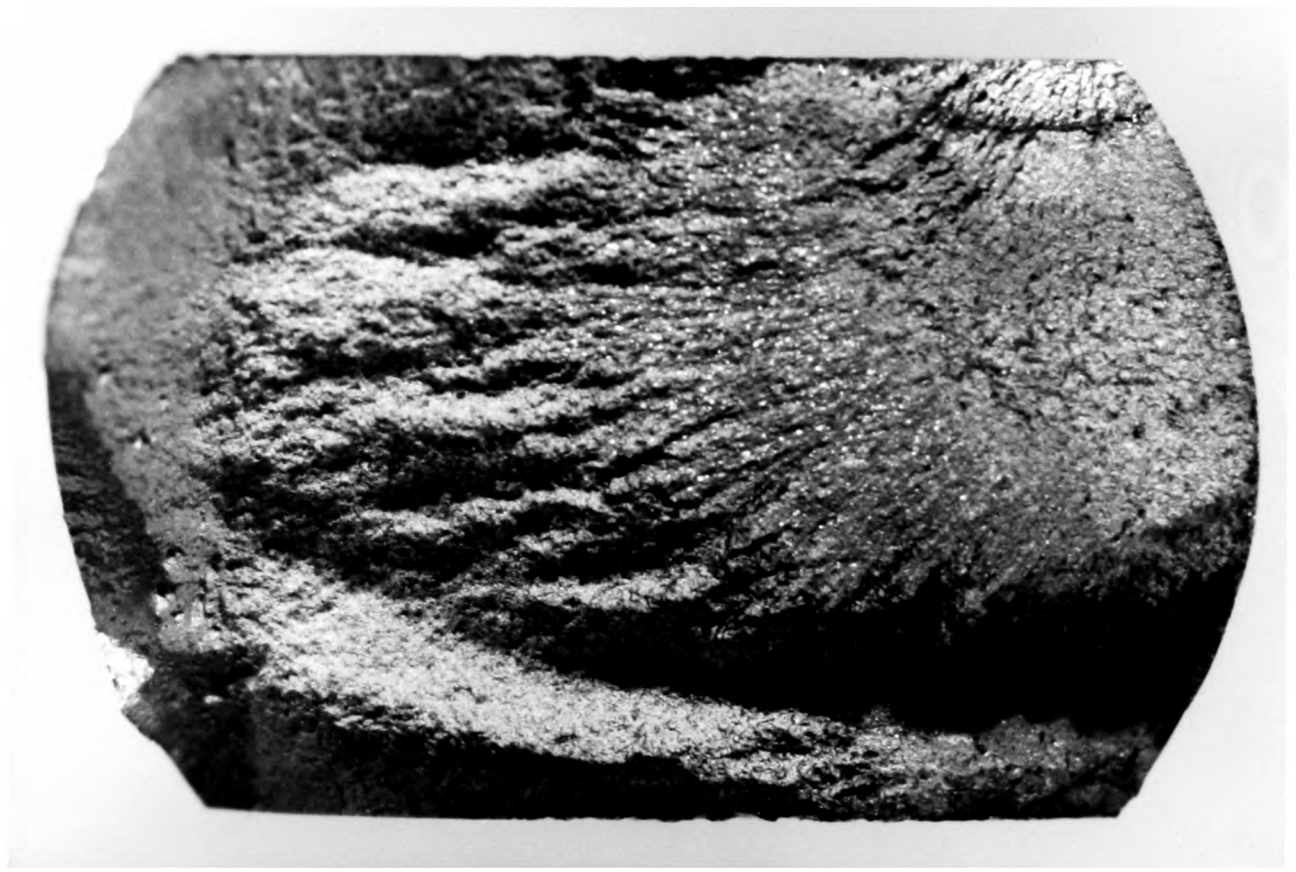

failures" often gave rise to anomalous results and were considered to be due to a misalignment of the fretting pads leading to non-uniform conditions along the contact length. The results of all experiments where such a failure occurred were discarded and the test repeated. Thus, all the results presented here represent tests in which reasonably uniform conditions were achieved along the contact length and a two-dimensional plane strain analysis is therefore employed in later sections.

3.2 Fatigue lives

The variation of fatigue life for experiments within each series is presented graphically in Figs. 3.1a-c. The horizontal axis was chosen to be the theoretical contact semi-width, a, calculated using the results of Hertz (1882). This was preferred to the radius of the indenters, since it enables a better comparison to be drawn between experiments of different series. The actual contact semi-width proved difficult to determine for reasons discussed in section 3.3 and was therefore not used.

In each series of tests it was found that large contact widths gave rise to short fatigue lives of the order of 10^6 cycles, whereas for small contact widths the specimens survived 10^7 cycles. An abrupt change between these two regimes was found to occur at a critical value of contact semi-width a_{crit} which was dependent on the following experimental parameters: alternating bulk stress in the specimen (σ), peak contact pressure (p_o), Tangential force ratio (Q/P), and coefficient of friction (f). This is precisely the phenomenon recorded by Bramhall (1973). Critical contact semi-widths (calculated from the Hertz theory)

are tabulated below for each series of experiments. A range of values for a_{crit} is given corresponding to the values of a at the largest contact to survive 10^7 cycles and the smallest to fail.

Series	Bulk Stress amplitude σ (MN/m^2)	Peak normal pressure p_o (MN/m^2)	Q/P	f	a_{crit} (mm)
1	92.7	157	0.45	0.75	0.28–0.38
2	92.7	143	0.24	0.75	0.54–0.72
3	92.7	143	0.45	0.75	0.18–0.27
4	77.2	143	0.45	0.75	0.36–0.54
5	61.8	120	0.45	0.75	0.57–0.71

The values of σ and p_o are similar to those used by Bramhall in his experiments, but detailed comparison of the results is not possible since values of Q/P were not recorded by him. Also, the estimated values for the coefficient of friction f are lower in his experiments.

For the purposes of discussing the effect of the various parameters on the results, it is convenient to regard series 3 as a base (a_{crit} = 0.18–0.27 mm). In series 1, a higher contact pressure was used and the critical contact semi-width increased to 0.28–0.38 mm. A similar effect was recorded by Bramhall. The higher contact pressure will increase the size of the compressive region beneath the contact and hence suppress the initiation and growth of cracks. The increased critical contact width might therefore be expected.

In series 2 a much lower tangential force was applied (Q/P = 0.24). This resulted in an increased critical contact width (a_{crit} = 0.54–0.72 mm). Again this might be expected since reducing Q will decrease the severity of fretting and consequently increase the value of a at which transition occurs. Bramhall does not vary the tangential force in his experiments, so no comparison can be made. Series 4 experiments were run at a lower bulk stress amplitude in the specimen (σ = 77.2 MN/m^2). Again an increased critical contact size resulted (a_{crit} = 0.36–0.54 mm), precisely the effect recorded by Bramhall. In series 5 both σ and p_o were reduced and an even larger increase in critical contact width resulted.

The present results therefore confirm the existence of a size effect as recorded by Bramhall (1973). There is an abrupt transition from low fatigue life ($\approx 10^6$ cycles) to a value of greater than 10^7 cycles. The same general dependence of the critical contact size on peak contact pressure and bulk stress amplitude is recorded, and the effect of reducing the tangential fretting force Q is also investigated. One remarkable feature of the present results is the lack of anomalous points (once those resulting from corner failures were discarded). Clearly the size of the contact has a significant effect on fatigue life for geometrically similar stress fields. This is a rather surprising result at first sight since, as in plain fatigue, the life might be expected to be dependent on the stress field alone. The main object of subsequent investigations carried out was to see if this effect could be explained by application of elastic stress analysis and fracture mechanics.

3.3 Investigation of results

In addition to the theoretical analysis presented in later chapters, the specimens and pads were examined in various ways after the experiments to gain additional insight into the fretting process. As stated in the introduction, a phase of oblique crack growth was observed on most of the failed specimens. This feature is shown in the typical section Fig. 3.4a. It is also clearly revealed on fracture surfaces examined under a scanning electron microscope. Figure 3.4b shows this shear lip particularly well, and it can be seen to extend for about 0.5 mm beneath the contact (the contact semi width a = 0.9 mm in this example). Little other useful information could be gained from examination of the fracture surfaces, since any details initially present were eradicated by the hammering action of the crack faces as they were brought together during the compressive part of the cycle.

Examination of the fretting scars produced on both specimens and pads was more revealing. Of particular interest was the small amount of fretting damage present on the intact specimens (e.g. Fig. 3.5a.) when compared with those which failed (Fig. 3.5b.). Figure 3.5b. also shows clearly the location of the crack on the surface of the specimen, near the edge of the fretting scar. Several scars were examined under a travelling optical microscope in an attempt to measure the real contact widths and to determine the boundaries of the central stick zone predicted by Mindlin (1949). Both proved difficult to record since the scar did not have definite regular boundaries. This is thought to be the result of two factors. First, the coefficient of friction was very low during the first few cycles of the test causing sliding to take place everywhere within the contact and damaging the entire area. Second, the

Fig. 3.4a Section of a failed specimen viewed under an optical microscope

Fig. 3.4b Fracture surface viewed under a scanning electron microscope

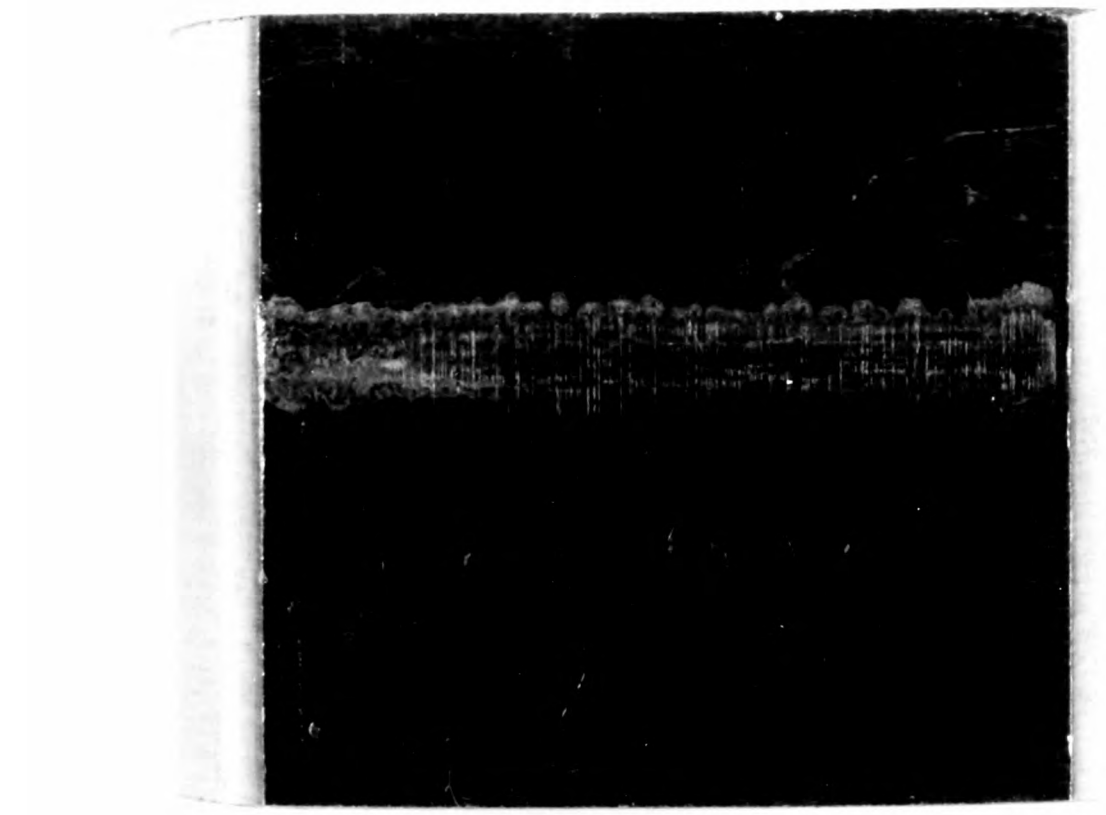

2 mm

Fig. 3.5 Fretting scars: (a) Intact specimen
(b) Failed specimen

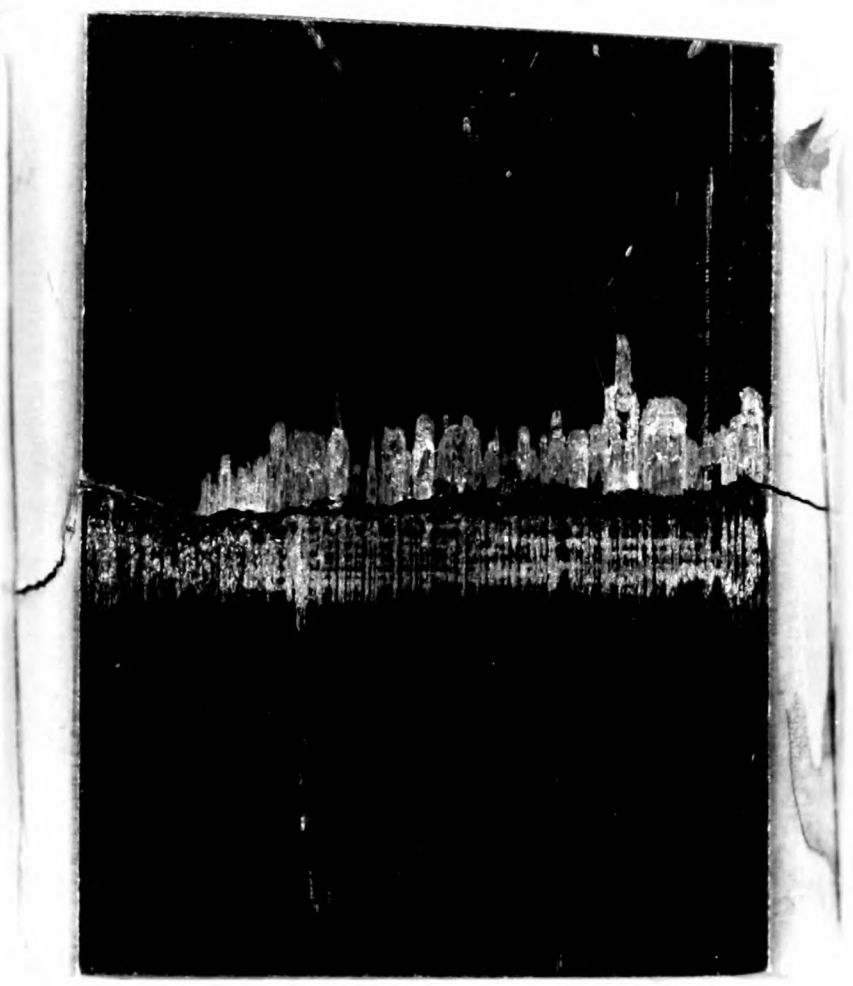

2 mm

surface roughness of both specimens and pads will have produced less distinct scar boundaries than might have been observed with a better surface finish.

A typical fretting scar produced on a pad is shown in Fig. 3.6 under the scanning electron microscope. The relatively deep scoring marks to the right of the main scar were caused by the specimen pulling through the pads when it broke and tend to obscure the edge of the scar. Within the scar itself, some degree of material transfer from the specimen is evident and this damage is noticeably greater in the two slip zones either side of the central stick zone. Thus there is some evidence to support the pattern of shear tractions predicted by Mindlin (1949).

Several of the specimens were sectioned longitudinally, mounted in resin, and polished in order to examine the crack trajectories and to detect any non-propagating micro-cracks present in the surviving specimens. Scanning electron microscope images are presented for a typical failed specimen in Fig. 3.7. A large number of cracks can be seen to have propagated away from the surface at a characterstic angle of between 45^{o} and 60^{o} to the free surface. At a higher magnification, the extensive fretting damage at the surface can be observed, together with several more micro-cracks. In contrast to this, examination of intact specimens revealed very little fretting damage at the surface and no cracks could be found. It is possible that, if any such cracks were present, they might have been obscured during the sectioning and polishing process, but the contrast in appearance with the failed specimens was quite marked and it seems unlikely that any significant cracks existed in the intact specimens. In order to economise on specimens, several of those which survived 10^{7} cycles were re-used in subsequent experiments by reversing them in the testing machine and

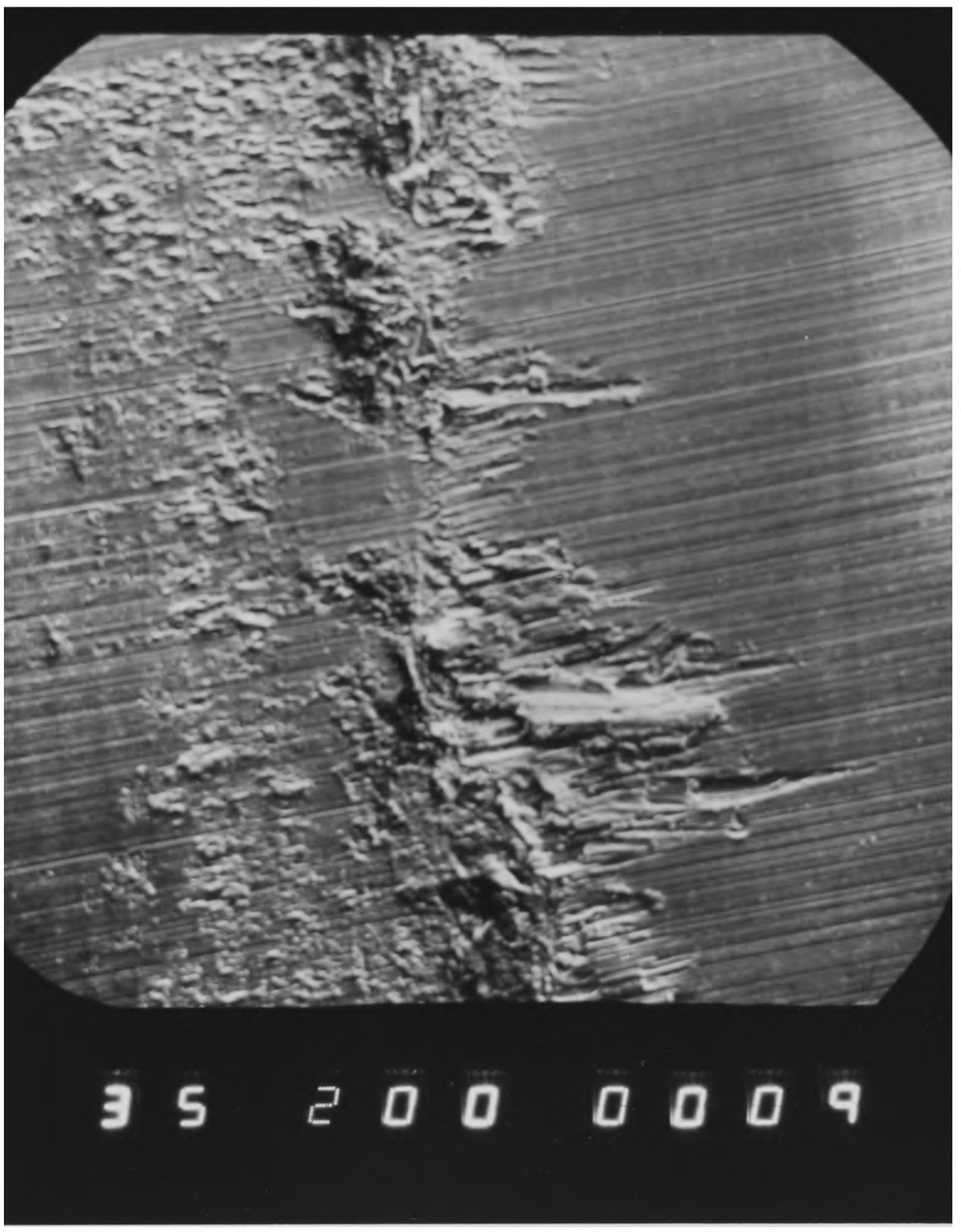

Fig. 3.6 Fretting scar on pad viewed under a scanning electron microscope

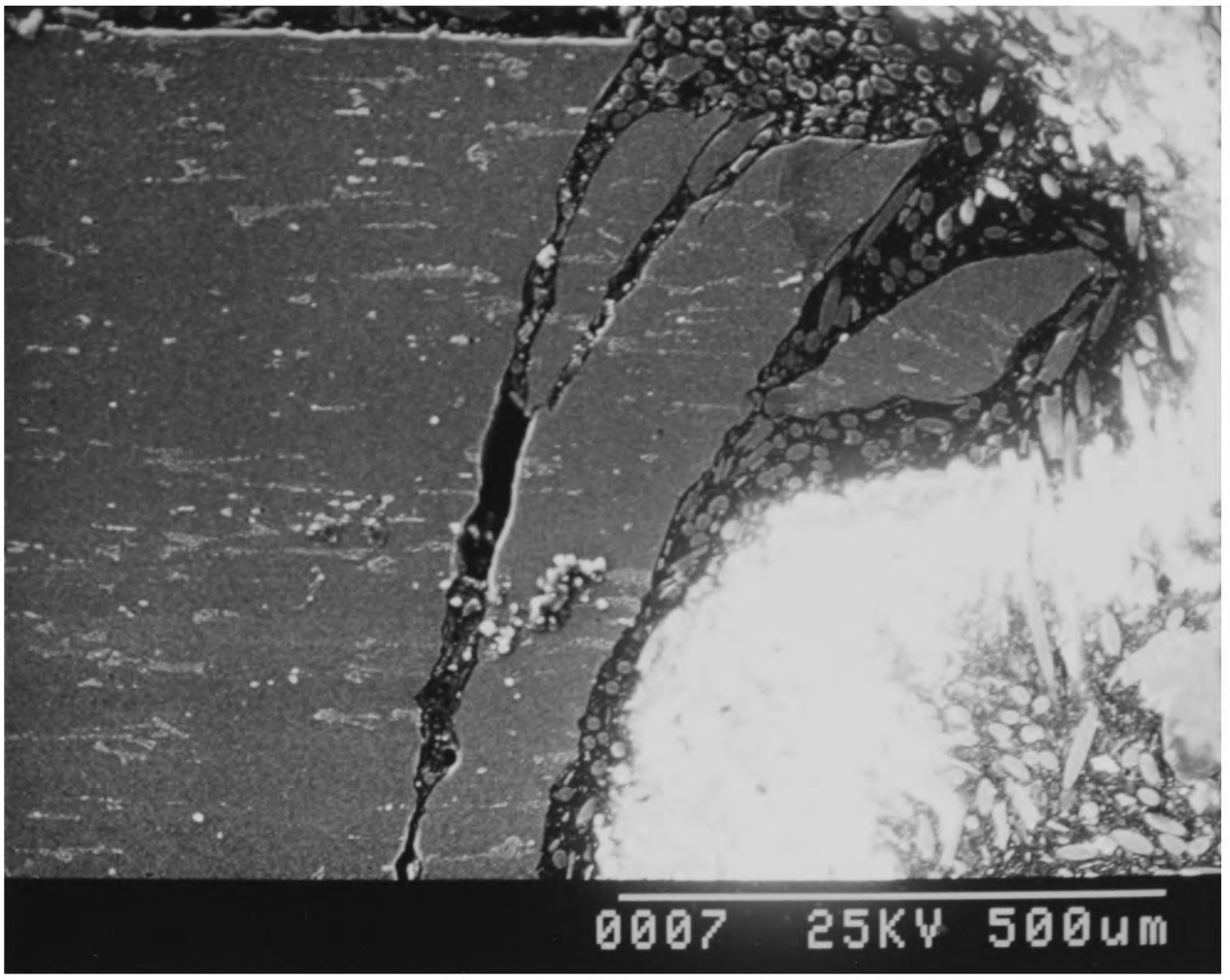

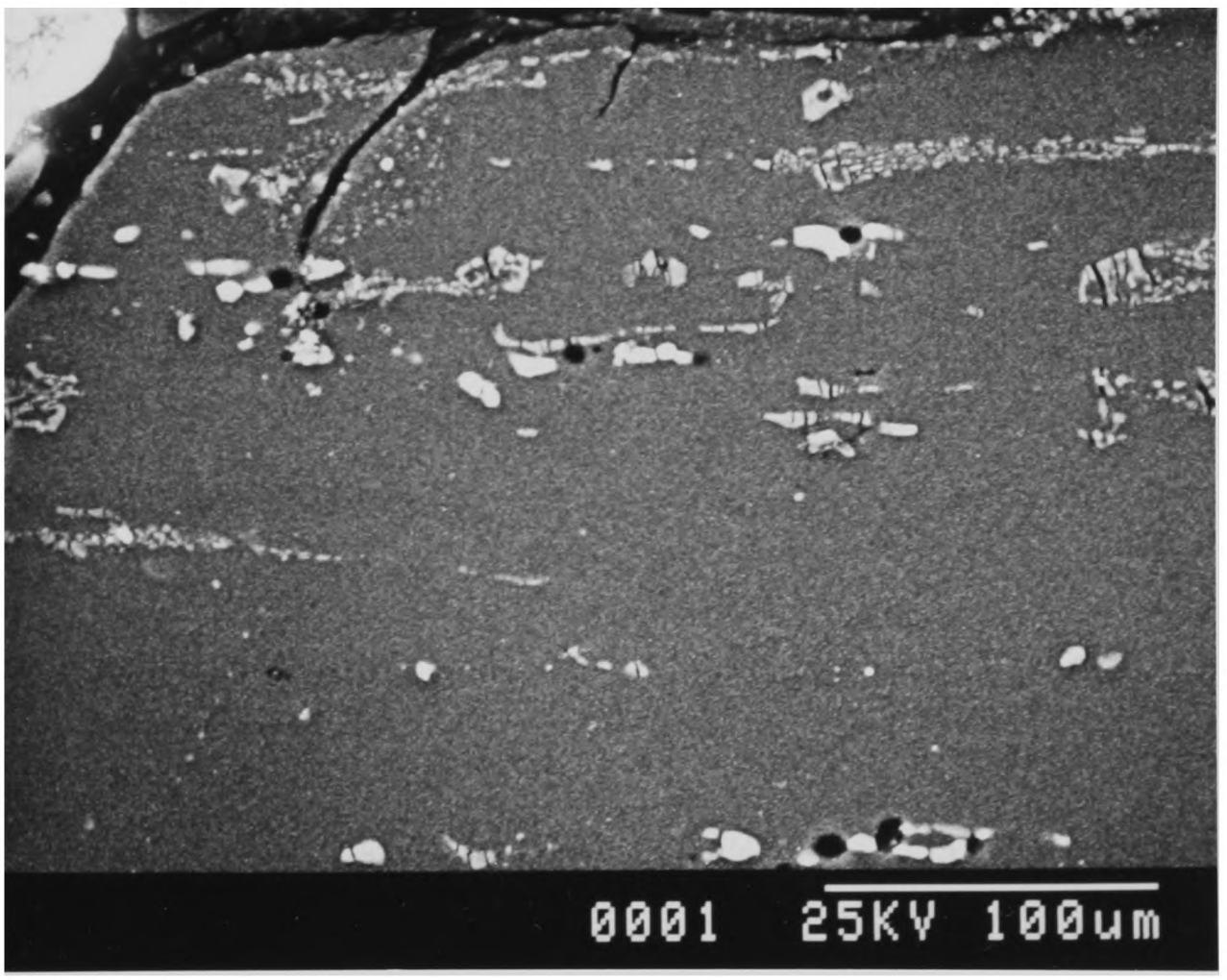

Fig. 3.7 Sections of a failed specimen viewed under a scanning electron microscope

bringing a different part of the surface into contact with the new pads. None of these specimens failed subsequently at the original fretting scar, as might have been expected if any significant cracks had been present.

The experimental evidence therefore seems to suggest that the reason for the survival of the intact specimens was that the fretting was insufficient to cause initiation of cracks. No evidence was obtained to support the alternative hypothesis that cracks self-arrested at contact semi-widths below a_{crit}.

3.4 Subsequent experiments

The evidence presented above suggests that fretting was far more severe in the larger contacts, despite the fact that the stress fields were geometrically similar. However, both stress and microslip are required to produce fretting fatigue and the very geometric similarity between contacts in the same series of experiments ensures that the amplitude of micro-slip scales with the size of contact. Several authors (e.g. Nishioka and Hirakawa (1969a)) report a variation in fatigue life with amplitude of micro-slip and this variation alone may well be the cause of the size effect reported.

If experiments are carried out in partial slip, as is the case here, the amplitude of micro-slip and the stress state are related, so that it is difficult to vary them independently. If experiments take place under fully sliding conditions the two quantities are independent, but practical difficulties arise. In sliding experiments wear may be significant and consequently the original profile of pads and specimen is lost. This prohibits a meaningful stress analysis and so is not suitable

for the current investigation.

One further possibility is, however, still open. Mindlin and Deresciewicz (1953) show that the amplitude of slip is a function of the degree of load reversal, maximum slip amplitude being obtained if Q is fully reversed. Thus, cycling between $+Q_o$ and $-Q_o$ will produce a larger slip amplitude than cycling between $+Q_o$ and 0, but will leave the peak stress state unchanged. To produce this effect with the experimental apparatus employed here would entail varying the minimum value of the cyclic bulk stress in the specimen (σ_{min}) whilst keeping σ_{max} unchanged. If σ_{min} is kept to negative values the amplitude of applied tension ($0 \rightarrow \sigma_{max}$) will be unaffected and thus the amplitude of tensile mode stress intensity factor (ΔK_I) will also remain unchanged.

In plain fatigue the threshold stress intensity factor amplitude ($\Delta K_I\big|_{th}$) is a function of $\sigma_{min}/\sigma_{max}$ (commonly known as the stress ratio or R-value). However, Pook (1978) shows that $\Delta K_I\big|_{th}$ is not particularly sensitive to R in the range $-1 < R < 0$ for alloys of the type used here. Hence the plain fatigue performance should be little affected by varying R in this range and any variation in fretting fatigue performance with the R-value would almost certainly be due to the variation in slip amplitude.

An additional series of experiments (series 6) were carried out to establish if the fretting fatigue performance did, indeed, vary with the degree of load reversal. The following parameters were chosen: pad radius = 150mm (constant), p_o = 120 MN/m^2, Q/P = 0.45, f = 0.75. The maximum alternating stress in the specimen (σ_{max}) was maintained constant at 61.8 MN/m^2, wheras the minimum value (σ_{min}) was varied between -61.8 MN/m^2 and zero for the five different experiments in the series. The variation of fatigue life with σ_{min} is shown in Fig. 3.8 and

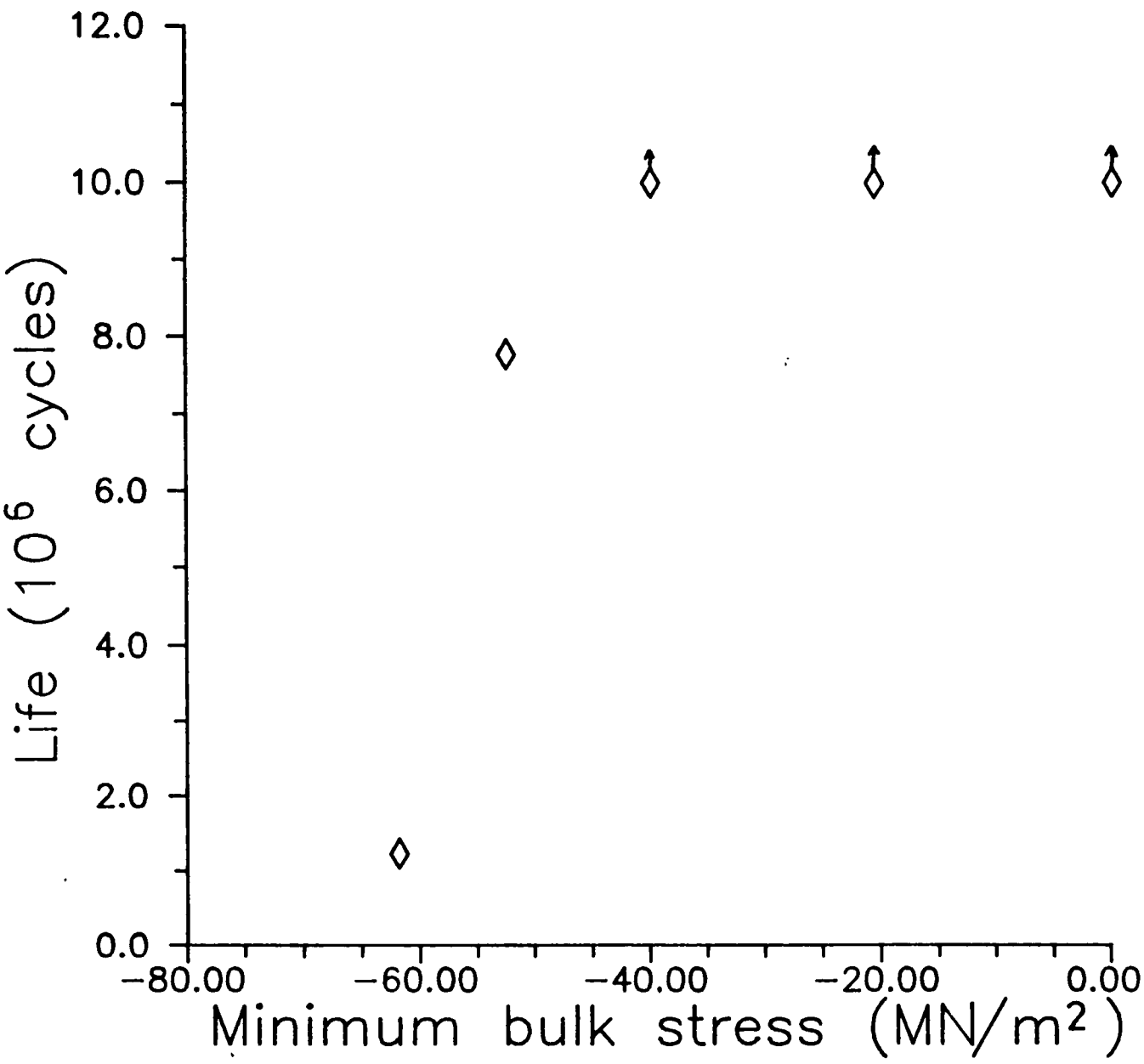

Fig. 3.8 Variation of fatigue life with degree of load reversal (series 6 experiments)

tabulated in Appendix A. The life can be seen to be short for high degrees of load reversal (and correspondingly high micro-slip) and in excess of 10^7 cycles for smaller amounts of compressive load. The dependence of fretting fatigue life on the amount of load reversal (and therefore slip amplitude) can be clearly seen from these results. Any model proposed to explain fretting fatigue should therefore incorporate the effect of micro-slip. This point will be returned to in chapter 9, when various possible models are discussed.

Chapter 4

Contact stress analysis

4.1 Hertz and Mindlin analyses

The first step in analysing the stress field developed at the contact between the pads and specimen in the fretting experiments is to determine the surface tractions developed. Previous analyses by Nishioka and Hirakawa (1969c) and O'Connor and Hills (1986), amongst others, have employed the results of Hertz (1882) and Mindlin (1949) and it is convenient initially to consider their results together with their inherent assumptions.

Hertz considered the contact of two long cylinders, with their axes parallel, under the action of a normal force P. Away from the ends of the cylinders, conditions of plane strain obtain and the analysis is essentially two-dimensional. A specialisation of this geometry is the case where the radius of one of the cylinders is infinite and the contact conditions modelled are those between a cylinder and a half-plane. This configuration is shown schematically in Fig.4.1a. The normal force P results in a contact patch of width 2a over which a pressure p(x) is developed. The principal assumptions of the Hertz theory may be summarised as:

(i) The surfaces are continuous and non conforming ($a \ll R$).

(ii) The strains are small ($a \ll R$)

(iii) Each solid may be considered as an elastic half-space.

(iv) That any shear tractions developed do not affect the normal

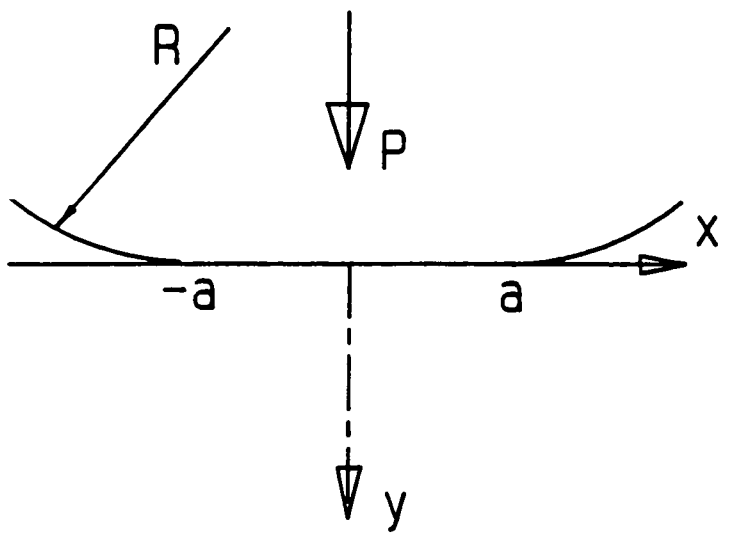

Fig. 4.1 Contact configurations: (a) Hertz

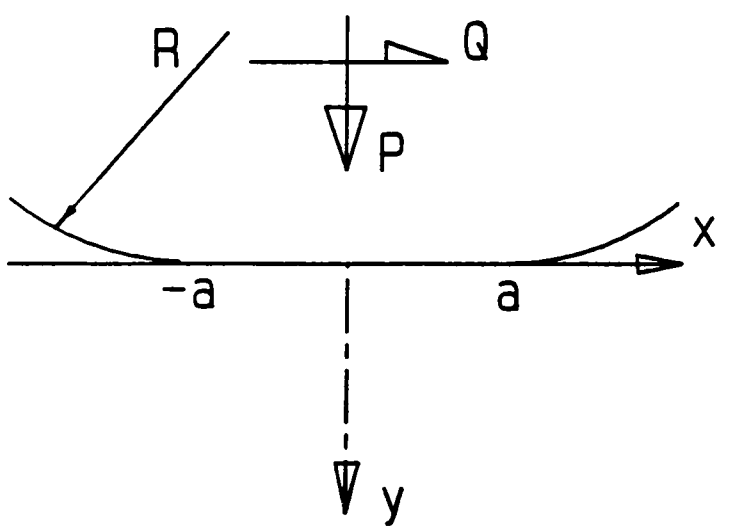

(b) Mindlin

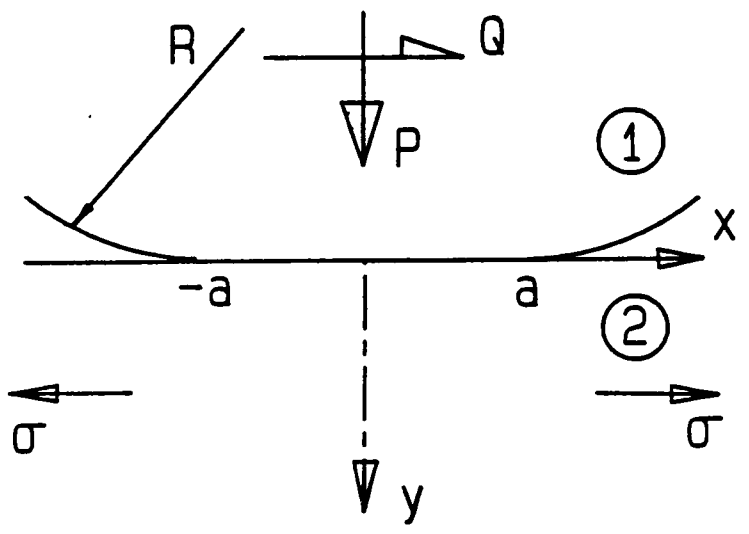

(c) Current model

pressure (i.e. the sufaces are frictionless, or the bodies are elastically similar).

The results of Hertz may now be summarised: a parabolic normal pressure distribution is developed,

$$p(x) = p_o \sqrt{1 - (x/a)^2} \qquad (4.1)$$

$$\text{where} \qquad p_o = \frac{2P}{\pi a} \qquad (4.2)$$

$$\text{and} \qquad a^2 = \frac{8 P R (1-\upsilon^2)}{\pi E} \qquad (4.3)$$

for the case of elastically similar bodies with Young's Modulus E and Poisson's Ratio υ.

In fretting experiments a tangential force Q is applied subsequently to the normal force P (Fig.4.1b). This configuration has been analysed by Mindlin for elastically similar bodies. The normal pressure distribution remains unchanged but shear tractions are developed to sustain the tangential force. A central stick zone $|x| < c$ is formed, bordered by two slip zones in which limiting friction acts. The shear tractions q(x) are given by:

$$q(x) = f p_o \sqrt{1 - (x/a)^2} + q'(x) \qquad (4.4)$$

$$\text{where} \qquad q'(x) = 0 \qquad a > |x| > c$$

$$\text{and} \qquad q'(x) = - f p_o \frac{c}{a} \sqrt{1 - (x/c)^2} \qquad |x| < c \qquad (4.5)$$

The size of the stick zone is revealed by considering tangential

equilibrium:

$$c/a = \sqrt{1 - Q/fP} \qquad (4.6)$$

In fretting experiments the tangential force Q is cycled to produce the necessary microslip. Mindlin and Deresciewicz (1953) considered this case and deduced that the resulting shear stress distribution is cyclic between limiting values of $\pm$ q(x) as defined in (4.4). The actual experimental configuration differs from that analysed by Mindlin in two important respects:

(i) The specimen thickness is only about 5 times greater than the larger contact widths and hence the validity of Mindlin's half-plane assumption must be called into question.

(ii) In Mindlin's analysis the only strains present are due to the contact forces themselves whereas the experimental configuration employed results in a tensile stress σ and a corresponding strain in the specimen which is not present in the fretting pads (Fig.4.1c). The previous analyses mentioned above account for this by superposing this bulk stress and the stresses due to a Mindlin contact. It is clear, however, that the presence of the bulk stress may affect the surface tractions arising at the contact. It is this latter effect which will be investigated in the current chapter.

4.2 Analysis of the loading case

The experimental configuration to be analysed is modelled in Fig.4.1c. The specimen is represented by a half plane on which rests the cylindrical fretting pad. A normal force P is applied to produce a Hertzian distribution of pressure. Subsequently a tangential force Q (< fP) is applied simultaneously with a remote bulk tensile stress σ in the surface of the half-plane. This accurately represents the action of the experimental apparatus where Q and σ are applied in phase. If the bulk stress is small [$\sigma a/Q \rightarrow 0$] the solution might be expected to be a perturbation of the Mindlin solution described above. The technique of Cattaneo (1938) might be employed and a parabolic distribution of shear stress superposed on the full slip solution within a displaced stick zone. However it is more useful to proceed with an alternative integral equation formulation which has more general application. Since the shear tractions are expected to be a perturbation of the Mindlin solution, a stick zone centred on x = e, and of width 2c, bordered by two slip zones of the same sign will be postulated. If the cylinder and the specimen are both modelled as elastically similar half-planes there is no coupling between direct and shear tractions and the boundary conditions at the interface are:

$$p(x) = q(x) = 0 \qquad |x| > a \qquad (4.7)$$

$$p(x) = p_o \sqrt{1 - (x/a)^2} \qquad |x| < a \qquad (4.8)$$

$$|q(x)| = fp(x) \qquad -a \leq x \leq e-c \quad \text{and} \quad e+c \leq x \leq a$$

$$|q(x)| < fp(x) \qquad |x-e| < c \tag{4.9}$$

For there to be no slip in the stick zones the surface strains must be equal, i.e.

$$\frac{\partial u_1}{\partial x} - \frac{\partial u_2}{\partial x} = 0 \qquad |x-e| < c \tag{4.10}$$

where u_1 and u_2 represent the x component of displacement in body 1 (the cylinder) and body 2 (the specimen), respectively.

Lastly the direction of slip in the slip zones must be opposite to the direction of q, i.e.

$$\text{sgn}(u_1 - u_2) = - \text{sgn}(q(x)) \qquad -a \leq x \leq e-c \quad \text{and} \quad e+c \leq x \leq a \tag{4.11}$$

For body 1 the surface strain is given by Muskhelishvili (1953a):

$$\frac{\partial u_1}{\partial x} = \frac{-(1-2\nu)(1+\nu)p(x)}{E} - \frac{2(1-\nu^2)}{\pi E} \int_{-a}^{a} \frac{q(\xi)}{(x-\xi)}\, d\xi \tag{4.12}$$

For body 2 a component of strain must be added as a result of the bulk tension:

$$\frac{\partial u_2}{\partial x} = \frac{-(1-2\nu)(1+\nu)p(x)}{E} + \frac{2(1-\nu^2)}{\pi E} \int_{-a}^{a} \frac{q(\xi)}{(x-\xi)}\, d\xi + \frac{\sigma}{E}(1-\nu^2) \tag{4.13}$$

Combining (4.12) and (4.13) yields:

$$\frac{\partial u_1}{\partial x} - \frac{\partial u_2}{\partial x} = - \frac{4(1-\nu^2)}{\pi E} \int_{-a}^{a} \frac{q(\xi)}{(x-\xi)}\, d\xi - \frac{\sigma}{E}(1-\nu^2) \tag{4.14}$$

q(x) is now written as

$$q(x) = -fp(x) + q'(x) = -fp_o \sqrt{1 - (x/a)^2} + q'(x) \qquad (4.15)$$

where $q'(x) = 0 \quad |x-e| < c$

Hence, substituting in (4.14) and invoking (4.10)

$$\int_{e-c}^{e+c} \frac{q'(\xi)}{(x - \xi)} d\xi = \frac{fp_o \pi x}{a} - \frac{\sigma \pi}{4} \qquad |x-e| < c \qquad (4.16)$$

Normalisation is carried out by setting $s = (x-e)/c$, $t = (\xi-e)/c$, and writing $k = \sigma a/(4fp_o)$ to give:

$$\int_{-1}^{1} \frac{q'(t)}{(s - t)} dt = \frac{fp_o \pi c}{a} \left[s + \frac{e}{c} + \frac{k}{c} \right] \qquad -1 < t < 1 \qquad (4.17)$$

This Cauchy integral equation has the solution (Muskhelishvili (1953b))

$$q'(s) = \frac{1}{\pi} \sqrt{1 - s^2} \int_{-1}^{1} \frac{fp_o c(\xi + (e/c) + (k/c))}{a \sqrt{1 - \xi^2} (\xi - s)} d\xi \qquad (4.18)$$

provided that the consistency condition is satisfied, namely

$$\int_{-1}^{1} \frac{(\xi + (e/c) + (k/c))}{\sqrt{1 - \xi^2}} d\xi = 0 \qquad (4.19)$$

This requires that

$$e = k = \frac{\sigma a}{4 f p_o} \qquad (4.20)$$

It now remains to check that boundary condition (4.11) is satisfied. This can be done in two ways: first, substitution of (4.20) into (4.14)

gives $(\partial u_1/\partial x - \partial u_2/\partial x)$ which is found to be positive for $x > (e+c)$ and negative for $x < (e-c)$. Hence, knowing that $u_1 - u_2 = 0$ in the stick zone we can show $u_1 > u_2$ outside. Alternatively the results of Poritsky (1950) may be used directly since q(x) and q'(x) are both parabolic. The full solution is therefore:

$$q(x) = - fp_o \sqrt{1 - (x/a)^2} \qquad x < e - c,\ x > e + c \tag{4.21}$$

$$q(x) = - fp_o \sqrt{1 - (x/a)^2} + \frac{c}{a} fp_o \sqrt{1 - ((x-e)/c)^2} \qquad |x - e| < c$$

where $e/a = \sigma/(4fp_o)$

The stick zone is thus shifted a distance e towards the front of the contact. A typical distribution of shear traction is shown in Fig.4.2. The Mindlin solution is recovered by setting $\sigma = 0$. The solution remains valid as long as $e+c \leq a$, i.e.

$$\frac{\sigma}{fp_o} \leq 4(1 - \sqrt{1 - Q/fP})$$

In order to develop a solution when this equality is not satisfied it is instructive to analyse the case when $Q = 0$.

4.2.1 Bulk tension alone

The analysis for the situation where the bulk tension alone is imposed follows broadly similar lines. Symmetry about $x = 0$ is expected, but with slip of opposite sign at the edges of contact. Boundary conditions (4.7)-(4.11) remain the same, except that the stick zone is $|x| < c$ i.e. $e = 0$. The appropriate version of (4.14) is therefore

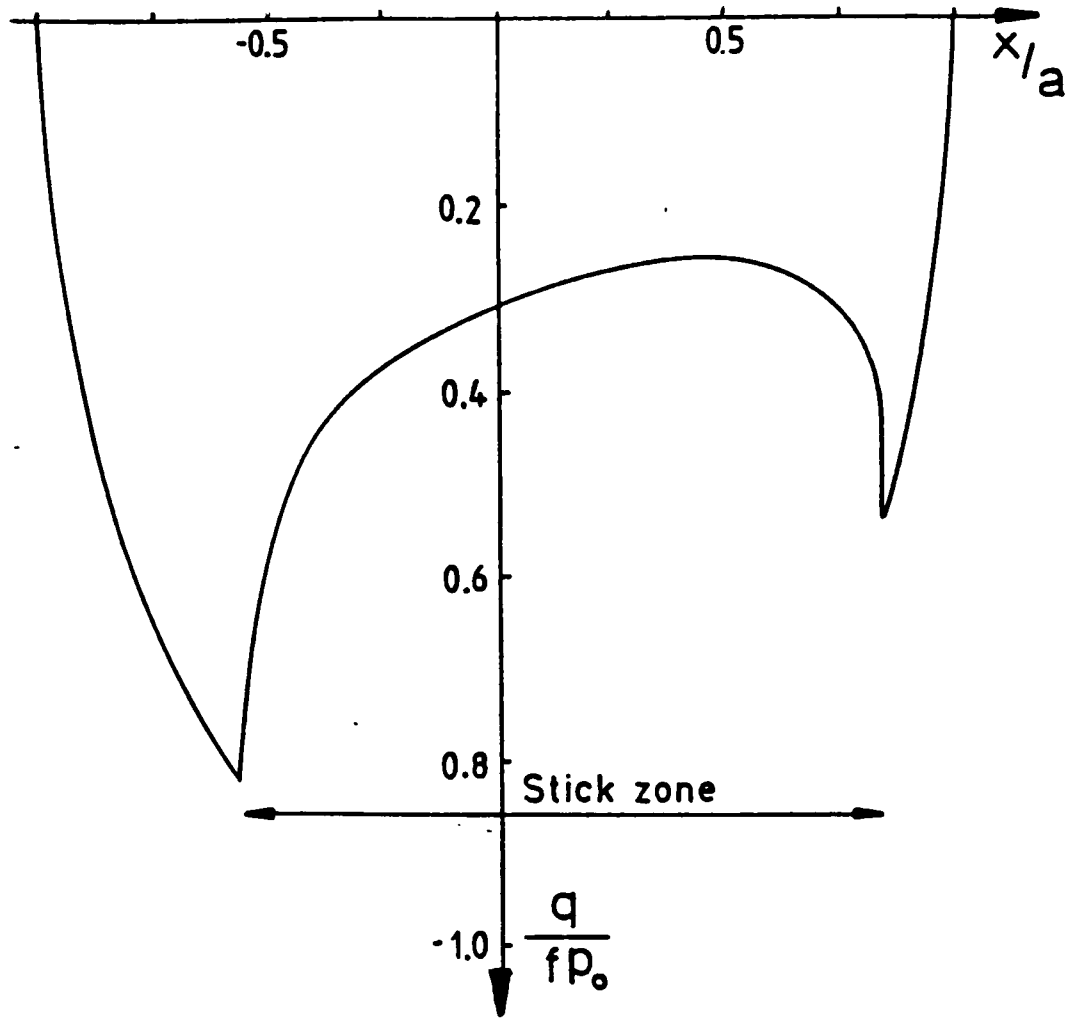

Fig. 4.2 Shear traction distribution, $Q/fP = 0.5$, $\sigma/fp_o = 0.5$

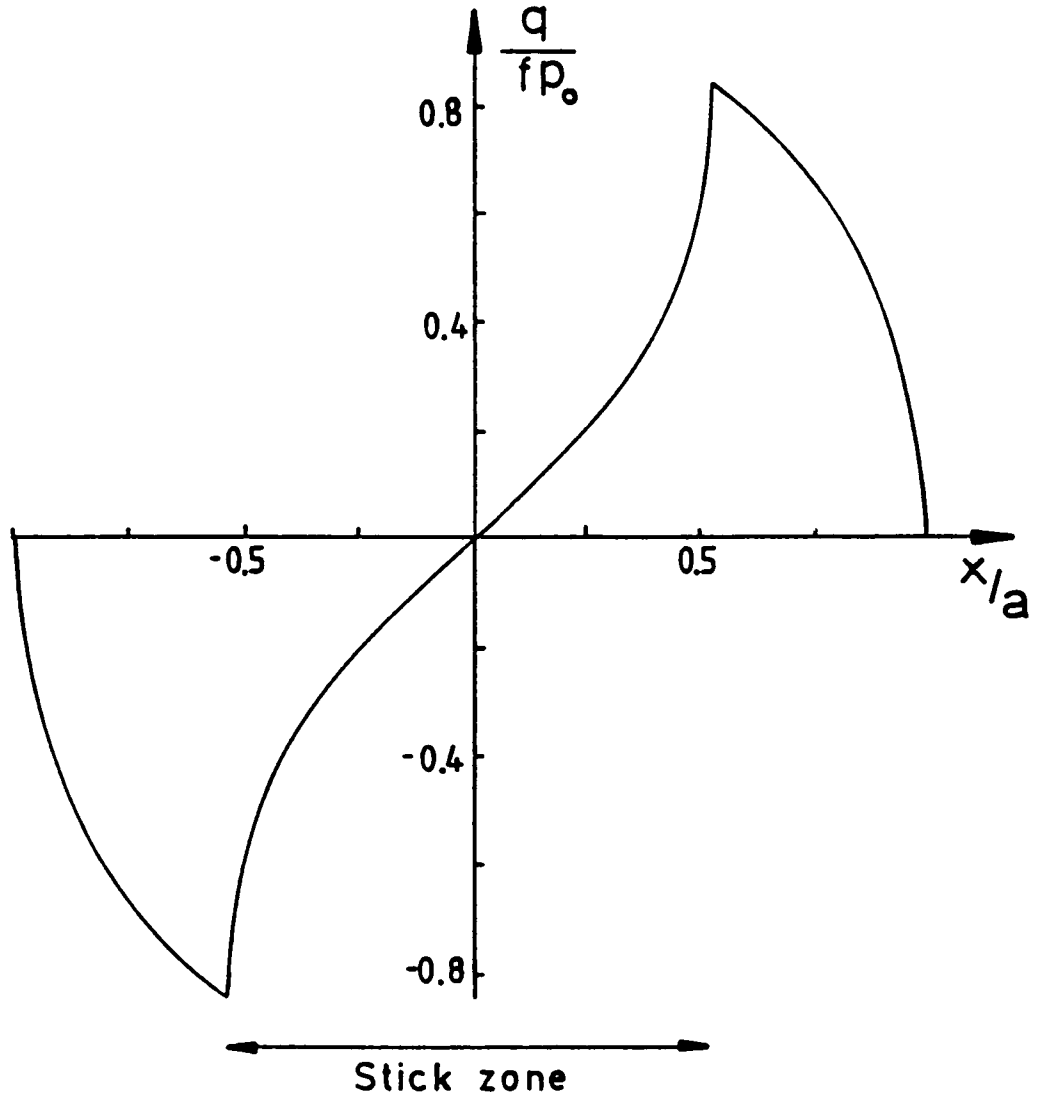

Fig. 4.3 Shear traction distribution due to bulk tension alone, $\sigma/fp_o = 0.5$

$$\int_{-a}^{a} \frac{q(\xi)}{(x - \xi)}\, d\xi + \frac{\sigma\,\pi}{4} = 0 \qquad |x| < c \qquad (4.22)$$

and

$$q(x) = -f p_o \sqrt{1 - (x/a)^2}\ \mathrm{sgn}(x) \qquad c \leq |x| \leq a \qquad (4.23)$$

It is convenient to write q as a perturbation on a straight line in the interval $|x| < c$ i.e.

$$q(x) = -f p_o \frac{x}{c} \sqrt{1 - (c/a)^2} + q''(x) \qquad |x| < c \qquad (4.24)$$

Thus, substituting (4.23) and (4.24) in (4.22) gives

$$\int_{-c}^{c} \frac{q''(\xi)}{(x - \xi)}\, d\xi = \frac{-\sigma\pi}{4} - \int_{-a}^{-c} \frac{f p_o \sqrt{1 - (\xi/a)^2}}{(x - \xi)}\, d\xi + \int_{c}^{a} \frac{f p_o \sqrt{1 - (\xi/a)^2}}{(x - \xi)}\, d\xi$$

$$+ \int_{-c}^{c} \frac{f p_o \xi \sqrt{1 - (c/a)^2}}{a(x - \xi)}\, d\xi$$

$$\equiv g(x,\sigma,c) \qquad |x| < c \qquad (4.25)$$

This equation is normalised by setting $s = \xi/c$ and $t = x/c$ to give

$$\int_{-1}^{1} \frac{q''(s)}{(t - s)}\, ds = G(t,\sigma,c) \qquad (4.26)$$

where G is the normalised form of g. c and σ are related variables and only one can be chosen at liberty. The relation between them is found by invoking the consistency condition of Muskhelishvili (1953b):

$$\int_{-1}^{1} \frac{G(\xi,\sigma,c)}{\sqrt{1 - \xi^2}}\, d\xi = 0 \qquad (4.27)$$

This side condition is enforced first and the integral (4.27) evaluated using Gauss–Chebyshev quadrature as described by Conte and DeBoor (1972).

In discretised form it is:

$$\frac{\pi}{n+1} \sum_{i=0}^{n} G(\xi_i,\sigma,c) = 0$$

where

$$\xi_i = \left[\frac{(2i + 1)\pi}{(n + 1)2}\right] \qquad i = 0,.....,n \qquad (4.28)$$

A particular value for c is chosen and $G(\xi_i,\sigma,c)$ found numerically using Clenshaw-Curtis integration as described by Piessens et. al. (1976). A value for σ consistent with that chosen for c is thus found and (4.26) can be written as

$$\int_{-1}^{1} \frac{w(s)\ \phi(s)}{(t - s)}\, ds = G(t,\sigma,c) \qquad (4.29)$$

where $\phi(s)$ is a bounded function and $w(s)$ an appropriate fundamental function modelling the expected behaviour of $q''(s)$.

The method of Erdogan et. al. (1973) is followed. It is noted that $q''(s)$ falls to zero at ± 1 and hence $w(s) = \sqrt{1 - s^2}$ is an appropriate choice. This permits the use of Gauss-Chebyshev integration to reduce (4.29) to a set of linear equations:

$$\sum_{i=1}^{n} \frac{1 - s_i^{\,2}}{n + 1}\ \frac{\phi(s_i)}{s_i - t_k} = G(t_k,\sigma,c)$$

where

$$s_i = \cos\left[\frac{i\ \pi}{n + 1}\right] \qquad i = 1,.....,n$$

$$t_k = \cos\left[\frac{\pi(2k - 1)}{2\ (n + 1)}\right] \qquad i = 1,.....,n+1 \qquad (4.30)$$

There are n+1 equations in the n unknowns $\phi(s_1)$, and, at first sight the problem appears overconstrained. However, the consistency condition has already been included in these equations (Erdogan et al. (1973)) and accordingly one of the equations may be dropped. Once a solution is found a check may be made to see that the extra equation is indeed satisfied. It is also important to check that boundary condition (4.11) is satisfied. A typical solution for $\sigma/fp_o = 2.0$ is given in. Fig.4.3. The central stick zone is bordered by equal slip zones of opposite sign. Figure 4.4 shows the variation of stick zone semi-width c with σ/fp_o.

4.2.2 Tangential force and tension

The remaining boundary problem to be solved is when Q and σ are applied simultaneously, but $(\sigma/fp_o) > 4(1 - \sqrt{1 - Q/fP})$. If the bulk stress is large a perturbation of the solution for Q = 0 outlined above might be expected. A similar approach is followed but, since there will no longer be symmetry, the stick zone boundaries are chosen to be $x = c_1, c_2$. The side-condition again reveals the consistent value for σ and the resulting integral equation is discretised and solved as before. The value of applied tangential force is calculated once the solution is known from

$$Q = \int_{-a}^{a} q(x)\, dx \qquad (4.31)$$

A typical distribution of shear traction is given in Fig.4.5 for $\sigma/fp_o = 2.0$, $Q/fP = 0.5$. By setting c2 = a and c1 = e-c the shifted Mindlin solution obtained initially for e+c = a can be recovered. Hence solutions are now known for all values of Q and σ.

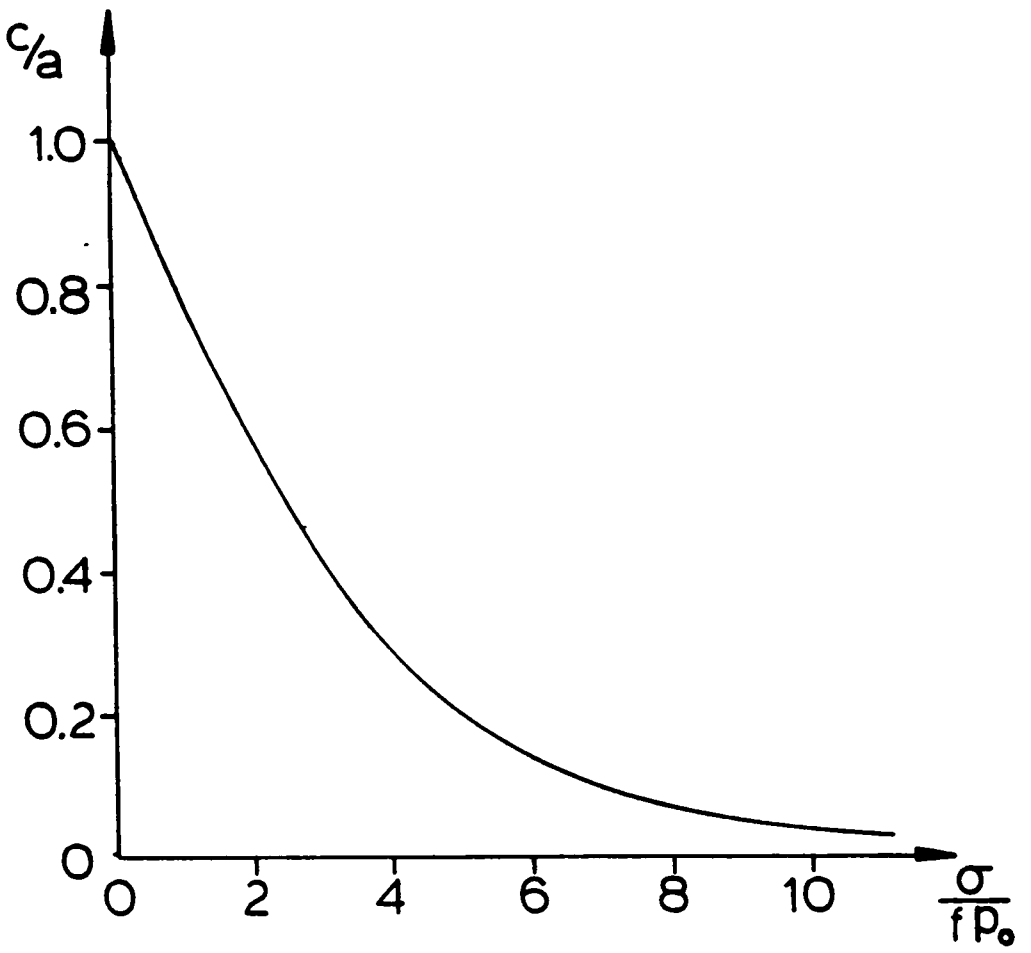

Fig. 4.4 Variation of stick zone semi-width with tension

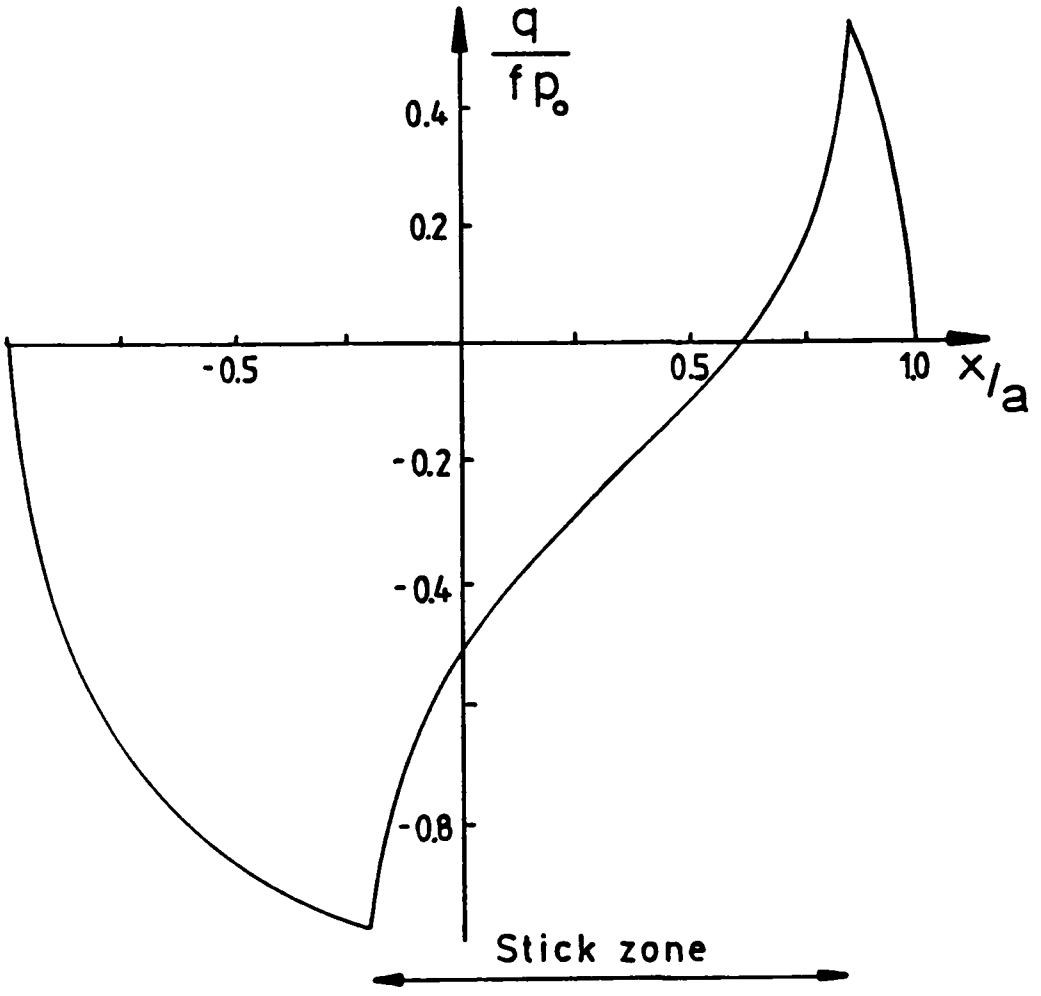

Fig. 4.5 Shear traction distribution, reverse slip case, Q/fP = 0.5, σ/fp_o = 2.0

4.3 Results - Loading phase

If Q and σ are increased simultaneously and proportionately from zero the resulting distribution of surface shear traction can take one of two basic forms. If $\sigma/fp_o \leq 4(1-\sqrt{1-Q/fP})$ the stick zone is bordered by slip zones of the same sign. The distribution of shear traction is similar to that described by Mindlin but with the centre of the stick zone shifted a distance $a\sigma/(4fp_o)$ towards the leading edge of the contact. It is interesting to note that in this case the size of the stick zone is independent of σ, which merely controls its position.

If $\sigma/fp_o > 4(1-\sqrt{1-Q/fP})$ the distribution is of the form shown in Fig.4.5. The stick zone is bordered by slip zones of opposite sign with reverse slip occurring at the leading edge. Figure 4.6 shows the stick zone boundaries for various values of σ/fp_o and Q/fP.

4.4 The unloading phase

In the fretting fatigue experiments carried out Q and σ are cycled and hence the case where loading and unloading take place must also be examined. Following the argument of Mindlin and Deresiewicz (1953), incremental loads $-\Delta Q$ $-\Delta\sigma$ are applied, superimposed on their respective maximum values. For no further slip to occur the incremental tractions at the edge of the contact would need to be infinite. Therefore it is postulated that reverse slip occurs at the edges of the contact and extends over the zones $-a < x < c'_1$ and $c'_2 < x < a$. The incremental change in tractions in these regions is known and a solution can thus be obtained for the change in traction in the region $c'_1 < x < c'_2$, where no incremental slip takes place, in the manner described above. Since c'_1

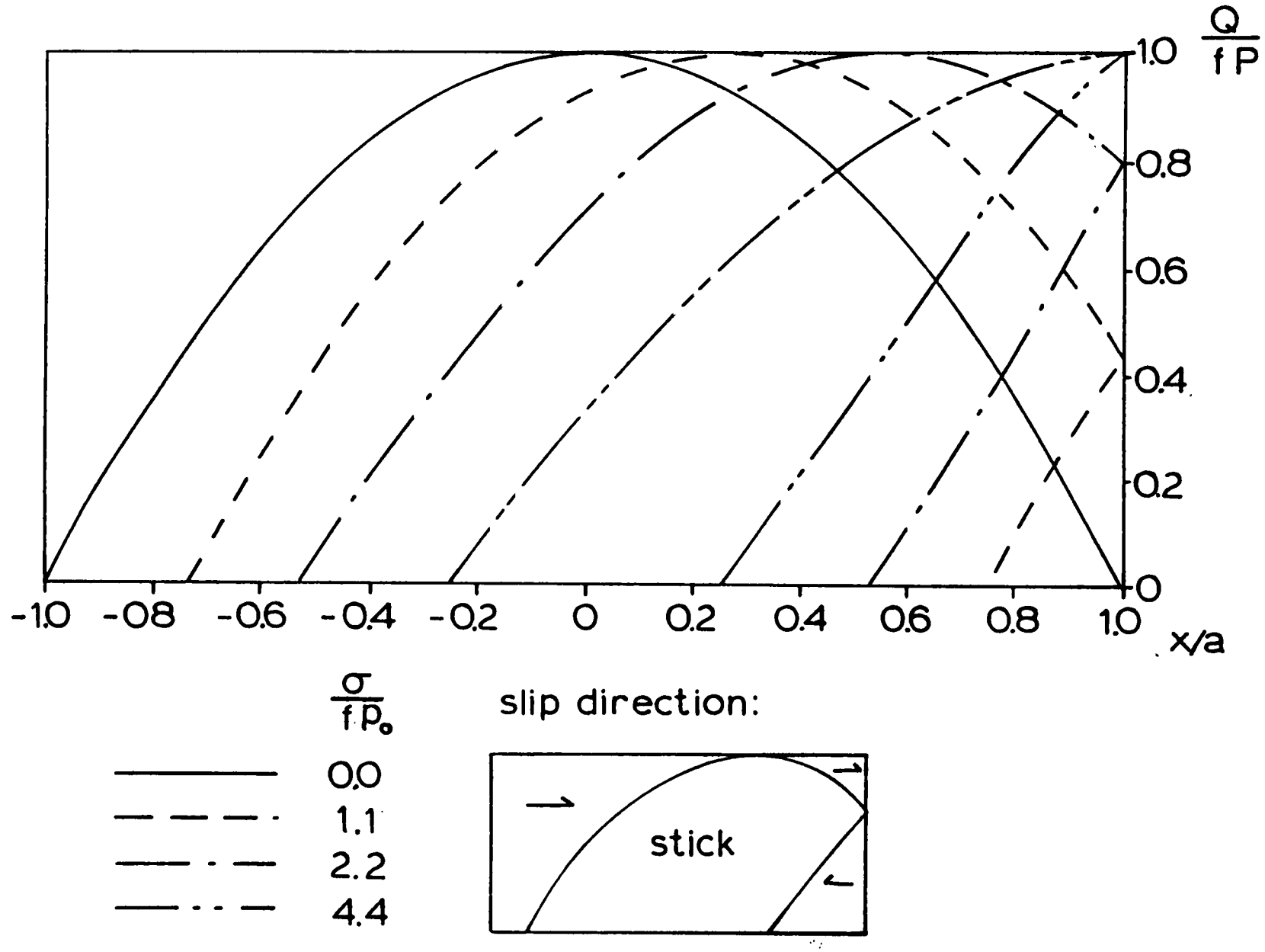

Fig. 4.6 Position of stick zone boundaries for different values of σ/fp_o and Q/fP

and c'_2 are unknown *a priori*, initial estimates are made and their values adjusted until the correct incremental changes in σ/fp_o and Q/fP are obtained. Addition of incremental and original tractions reveals the complete traction distribution at that point in the cycle.

Figure 4.7 shows the shear traction distribution at three points in the cycle: at maximum forward load, with the load reduced to zero, and at maximum reversed load. Two types of distribution are displayed: (a) $Q_{max}/fP = 0.5$, $\sigma_{max}/fp_o = 0.55$ (the shifted Mindlin case) and (b) $Q_{max/fP} = 0.38$, $\sigma_{max}/fp_o = 2.27$ (the reverse slip case). It is evident that non-zero residual shear tractions arise when Q and σ are reduced to zero, but that when the loading is fully reversed the stick zone is coincident with that produced by the initial loading but with the shear tractions reversed. It can be seen that, on reloading, the shear tractions will be equal and opposite to those produced on unloading and that cyclic shear tractions are produced by the in-phase cycling of Q and σ.

4.5 Evaluation of stresses in the specimen

Once the distribution of surface tractions has been determined it is possible to calculate the stresses developed in the specimen, which is modelled here as a half-plane. These stresses will be severest when Q and σ take their maximum values and this case will be considered here. The experimental results described in Chapter 3 show that fretting fatigue cracks initiate at or near the trailing edge of the contact ($x = -a$) and the effect of the modified traction distribution on the stress state here is of particular interest. Any modification of the Mindlin solution will be most apparent at this point since the only

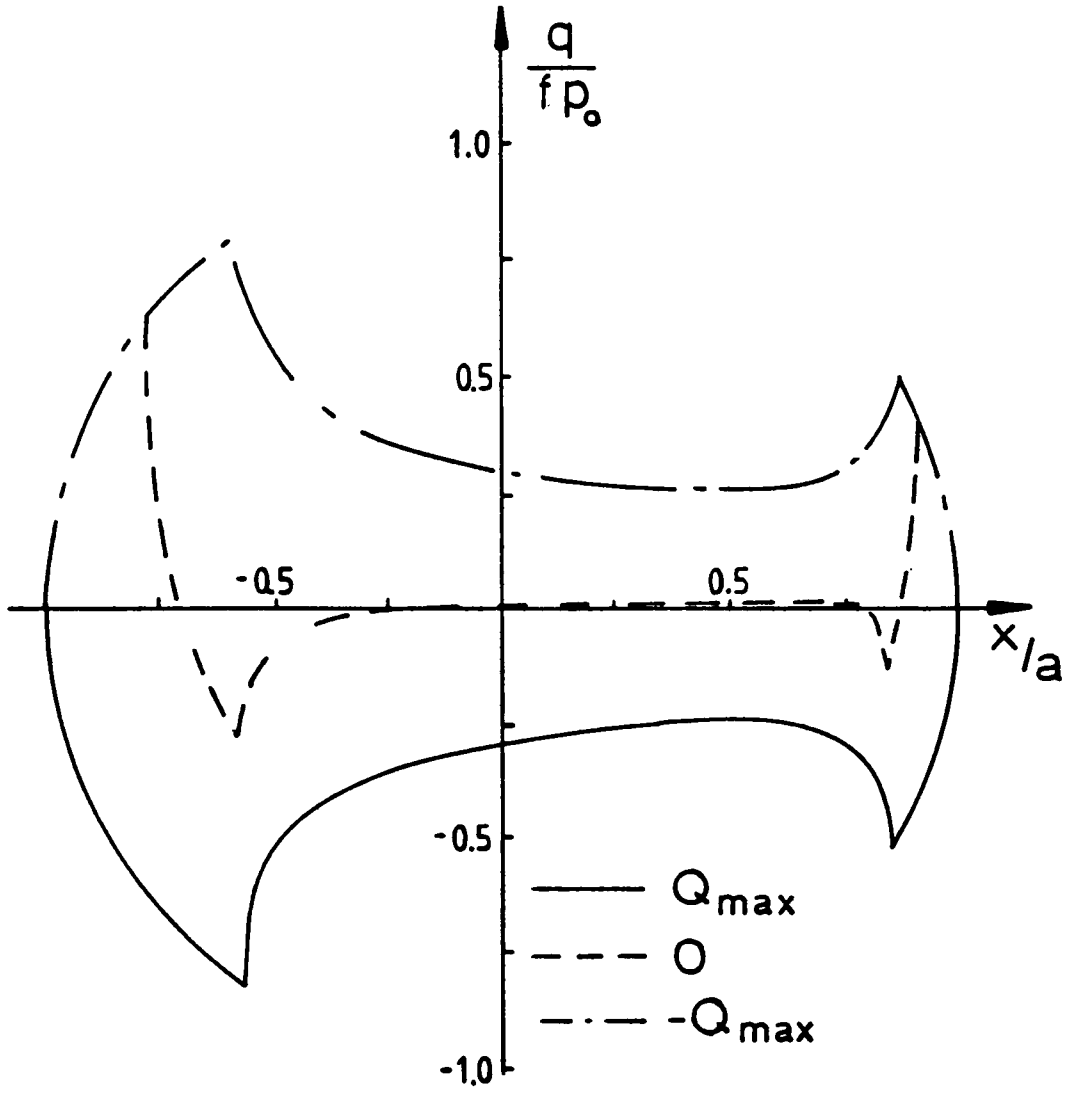

Fig. 4.7 Shear traction distributions during unloading:
(a) Shifted Mindlin case, $Q_{max}/fP = 0.5$, $\sigma_{max}/fp_o = 0.55$

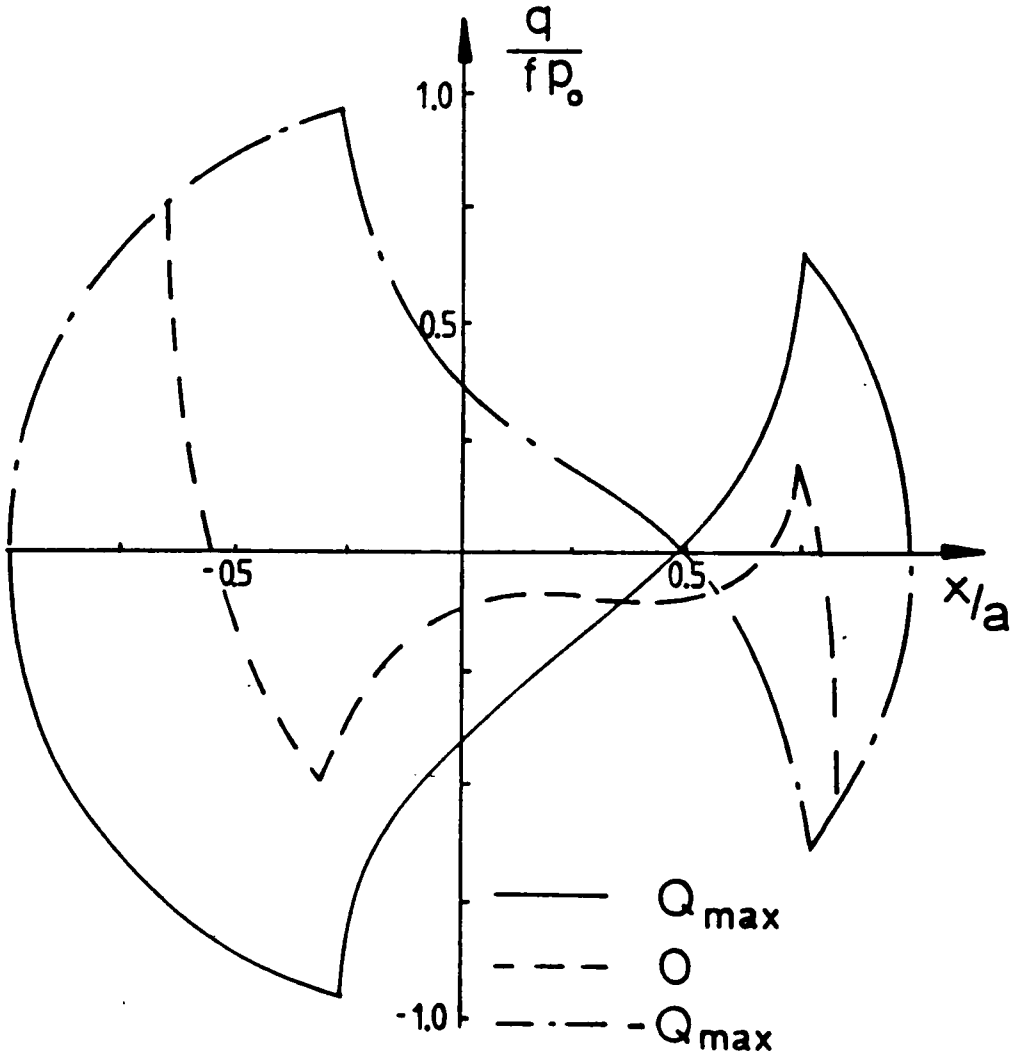

(b) Reverse slip case, $Q_{max}/fP = 0.38$, $\sigma_{max}/fp_o = 2.27$

non-zero stress components acting are (i) a direct stress in the x direction due to Q (σ_{xxq}) and (ii) the bulk tensile stress in the specimen (σ). The stress component σ_{xxq} is best found by integrating the solution of Flamant (1892) for the surface stresses induced by a line load on a half-space.

$$\sigma_{xxq} = \frac{-2}{\pi} \int_{-a}^{a} \frac{q(x)}{(x + a)}\, dx \qquad (4.32)$$

An accurate evaluation of the integral is obtained by writing q(x) as a perturbation on the full-slip solution as in (4.15) to give:

$$\sigma_{xxq} = \frac{-2}{\pi} \int_{-a}^{a} \frac{-fp_o\sqrt{1 - (x/a)^2}}{(x + a)}\, dx \; - \frac{2}{\pi} \int_{-a}^{a} \frac{q'(x)}{(x + a)}\, dx$$

$$= 2fp_o - \frac{2}{\pi} \int_{-a}^{a} \frac{q'(x)}{(x + a)}\, dx \qquad (4.34)$$

The remaining integral may be accurately evaluated since q'(x) = 0 in the trailing slip zone and the integral is thus non-Cauchy. The variation of σ_{xxq} with bulk stress is shown in Fig.4.8 for three values of Q/fP. It can be seen that, for Q/fP < 1.0, increasing the bulk stress also increases the stress induced by the contact at the initiation site.

To investigate the stresses induced below the surface and, in particular, to see how these vary from the Mindlin solution it is again convenient to describe the traction distribution as a perturbation on the full-slip solution:

$$p(x) = p_o \sqrt{1 - (x/a)^2}$$

$$q(x) = -fp_o \sqrt{1 - (x/a)^2} + q'(x) \qquad (4.35)$$

The stresses induced by the parabolic components may be evaluated using

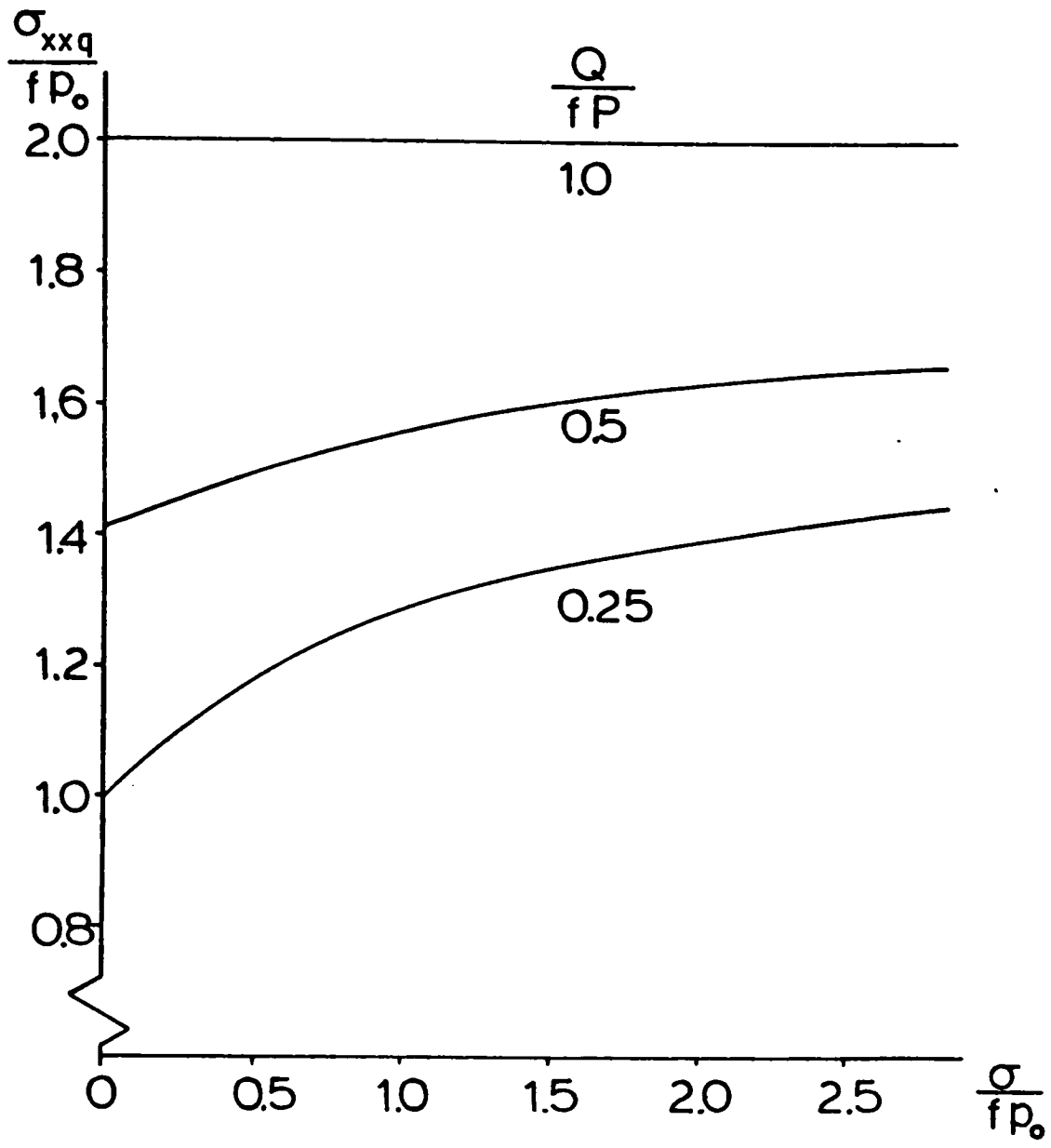

Fig. 4.8 Variation of stress component at trailing edge of contact with σ/fp_o

the results of Sackfield and Hills (1985), whereas q'(x) is modelled by a piecewise linear function and the results of Bentall and Johnson (1968) employed to deduce the induced stress field. To these two components must be added the bulk tensile stress in the specimen σ. Figure 4.9 shows contours of maximum principal stress for series 1 experiments ($Q/fP = 0.6$, $\sigma/fp_o = 0.79$, $f = 0.75$) (a) for the results of the current analysis and (b) for the Mindlin case. The effect of the modified analysis is not great, except for a region immediately under the contact. This might have been expected from St.Venant's principle. The relatively large value of σ tends to dominate the stress field away from the contact and this effect is similar in both cases. Principal stress directions and maximum shear stress directions are shown in Fig.4.10 and are almost identical for both the Mindlin and present analyses.

4.6 Discussion of results

Surface traction distributions have been derived for the experimental configuration which differ substantially from those given by Mindlin (1949) due to the presence of the bulk stress in the specimen. The principal effect is to shift the stick zone away from the trailing edge of the contact and to increase the size of the trailing slip region in which fretting fatigue cracks initiate. Figure 4.11 compares the surface shear tractions derived here with the results of the Mindlin analysis. For series 1 experiments, (which are typical of most of the other experimental series) Fig. 4.11a clearly shows the displaced stick zone. In series 2 (Fig. 4.11b) the applied tangential force Q is smaller and $\sigma/fp_o > 4(1 - \sqrt{1 - Q/fP})$. Thus the resulting shear traction

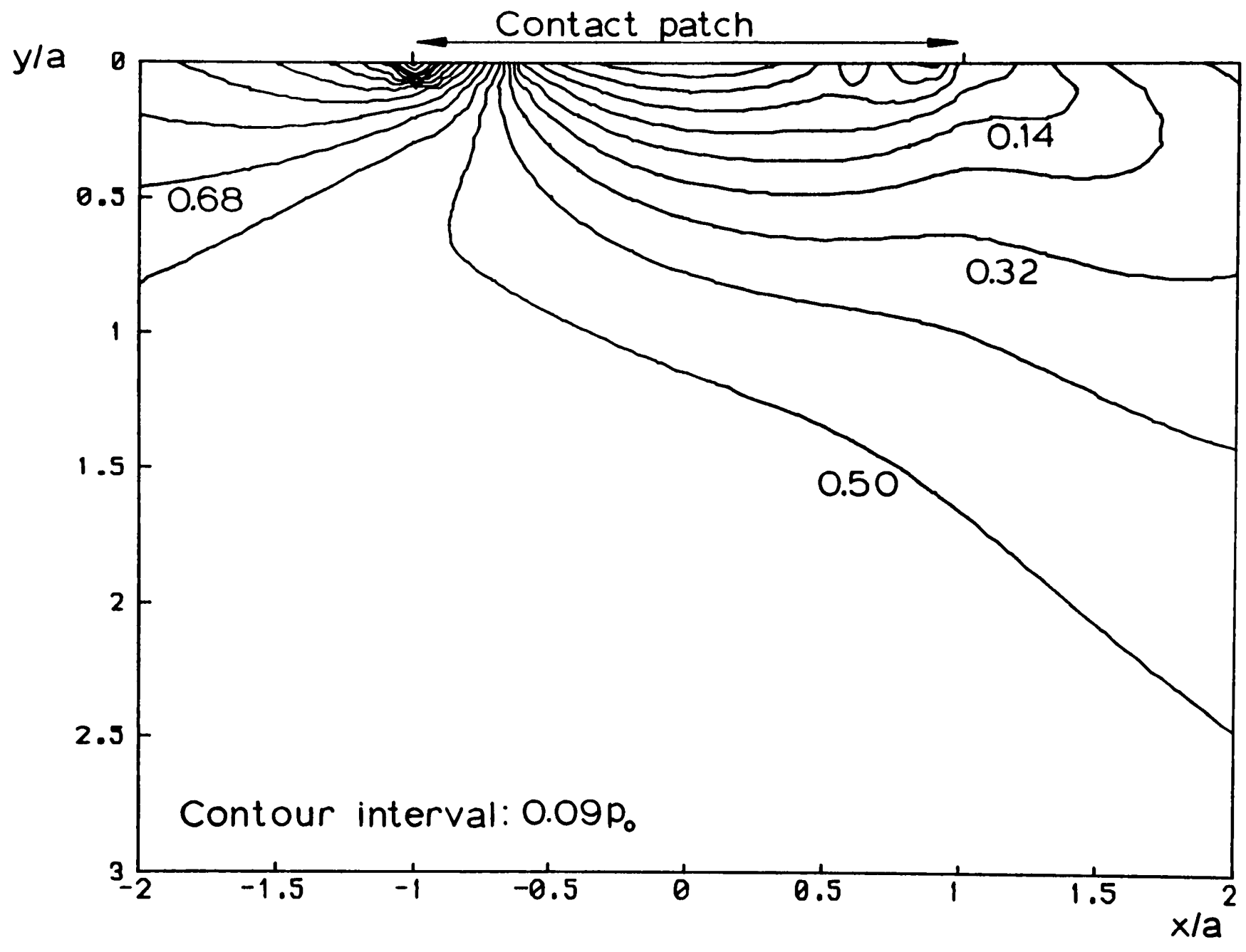

Fig. 4.9a Contours of most positive principal stress (σ/p_o) for series 1 experiments, incorporating shifted stick zone

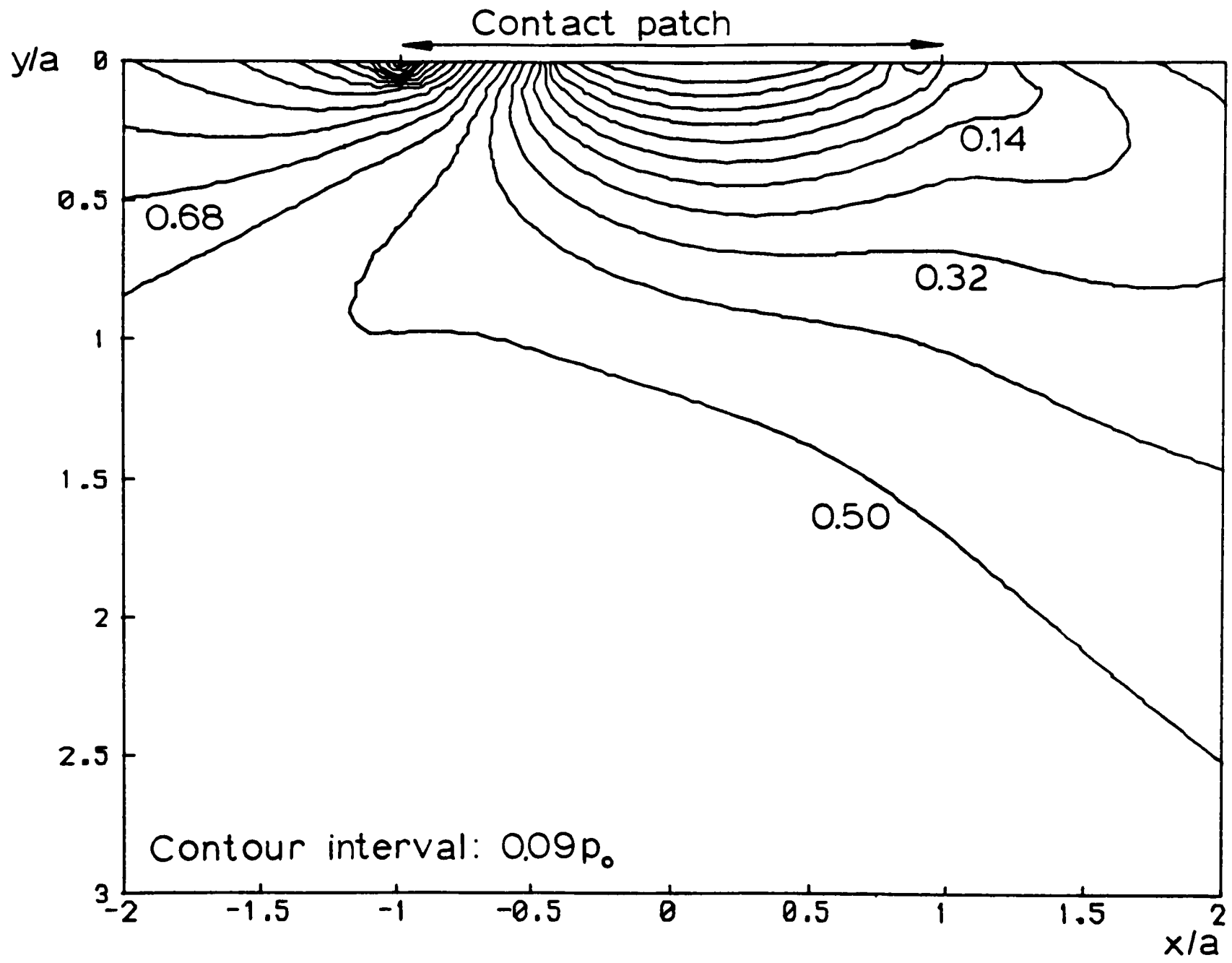

Fig. 4.9b Contours of maximum principal stress (σ/p_o) for series 1 experiments, Mindlin approximation

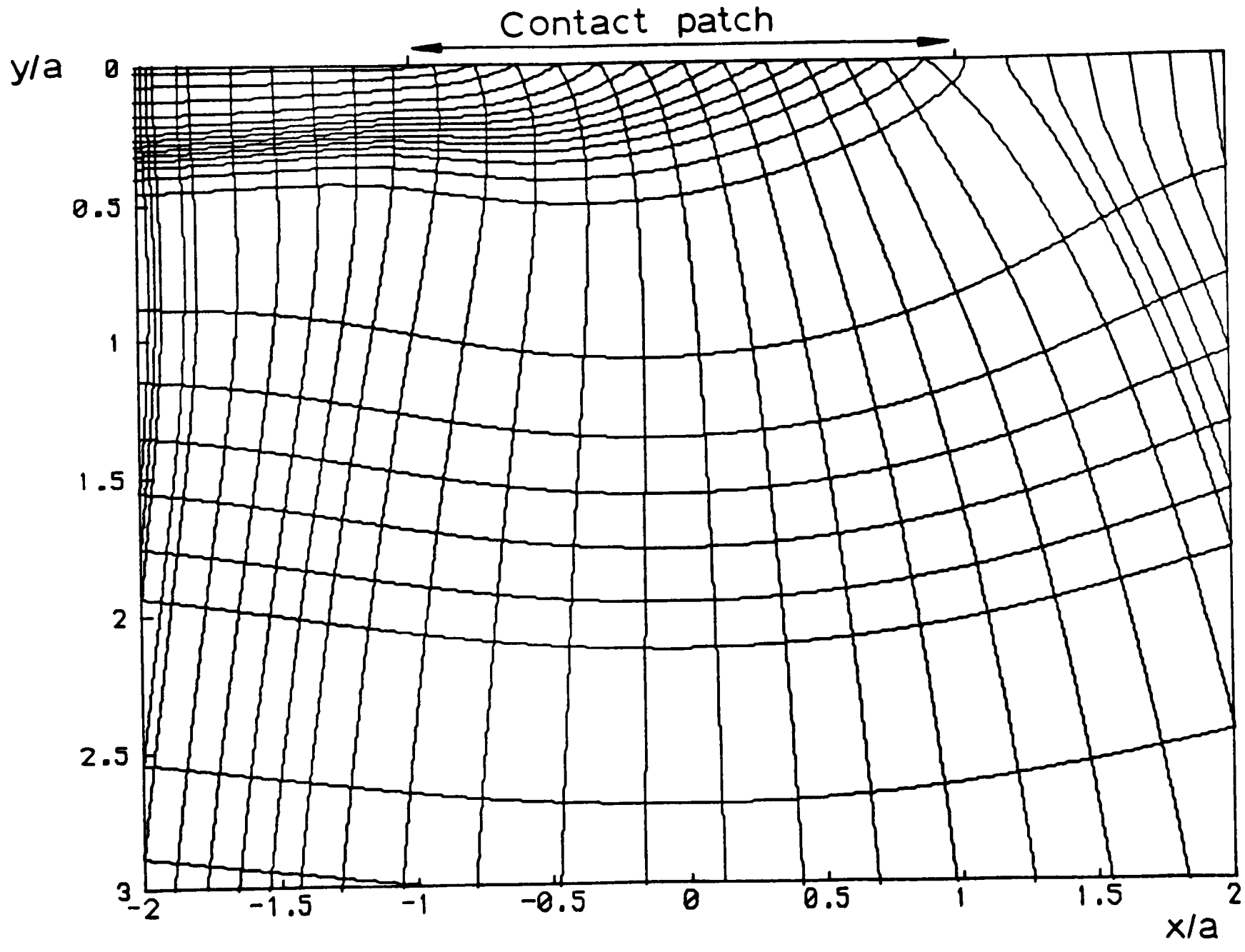

Fig. 4.10a Principal stress directions, series 1 experiments

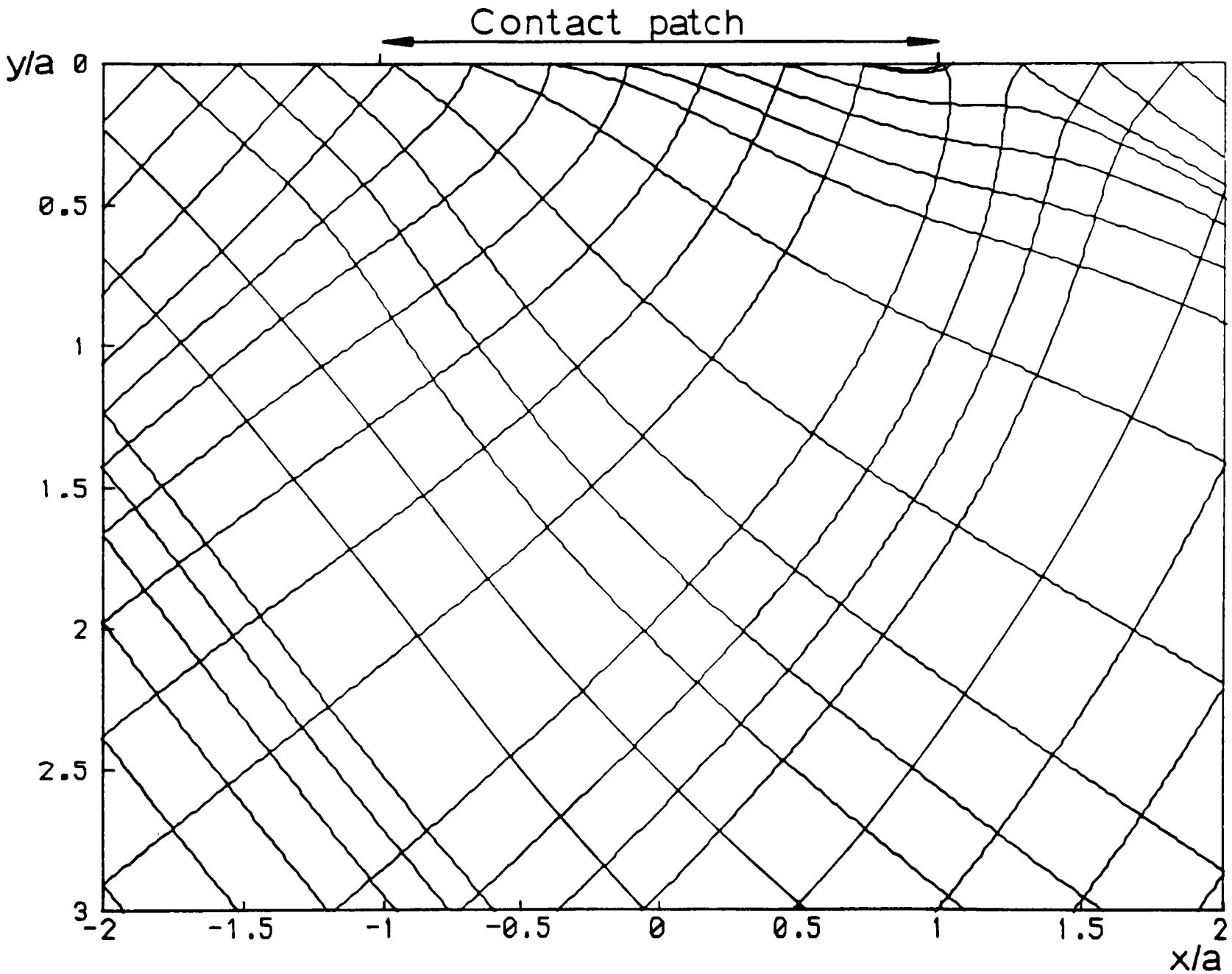

Fig. 4.10b Directions of maximum shear stress, series 1 experiments

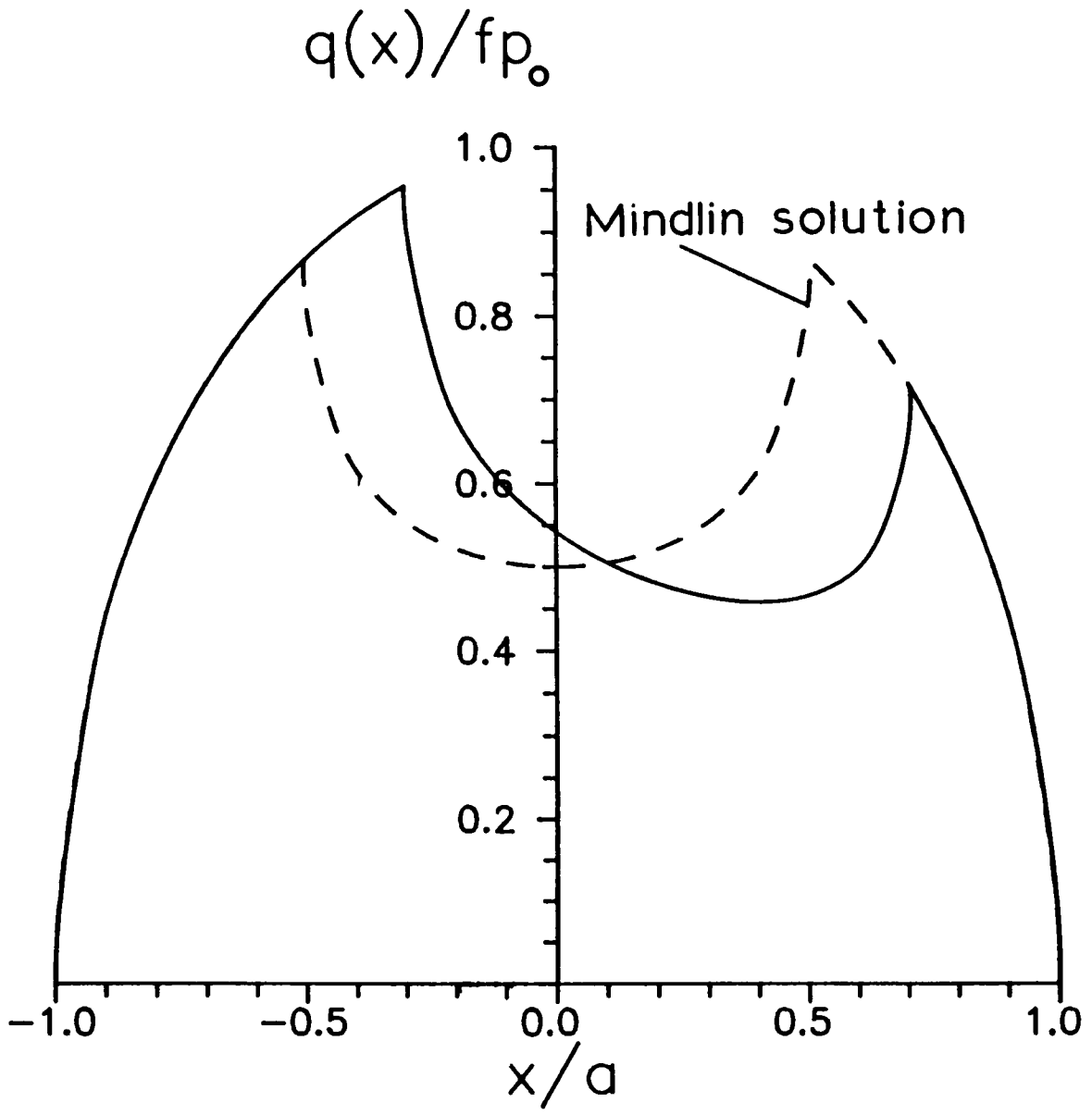

Fig. 4.11 Comparison of shear tractions developed with Mindlin model
(a) Series 1 experiments

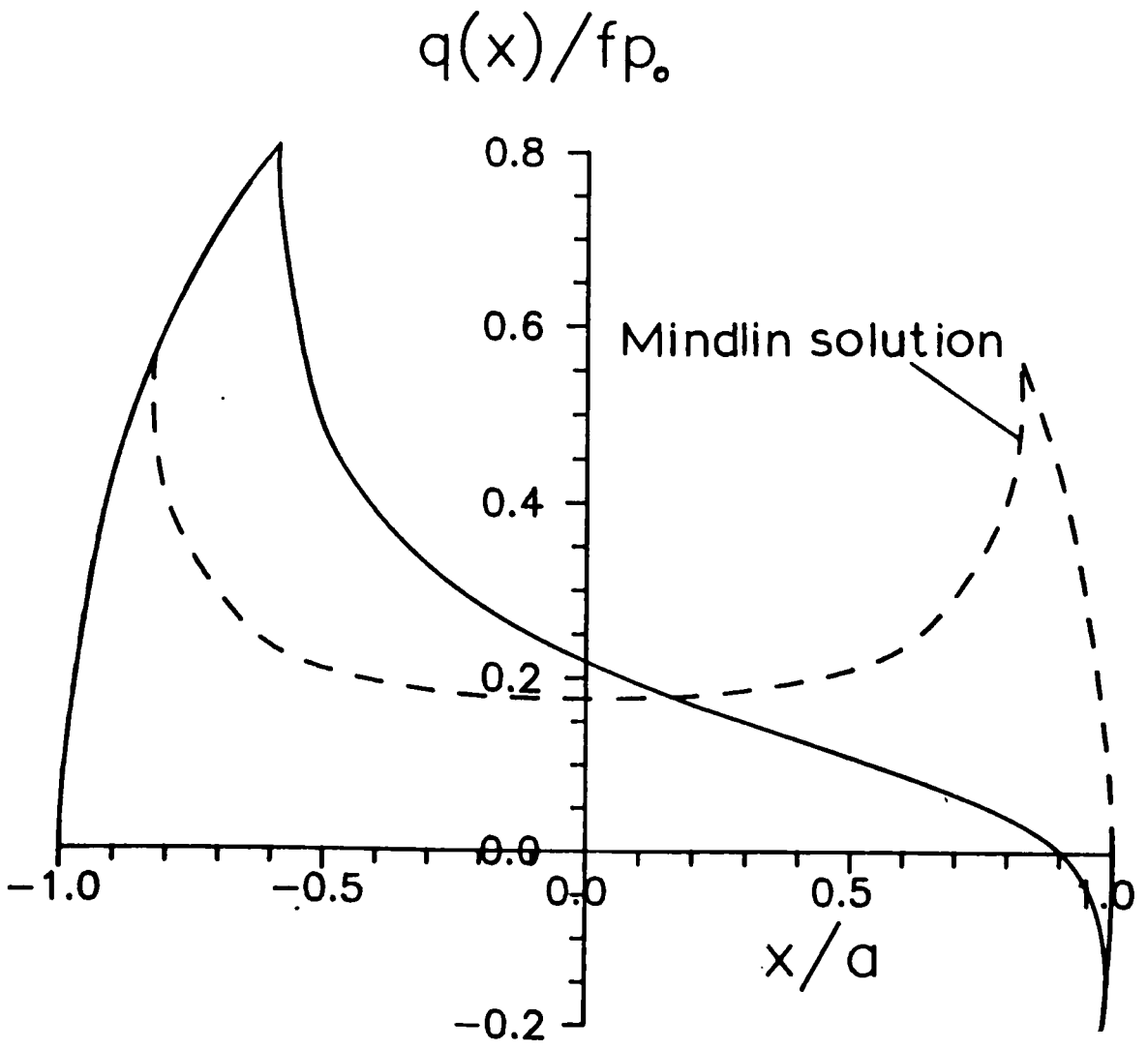

(b) Series 2 experiments

distribution contains a region of reverse slip at the leading edge of the contact. Series 2 was the only configuration tested to exhibit this phenomenon.

The current analysis reveals shear traction distributions which differ from Mindlin's in two important respects: (i) The tensile stress induced in the trailing slip zone is increased, although this effect is less marked as $Q/fP \rightarrow 1.0$, (ii) The trailing slip zone is enlarged and the amplitude of micro-slip experienced at the edge of the contact is consequently increased. Hence, in the region where fretting fatigue cracks initiate, both the tensile stress and the amplitude of micro-slip are larger than predicted if the Mindlin analysis is employed.

Chapter 5

The effect of finite specimen thickness

5.1 Introduction

As stated in chapter 4, one of the assumptions of the Hertz theory of elastic contact is that both contacting bodies may be represented as half-planes, i.e. that the dimensions of the bodies are large compared with the dimensions of the contact itself. In fretting fatigue experiments both specimen and pads have finite dimensions but previous analyses by Nishioka and Hirakawa (1969c) and Milestone (1970), inter alia, have retained the half-plane assumption. The validity of this approach must clearly be called into question if the contact semi-width is of the same order as the dimensions of the bodies themselves. In particular, the specimen thickness in the current experiments is only about 5 times the contact width for the larger contacts. Bentall and Johnson (1968) have shown that for plane rolling contact the thickness of an elastic strip moving between two elastic rollers has a significant effect on the resulting surface tractions. It was decided, therefore, to investigate the effect of the specimen thickness on the surface tractions developed in fretting and consequently to test the validity of the half-plane assumption for analysing the current experiments.

Elastic contact problems involving strips can, in principle, be formulated using Sneddon's integral transform methods (Sneddon (1951)). However, in practice two problems arise; first, the integrals developed are often difficult to evaluate accurately, since they are over a semi-infinite range and incorporate slowly decaying oscillatory kernels.

Secondly, mixed boundary value problems cannot readily be formulated. Instead, a hybrid method due to Bentall and Johnson (1968) is adopted. A schematic view of the geometry is shown in Fig. 5.1a.

Whereas in half-plane problems an integral equation relating the surface displacements to a continously varying traction distribution can easily be composed (Muskhelishvili (1953a)), for strip problems this is not feasible, owing to the complexity of the influence function. Instead, a piecewise linear idealisation of the true traction is utilised, which consists of a series of overlapping triangles, Fig. 5.2. The first step in the solution is to determine the surface displacements at some point m due to a triangle of traction (direct or shear) centred on a point n. When this building block has been established, a wide variety of contact geometries may be analyzed by formulating what is, essentially, a discretised form of the integral equation method. Details of the derivation of these influence functions are given by Bentall and Johnson (1968) and here, after summarising the results needed, the solution of the boundary value problems is addressed.

5.2 Influence functions

The problem outlined above where two cylinders indent a strip as shown in Fig. 5.1a has the following surface boundary conditions outside the contact;

$$\sigma_{yy} = \tau_{xy} = 0 \qquad |x| > a \ , \ y = \pm h \qquad (5.1)$$

where a is the contact semi-width and h the strip semi-thickness. Arguments of symmetry about x = 0 may be used to augment (5.1), giving

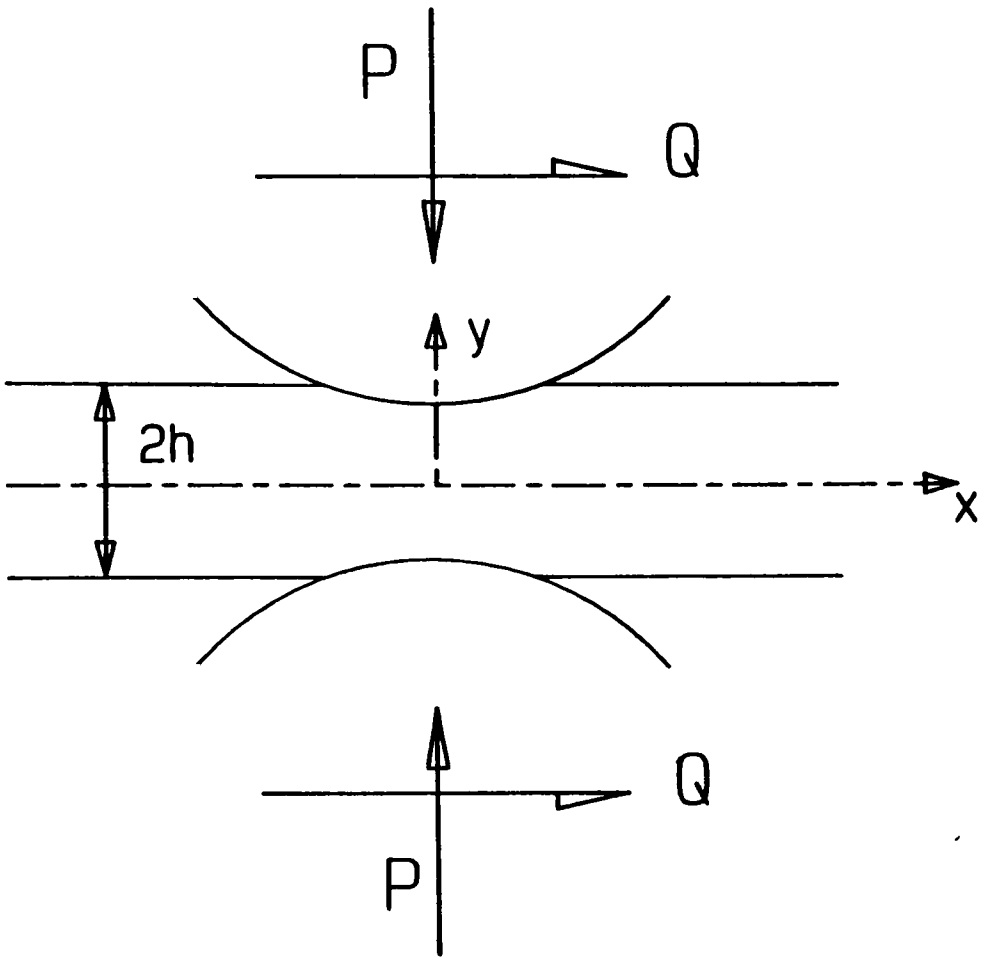

Fig.5.1 Contact configurations

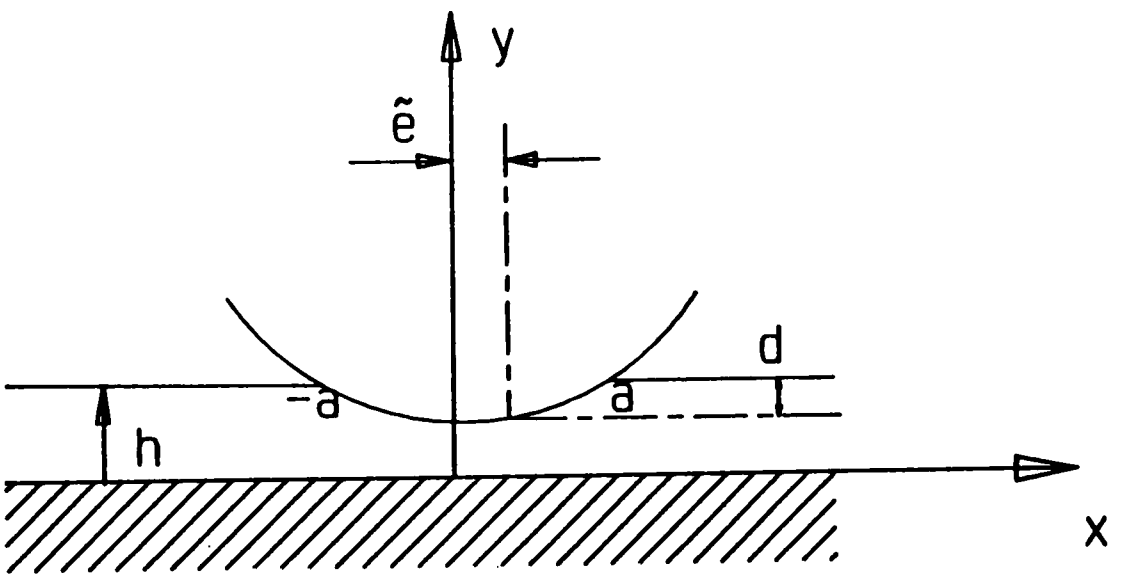

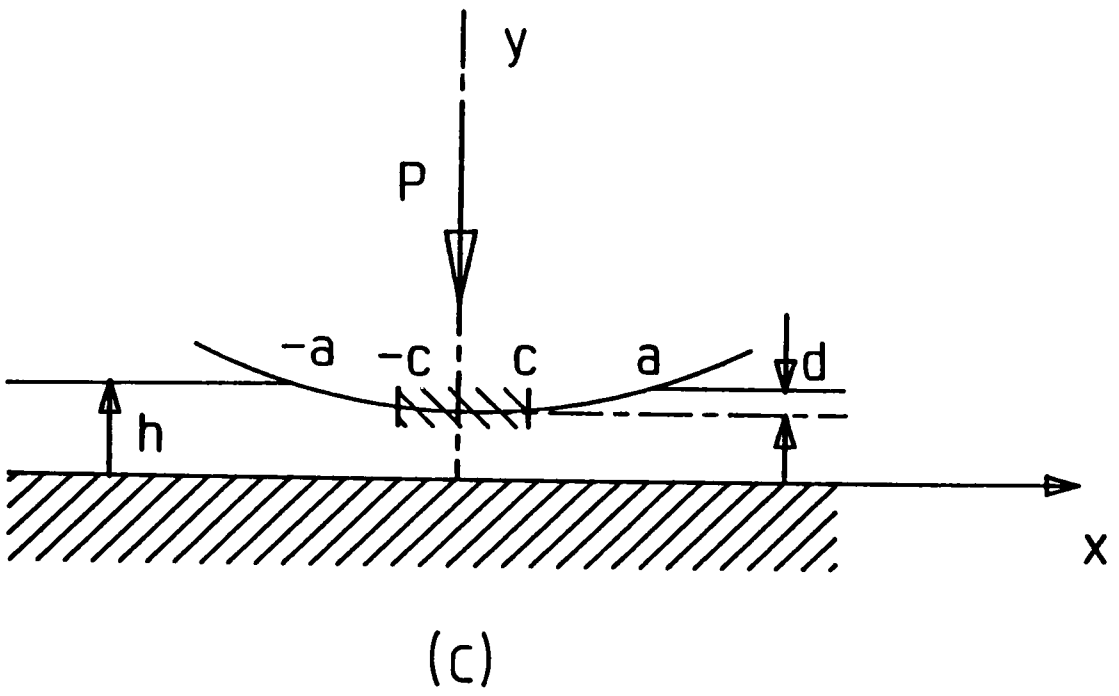

(c)

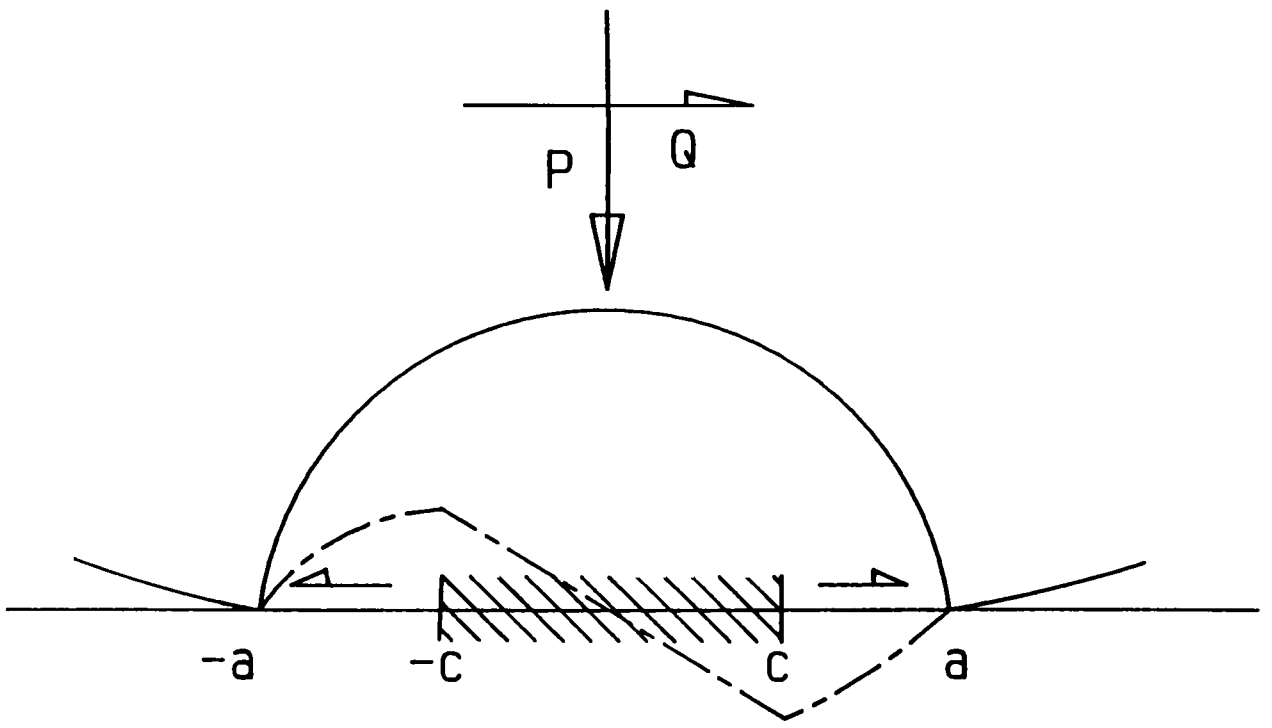

(d)

Fig. 5.1 Contact configurations

the following:

$$\sigma_{yy} = \tau_{xy} = 0 \qquad |x| > a,\ y = h \qquad (5.2)$$

$$\tau_{xy} = v = 0 \qquad y = 0 \qquad (5.3)$$

whereupon the problem is seen to be identical to that of an elastic strip of thickness h resting on a rigid frictionless substrate as shown in Fig. 5.1b.

In general, coupling between shear and direct tractions may lead to an asymmetric distribution of direct traction. This would result in the centre of contact not being coincident with the centre of the indenter. Accordingly the origin is taken as the centre of the contact and the centre of the indenter assumed to be displaced by an amount $\tilde{e}$. To reduce the number of independent variables contact between a cylinder and an elastic strip having the same elastic constants, viz. Poisson's ratio υ and modulus of rigidity μ will be considered. The problem is formulated below for conditions of plane strain.

Direct and shear tractions over the contact are each represented by 2S overlapping triangles with equal bases (Fig 5.2). The heights of the nth triangles are p_n and q_n, which represent the magnitudes of the direct and shear tractions respectively at x = na/S. The relative vertical and horizontal displacements v(m), u(m) due to the total direct and shear force exerted are now extracted from Bentall and Johnson (1968)

$$\frac{v(m)}{a} = \sum_{n=-(s-1)}^{s-1} \bar{P}_n \left[\frac{H}{2} \{I_{AO} + I_A(m-n)\} + \frac{1}{2S} \{I_{AR}(m-n) - I_{AR}(n)\} \right.$$

$$\left. + \frac{1}{2S} I_{AR}(m-n) \right] - \sum_{n=-(s-1)}^{s-1} \bar{Q}_n \left[\frac{H}{2} I_B(m-n) - \frac{1}{8S} \frac{1-2\upsilon}{1-\upsilon} I_{BR}(n) \right] \qquad (5.4)$$

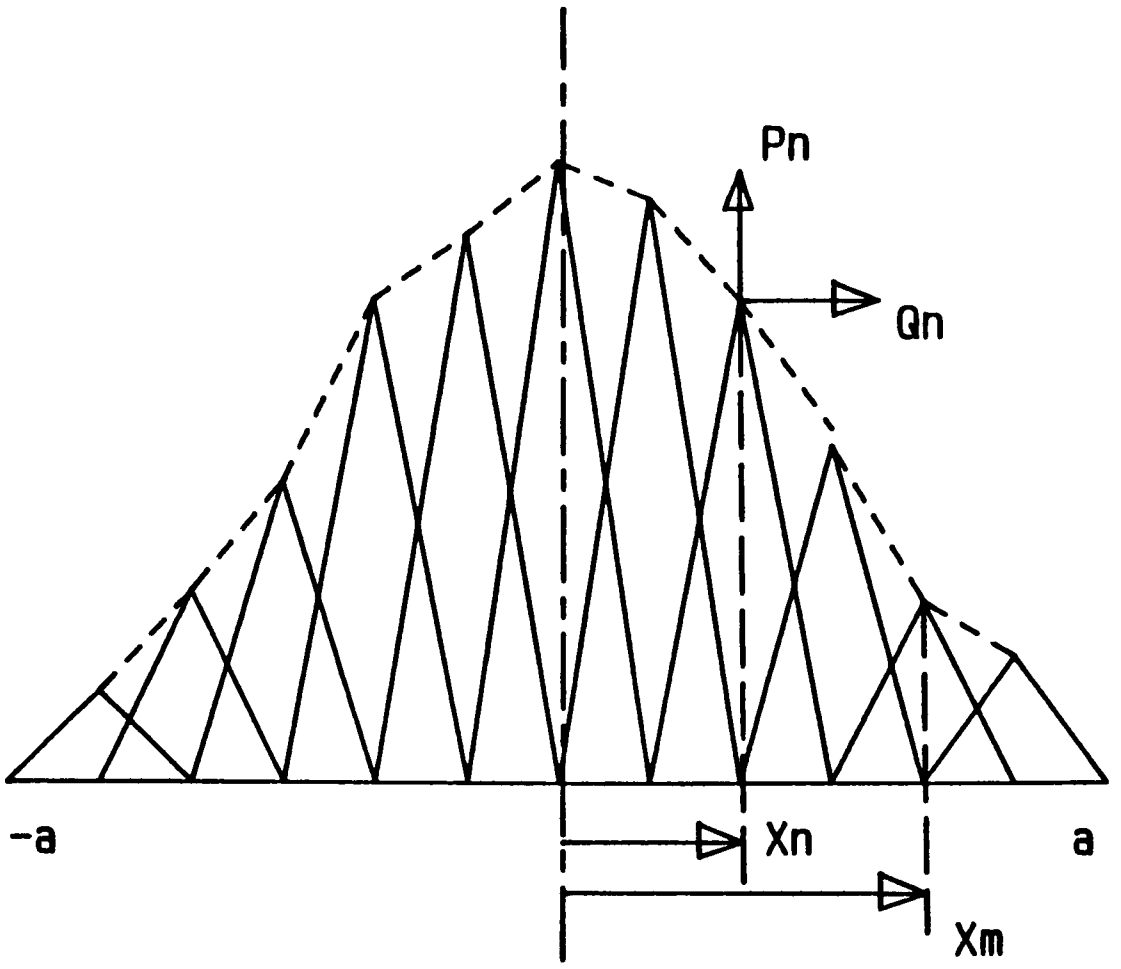

Fig. 5.2 Discretised model of surface tractions

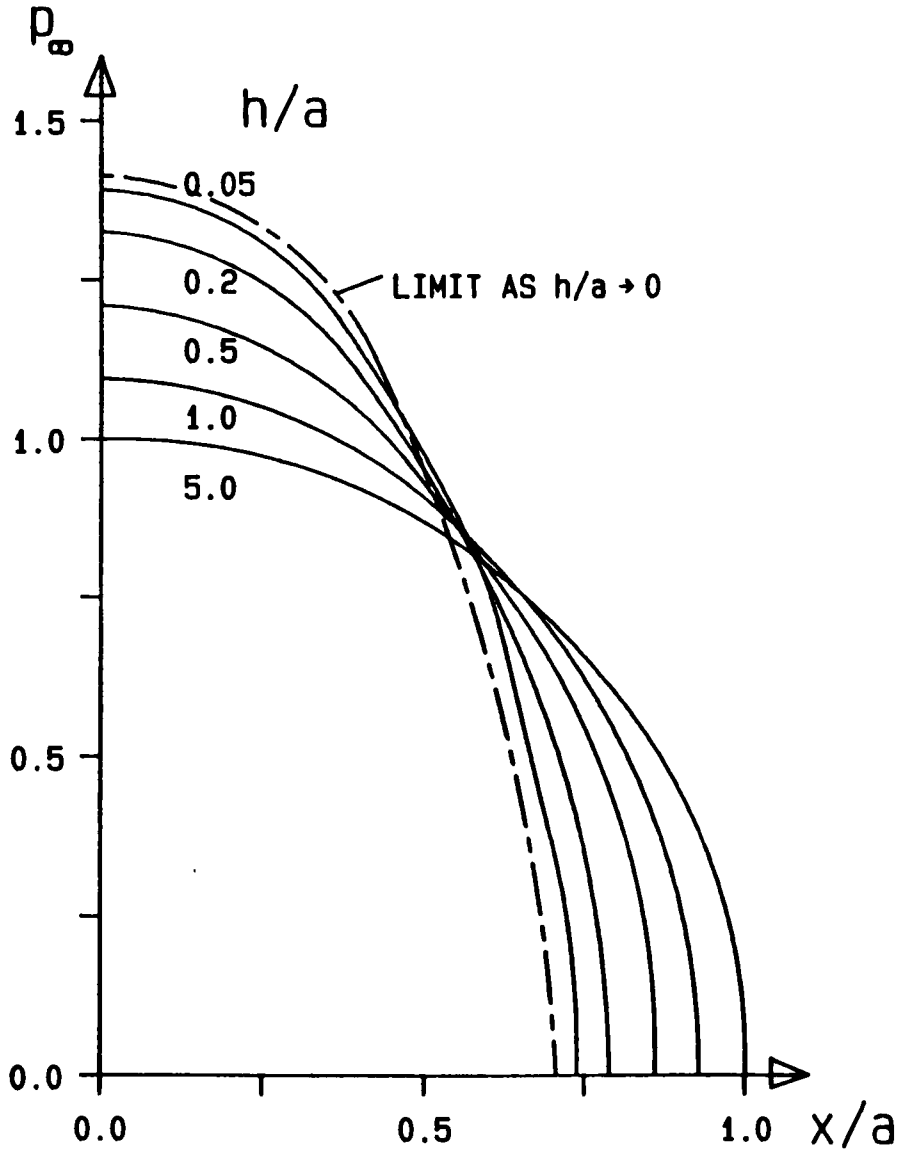

Fig. 5.3 Frictionless indentation, direct tractions (symmetric)

$$\frac{u(m)}{a} = \sum_{n=-(s-1)}^{s-1} \bar{P}_n \left[\frac{H}{2} \{I_B(m-n) + I_B(n)\} \right]$$

$$- \sum_{n=-(s-1)}^{s-1} \bar{Q}_n \left[\frac{H}{2} \{I_D(m-n) - I_D(n)\} - \frac{1}{S} \{I_{AR}(m-n) - I_{AR}(n)\} \right] \qquad (5.5)$$

Where $\bar{P}_n = p_n/\bar{p}$, $\bar{Q}_n = q_n/\bar{p}$, $\bar{p} = P/2S$, $H = h/a$ and the functions I are precisely as defined by Bentall and Johnson, q.v., and tabulated for convenience in Appendix B.

Following Hertz, the relative vertical displacement within the contact zone is approximated by a parabola. An allowance is made for the eccentricity $\tilde{e}$, so that

$$\frac{v(m)}{a} = \frac{2DR\alpha^2}{a} + \frac{2m\eta\alpha^2}{S} - \frac{m^2\alpha^2}{S^2} \qquad (5.6)$$

where $\eta = \tilde{e}/a$, $D = d/a$ (d being the rigid body normal approach), $\alpha = a/a_\infty$ (a_∞ being the contact half-width predicted by the Hertzian solution), and R is the radius of the cylinder. Restrictions on the variation of the relative tangential displacement depend on the exact contact configuration. Note that within a stick zone the relative tangential strain ϵ_r (i.e. $\epsilon_{xx}^{indenter} - \epsilon_{xx}^{strip}$) between adhered points is equal to the value when they first entered the stick zone whilst in the slip zones the direct and shear tractions are related by the coefficient of friction, f, ie.

$$q = \pm \mid fp \mid \qquad (5.7)$$

Before analysing the fretting problem, which is relatively complex, it is instuctive to develop the technique by treating a range of simpler configurations first. These are described below in sections 5.3 → 5.6.

5.3 Frictionless Indentation

The simplest problem which may be treated is normal indentation by a frictionless cylinder Fig. 5.1b. At low loads, ie. $a \ll h$, the contact is Hertzian, since the strip approximates a half-plane. At finite loads, the numerical solution must be used. Equations (5.4) and (5.6) are equated for all values of $-S \leq m \leq S$. Thus the vertical displacement is matched at 2S+1 points, including the edges of contact. A further equation arises from the requirement of vertical equilibrium, ie.

$$\sum_{n=-(s-1)}^{s-1} \bar{P}_n = P/\bar{p} = 2S \qquad (5.8)$$

The unknowns are the 2S-1 ordinates of the contact pressures $\bar{P}_n$, together with the rigid body normal approach d, α (a measure of the contact patch size) and the eccentricity $\tilde{e}$. Thus the problem has been reduced to 2S+2 simultaneous equations in 2S+2 unknowns and may readily be solved using a computer library routine. As expected from symmetry $\tilde{e}$ is found to be zero. The distribution of normal traction is shown in Fig. 5.3 for several values of h/a . The pressure, p is normalised with respect to p_∞, the maximum Hertzian contact pressure and the results were calculated with S=20. The major effect of the finite strip thickness can be seen to be a reduction in contact area, compared to the Hertzian solution and a corresponding increase in peak pressure. The limiting

case for large h/a is Hertzian contact of a cylinder on a half-plane. The opposite limit (h/a → 0) corresponds to Hertzian contact of two cylinders of radius R ($a/a_\infty = 1/\sqrt{2}$, $p_{max}/p_\infty = \sqrt{2}$). This is as expected since for thin strips the displacements within the strip are small compared with those in the cylinders.

5.4 Sliding contact

It is now appropriate to introduce tangential tractions in addition to the normal pressure already considered. Rather than proceeding to the partial slip case immediately it is simpler to consider first the case of fully sliding contact. For quasi-static sliding contact between the impressed cylinder and the strip, numerical solution is again acheived by combining (5.4) and (5.5) and using (5.7). In this case there is no longer symmetry, and $\tilde{e}$ is non-zero. Again there are 2S+2 knowns and unknowns (if only the 2S-1 $\bar{P}_n$ are treated as unknown tractions) and the shear components are related by (5.7) (ie. q = fp). Fig. 5.4 shows distributions of normal and shear tractions at several different values of h/a for f = 0.3 and υ = 0.3. These results were obtained with S=10.

Again the major effect of the finite strip thickness can be seen to be a reduction in the contact area and an increase in the peak pressure. The coupling between shear and direct tractions produces some asymmetry in the results but the effect is not large at this value of f.

5.5 Adhesive indentation

As a prelude to analysing the fretting problem, normal indentation where the interfacial friction is finite but Q=0 will be treated. This

configuration is considerably more complex than the previous ones, and a satisfactory initial simplification of the problem is to assume that the coefficient of friction is sufficiently high to prevent relative displacement between corresponding points on the two bodies once within the contact zone, ie. that no slip takes place. As the applied load is increased, the contact patch grows and new surface particles come into contact. The relative strain between such points remains constant once they enter the contact and, since there is no rigid body tangential displacement, the relative displacement u_r also remains constant. The solution needs to ensure that, for all pairs of adhered points, u_r remains at the same value as when the two points entered the contact.

One difficulty is that the displacements of such points before they enter the contact zone are not known *a priori*. Further, since the displacement of points within the strip is an unknown function of the ratio h/a, the problem is not self-similar, unlike those treated by Spence (1968,1975), and hence an incremental solution, as first used by Goodman (1962) in his analysis of contact between dissimilar spheres, is necessitated.

The solution proceeds as follows: at large values of h/a the geometry approximates to the Hertzian case of two half-planes and the values of u_r are expected to be small within the contact. It is therefore reasonable to assume an approximately linear variation of u_r with x for some large value of h/a (= h/a_o, say). It is then possible to specify the relative tangential displacements at the matching points (u_m) in terms of the values at the edges of the contact $u(+a_o)$, $u(-a_o)$, which are as yet unknown. Thus the 2S+1 tangential matching equations are obtained by substituting for u_m in (5.5). There are now 4S+3 equations, and the correponding unknowns are; 2S-1 values of $\bar{P}_n$, 2S-1 values of $\bar{Q}_n$,

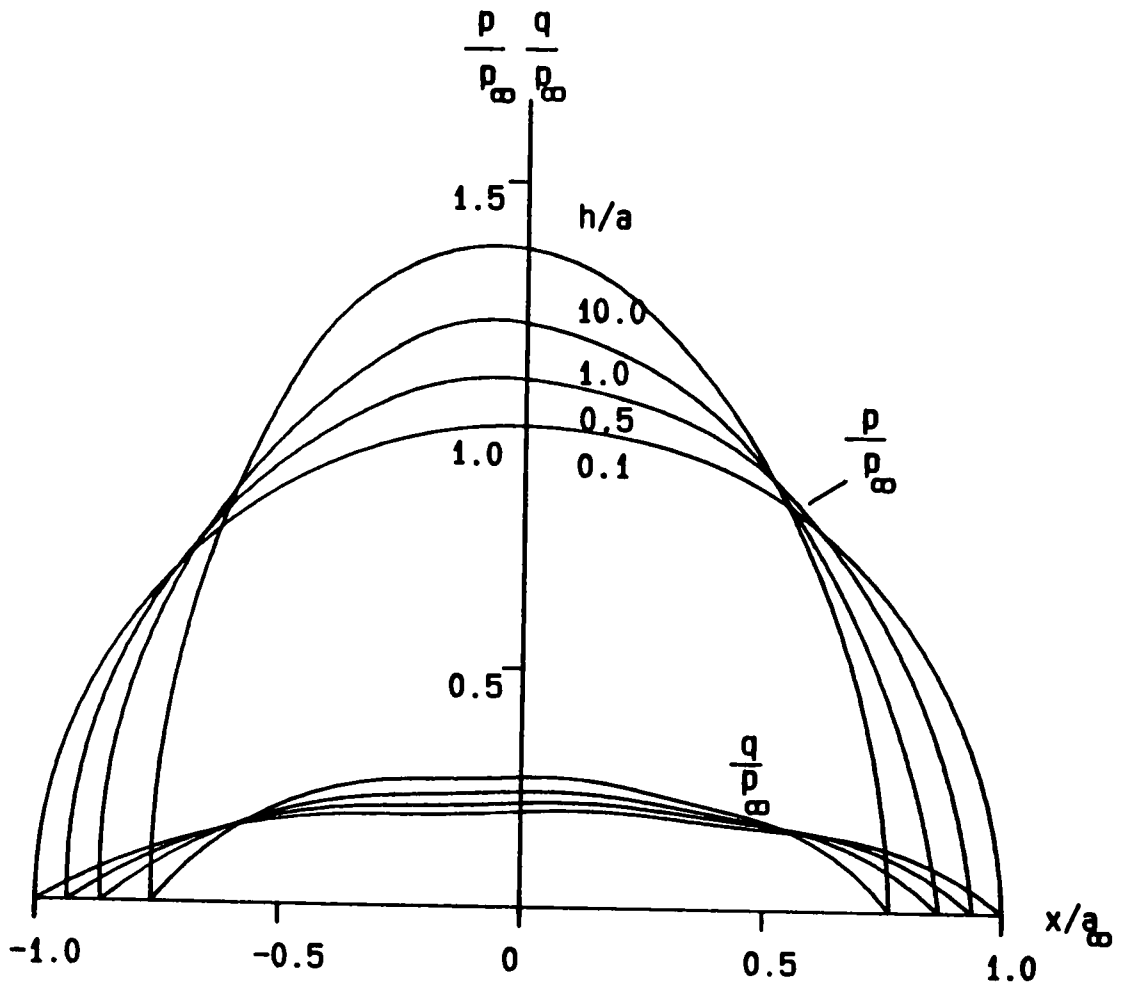

Fig. 5.4 Sliding contact, f = 0.3, ν = 0.3, surface tractions

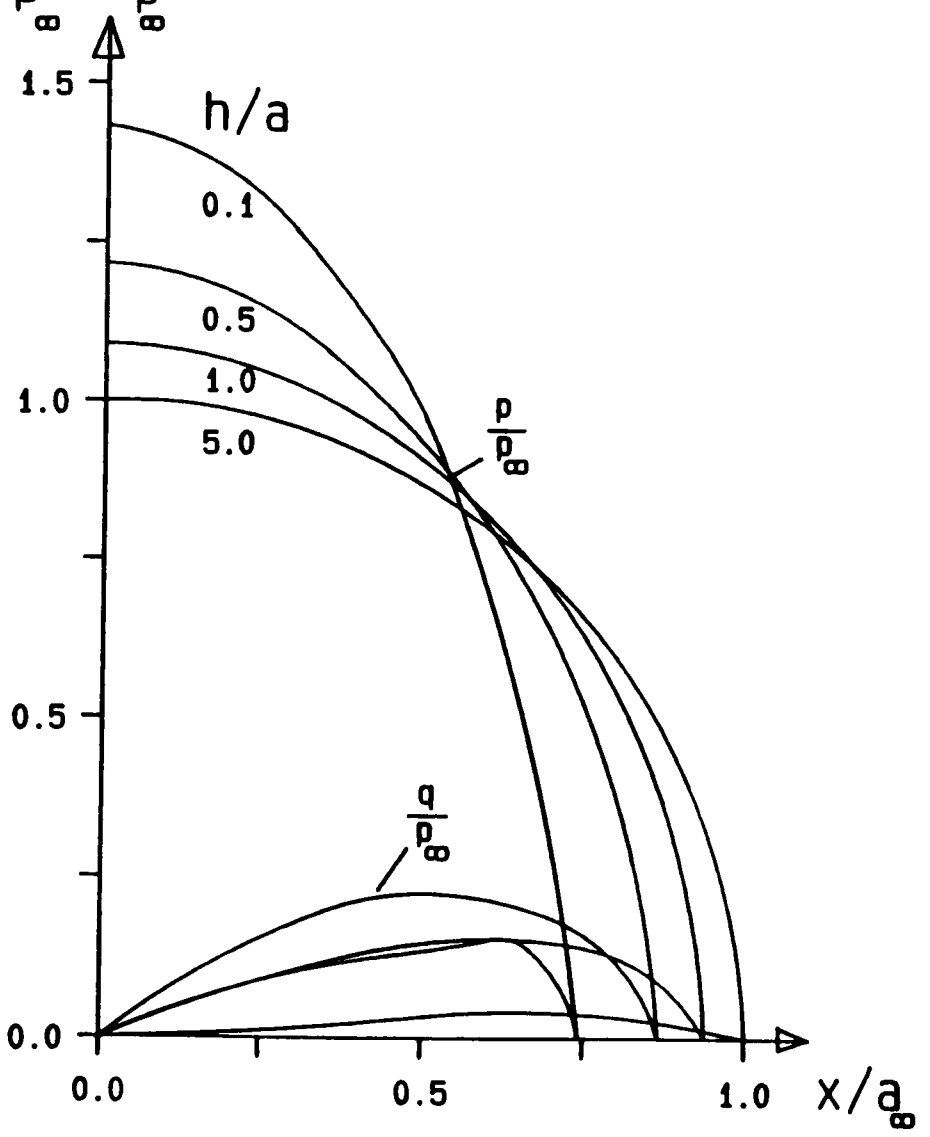

Fig. 5.5 Adhesive indentation, ν = 0.3
(a) Direct tractions (symmetric) and shear tractions (anti-symmetric)

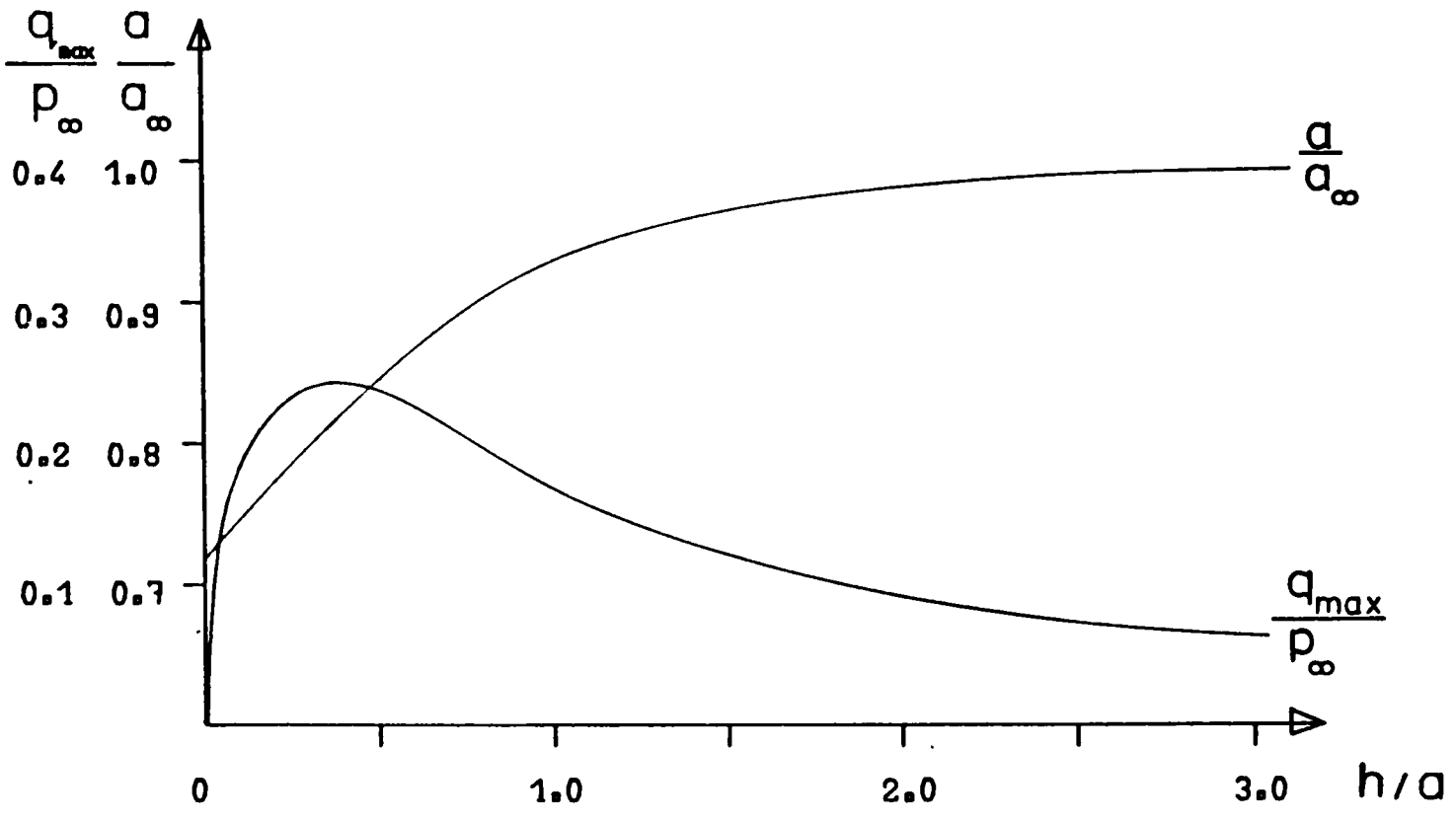

Fig. 5.5 Adhesive indentation, $\nu = 0.3$

(b) Variation of contact size and maximum shear stress with h/a

(c) Variation of relative tangential displacement within the contact with position

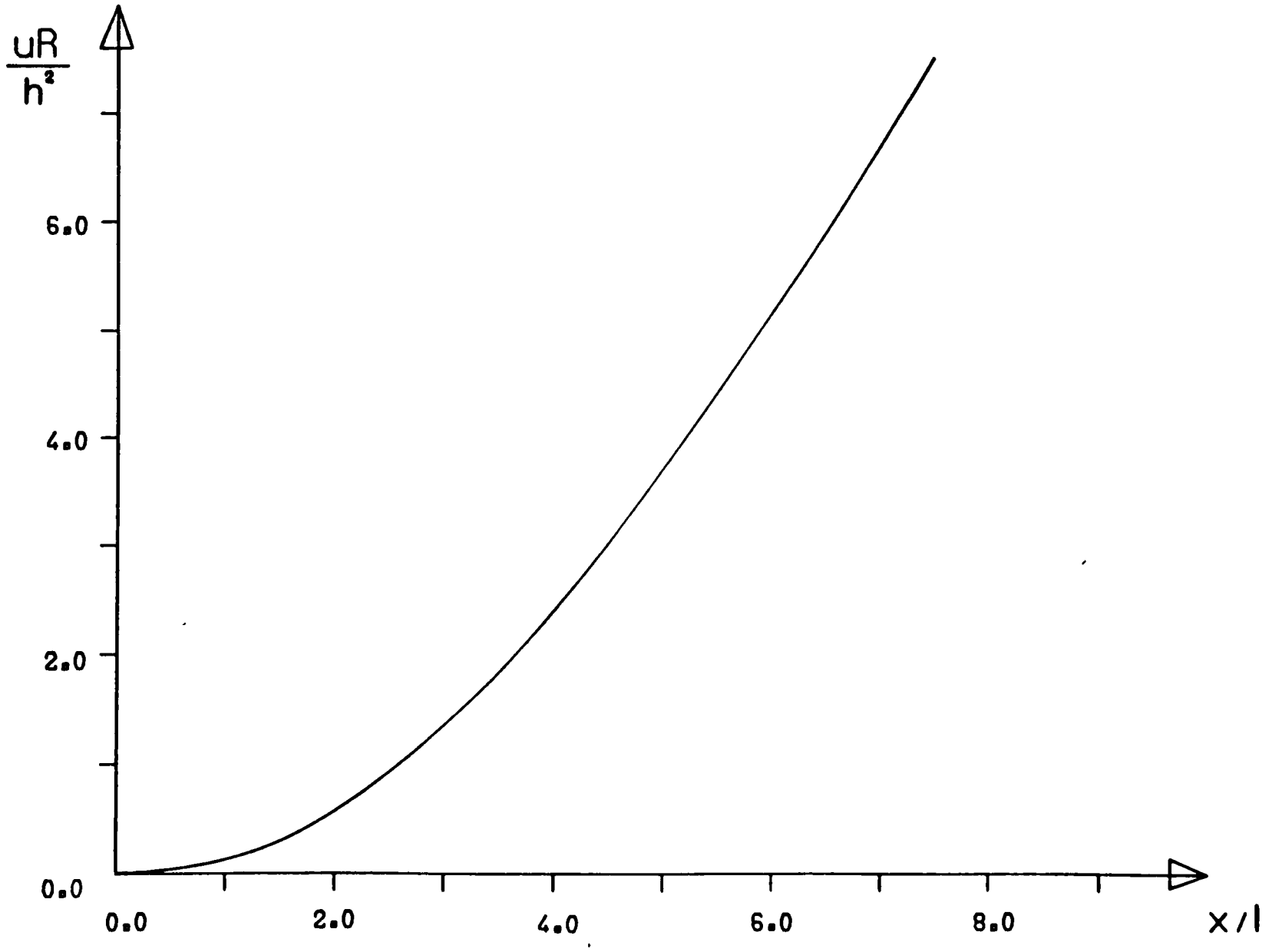

η, α, D, $u(+a_o)$, and $u(-a_o)$.

The solution reveals the values of u at $x/h = \pm a_o/h$. A small load increment is now made such that the contact grows to $x = \pm a_1$. Linear interpolation of the previous solution is used to determine u_m for all matching points within the range $|x| \leq a_o$ and the variation over the small intervals $a_o > |x| \geq a_1$ is assumed linear. The solution of the second step can now be found since the values of u_m at all matching points are either known from the previous solution or can be expressed in terms of $u(\pm a_1)$. Hence, the incremental solution proceeds by taking small steps in h/a from an initial value which is sufficiently large for the variation of u_r to be assumed linear. Once four values of $u(a_i)$ are known a fitted cubic spline is used in place of linear interpolation to determine u_m.

Results were calculated with S = 10 and for $\upsilon = 0.3$. Fig. 5.5a shows the normal and shear stress distributions for various values of h/a. Fig. 5.5b shows the variation of a/a_∞ and the maximum shear traction with h/a. It will again be noted that as $h/a \to 0$, and $h/a \to \infty$ the contact becomes Hertzian. Between these limits, the finite strip causes significant shear tractions at the interface which reach a maximum at $h/a \approx 0.35$. Fig 5.5c shows the variation of u with x within the stick zone.

5.6 Frictional Indentation

The restriction that the coefficient of friction is sufficiently high to sustain stick throughout the contact is now relaxed. It has been shown by Goodman (1962), for the case of point contact between dissimilar bodies, that although the shear traction falls continuously to zero at

the edge of contact, the ratio q/p becomes infinite there. Bentall and Johnson (1968), however, show that for rolling contact between a strip and a cylinder this ratio falls to zero at the edges of contact. Because of the discrete nature of the numerical analysis it is only possible to examine this ratio at the 2S-1 points n. If full stick is assumed, the highest value of q/p predicted by the present numerical solution with S set to 10 is 0.328 at h/a = 0.343, $|x|/a = 0.9$. Thus if $f < 0.328$, the solution produced by assuming adhesion everywhere is violated. If $f > 0.328$ possible violations may occur at $x/a > 0.9$ but cannot be detected without increasing S.

For values of f where violations occur an iterative scheme is adopted to overcome the problem. At each load increment stick is first assumed. The outer points are then checked for violations of the friction law and where these are detected $\bar{Q}_n$ is replaced by $\pm f\bar{P}_n$ as appropriate. The matching of the tangential displacement is discarded within the new slip zone $c \leq |x| \leq a$ (Fig.1c). A new solution is now obtained, and again checks for violations are carried out. If necessary, further points are permitted to slip until a satisfactory result is obtained. Values of $u(\pm c)$ are recorded for incorporation at the next load step, which can now be taken. Fig. 5.6 shows the results obtained for $f = 0.2$, $\upsilon = 0.3$ with $S = 20$. The variation of the stick zone boundaries and the size of the contact patch is shown in Fig. 5.7. It is seen that for $h/a \geq 2.0$ the contact is effectively Hertzian. As the load is increased the slip zones develop, reaching a maximum proportion of the contact at about h/a = 0.6. As the load is increased further the slip zone rapidly recedes so that as $h/a \rightarrow 0$ normal Hertzian conditions again apply.

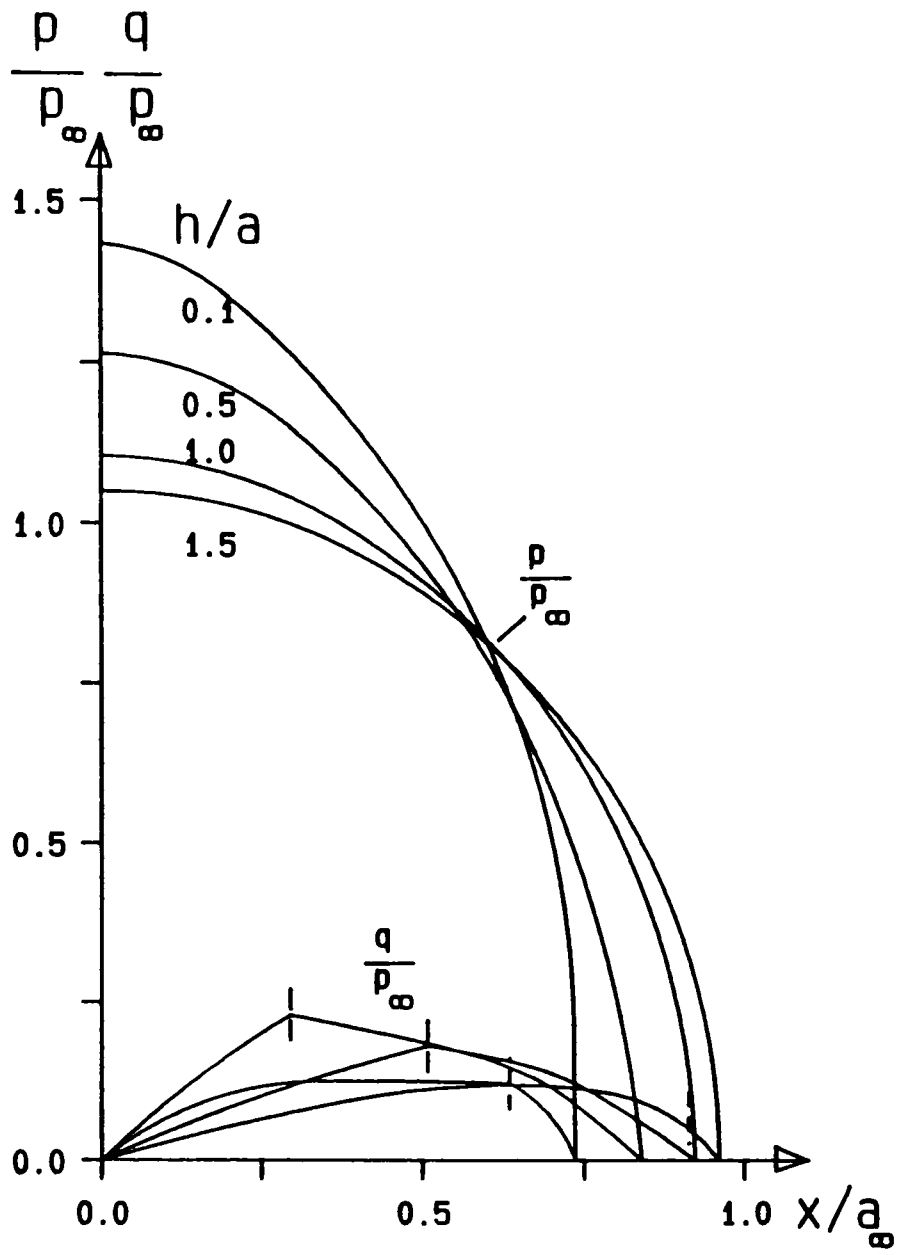

Fig. 5.6 Frictional indentation, $\nu = 0.3$, $f = 0.2$
(a) Direct tractions (symmetric) and shear tractions (anti-symmetric)
(b) Variation of contact size and maximum shear traction with h/a

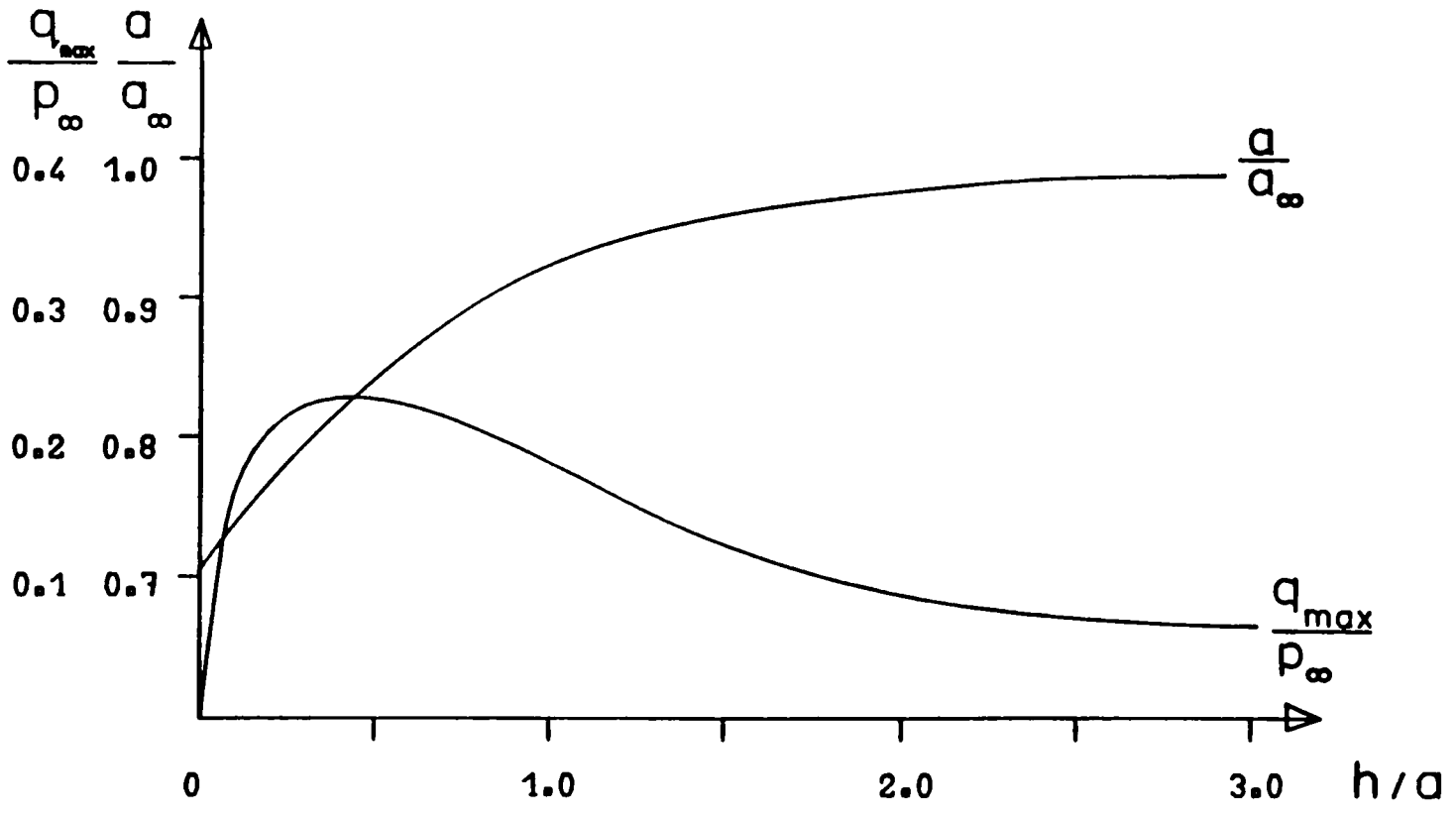

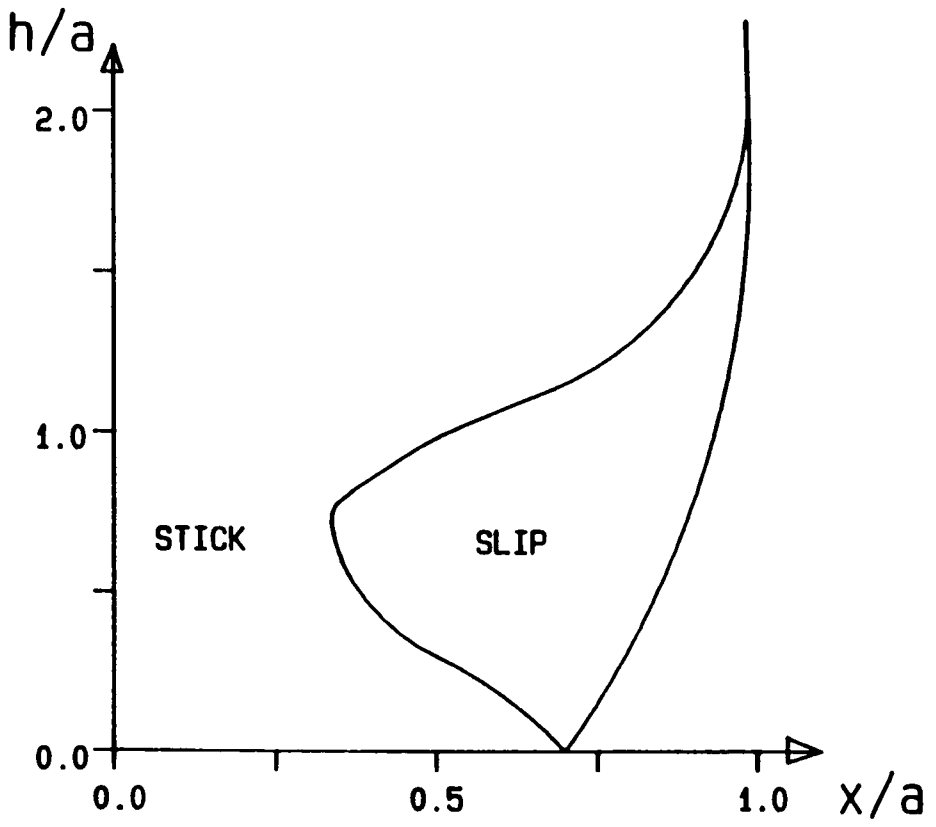

Fig. 5.7 Frictional indentation, $\nu = 0.3$, $f = 0.2$, stick and slip zones

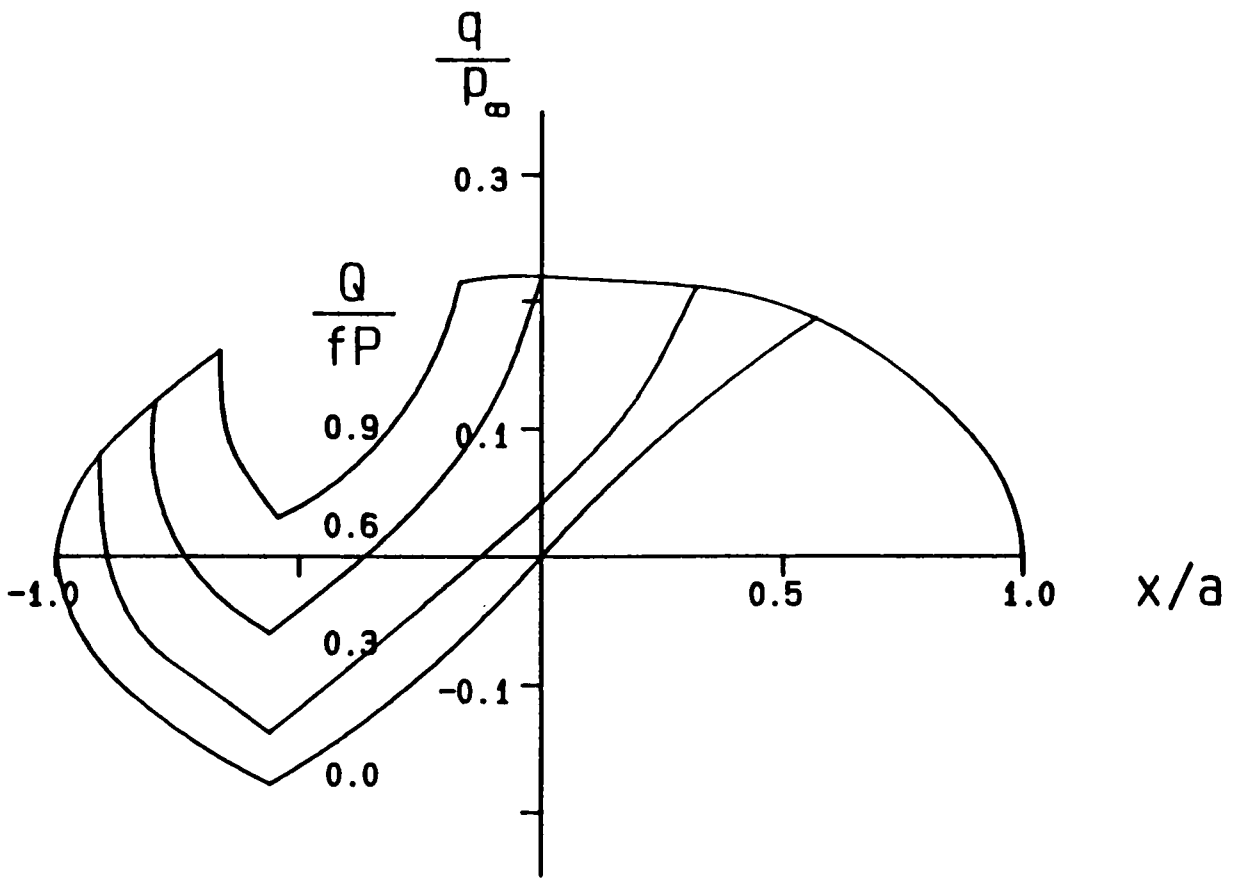

Fig. 5.8 Mindlin-type contact, $h/a = 1.0$, $\nu = 0.3$, $f = 0.2$, shear traction distributions

5.7 The Mindlin Problem

As stated at the outset, the object of the present chapter is to assess the influence of finite strip thickness on the analysis of fretting fatigue. In the classical Mindlin analysis of the half-plane problem two elastically similar bodies are pressed normally together so that they stick everywhere, and then a tangential force less than that needed to cause sliding is applied, giving rise to a central stick zone bordered by slip of the same sign.

In the present configuration, slip zones of opposite sign already exist before the tangential force is applied. As soon as such a force is applied the magnitude of the shear stress on one side is augmented, whilst the other is reduced, Fig. 5.1d. This is accompanied by a small relative displacement in the direction of the augmented shear. Note, however, that in the slip zone where the shear traction is depleted, the shear traction and relative 'slip velocity' are of opposite sign. This violates the friction law and hence instantaneous adhesion results ($-a < x < -c$, Fig. 5.1d). As the magnitude of Q is increased, slip is expected to re-start at $x = -a$, but to be of the same sign as that in the interval $c < x < a$.

The starting conditions for the solution of this loading are the final conditions for frictional indentation, but with an infinitesimal load increment δQ applied so that the stick zone extends over $-a < x < c$. The relative tangential displacement u is already known for $-c < x < c$ and may be calculated for $-a > x > -c$ using (5.5). The application of a shear force Q results in a relative displacement δ_t between distant points in the bodies, so that the tangential matching

condition expressing ϵ_r = constant becomes;

$$u_m = u_{mo} + \delta_t \tag{5.9}$$

Where u_{mo} are the values determined before Q is applied. The further unknown δ_t gives a measure of the tangential compliance. The problem is rendered determinate by introducing the second (tangential) equilibrium equation;

$$\sum_{n=-(S-1)}^{S-1} \bar{Q}_n = Q/\bar{p} = 2SQ/P \tag{5.10}$$

Again an iterative solution is pursued. The required value of Q/P is chosen and the stick zone taken initially to be $-a < x < c$. If violations occur either or both outer points are allowed to slip and the problem re-solved. The method proceeds until a satisfactory solution is obtained. It should be noted that an incremental approach is not required since the stick zone recedes and u_{mo} is known everywhere. Shear traction distributions for a range of values of Q/fP are given in Fig. 5.8 for $h/a = 1.0$, $f = 0.2$, and $\nu = 0.3$. For these values of h/a and f coupling between shear and direct tractions is so small that the direct tractions are almost identical to the case when $Q = 0$. Similarly the variation of a/a_∞ with Q is sufficiently small to be neglected. Fig. 5.9 summarises the variation of stick zone boundaries with Q/fP for $h/a = 1.0$, $f = 0.2$, and $\nu = 0.3$.

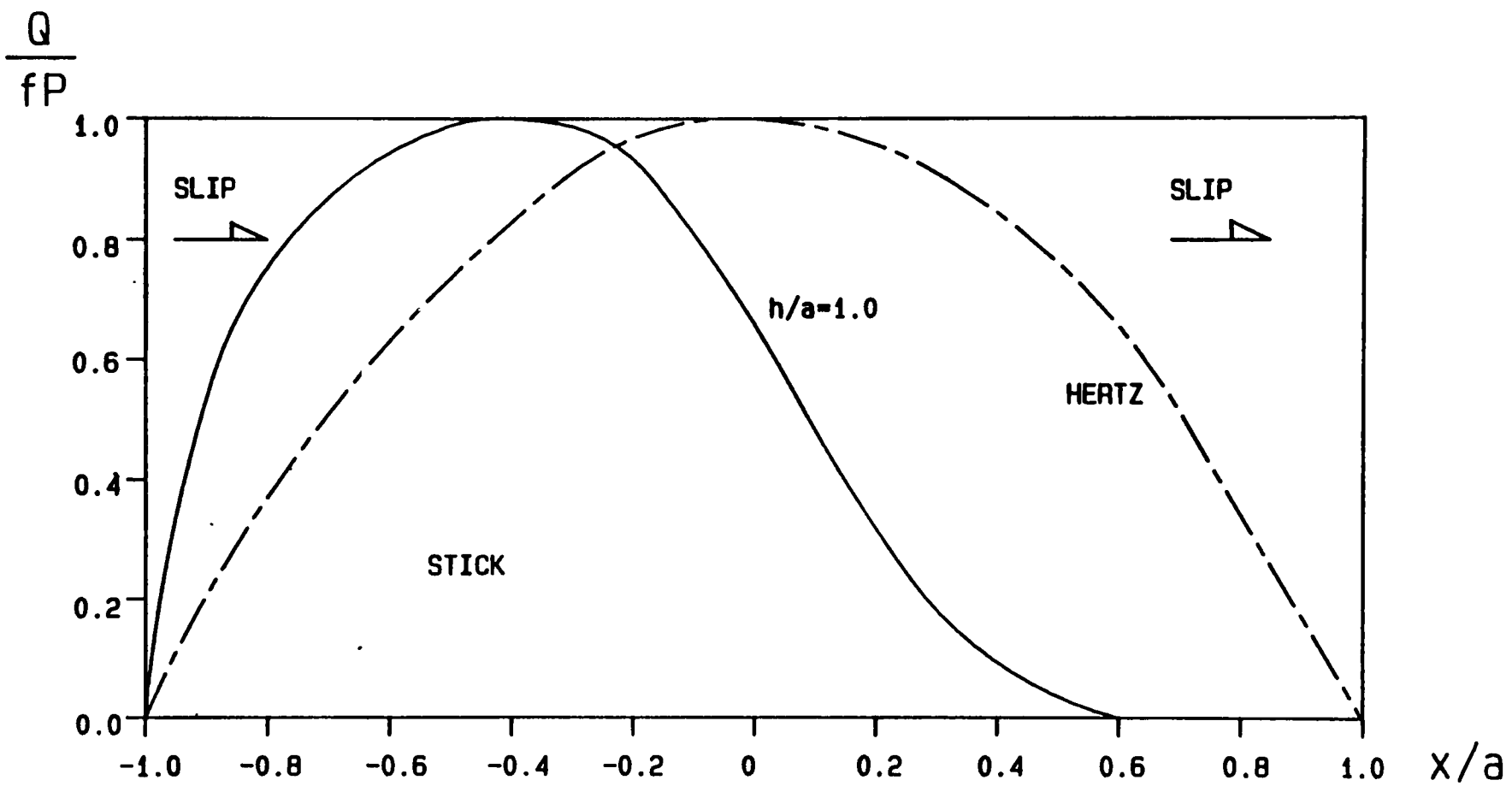

Fig. 5.9 Mindlin type contact, $\nu = 0.3$, $f = 0.2$, stick and slip zones

5.8 Discussion

In order to assess the effect of finite specimen thickness on the surface traction distribution in fretting fatigue, a range of frictionless and frictional contact problems of an elastic strip indented by two rollers has been studied. For each, the interfacial tractions have been deduced using the method of Bentall and Johnson (1968). It has been shown that the largest discrepancies from Hertzian theory occur at $h/a \approx 0.4$ and that if h/a is greater than 5.0, differences are negligible. The results confirm that the contact pressure is still approximately parabolic (Figs. 5.3, 5.5a, 5.6a) but that the contact size and peak pressure are considerably altered. Fig. 5.10 may be used to calculate both these quantities for any known load since the equivalent Hertzian contact size a_∞ is easily found. These results are presented for the case of adhesive indentation, but are almost identical for the other configurations studied.

The effect of finite strip thickness on the form of the contact pressure distribution for a sliding contact is slight (Fig. 5.4) and is very much less than the influence of a dissimilarity between elastic constants as discussed by Hills and Sackfield (1985). Indeed, a general result of the current investigations is that the effect of coupling between the shear and direct tractions is small and that for practically realisable coefficients of friction, the magnitude of surface vertical displacements induced by shear is much less than the initial curvature. It would therefore be entirely reasonable, for all strip thicknesses, to solve directly for the pressure, neglecting the effect of $q(x)$. This would considerably facilitate the solution.

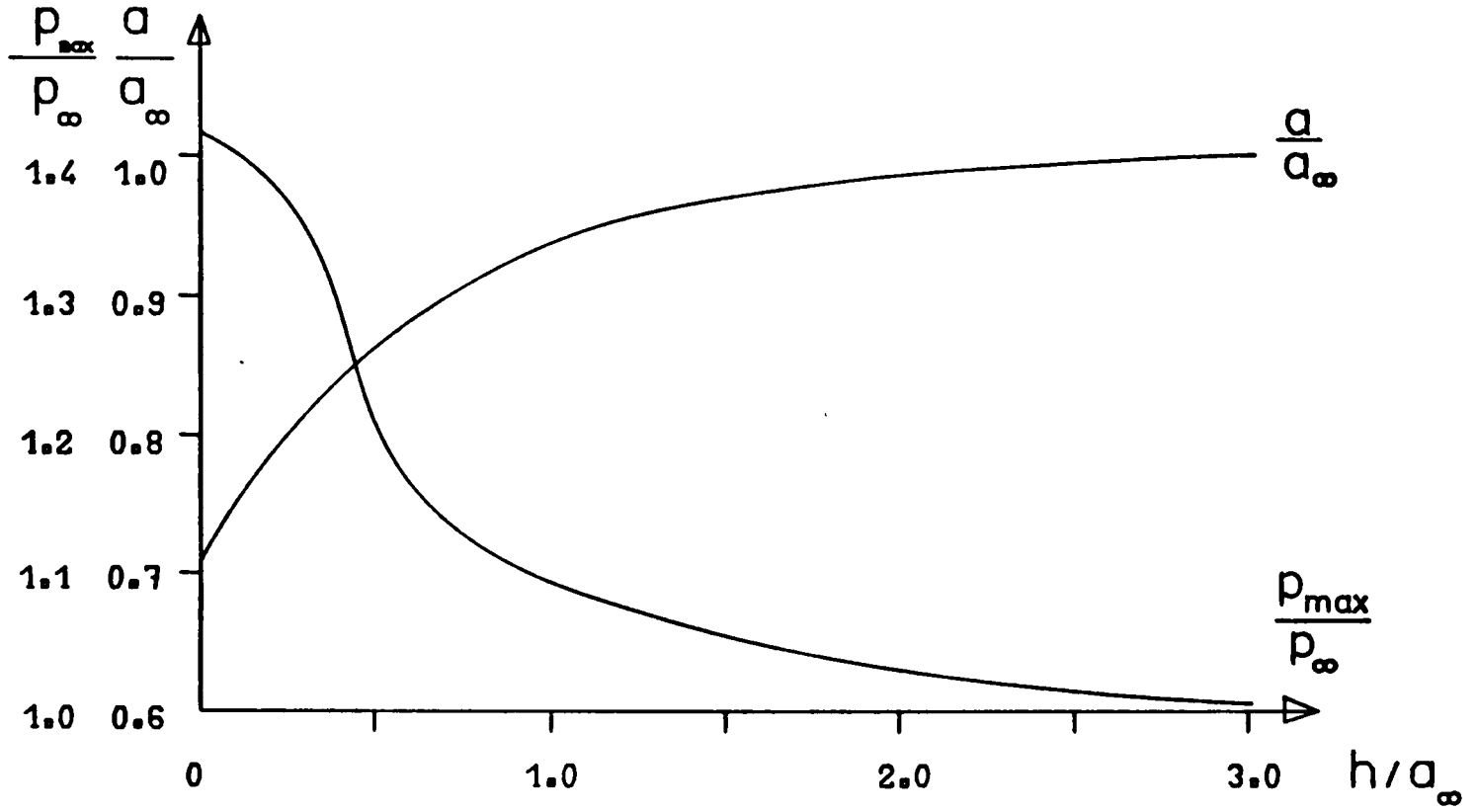

Fig. 5.10 Variation of contact size and peak pressure with normalised strip width, adhesive indentation, $\nu = 0.3$

Adhesive and frictional indentation problems require an incremental solution, which is rather expensive in computing time but gives satisfactory results with S = 10 or greater. The effect of finite friction on the results for normal indentation is not significant at realistic values of f, as noted by Bentall and Johnson (1968) The effect on the direct traction is very small, being confined to a slight attenuation near the edges of contact and a corresponding increase at x/a $\approx$ 0.5 . There is, however, a more pronounced shift in the shear traction distribution towards the centre of the contact (c.f. Figs. 5.5a, 5.6a).

Of most importance to the fretting problem is the effect of finite strip thickness on stick/slip zones for Mindlin contact. This has been found (Figs. 5.8 & 5.9) and is quite significant for thin specimens (h/a $\rightarrow$ 0). It may be seen from Fig. 5.9 that one stick zone grows considerably at the expense of the other, affecting the amplitude of microslip, which is of considerable interest in the analysis of fretting fatigue. In the present series of experiments 5.5 < h/a < 70. This is well outside the range of values (h/a < 2.0, Fig. 5.10) where the specimen thickness has any significant effect on the surface traction distribution. The use of the half-plane approximation is therefore entirely appropriate in the experimental analysis and it would have been possible to decrease the specimen thickness even further. This would have reduced the overall tensile load required and allowed the testing machine to operate at a higher frequency. Drawing on the results of this chapter, the half-plane approximation has been retained for all subsequent analysis of the present experiments.

Chapter 6

The effect of dissimilar materials

6.1 Introduction

One of the major practical difficulties of the fretting experiments carried out was that edge effects were present due to the finite width of the fretting pads and specimen. The traction distribution at the edges of contact will be affected and consequently fretting conditions here will differ from those at the centre. The plane strain analysis carried out is not therefore applicable at the contact edges and failures resulting from the edge conditions cannot readily be analysed. One possible method of circumventing this difficulty is to use barrelled rollers for the fretting pads. The axial profile variation of these rollers could be adjusted to give constant conditions across the width of contact. Such rollers would, however, be complicated to machine and the use of commercially available rollers from roller bearings becomes attractive.

An immediate difficulty arises in using such rollers with elastically dissimilar materials in that the Mindlin (1949) analysis is only valid for materials with similar elastic constants. A knowledge of the surface tractions developed by contact of dissimilar elastic cylinders is therefore required before use of steel rollers in the fretting of aluminium alloy can be contemplated. In this chapter the effect of using dissimilar elastic materials will be analysed quantitively. Although the results are of use in planning future work,

no experiments were, in fact, carried out with dissimilar materials since they did not prove 'necessary' in practice.

Analyses of the contact of dissimilar elastic bodies have been carried out by Spence (1968,1986) for contact under the influence of normal and oblique forces. Such frictional contacts are, however, history dependent and the experimental configuration, where the tangential load is applied subsequently to the normal load has not previously been analysed for dissimilar cylindrical indenters. Since the contact is history dependent, the problem of normal indentation, previously considered in detail by Spence (1968,1973) must be treated first. Spence's solution concentrates on a rigid, flat-ended punch, and uses an iterative scheme to develop a coupled solution. In this chapter a numerical technique is developed which is capable of providing a solution for the contact of cylindrical surfaces under both normal and tangential forces.

6.2 Formulation

The configuration to be analysed is shown in Fig.6.1. Dissimilar cylinders 1 and 2 are in contact under the action of a normal force P. The tangential force Q is initially zero. The vertical surface displacements of bodies 1 and 2, approximated as half-planes, in terms of the distributed direct and shear tractions p(x), q(x) are given by Johnson (1985), Noble and Spence (1971) as

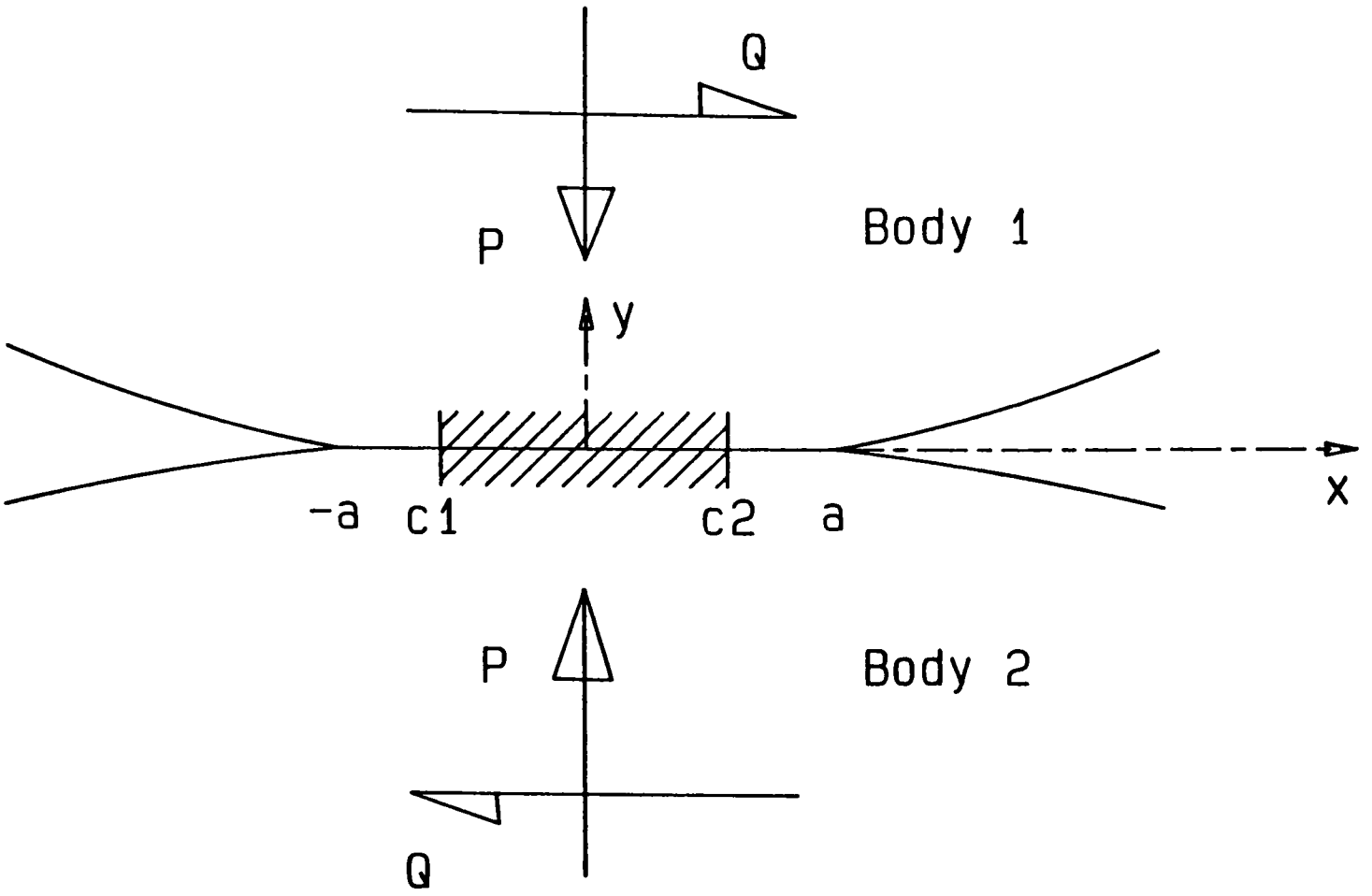

Fig. 6.1 Contact configuration

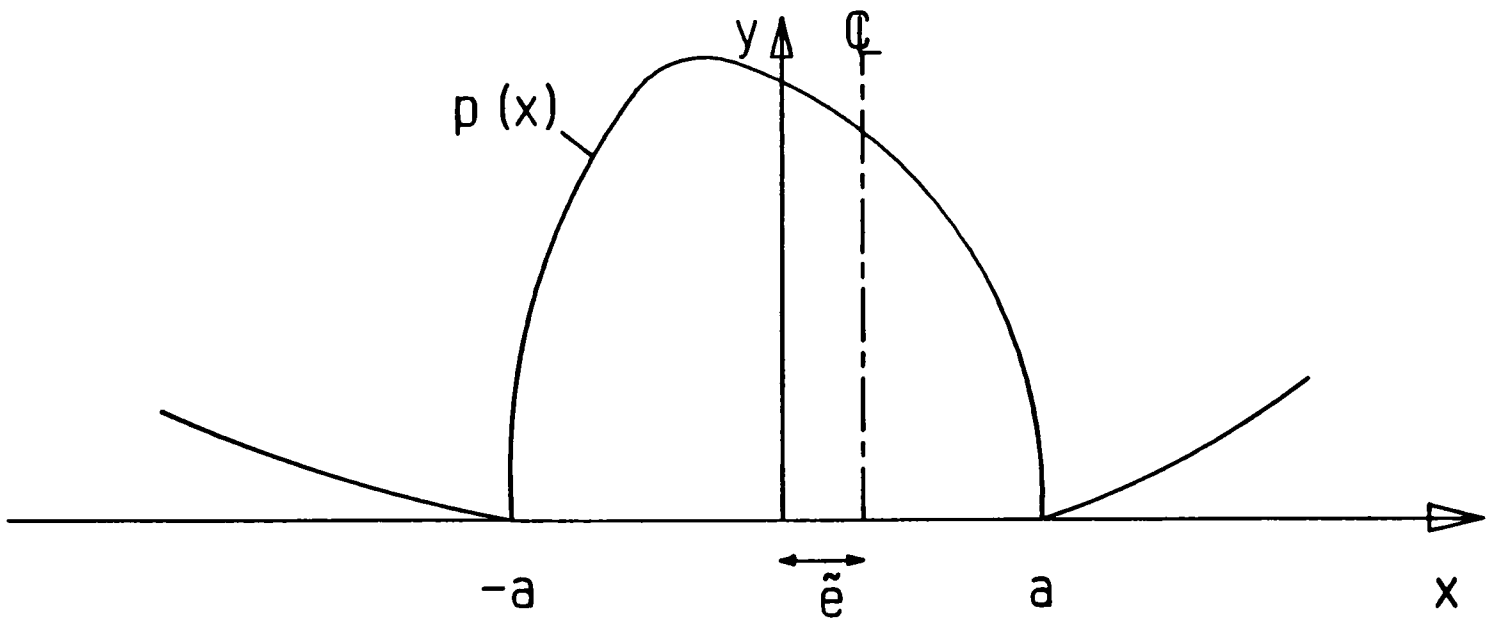

Fig. 6.2 Eccentricity of contact patch due to coupling

$$\frac{\partial v_1(x)}{\partial x} = \frac{\chi_1 + 1}{4\,\mu_1\,\pi}\int_{-a}^{a}\frac{p(\xi)\,d\xi}{x-\xi} - \frac{\chi_1 - 1}{4\,\mu_1}\,q(x) \qquad (6.1a)$$

$$\frac{\partial v_2(x)}{\partial x} = -\frac{\chi_2 + 1}{4\,\mu_2\pi}\int_{-a}^{a}\frac{p(\xi)\,d\xi}{x-\xi} - \frac{\chi_2 - 1}{4\,\mu_2}\,q(x) \qquad (6.1b)$$

where $|x| < a$ is the interval over which the tractions are distributed (Fig. 6.1), $\chi = 3 - 4\upsilon$ in plane strain, υ being Poissons ratio, and the subscripts 1 and 2 refer to bodies 1 and 2 respectively. If the contact semi-width is much less than the radii of curvature R_1, R_2 of the contacting bodies, the surfaces may be approximated as parabolae and (6.1a) and (6.1b) are related by

$$\frac{\partial v_1}{\partial x} - \frac{\partial v_2}{\partial x} = -\,k\,x \qquad (6.2)$$

where $k = 1/R_1 + 1/R_2 = 1/R$

Thus

$$\frac{1}{\pi}\int_{-a}^{a}\frac{p(\xi)}{x-\xi}\,d\xi - \beta\,q(x) = -\frac{k\,x}{A} \qquad |x| < a \qquad (6.3)$$

where

$$A = \frac{1-\upsilon_1}{\mu_1} + \frac{1-\upsilon_2}{\mu_2}$$

and

$$\beta = \frac{\frac{1-2\upsilon_1}{2\mu_1} - \frac{1-2\upsilon_2}{2\mu_2}}{\frac{1-\upsilon_1}{\mu_1} + \frac{1-\upsilon_2}{\mu_2}} \qquad \text{(Dundurs' Constant)}$$

The tangential surface displacements are given by Johnson (1985), Noble and Spence (1971) as

$$\frac{\partial u_1(x)}{\partial x} = \frac{\chi_1 + 1}{4\,\mu_1 \pi} \int_{-a}^{a} \frac{q(\xi)\,d\xi}{x - \xi} + \frac{\chi_1 - 1}{4\,\mu_1}\, p(x) \qquad (6.4a)$$

$$\frac{\partial u_2(x)}{\partial x} = -\frac{\chi_2 + 1}{4\,\mu_2 \pi} \int_{-a}^{a} \frac{q(\xi)\,d\xi}{x - \xi} + \frac{\chi_2 - 1}{4\,\mu_2}\, p(x) \qquad (6.4b)$$

Following Spence, a central stick zone is anticipated where prior straining of surface points before they enter the stick zone is proportional to $|x|$, due to self-similarity, Spence (1973). The bordering slip zones are of opposite sign. Thus

$$\frac{1}{\pi} \int_{-a}^{a} \frac{q(\xi)}{x - \xi}\, d\xi + \beta\, p(x) = \frac{C|x|}{A} \qquad |x| < c \qquad (6.5)$$

where C is a constant, unknown at this stage, and

$$q(x) = f\, p(x)\, \mathrm{sgn}(\beta x) \qquad c \leq |x| \leq a \qquad (6.6)$$

where f is the coefficient of friction. In addition, vertical equilibrium requires that the contact pressure be related to the applied load P by

$$P = -\int_{-a}^{a} p(x)\, dx \qquad (6.7)$$

The negative sign arises because P is taken as positive downwards, whereas p(x) is positive in tension (Fig. 6.1). Conditions of symmetry dictate that q(x) is an odd function, so that there is no resultant horizontal force. The slip direction must also be consistent with the direction of the friction force, so that for (6.6) to be true we must

verify *a posteriori* that

$$\text{sgn}(h(x)) = \text{sgn}\ (\beta x) \qquad c \leq |x| \leq a \qquad (6.8)$$

where

$$h(x) = \frac{\partial u_1}{\partial x} - \frac{\partial u_2}{\partial x} \qquad (6.9)$$

Cauchy integral equations (6.3) and (6.5) supplemented by (6.6) and (6.7) constitute a well-posed problem. However, the exact solution by the Weiner-Hopf technique is difficult, Spence (1968). A common approximation is to neglect the effect of shear tractions on vertical displacements (i.e. to drop the second term in (6.3)). This technique, known as the uncoupled approximation, was first employed by Goodman (1962) and is satisfactory if Poisson's ratio is large. The fully coupled problem, where the second term is retained will be treated here by a numerical technique which is appropriate for both normal indentation and the subsequent application of a tangential force.

6.3 Normal indentation

The numerical technique used is similar to that employed in chapter 4. A quadrature based on the representation of $p(x)$, $q(x)$ as families of Chebyshev polynomials was adopted (Erdogan, Gupta and Cook, (1973). This is ideally suited to representation of integrals with Cauchy singularities, and correctly accounts for the behaviour of the integrand as $x \to \xi$.

It is first recognised that, once a tangential force is applied, the contact pressure may become asymmetric (Fig 6.2) leading to a contact patch which is not central about the centreline of the indenter. Accordingly, the approach of Bentall and Johnson (1968) is followed and

the origin taken as the centre of the contact patch rather than the centreline of the indenter. An eccentricity $\tilde{e}$ is allowed for between this centreline and the origin. It should be noted that for the normal phase of loading, symmetry suggests that $\tilde{e}$ will be zero, but it is incorporated to facilitate the use of the same family of equations for the sequel, where a tangential load is applied.

Thus (6.3) must now be written as

$$\frac{1}{\pi} \int_{-a}^{a} \frac{p(\xi)}{x - \xi} d\xi - \beta\, q(x) = - \frac{k(x - \tilde{e})}{A} \qquad (6.10)$$

Equations (6.10) and (6.5) are normalised by substituting; $r = x/a$, $\eta = \tilde{e}/a$, $\tau = c/a$, $\zeta = \xi/a$, $\hat{p}(x) = \frac{a\, p(x)}{P}$, and $\hat{q}(x) = \frac{a\, q(x)}{P}$, giving

$$\frac{1}{\pi} \int_{-1}^{1} \frac{\hat{p}(\zeta)}{(r - \zeta)} d\zeta - \beta\, \hat{q}(r) = - \frac{k\, a^2 (r - \eta)}{A\, P} \qquad |r| < 1 \qquad (6.11)$$

and

$$\frac{1}{\pi} \int_{-1}^{1} \frac{\hat{q}(\zeta)}{(r - \zeta)} d\zeta + \beta\, \hat{p}(r) = \frac{C\, a^2\, |r|}{A\, P} \qquad |r| < \tau \qquad (6.12)$$

Since there is a central stick zone $|r| < \tau$ we represent $\hat{q}$ as

$$\hat{q}(r) = f\, \hat{p}(r)\, \mathrm{sgn}(r) \qquad |r| > \tau \qquad (6.13a)$$

$$\hat{q}(r) = f\, \hat{p}(\tau) \frac{r}{\tau} + \hat{q}'(r) \qquad |r| \leq \tau \qquad (6.13b)$$

where $\hat{q}'(r)$ is an unknown function equal to zero at $r = \pm \tau$. In subsequent equations it is assumed that $\beta > 0$.

Thus, (6.12) becomes

$$\frac{1}{\pi}\int_{-\gamma}^{\gamma}\frac{\hat{q}'(\zeta)}{(r-\zeta)}\,d\zeta = \frac{f}{\pi}\int_{-1}^{\gamma}\frac{\hat{p}(\zeta)}{(r-\zeta)}\,d\zeta - \frac{f\hat{p}(\gamma)}{\pi\gamma}\int_{-\gamma}^{\gamma}\frac{\zeta}{(r-\zeta)}\,d\zeta$$
$$- \frac{f}{\pi}\int_{\gamma}^{1}\frac{\hat{p}(\zeta)}{(r-\zeta)}\,d\zeta - \beta\,\hat{p}(r) + \frac{C\,a^2\,|r|}{A\,P} \qquad (6.14)$$

The method of Erdogan, Gupta and Cook (1973) is now used to reduce this integral equation to a set of simultaneous linear equations. The first integral is normalised by setting $s = r/\gamma$ and $z = \zeta/\gamma$. $\hat{q}'(z)$ is written as the product of a bounded function $\phi(z)$ and a weighting function $w(z) = \sqrt{1 - z^2}$. This permits the use of Gauss-Chebyshev quadrature to discretise (6.14) giving

$$\sum_{i=1}^{n}\frac{1 - z_i^2}{n+1}\,\frac{\phi(z_i)}{s_k - z_i} = \frac{f}{\pi}\int_{-1}^{\gamma}\frac{\hat{p}(\zeta)}{(r_k - \zeta)}\,d\zeta - \frac{f\hat{p}(\gamma)}{\pi\gamma}\int_{-\gamma}^{\gamma}\frac{\zeta}{(r_k - \zeta)}\,d\zeta$$
$$- \frac{f}{\pi}\int_{\gamma}^{1}\frac{\hat{p}(\zeta)}{(r_k - \zeta)}\,d\zeta - \beta\,\hat{p}(r_k) + \frac{C\,a^2|r_k|}{A\,P} \qquad (6.15)$$

where

$$z_i = \cos\left[\frac{i\,\pi}{n+1}\right] \qquad i = 1,\ldots n$$

$$s_k = \cos\left[\frac{\pi\,(2k-1)}{2\,(n+1)}\right] \qquad k = 1,\ldots n+1$$

$$r_k = \gamma s_k$$

Similarly, (6.11) is discretised by setting $\hat{p}(r) = \psi(r)\sqrt{1 - r^2}$ to give

$$\sum_{i=1}^{n} \frac{1 - r_i^2}{n + 1} \frac{\psi(r_i)}{t_k - r_i} = \beta \hat{q}(t_k) - \frac{k a^2 t_k}{A P} + \frac{k a^2 \eta}{A P} \qquad (6.16)$$

where

$$r_i = \cos\left[\frac{i \pi}{n + 1}\right] , \qquad i = 1,\ldots n ,$$

$$t_k = \cos\left[\frac{\pi (2k - 1)}{2 (n + 1)}\right] , \quad k = 1,\ldots n+1 .$$

A partial check on the implementation of the above equations on a computer may be carried out by setting $\beta = 0$ in (6.16) and solving (6.15) and (6.16) to obtain a numerical solution to the uncoupled problem treated analytically by Nowell, Hills, and Sackfield (1988). Equation (6.16) now leads directly to the Hertzian solution

$$\hat{p}(r) = - \frac{2}{\pi} \sqrt{1 - r^2} \qquad (6.17)$$

which is substituted into (6.15). The required ratio of β/f is chosen and an appeal to self-similarity is made to determine the consistent stick zone size, τ. This is given by Spence (1973) as

$$\beta K(\tau) = f K'(\tau) \qquad (6.18)$$

for all polynomial indenters, when the problem is treated as uncoupled. Here $K(\tau)$ is a complete elliptic integral and the notation $K'(\tau)$ implies replacing the argument τ by $\sqrt{1 - \tau^2}$. The integrals on the right hand side of (6.15) are evaluated numerically using Clenshaw-Curtis integration (Piessens, Van Roy-Branders and Mertens, (1976)) and (6.15) solved as a set of n+1 linear equations in n+1 unknowns (n values of $\phi(z_i)$ together with $\frac{C a^2}{A P}$). Numerical results obtained in this way with n = 20 are almost indistinguishable from those obtained theoretically (Nowell, Hills, and Sackfield (1988)). As might be expected from arguments of self-simlarity, the consistent value of τ

leads to a solution where h(x) and h'(x) are continuous at the stick/slip boundary.

The solution of the fully coupled problem is more complex. This time β and f appear independently rather than as the ratio β/f. Again an appeal to self-similarity is made to determine the consistent stick zone size τ. The exact solution (Spence (1973)) involves the Perron root of an infinite matrix, but alternative more tractable approximations are given, viz. as the root of one of the following equations, which are asymptotic solutions, but in practice enable the entire range of values of τ to be covered accurately. If $\tau \lesssim 0.6$,

$$\frac{\pi \ \alpha}{\ln \{(1 - \beta^2)^{-1}\}} = \left[\frac{K'(\tau)}{K(\tau)} - \frac{\pi \ \theta}{3}\right]^{-1} \qquad (6.19)$$

where $f\beta = \tan(\pi\theta)$ and K' and K are the elliptic integrals already defined, whilst if $\tau > 0.6$

$$\frac{\tan^{-1} f}{\kappa} = \tanh^{-1} \tau + \aleph(\tau,\kappa) + \ln 2 \qquad (6.20)$$

where

$$\kappa = \frac{2}{\pi} \tanh^{-1} \beta$$

and

$$\aleph(\theta,\kappa) \approx \frac{\theta \ \pi^2}{12}\left[1 + 0.2326 \ \pi\theta + \frac{\pi^2}{15}\left[\theta^2 - \frac{\kappa^2}{4}\right]\right]$$

Once τ has been determined, the coupled equations (6.15) and (6.16) are solved by sequential iteration. As a starting point, a Hertzian distribution is assumed for $\hat{p}(r)$. Equation (6.15) is now solved for ϕ, allowing an estimate $\hat{q}_o(s)$ for $\hat{q}$ to be calculated. Krenk's interpolation formulae (Krenk (1975)) are then used to evaluate $\hat{q}_o$ at the correct

collocation points t_k for (6.16) and this set of equations can now be solved in conjunction with the discretised form of (6.7) to find a revised pressure distribution $\hat{p}_1(r)$. Iteration between the two sets of equations continues until convergence is achieved, whereupon distributions $\hat{p}_n(r)$, $\hat{q}_n(s)$ have been found which satisfy both (6.15) and (6.16) and are thus solutions to the coupled problem. Also revealed are numerical values for $\frac{C\,a^2}{A\,P}$, $\frac{k\,a^2}{A\,P}$ (the contact law), and $\frac{k\,a^2\,\eta}{A\,P}$ (the eccentricity, which, as expected, is found to be zero for the case of normal indentation). These three supplementary values are found since the solutions for $\hat{p}(x)$ and $\hat{q}(x)$ are both bounded and enforcement of the associated side condition gives rise in the numerical quadrature to an extra equation (equations 6.15 and 6.16). Further, the requirement of vertical equilibrium yields an additional equation, and thus there are 2n+3 equations for as many unknowns.

In all the cases studied convergence to three significant figures was found to have occurred before four complete iterations. As with the uncoupled case, choice of the consistent value for γ (from self-similarity) gave results which were continuous in h(x) and h'(x) at the stick/slip interface. It would therefore have been possible to use this condition to determine γ instead of Spence's results (equations 6.19,6.20), to make the analysis self-contained, but this technique would have required a further sequence of iteration.

6.4 Results - Normal indentation

As stated above, the numerical analysis of the uncoupled problem gave almost identical results to an analytical solution due to Sackfield (Nowell, Hills, and Sackfield (1988)). Satisfactory results were

obtained with n set to 10 or greater. Those presented here used a value of 20 since there was no significant penalty in computing time and more data points are obtained. Variation of the stick zone size with β/f is shown in Fig. 6.3., together with the corresponding results for the coupled case. As expected, coupling only has a significant effect at higher values of β/f. Although values of stick zone size can be calculated for $|\beta| > 0.5$ these never occur in practice and are not shown.

Figure 6.4 shows the traction distributions obtained using the uncoupled approximation, whereas Fig. 6.5 demonstrates the effect of coupling on surface tractions for two sample cases ($\beta = 0.2$, $f = 0.8$, and $\beta = 0.4$, $f = 0.5$). The first represents a typical value of β for dissimilar materials (eg. Alumina on glass) with a high coefficient of friction. The uncoupled and fully coupled solutions are almost identical at this value of β although both are significantly different from the Hertz solution as substantial shear tractions arise. Figure 6.5b shows the larger difference between the two solutions at $\beta = 0.4$, which is about the largest value conceivable for real materials (steel on concrete). It can be seen that coupling increases the peak contact pressure at the expense of that nearer the edges of contact. There is a corresponding decrease in the contact area. The ratio of actual to Hertzian contact area can be found from Fig. 6.6. although it should be noted that the effect is only slight at practical values of β and f. Real contact areas are never less than 90% of those predicted by Hertz.

Figure 6.7 demonstrates the variation of the parameter $\frac{C\,a^2}{A\,P}$, which characterises the relative strain in the stick zone, with β and f. Once again divergence between the fully coupled solution and the uncoupled approximation is only significant at high values of β/f (>1.0).

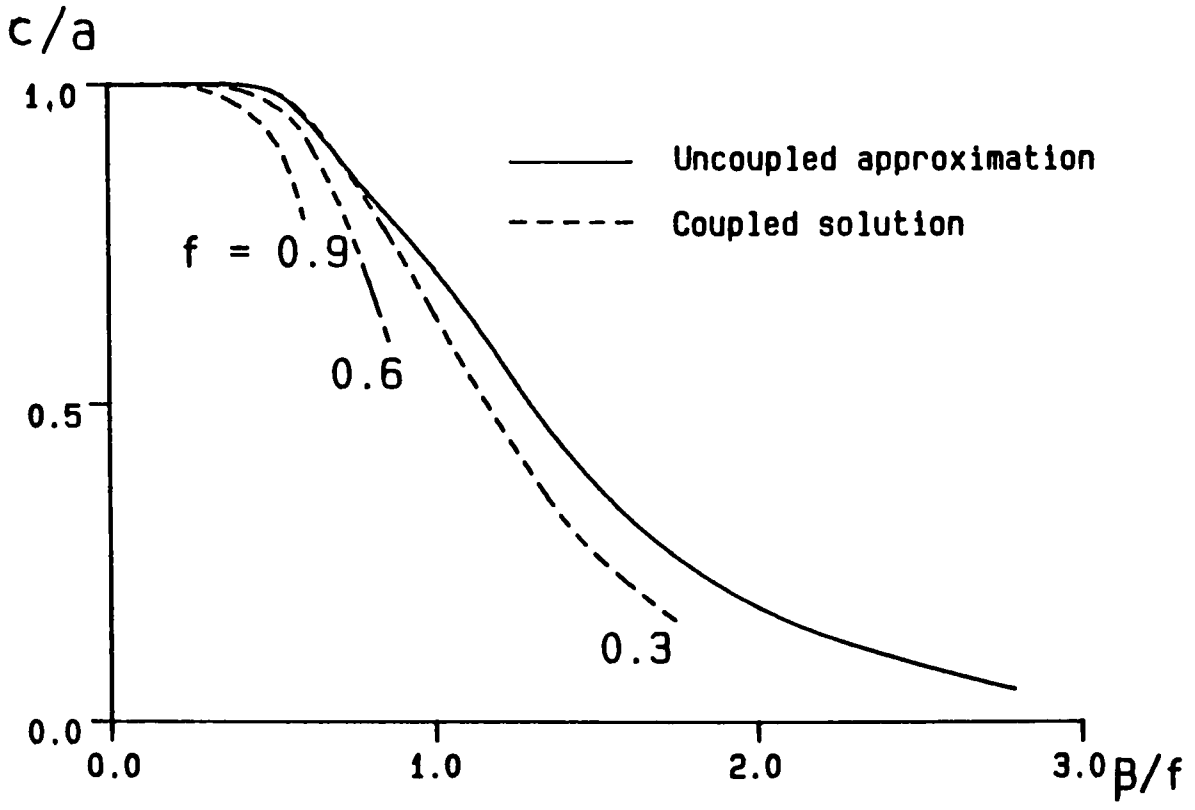

Fig. 6.3 Variation of stick zone size with β and f

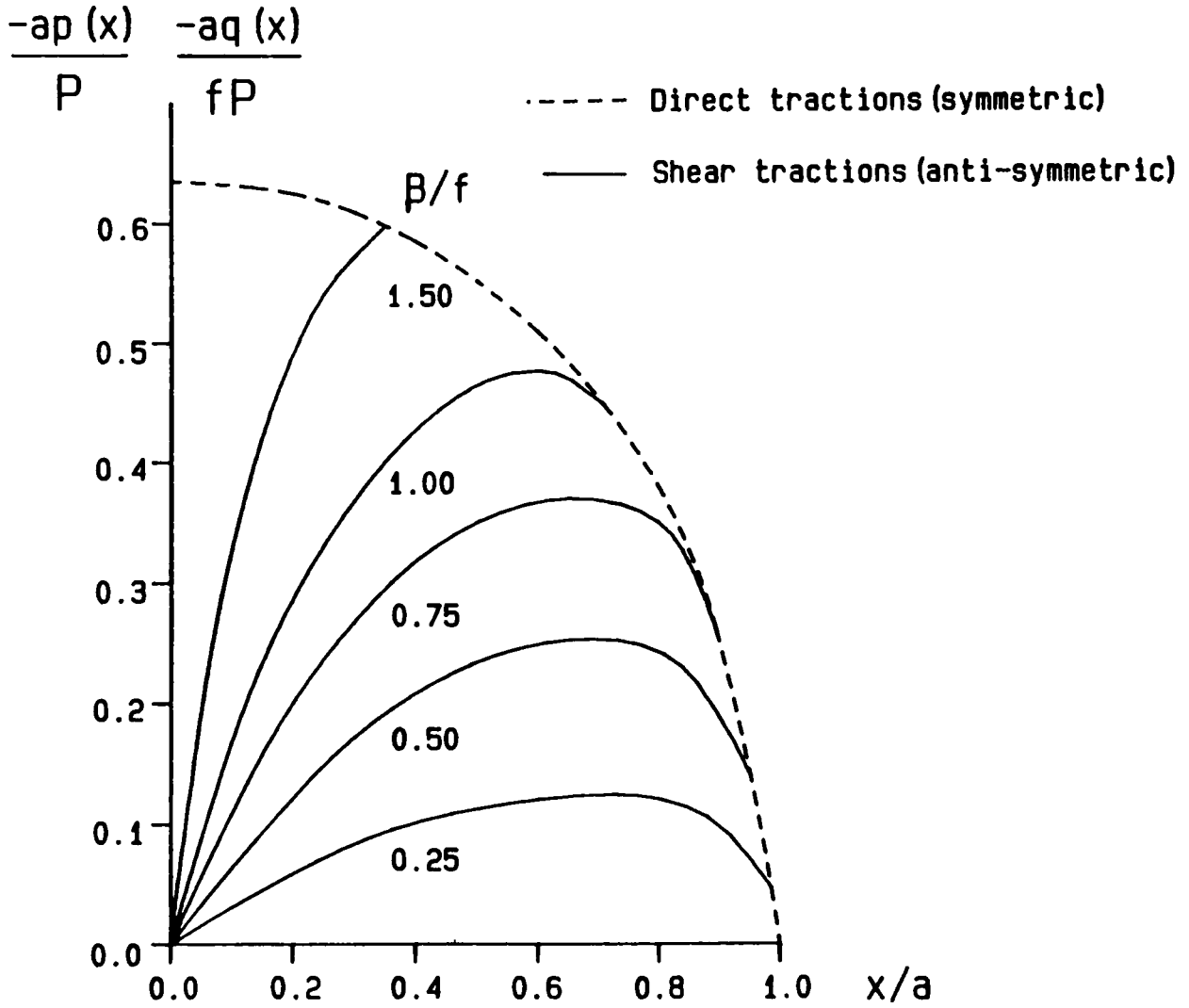

Fig. 6.4 Uncoupled approximation, direct (symmetric) and shear (antisymmetric) tractions

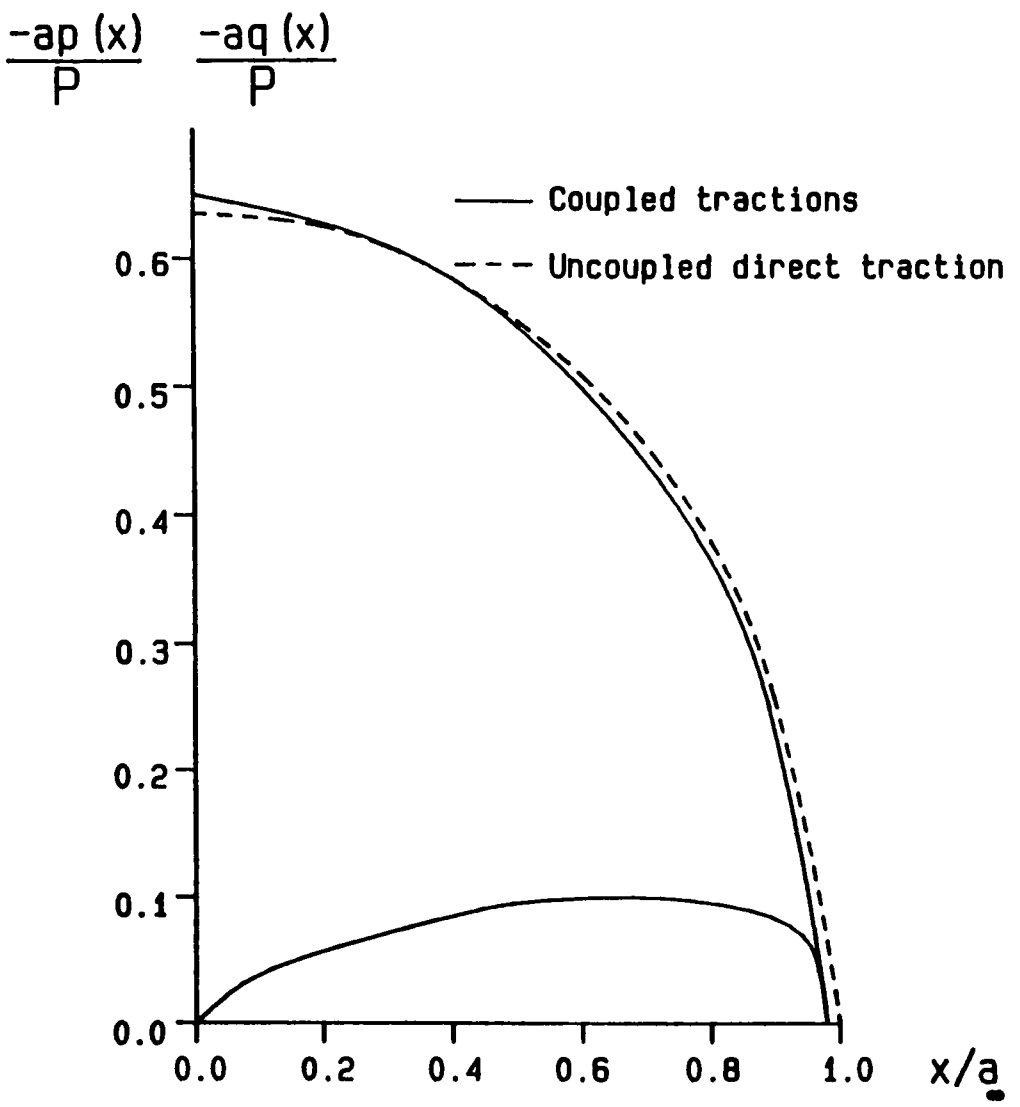

Fig. 6.5 Coupled case, direct (symmetric) and shear (anti-symmetric) tractions
(a) $\beta = 0.2$, $f = 0.8$, $c/a = 0.99975$
(b) $\beta = 0.4$, $f = 0.5$, $c/a = 0.750$

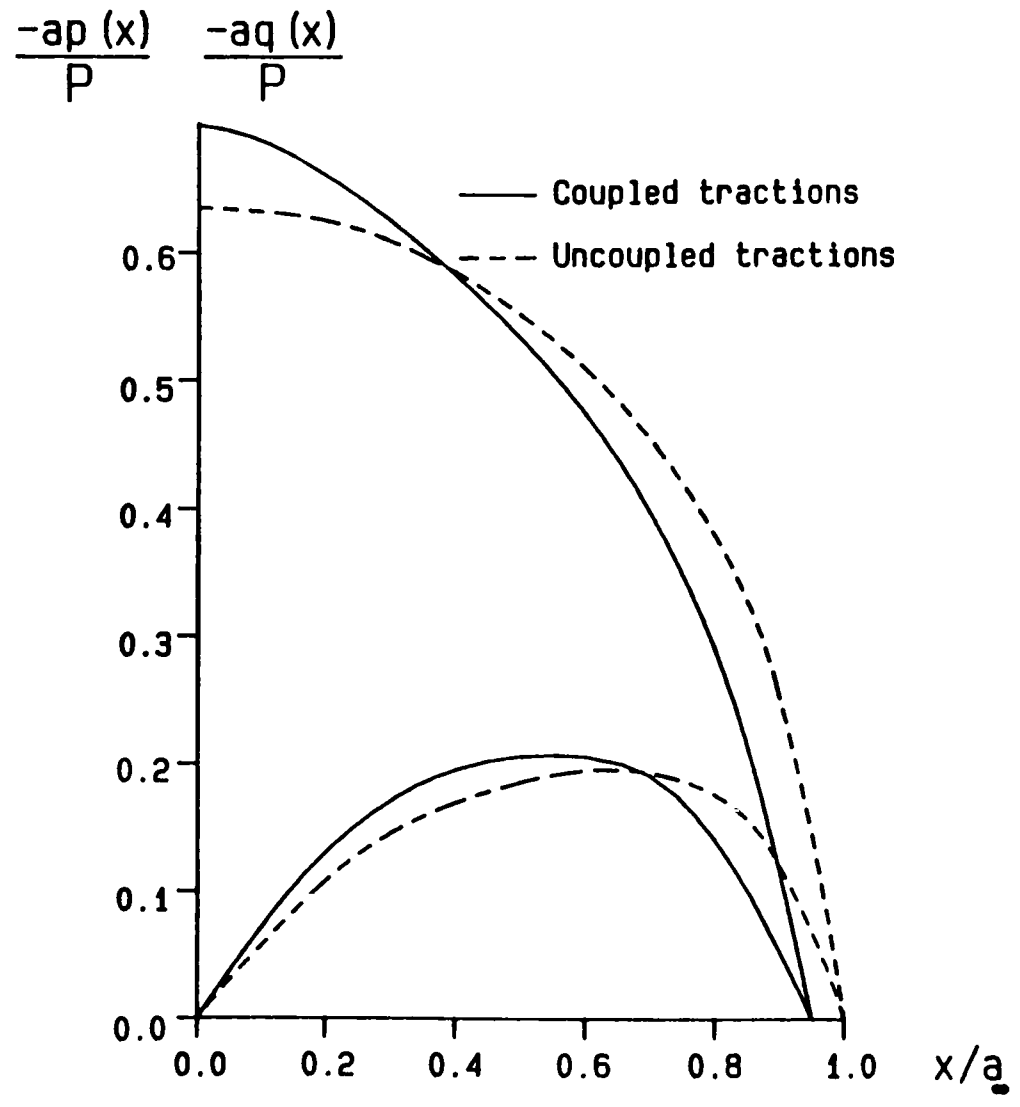

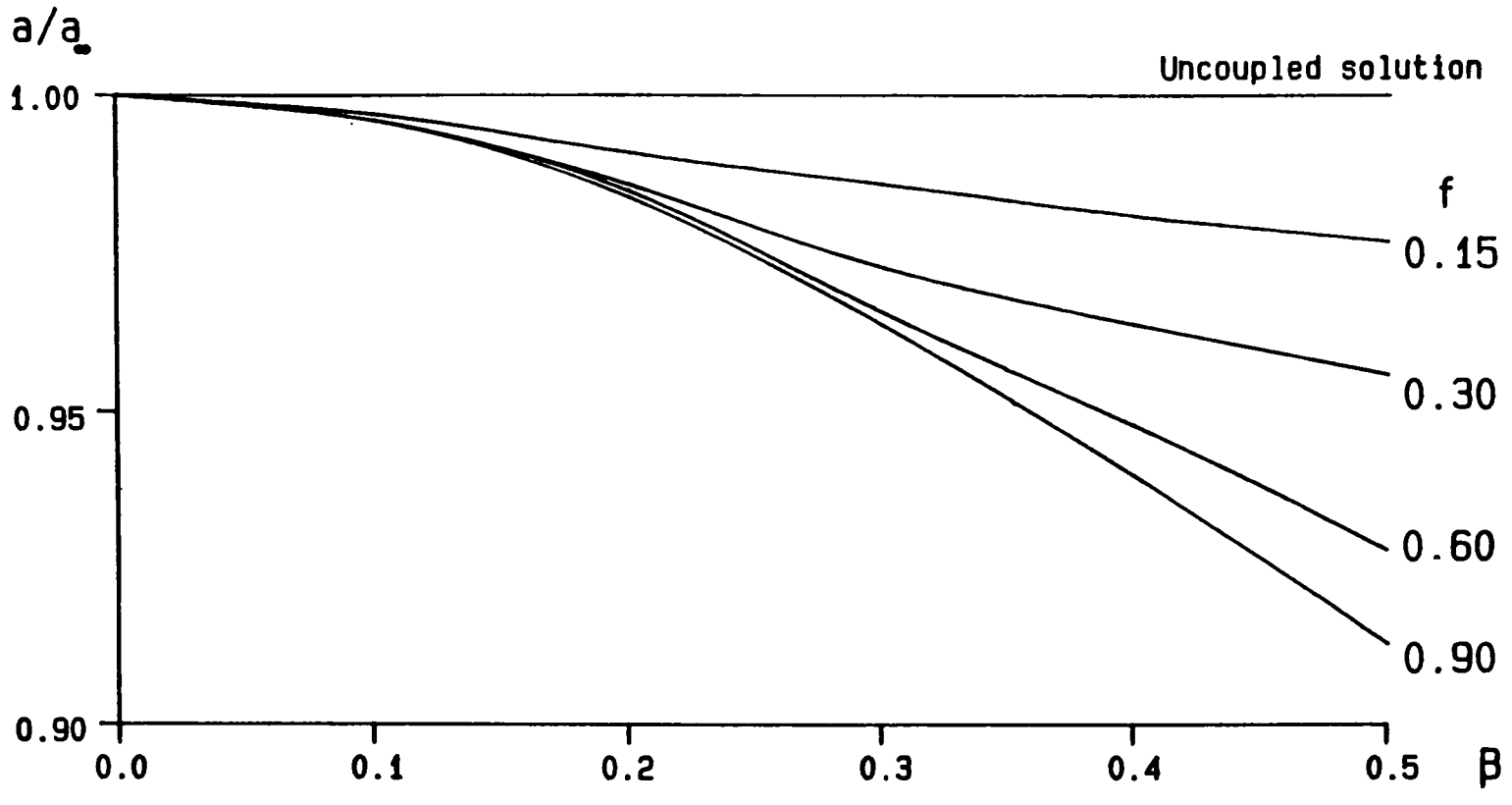

Fig. 6.6 Variation of contact size with β and f

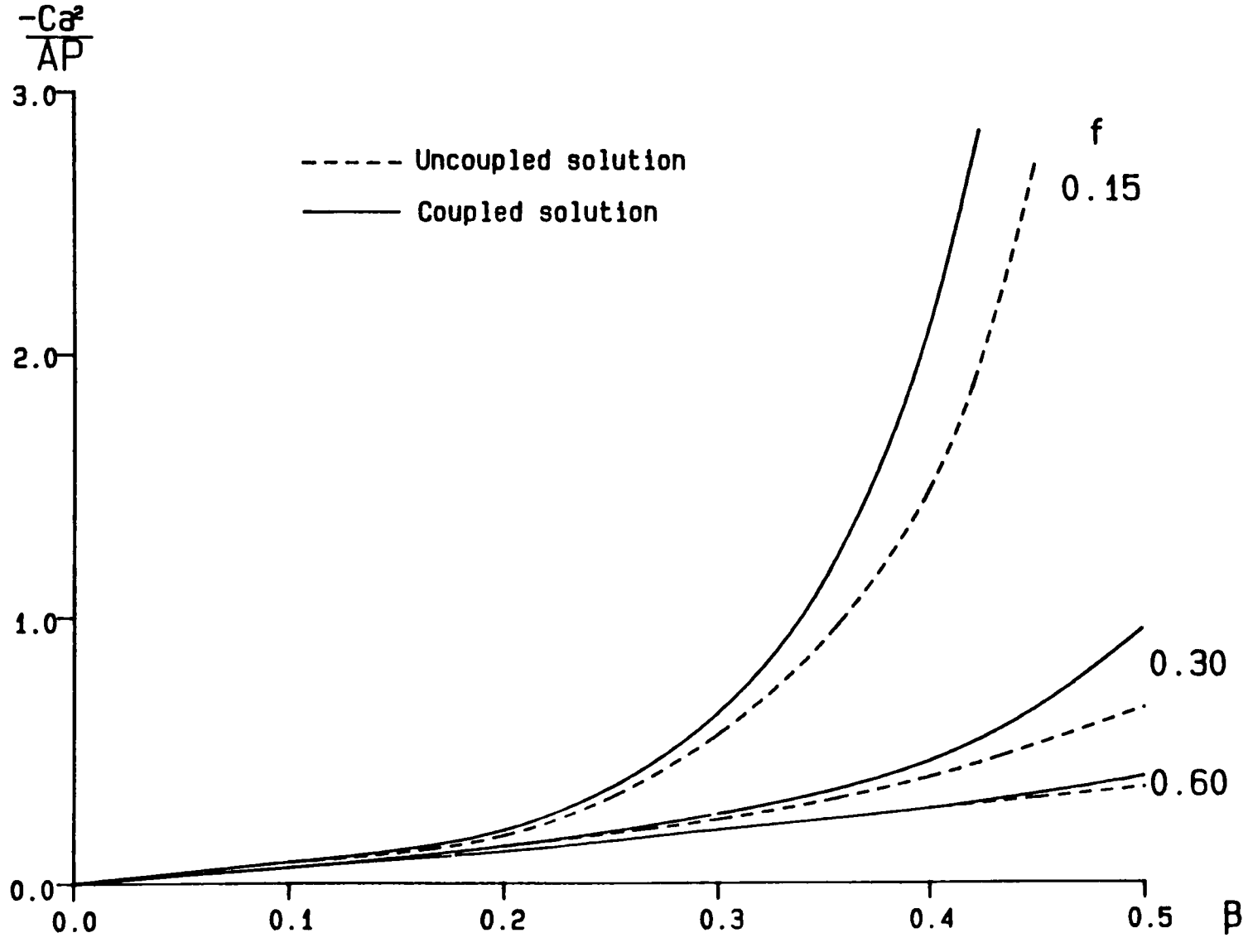

Fig. 6.7 Variation of Ca^2/AP with β and f

6.5 Tangential loading

In fretting fatigue experiments the indenters are first pressed against the specimen by a normal load and then subjected to an oscillating tangential load to produce the fretting. As a first step towards the solution of this problem it is convenient to consider the case where dissimilar cylinders are first loaded by a normal force P and then subjected to a monotonically increasing tangential force Q. This is effectively the equivalent of the Mindlin problem for dissimilar elastic cylinders.

At the end of the normal phase of loading shear tractions similar to those shown in Figs 6.5. exist whereby a central stick zone $-c < x < c$ is bordered by slip zones with shear tractions of opposite sign, Fig. 6.8a. Consider now an incremental tangential force ΔQ applied to the contact. The effect will be to increase the shear tractions in one slip zone and decrease them in the other. This is accompanied by a small relative displacement in the direction of the augmented shear. In the region of depleted shear ($-a < x < 0$). the shear tractions and relative 'slip velocity' have opposite sign, which violates the friction law (6.8) and hence instantaneous adhesion results over the region $-a < x < c$, Fig. 6.8b. As Q is increased further, slip re-starts at $x = -a$, but in the same direction as that in the interval $c < x < a$.

The application of a tangential force Q therefore results in an instantaneous growth of the stick zone followed by a monotonic reduction in its size. This effect can be exploited to solve the problem in the following way; surface tractions at the end of the normal loading phase are found using the method of section 6.3. The resulting values of relative tangential strain ($h(x) = \frac{\partial u_1}{\partial x} - \frac{\partial u_2}{\partial x}$) throughout the contact are

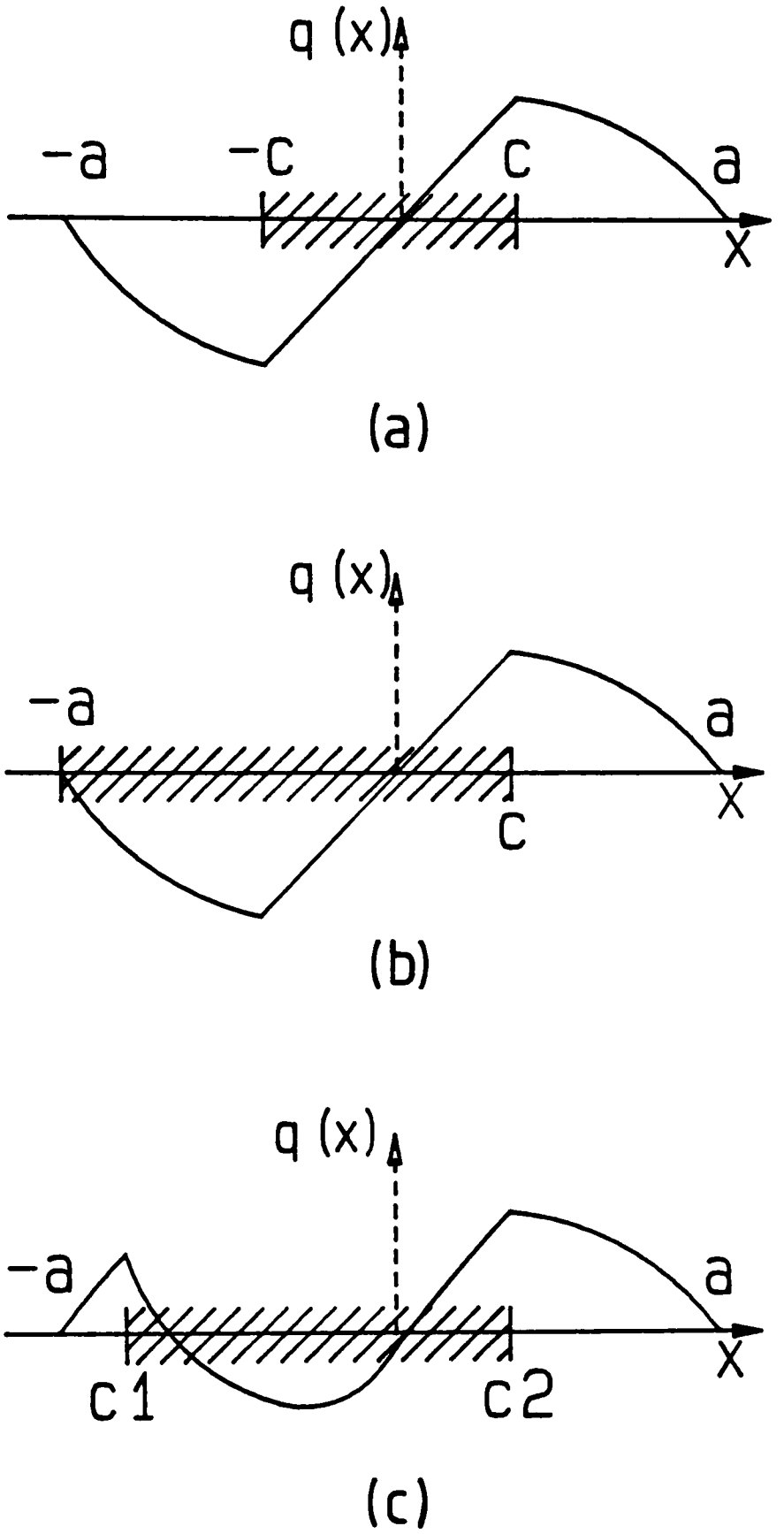

Fig. 6.8 Schematic shear traction distributions
(a) after normal loading
(b) with incremental tangential force ΔQ applied
(c) with significant tangential force applied

then calculated using (6.4) and stored. Adhesion is now expected over the range $c1 < x < c2$, Fig. 6.8c, bordered by slip of the same sign, and consequently (6.12) is re-written as

$$\frac{1}{\pi} \int_{\gamma 1}^{\gamma 2} \frac{\hat{q}''(\zeta)}{(r - \zeta)} \, d\zeta = \frac{-f}{\pi} \int_{-1}^{1} \frac{\hat{p}(\zeta)}{(r - \zeta)} \, d\zeta - \beta \hat{p}(r) + \frac{a^2}{A P} h(r) \tag{6.21}$$

where

$$\hat{q}(r) = f \hat{p}(r) + \hat{q}''(r) \qquad \gamma 1 < r < \gamma 2$$

and $\gamma 1 = c1/a$, $\gamma 2 = c2/a$. This equation is then discretised in a similar manner to (6.14) and solved in conjunction with (6.16). An immediate difficulty arises, however, in that $\gamma 1$ and $\gamma 2$ are unknown *a priori*. But, it will be noted that discretisation of (6.21) yields (n+1) equations in n unknowns $\phi(z_i)$, since in this case there is no constant C to be determined, as the stick zone is receding. The (n+1)th equation is equivalent to the consistency condition for the integral equation (Erdogan, Gupta and Cook (1973)) and the procedure adopted is as follows: trial values of $\gamma 1$ and $\gamma 2$ are chosen and the (n+1)th equation dropped. The coupled sets of equations are then solved using the iterative technique developed in section 6.3. Next, a check is made to see if the solution satisfies the (n+1)th equation and, if is not, $\gamma 2$ is adjusted and the problem re-solved[1]. Once a consistent solution has been acheived the value of the applied force Q producing this distribution of tractions

---

[1]This procedure is needed since what is, in reality, an incremental problem is being solved by finite steps. The enforcement of the side condition is equivalent to ensuring (6.8) obtains within the slip zones, and $|q(x)| < -fp(x)$ in the stick zones.

is calculated using

$$Q = \int_{-a}^{a} q(x)\, dx \qquad (6.22)$$

Although frictional loading problems should generally be treated incrementally because of the dependence on previous load history, in this case the stick zone is always receding and it is permissible to go straight from the result for normal indentation to that for any subsequently applied tangential load.

6.6 Results - tangential loading

Results are given in Fig. 6.9a for $\beta = 0.4$, $f = 0.5$, which gives rise to the maximum amount of coupling that is likely to occur in practice. It will be seen that the stick zone is substantially offset when compared with that predicted by the Mindlin-Cattaneo analysis whose results are plotted for comparison in Fig. 6.9b. The asymmetric distribution of direct tractions can be clearly seen in Fig. 6.9a for $Q/fP = 0.9$ and it is this which leads to the tangentially shifted contact patch predicted in section 6.3. At intermediate values of β or low f coupling is modest and the approximation including only one coupling term (Goodman's approximation) may be used to obtain accurate results without necessitating the iterative approach. Figures 6.3, 6.6, and 6.7 may be used as a guide to the divergence of the two solutions (ie. retaining one or both coupling terms) for given values of β and f.

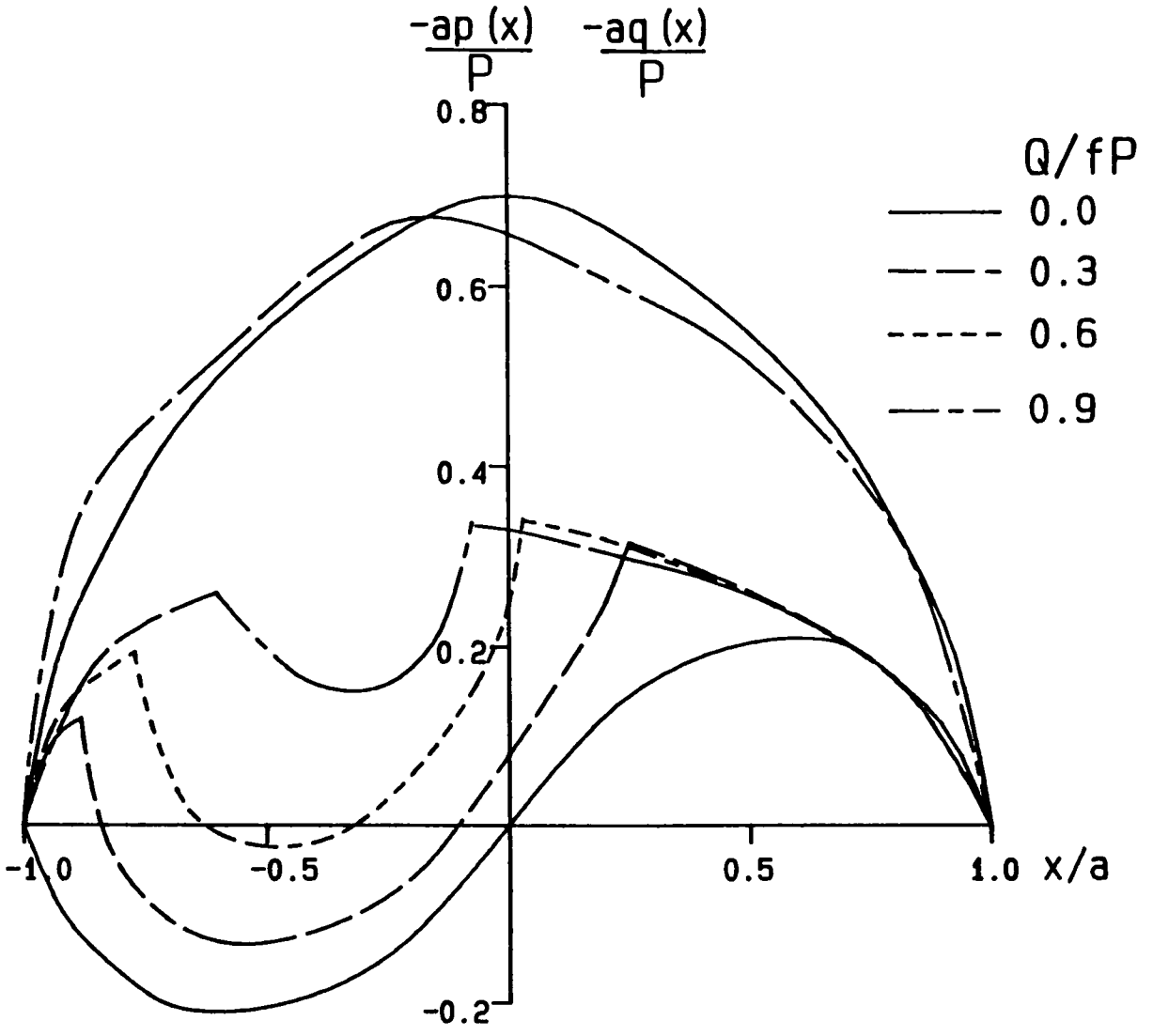

Fig. 6.9 Surface tractions during application of monotonically increasing tangential force, f = 0.5
(a) coupled case, $\beta = 0.4$
(b) elastically similar solution (Mindlin)

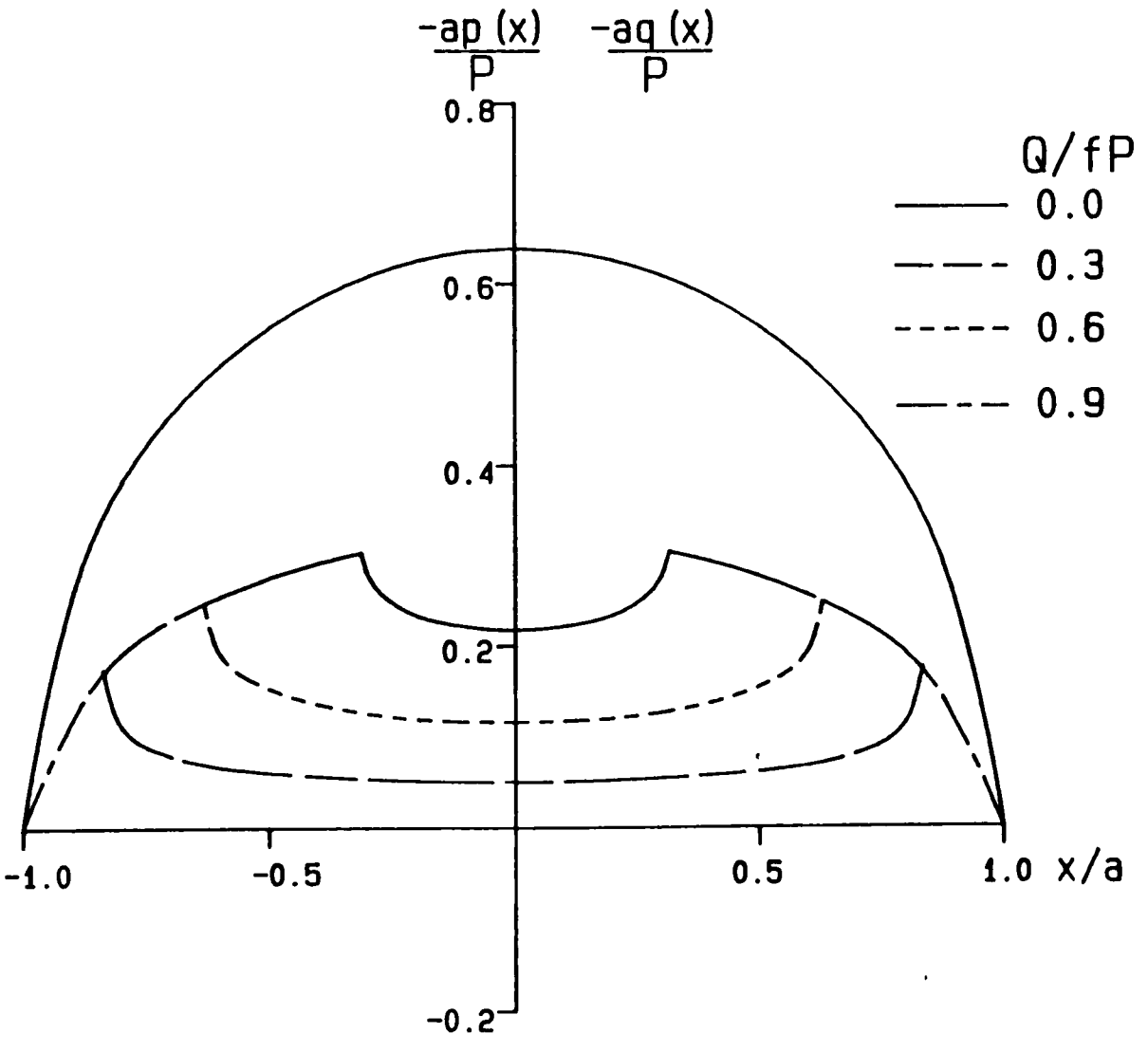

6.7 Oscillating Tangential force

It is now possible to extend the technique to model the effects of an oscillating tangential force varying between the limits $\pm Q_{max}$. Suppose Q is increased from 0 to $+Q_{max}$ in the manner described above. Subsequent application of an increment $-\Delta Q$ will result in instantaneous stick over the entire contact area, followed by the onset of reverse slip at the edges as the magnitude of this reverse load is increased (Mindlin and Deresiewicz (1953)).

The basic solution for monotonically increasing Q can be adapted in the following way; a solution is obtained for the application of P followed by $+Q_{max}$. h(r) is then calculated under this loading and stored. Equation (6.21), is now re-solved with new stick zone boundaries $\gamma 1'$ and $\gamma 2'$ and reverse slip in the regions $-1 < r < \gamma 1'$, and $\gamma 2' < r < 1$. $\gamma 1'$ and $\gamma 2'$ are adjusted until they are are both self-consistent, and the resultant shear force is equal to $-Q_{max}$. This process may then be continued if a forward load is re-applied.

Space considerations preclude a comprehensive presentation of the results, since β, f, and Q_{max}/fP are all independent variables. Typical results are shown in Fig. 6.10a for a case where the uncoupled approximation has been retained ($\beta/f = 1.0$, $Q_{max}/fP = 0.5$). and in Fig 6.10b for the corresponding problem where $\beta = 0$, ie. the bodies are elastically similar, and the Mindlin-Cattaneo model applies. In all the cases studied steady state traction distributions had evolved after the application of three complete loading cycles. It will be noted that in the example shown, the steady state stick zone is much larger than that when the tangential force is first applied, and is similar to that predicted by the Mindlin analysis, although the shear traction

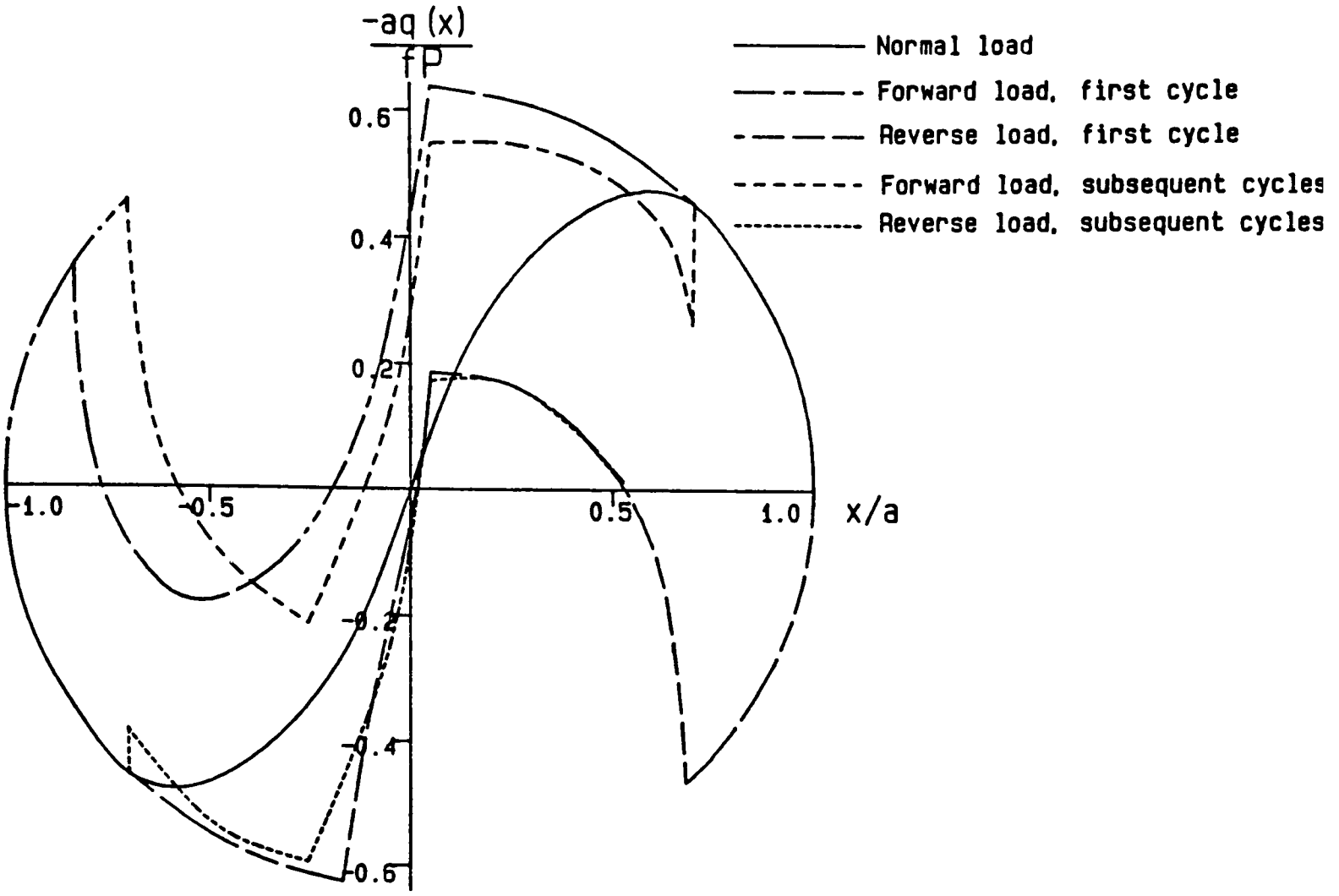

Fig. 6.10 Shear tractions during cyclic loading, $Q_{max}/fP = 0.5$

(a) uncoupled solution, $\beta/f = 1.0$
(b) elastically similar solution Mindlin)

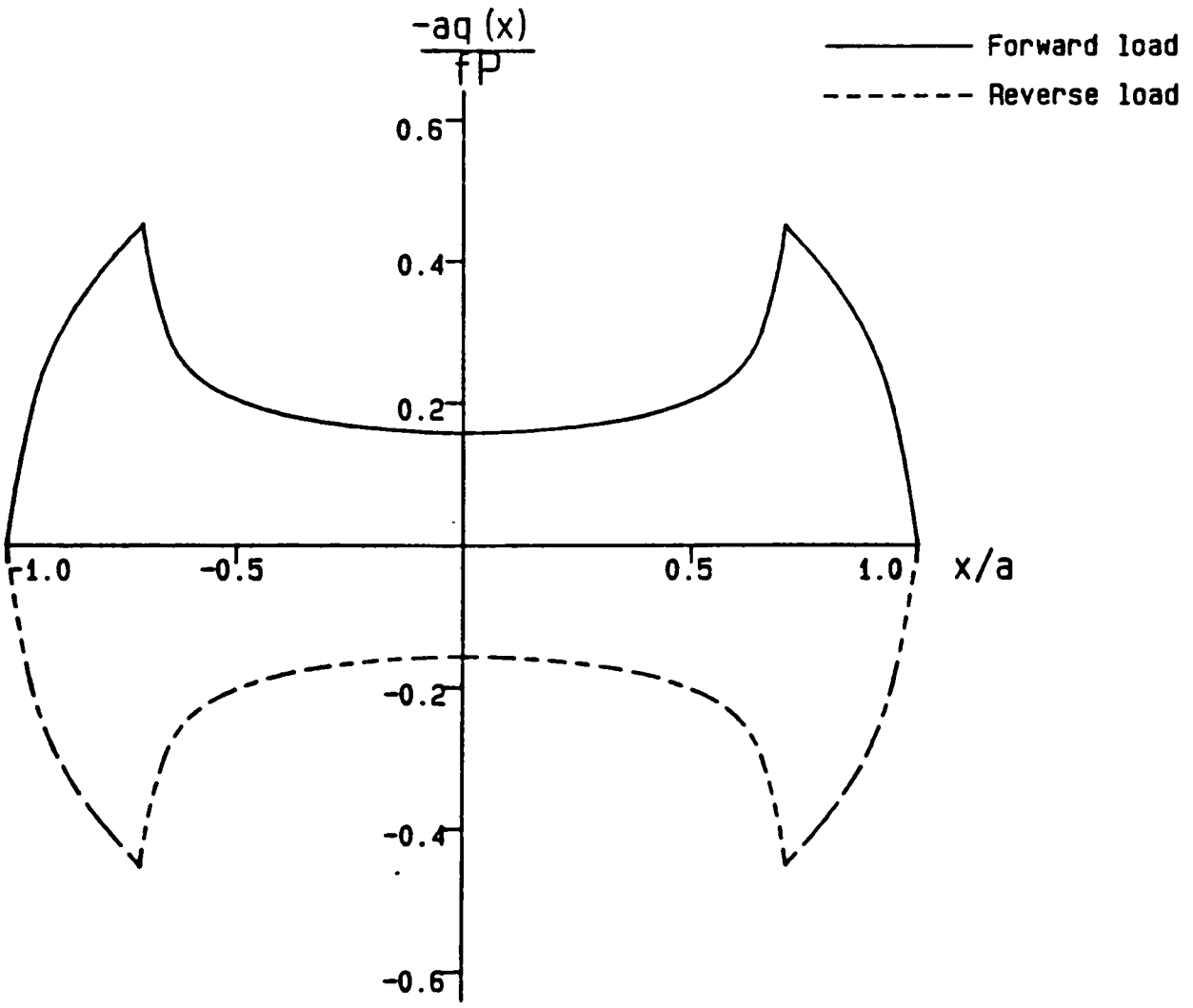

distribution is substantially altered. A similar problem of fretting of a rigid crowned indenter on an elastic strip has been studied by Keer and Farris (1986) and they too report a complex variation of the stick-slip boundary during the first few cycles of fretting together with a growth of the stick zone.

6.8 Discussion

A numerical technique has been developed to deduce the interfacial tractions which arise during the contact of dissimilar elastic cylinders under normal and tangential loading. The results may be are compared to those produced by an analytical treatment of the case where the effect of shear tractions on normal displacement is neglected (Nowell, Hills, and Sackfield (1988)). The results of both analyses with this uncoupled assumption are in excellent agreement. The numerical technique can be extended to treat the fully coupled case as first developed by Spence (1973) for a flat punch. The results show that the uncoupled approximation is reasonable for values of $\beta/f < 1.0$, which will be the case in most practical applications since β rarely exceeds 0.2 for contact between engineering materials, and low values of friction give rise to proportionately small shear tractions.

The previously unsolved problem posed by subsequent application of normal and tangential loads may be treated by this numerical approach and results have been presented for application of both monotonically increasing and oscillating tangential loads. The growth of the stick zone during the first few cycles is found to be complex and each specific problem of this nature is best analysed separately. The analysis renders the use of cylindrical indenters possible in fretting tests on dissimilar

elastic materials for which a subsequent stress analysis is contemplated.

In practice, steel indenters were not used in the present series of experiments on the fretting of aluminium alloy. It proved difficult to obtain the required barrelled rollers in a sufficiently large range of diameters to permit a reasonable variation of contact semi-widths. The original problem, that edge conditions might affect the fatigue life of the specimen was not found to be a serious difficulty, provided that sufficient care was taken in aligning the fretting pads. The use of pressure sensitive film helped considerably in this respect.

The use of elastically dissimilar fretting pads may, however, have certain advantages. The surface roughness of the pads can have a significant effect on the surface traction distribution, as will be discussed in chapter 8. The higher quality of finish obtainable with steel pads might prove beneficial in fretting tests on aluminium alloys. The present analysis would be useful in analysing such a configuration and in assessing the degree of approximation implicit in applying the Mindlin (1949) analysis to the configuration.

A similar problem to that analysed in this chapter is that of tractive rolling of dissimilar elastic cylinders. This problem was first solved by Bentall and Johnson (1967) using a piece-wise linear model, although their paper concentrates largely on 'free' rolling where no net shear force is transmitted between the rollers. The integral equation technique can be extended to treat this configuration and the analysis brings out several interesting points. The treatment of this configuration is included here in Appendix C since it may be helpful to study it in the context of the other contact problems dealt with in the main body of the thesis. It has, however, no direct application to the fretting problem.

Chapter 7

The effect of surface roughness

7.1 Introduction

The analysis carried out so far to determine the contact stresses has retained the assumption, implicit in the Hertz analysis, that the surfaces are smooth. Real surfaces all exhibit some degree of surface roughness although it is possible by precision finishing to reduce this to a degree where the amplitude of the roughness is so small as to have negligible effect on the Hertz solution.

In preparing the pads and specimens for the experiments reasonable care was taken to ensure that a good surface finish was produced without going to the elaborate lengths that would be involved in surface polishing. A surface roughness of 0.4 μm r.m.s. was specified for both the pads and specimens. The fretting pads were produced by milling on an N/C machining centre and a surface finish of 0.3 μm r.m.s.was obtained. A typical Talysurf trace taken parallel to the axis of the cylindrical portion of a pad is shown in Fig. 7.1.

The surface of the specimens to be subjected to fretting was finished by surface grinding perpendicular to the specimen axis. The alloy used did not react well to this process and surface values in the range 0.5 → 1.0 μm r.m.s. were obtained. This represented an improvement on the unground surface, but was not as good as that obtained on the pads. A typical Talysurf trace taken perpendicular to the direction of grinding is presented in Fig. 7.2. The almost regular grinding marks can clearly be seen. These have a wavelength of about 0.15 mm, which is of

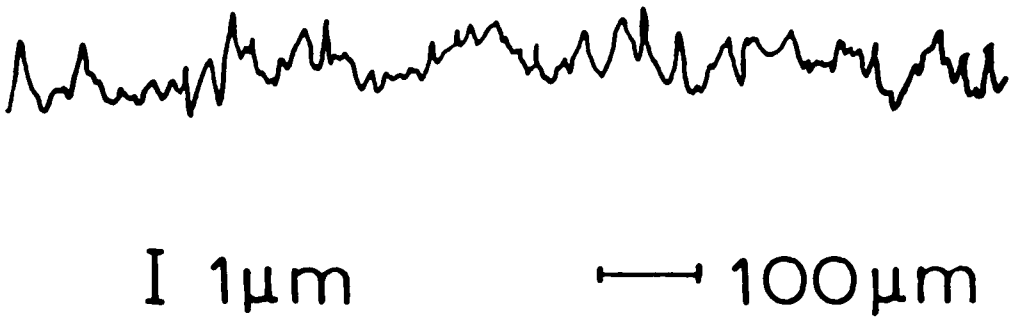

Fig. 7.1 Surface profile of fretting pads

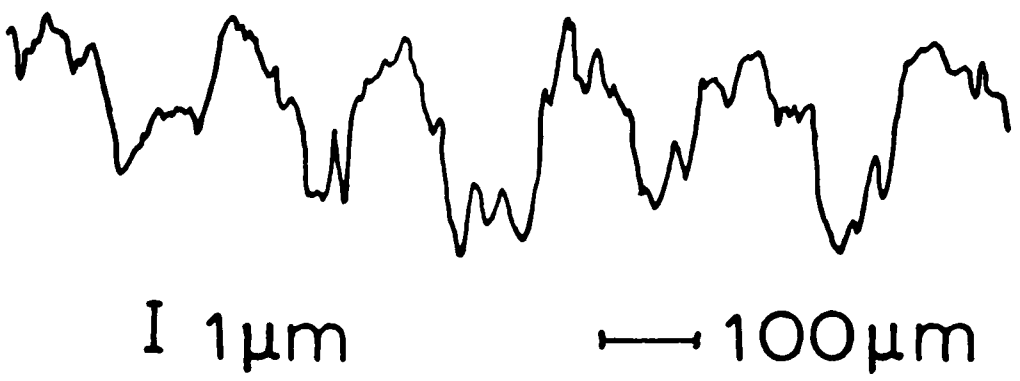

Fig. 7.2 Surface profile of specimen

the same order as the experimental contact widths (0.2 → 2.0 mm). The presence of such undulations will clearly affect the surface tractions developed and, to some degree, the corresponding subsurface stress state. From St. Venant's principle, the stress state distant from the surface might be expected to be the same as that produced by smooth contact. In order to test the validity of applying a smooth model to the analysis of contact of rough surfaces it is important to determine the region of the half plane over which the roughness has a significant effect on the stress field.

7.2 Random rough surfaces

Surface roughness has two distinct effects on the surface tractions developed between contacting elastic bodies. Before discussing these a distinction must first be drawn between the true pressure at a point p(x) and the mean pressure or expected pressure p^*. This mean pressure is given by:

$$p^*(x) = \int_0^\infty \phi(\xi)p(\xi)\, d\xi \qquad (7.1)$$

where $\phi(\xi)$ represents the probability that $p = p(\xi)$.

Instead of producing continuous contact, rough bodies will interact at a series of discrete points corresponding to the tips of asperities. The actual pressure distribution will therefore consist of a number of areas of concentrated pressure, separated by regions in which no contact takes place and no surface tractions arise. Second, roughness will render the surface layer more compliant than for a smooth body and the mean (or statistically expected) pressure distribution will be affected

so that the discrete contacts occur over a larger area than the region of continuous contact for smooth bodies. These two effects are illustrated diagramatically in Fig. 7.3.

The contact of randomly rough spheres has been analysed by Greenwood and Tripp (1967). The model adopted is to assume that a rough sphere can be represented by a smooth sphere covered in hemispherical asperities with constant curvature but a Gaussian distribution of heights. The analysis leads to a bell-shaped distribution of mean pressure such as that already presented in Fig. 7.3. The maximum value of this mean pressure distribution is lower than the Hertzian peak pressure. One consequence of assuming a Gaussian distribution for asperity heights is that there is always a finite, if small, probability that the surfaces will interact at any distance from the centre of the contact. Thus the mean pressure distribution approaches zero asymptotically as $r \to \infty$. Hence the contact area predicted is not precisely defined. Greenwood and Tripp overcome this difficulty by defining an effective radius of the contact circle a^* where

$$a^* = \frac{3\pi \int_0^\infty r p^*(r)\, dr}{4 \int_0^\infty p^*(r)\, dr} \qquad (7.2)$$

The radius of this effective contact circle is found to be larger than the Herzian value for all rough surfaces.

The contact of rough cylinders has been similarly analysed by Lo (1969). The analysis is not truely two dimensional, since the asperities are modelled as hemispheres in a similar manner to the approach of Greenwood and Tripp. Drawing from the results of their paper, Lo obtains

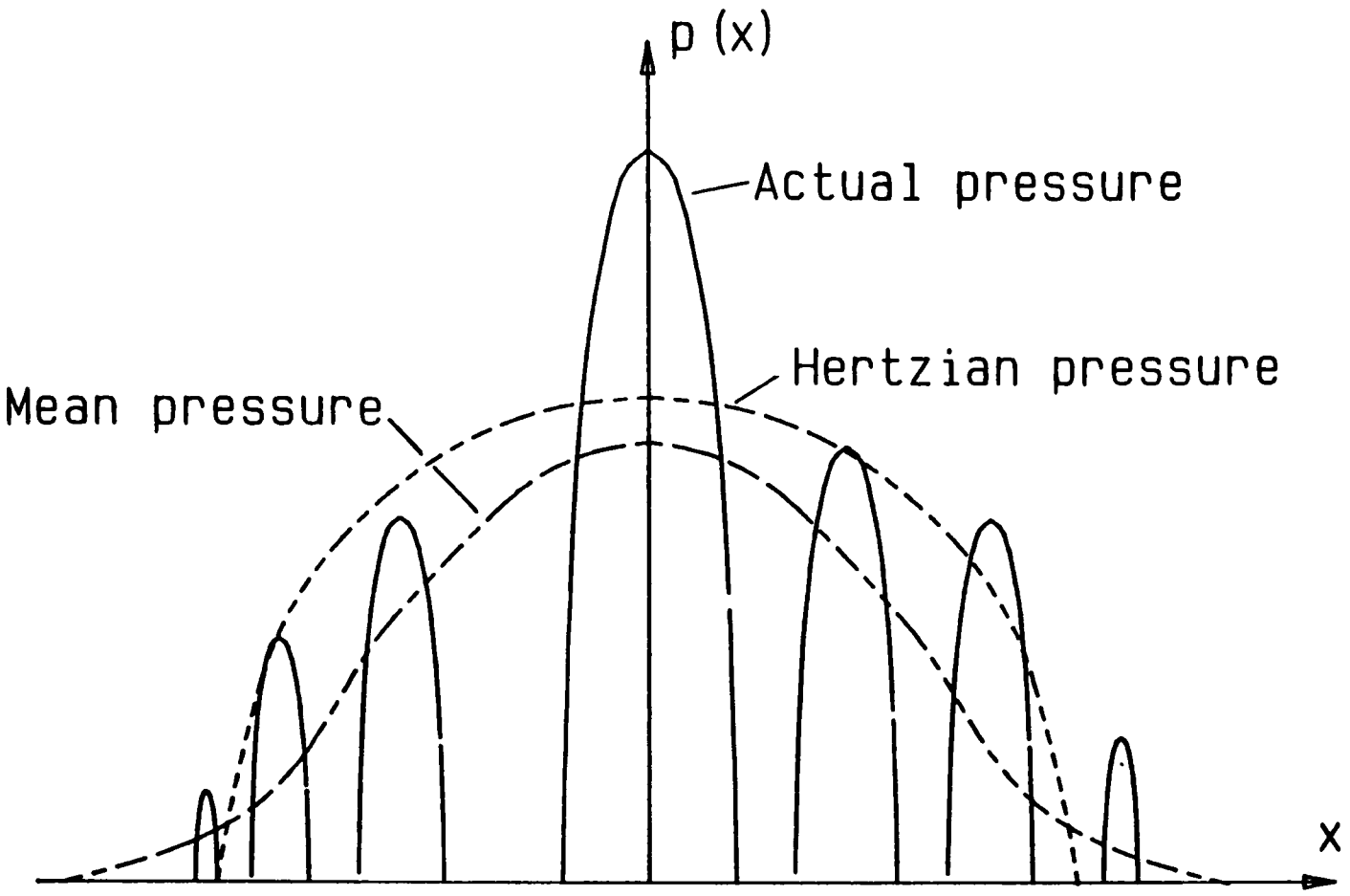

Fig. 7.3 Comparison of mean and actual pressure distributions for a rough surface with the Hertz solution

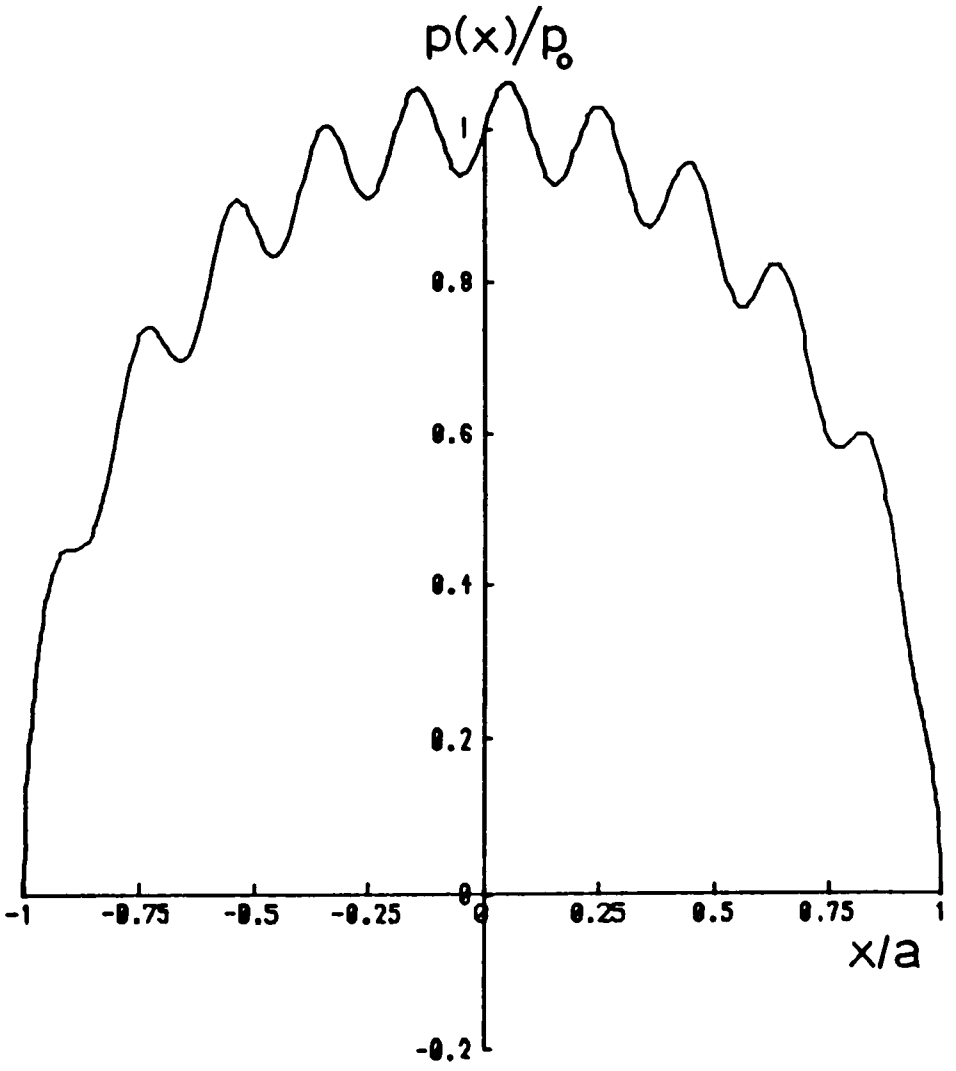

Fig. 7.4 Typical pressure distribution for contact of a smooth cylinder with a sinusoidally rough half-plane, $\lambda/a = 0.2$, $YR/a\lambda = 0.01$

an approximate result for the contact of cylinders by assuming a bell-shaped pressure distribution of the form

$$p^*(x) = p_o^* \left(1 - (x/a^*)^2\right)^2 \qquad 0 \leq x \leq a^* \qquad (7.3)$$

where p_o^* and a^* are constants to be determined for a particular contact configuration. This assumption is reasonable at high roughness values, but unlike the more accurate numerical analysis of Greenwood and Tripp it does not tend to the Hertzian solution at low values of surface roughness.

It is possible to analyse measurements taken from the experimental surfaces using Lo's method and to obtain estimates for the peak mean pressure and contact semi-width. These predict that the peak mean pressure is between 66% and 88% of the Hertzian value for the range of contact sizes used in the experiments. Predictions for the semi-width of contact lie between 1.6 and 2.3 times the corresponding Hertzian values. Measurements of real contact width were taken from the fretted specimens by examining the size of the scar. This gives an upper bound for the contact semi-width since some sliding will have taken place at the beginning of the experiment causing the scar to be larger than the contact width. These measurements show that the real contact width in the experiments is always less than 1.15 times the Hertz value, i.e. well below the predictions of Lo's technique.

Two possible reasons for this discrepancy can be advanced. The failure of Lo's method to approximate the Hertz solution at low roughness values leads to an overestimate of the contact size for relatively smooth surfaces such as those employed in the experiment. Second, Lo's technique is based on the assumption that a large number of contacts are

present. The wavelength of the grinding marks shown in Fig. 7.2 is about 0.15mm, so that the number of these large asperity contacts in present in the experiments lies between 2 and 15. Thus the statistical assumptions in Lo's analysis are not valid for the current experimental configuration.

In order to assess the validity of applying a smooth model to the experimental analysis a model is required which will reveal the actual traction distribution present and compare the subsurface stress field with that produced by Hertz contact.

7.3 Analysis

The talysurf trace presented in Fig. 7.2 reveals that the asperities have similar heights and a reasonably regular spacing. An appropriate model for such a ground surface might therefore be a regular series of asperities of constant height and tip curvature. A first approach to solving the problem would be to represent this roughness as a sine wave of amplitude Y and wavelength λ superimposed on the cylindrical profile of the surface. The integral equation for contact pressure (6.3) thus becomes:

$$\frac{\partial v_1}{\partial x} - \frac{\partial v_2}{\partial x} = \frac{4(1-\upsilon^2)}{\pi E} \int_{-a}^{a} \frac{p(\xi)}{(x-\xi)} d\xi = -\frac{x}{R} + \frac{2\pi Y}{\lambda} \cos(2\pi x/\lambda) \qquad (7.4)$$

This equation can be solved by the numerical technique outlined in chapter 4 to give the resulting pressure distribution. The effect of the sinusoidal roughness is to produce a sinusoidal ripple superimposed on the Hertzian pressure distribution as shown in Fig. 7.4. The amplitude of this ripple increases with increasing Y or decreasing λ. At the values recorded experimentally, the amplitude is so large that negative

pressures are implied at the troughs. This is clearly physically impossible and discontinuous contact must result. Hence to analyse the experimental configuration a technique must be developed which takes account of this phenomenon whereby contact takes place at a number of discrete points close to the asperity tips.

The model adopted is shown in Fig. 7.5. A smooth elastic cylinder of radius R represents the fretting pad and is in contact with a rough elastic half-plane under the action of a normal force P. The surface roughness caused by the grinding marks is represented by a series of part-cylinders of radius ρ and spacing λ. As the cylinder and half-plane are brought into contact a few asperity tips will contact. If the load is increased, more asperities will be brought into the contact and simultaneously the load on the central asperities will increase. Eventually, if a large number of contacting asperities are involved the mean pressure distribution will be approximately Hertzian. Further, if the surface of each asperity is considered to be cylindrical then each of the individual contacts will be Hertzian. Modelling the cylinder as a parabola gives the relative vertical displacement at any contacting peak as:

$$v(x) = d - \frac{x^2}{2R} \tag{7.5}$$

where d is the relative displacement of the bodies at $x = 0$. If the effect of the overall deformation of the cylinder on the displacement for all points within a particular asperity contact is assumed to be uniform then the displacement v_n required at that asperity can be written as:

$$v_n = d - \frac{(\lambda n)^2}{2R} \qquad 0 \leq |n| \leq N \tag{7.6}$$

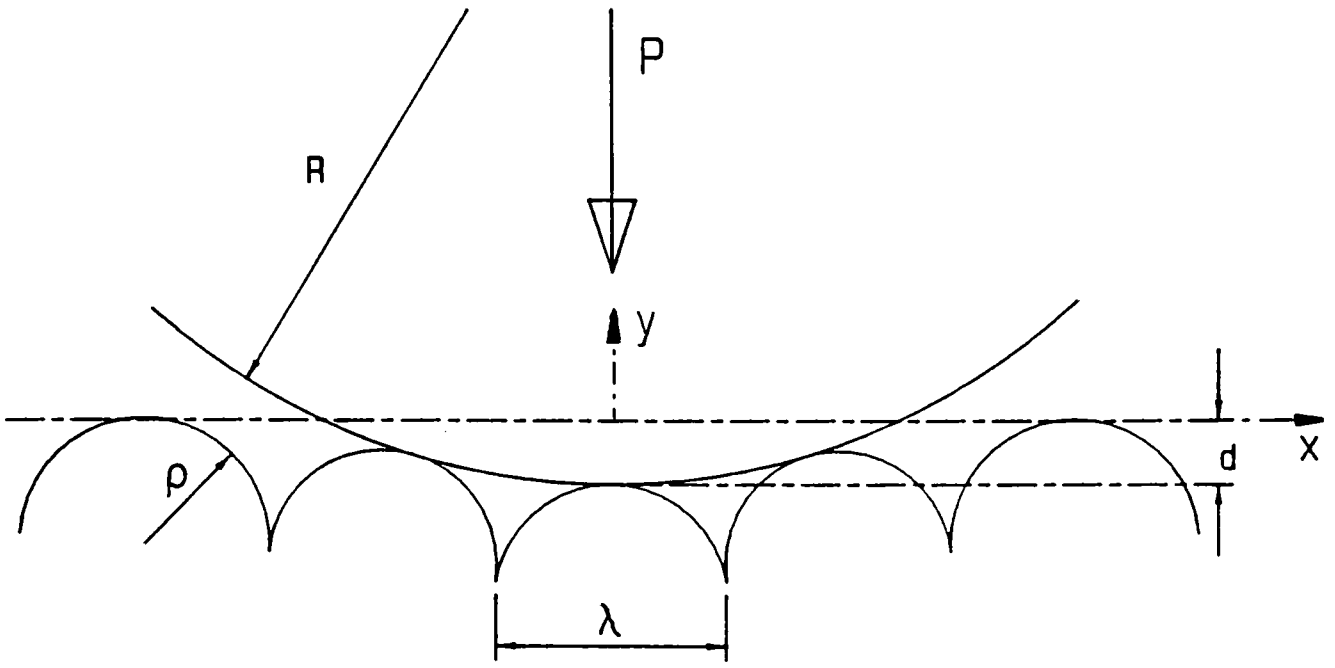

Fig. 7.5 Model of contact for ground surfaces

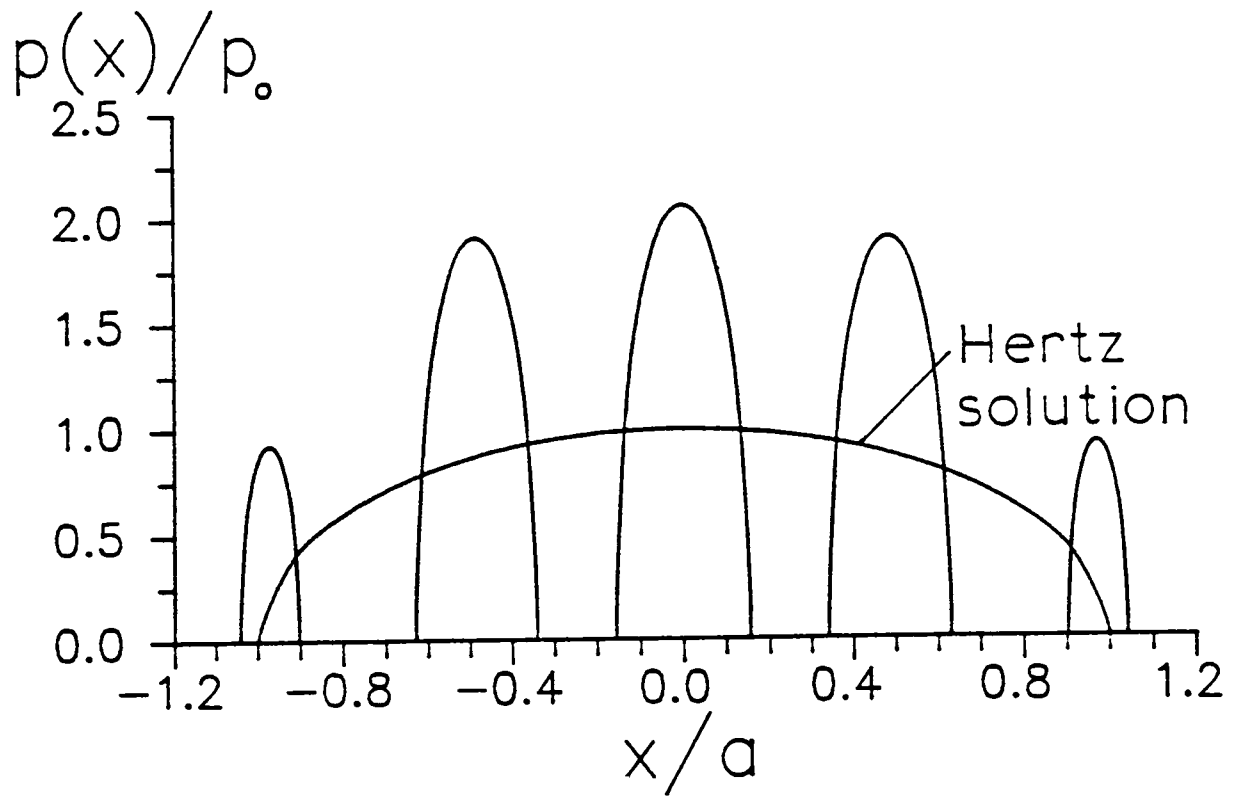

Fig. 7.6 Contact pressure distribution, $P/\pi E^{*}R = 1.52 \times 10^{-4}$, $\rho/R = 0.0751$, $\lambda/R = 0.012$

where n defines the asperity location and 2N + 1 asperities are in contact (The central asperity is assumed to lie at x = 0). The displacements caused by the individual contacts can be found from the results of Poritsky (1950), provided that the half-plane assumptions are retained for each individual asperity contact. If the load carried by the nth asperity is P_n and the corresponding semi-width of contact a_n, then:

$$v_n = \frac{-2P_n}{\pi E}(1 - \upsilon^2)\left[\frac{x - \lambda n}{a_n}\right]^2 + \text{constant} \qquad |x - \lambda n| \leq a_n$$

$$= \frac{-2P_n}{\pi E}(1 - \upsilon^2)\left[\ln|X| + \frac{1}{2X^2}\right] + \text{constant} \qquad |x - \lambda n| > a_n \tag{7.7}$$

for each body, where $X = \frac{|x - \lambda n|}{a_n} + \sqrt{\frac{(x - \lambda n)^2}{a_n^2} - 1}$

In terms of the displacement relative to that at x = 0, viz. $(v_n - d)$, the equations become:

$$v_n - d = \frac{-2P_n}{\pi E}(1 - \upsilon^2)\left[\frac{(x - \lambda n)^2}{a_n^2} - \ln|Z| - \frac{1}{2Z^2}\right] \qquad |x - \lambda n| \leq a_n$$

$$= \frac{-2P_n}{\pi E}(1 - \upsilon^2)\left[\ln|X| + \frac{1}{2X^2} - \ln|Z| - \frac{1}{2Z^2}\right] \qquad |x - \lambda n| > a_n \tag{7.8}$$

where $Z = \frac{|\lambda n|}{a_n} + \sqrt{\frac{(\lambda n)^2}{a_n^2} - 1}$

The combined affect of the 2N + 1 asperity contacts on both bodies may be summed to give the total displacement at the mth asperity :

$$2(v - d)_m = 2\sum_{n=-N}^{N}(v_n - d)_m = \frac{-(\lambda m)^2}{2R} \tag{7.9}$$

where $(v_n - d)_m$ is obtained by substituting $x = \lambda m$ in (7.8)

There are 2N of these equations, corresponding to $m = -N,\ldots,-1,1,\ldots,N$ (i.e. there is no equation for $m = 0$). An additional equation is obtained from the requirement for overall equilibrium:

$$\sum_{n=-N}^{N} P_n = P \qquad (7.10)$$

There are now $2N + 1$ equations, which alow the problem to be solved in conjunction with the Hertzian relationships between P_n and a_n, namely

$$a_n^2 = 4P_n\rho(1 - \upsilon^2)/\pi E \qquad (7.11)$$

An iterative solution method is adopted, with initial estimates for P_n and a_n being obtained from the smooth Hertz solution. The number of contacts $(2N + 1)$ must also be guessed initially and the final solution checked for consistency. This requires that all P_n are positive and that there is no contact for asperities outside the contact ($|n| > N$). Once the correct value has been chosen for N, convergence to consistent values of P_n, a_n takes place after $3 \rightarrow 4$ iterations. The solution is found to be dependent on the following normalised variables: load $(P/\pi E^* R)$, asperity spacing (λ/R), and asperity curvature (ρ/R). The quantity E^* represents the usual equivalent Young's Modulus given by

$$E^* = \frac{E}{2\,(1 - \upsilon^2)}$$

for elastically similar bodies.

7.4 Results and discussion

In order to analyse the experimental contact configurations, measurements of asperity separation (λ) and tip radius (ρ) must be made.

These can be obtained from the Talysurf trace (Fig. 7.2). The separation is not difficult to estimate, but a degree of judgement is required in obtaining a representative value for ρ. The pressure distribution at each individual asperity is highly sensitive to ρ, but the distribution of asperity loads P_n and hence the subsurface stress field is relatively *insensitive*. Thus, for the purposes of examining this interior stress field an accurate estimate is not required. A value of $\rho = 0.94$mm was chosen to be representative of the long wavelength grinding marks.

A typical pressure distribution obtained by this technique is shown in Fig. 7.6, together with the Hertz solution for smooth contact. In this case there are 5 discrete contacts and the maximum pressure developed is 2.07 times the equivalent maximum Hertz pressure p_o although, as discussed above, this result is highly sensitive to the chosen value of ρ. This peak pressure ratio varies between 3.64 and 3.76 for the range of contact conditions covered in the experiments and the chosen estimate for ρ.

Once the surface tractions are known, the subsurface stress field can be calculated using the technique outlined in chapter 4 by summing the contributions from each individual asperity contact. Contours of most positive principal stress are presented in Fig. 7.7a for $P/\pi E^* R = 1.27 \times 10^{-5}$, $\lambda/R = 0.001$, $\rho/R = 0.006$, which results in 15 asperity contacts. The corresponding plot for smooth contact is shown in Fig. 7.7b and it can be seen that the perturbation to the stress field caused by the surface roughness is restricted to a shallow surface layer with a depth equal to about 5% of the contact width.

The analysis so far has been restricted to the application of a purely normal force. The extension of the technique to analyse cases where a tangential force less than limiting friction is also applied

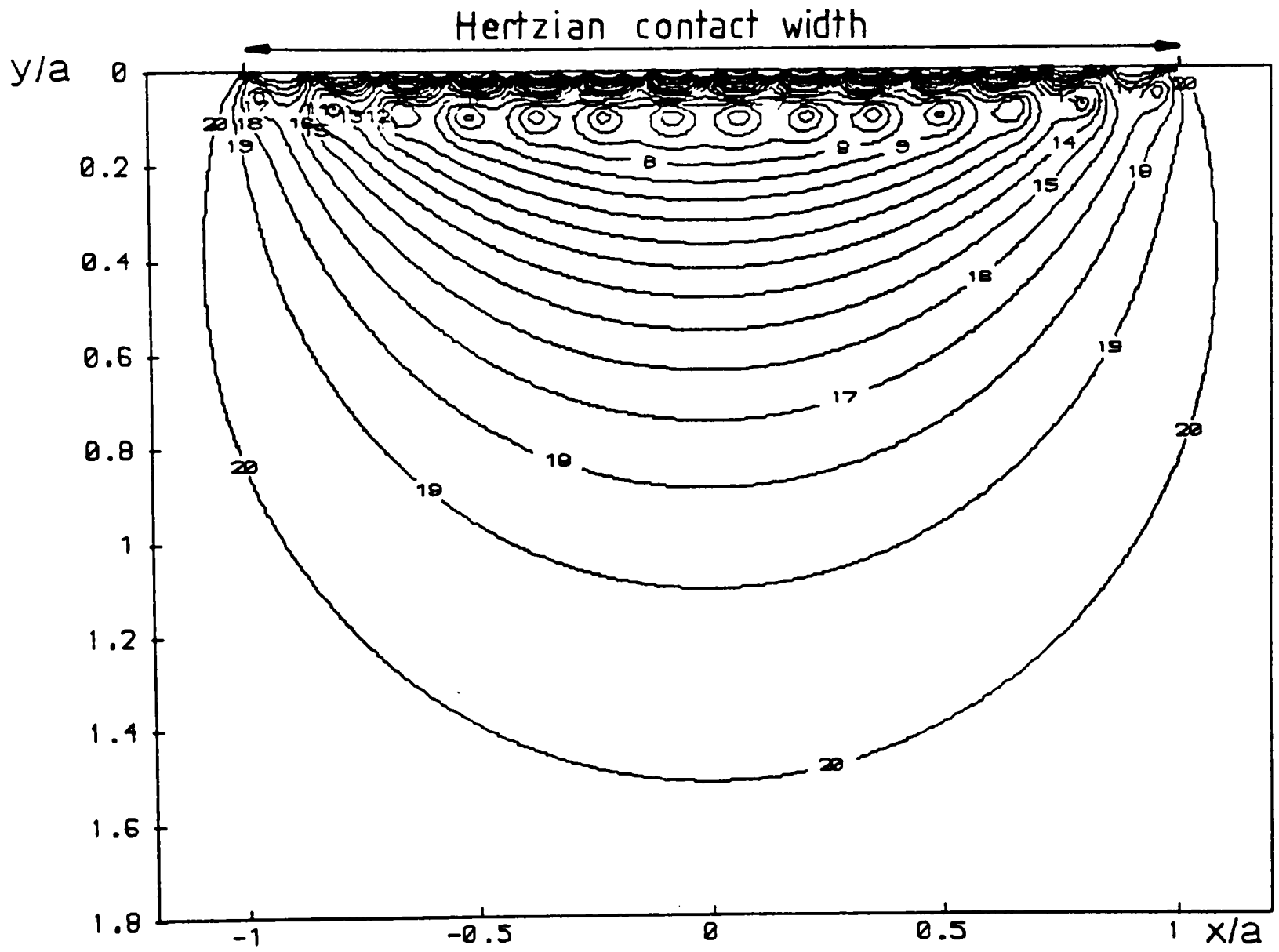

CONTOUR KEY	
1	-1.00
2	-0.95
3	-0.90
4	-0.85
5	-0.80
6	-0.75
7	-0.70
8	-0.65
9	-0.60
10	-0.55
11	-0.50
12	-0.45
13	-0.40
14	-0.35
15	-0.30
16	-0.25
17	-0.20
18	-0.15
19	-0.10
20	-0.05
21	0.00

Fig. 7.7a Contours of most positive principal stress (σ/p_o)

Rough contact, $P/\pi E^* R = 1.27 \times 10^{-5}$, $\lambda/R = 0.001$, $\rho/R = 0.006$ (15 contacts)

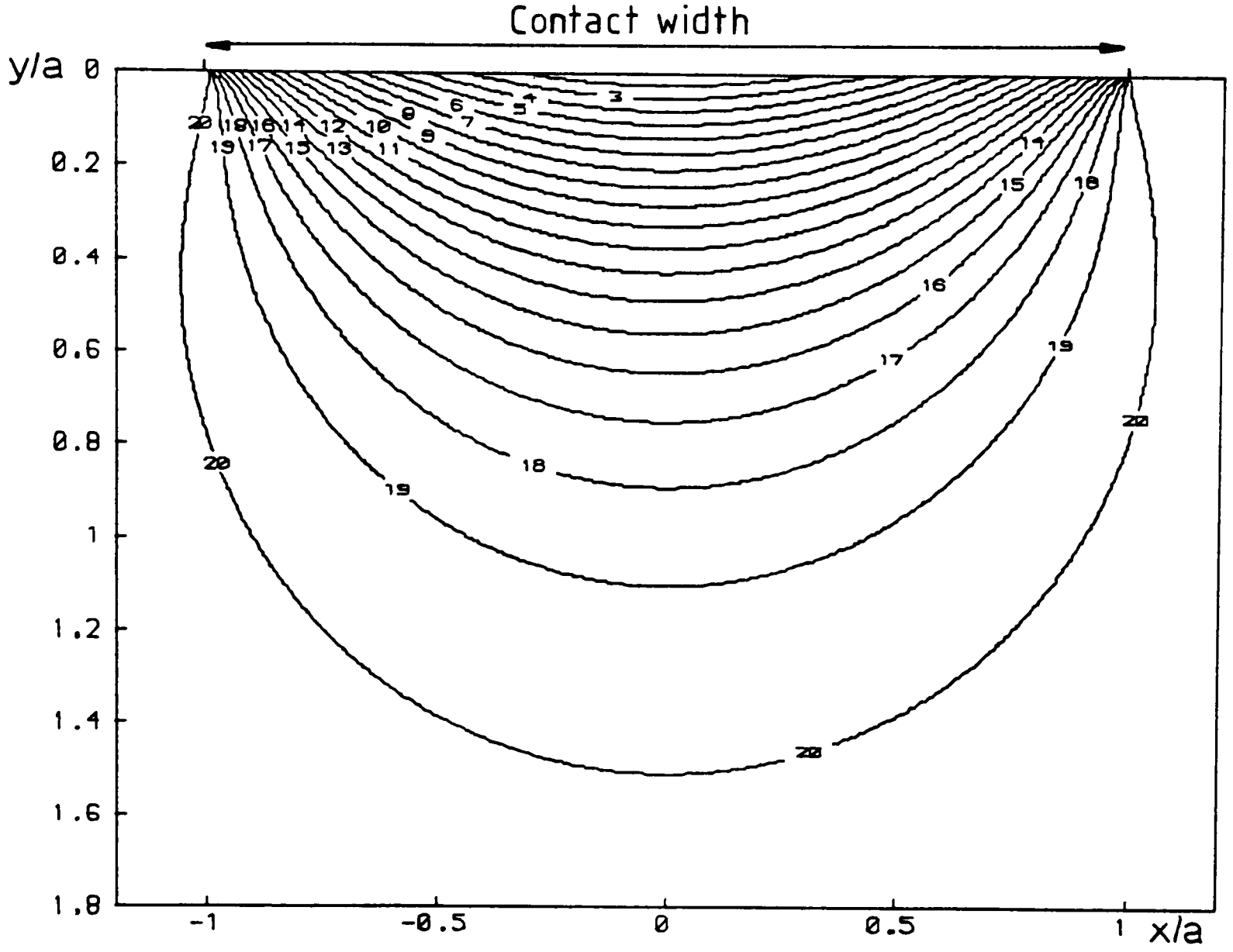

CONTOUR KEY	
1	-1.00
2	-0.95
3	-0.90
4	-0.85
5	-0.80
6	-0.75
7	-0.70
8	-0.65
9	-0.60
10	-0.55
11	-0.50
12	-0.45
13	-0.40
14	-0.35
15	-0.30
16	-0.25
17	-0.20
18	-0.15
19	-0.10
20	-0.05
21	0.00

Fig. 7.7b Contours of most positive principal stress (σ/p_o)

Smooth contact (Hertz)

would inevitably be complex, but fully sliding contact can easily be dealt with since q(x) = fp(x) everywhere. An approximate model of the stress field beneath the experimental contact configurations can thus be set up by applying the correct values of normal force (P), tangential force (Q) and bulk stress σ, but with the coefficient of friction reduced so that f = Q/P and the contact is fully sliding.

To model series 3 experiments, which are typical of the range of conditions examined, values of Q/P = 0.45, σ/p_o = 0.648, and hence f = 0.45 were chosen and the measured values of ρ and λ employed. Figure 7.8a shows the stress field under the largest contact of the series (R = 150mm). In this case 15 asperities are in contact. The corresponding Hertzian stress field for the series is shown in Fig.7.8b and, once again the effect of the rough surface is confined to a thin layer y/a < 0.1. As the radius of the fretting pad is reduced the overall contact size is also reduced and the number of asperity contacts decreases. For R = 75mm (Fig. 7.9a), the number of contacts has decreased to 7 and the depth of the affected layer is now about 10% of the contact width (y/a < 0.2). For R = 25mm there are only 3 asperities in contact and the affected layer now extends to y/a = 0.6. Even so, cracks growing from the trailing edge of the contact (x/a = -1.0) and inclined under the contact pass through the region where the principal stress values are least affected by the surface roughness and the Hertzian stress field may therefore be considered appropriate in calculating stress intensity factors for crack lengths greater than about 0.3a.

The model developed is necessarily simplified and no attempt has been made to model the stick/slip pattern caused by a tangential force less than limiting friction. Similarly, the contact has been assumed to

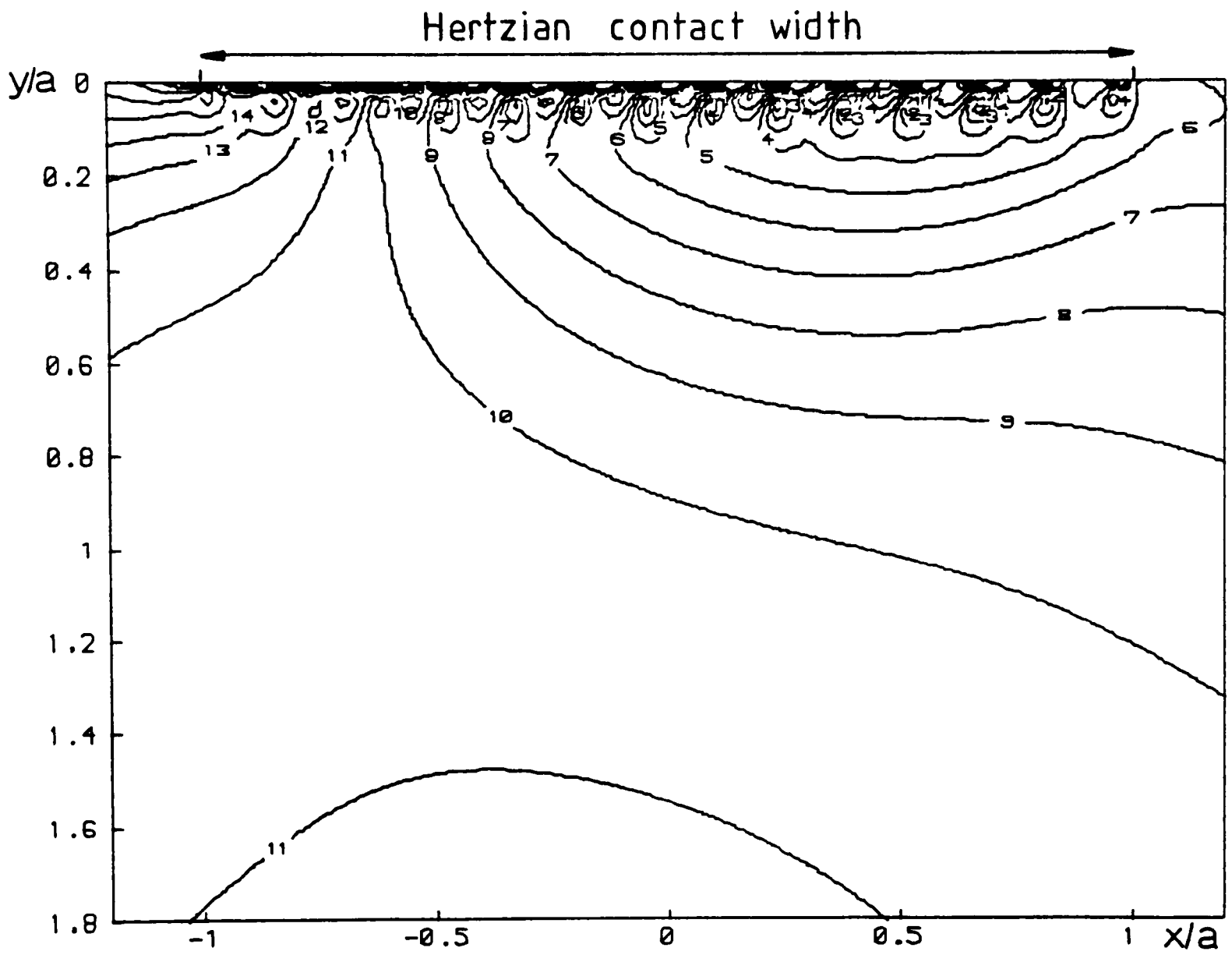

CONTOUR KEY	
1	-0.40
2	-0.30
3	-0.20
4	-0.10
5	0.00
6	0.10
7	0.20
8	0.30
9	0.40
10	0.50
11	0.60
12	0.70
13	0.80
14	0.90
15	1.00
16	1.10
17	1.20
18	1.30
19	1.40
20	1.50
21	1.60

Fig. 7.8a Contours of most positive principal stress (σ/p_o) for series 3 experiments

Rough contact, R = 150 mm, (15 contacts)

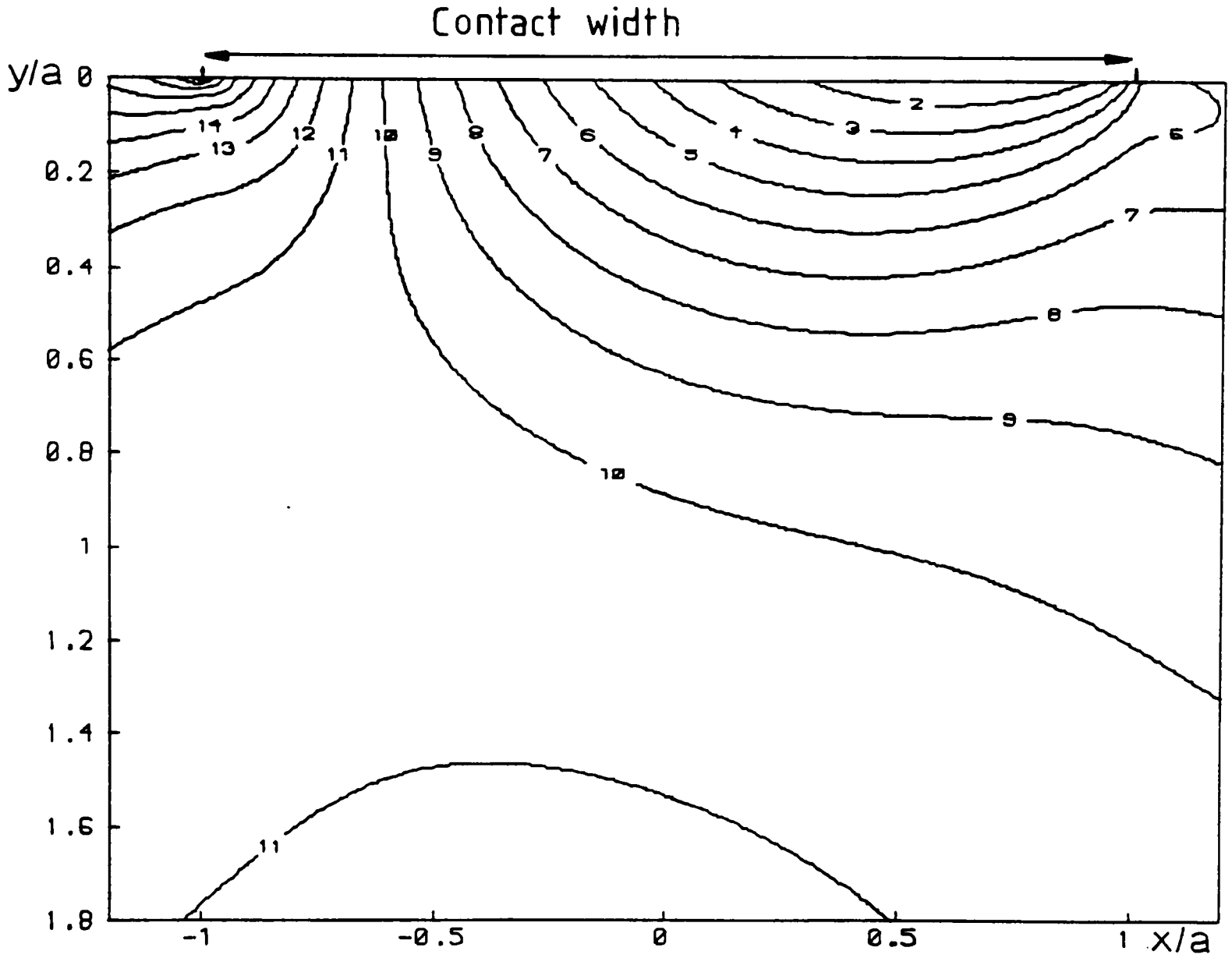

CONTOUR KEY	
1	-0.40
2	-0.30
3	-0.20
4	-0.10
5	0.00
6	0.10
7	0.20
8	0.30
9	0.40
10	0.50
11	0.60
12	0.70
13	0.80
14	0.90
15	1.00
16	1.10
17	1.20
18	1.30
19	1.40
20	1.50
21	1.60

Fig. 7.8b Contours of most positive principal stress (σ/p_o) for series 3 experiments

Smooth contact

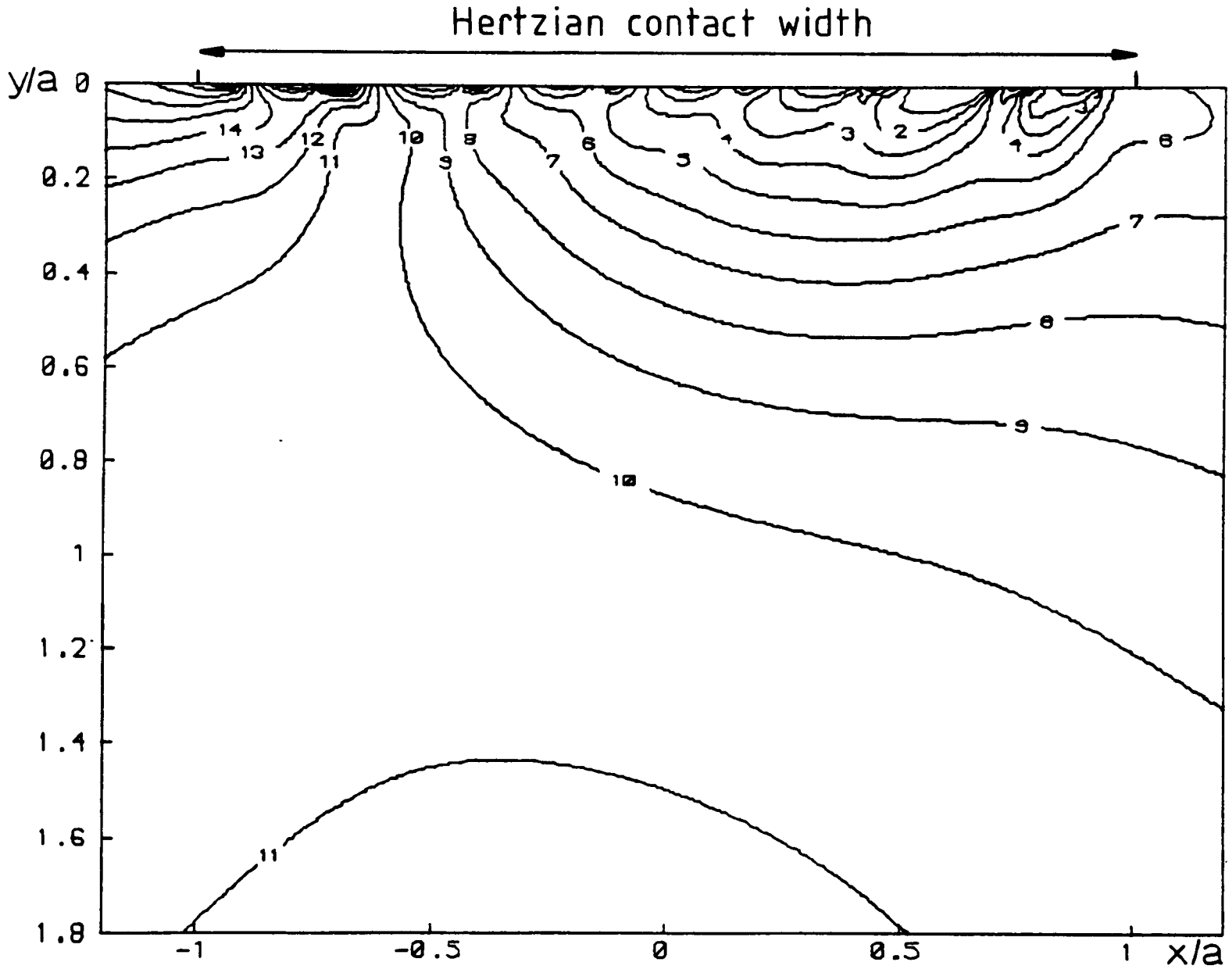

CONTOUR KEY	
1	-0.40
2	-0.30
3	-0.20
4	-0.10
5	0.00
6	0.10
7	0.20
8	0.30
9	0.40
10	0.50
11	0.60
12	0.70
13	0.80
14	0.90
15	1.00
16	1.10
17	1.20
18	1.30
19	1.40
20	1.50
21	1.60

Fig. 7.9a Contours of most positive principal stress (σ/p_o) for series 3 experiments

Rough contact, R = 75 mm, (7 contacts)

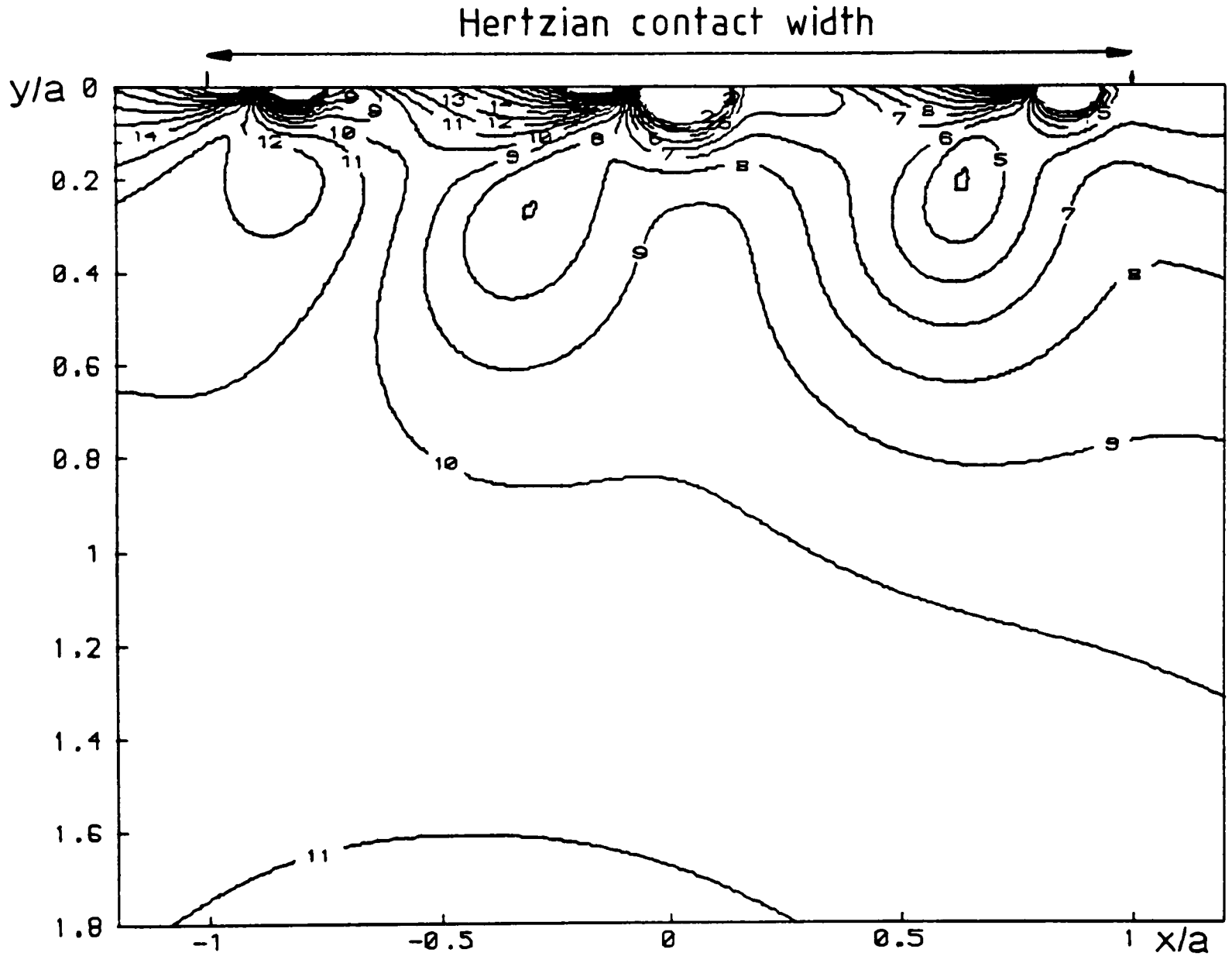

CONTOUR KEY	
1	-0.40
2	-0.30
3	-0.20
4	-0.10
5	0.00
6	0.10
7	0.20
8	0.30
9	0.40
10	0.50
11	0.60
12	0.70
13	0.80
14	0.90
15	1.00
16	1.10
17	1.20
18	1.30
19	1.40
20	1.50
21	1.60

Fig. 7.9b Contours of most positive principal stress (σ/p_o) for series 3 experiments

Rough contact, R = 25 mm, (3 contacts)

be symmetrical about x = 0, although in practice there can be any degree of phase shift. However, the effect of roughness has been demonstrated to be confined to the surface layer and some estimates of the size of this affected zone obtained. No account has been taken of asperity plasticity, although the high peak pressures predicted would certainly entail some degree of plastic deformation. This would reduce the peak pressures and probably reduce the size of the surface layer affected by the roughness.

The Hertzian stress field has been shown to provide a reasonable model for that existing under rough surfaces remote from a thin surface layer. In calculating stress intensity factors for the current experiments, the use of the Hertzian stress field would seem to be reasonable for those contacts where more than 7 asperities are involved and the crack length is greater than about 0.1a. At smaller contact widths, similar to the smallest two used experimentally the approximation is less good, but since the exact number and height of asperities within the contact is unknown, it may be regarded as a best estimate of the stress field.

The surface stress state is highly dependent on surface roughness, although it should be noted that the region of high tensile stress at the trailing edge of the contact (x/a = -1.0) is present in all the cases studied. The importance of seeking a good surface finish for experimental specimens is clearly emphasized, but it should be recognised that real contacts liable to undergo fretting are unlikely to have such a good finish and some consideration of surface roughness effects will be inevitable in seeking to apply experimental results.

Drawing from the results of this analysis, the stress field generated by contact of smooth surfaces has been used for the purposes of

calculating stress intensity factors in the following chapter. It is recognised that the degree of approximation involved is significant for the smaller contact widths, but, since no measurements of actual surface profile under the contact were made, this is the best available option.

Chapter 8

Calculation of stress intensity factors

8.1 Introduction

The stress field within the specimen under fretting conditions has been determined (Chapter 4) and it has been shown that the representation of the specimen as a smooth half-plane is reasonable in calculating these stresses (Chapters 5, & 7). The next step in the analysis must be to calculate stress intensity factors for cracks growing under the influence of this stress field. Only then can crack growth rates and conditions for self arrest be meaningfully discussed. As shown in chapter 3, fretting fatigue cracks initiate near the edge of the contact and grow for some distance obliquely under the contact before turning to a direction normal to the free surface. This phenomenon has been widely reported by many authors, including Nishioka and Hirakawa (1969b), and Sato, Fujii and Kodama (1986). Calculation of stress intensity factors for cracks under fretting conditions has been carried out by Rooke and Jones (1977) and O'Connor and Hills (1986) but the techniques are only applicable to cracks which are perpendicular to the free surface. A method of analysing slant cracks would clearly be a useful tool in assessing the experimental results.

In addition to fretting fatigue, slant cracks near the free surface also occur widely in wear and rolling contact fatigue problems (e.g. Fleming (1977), Way (1935)) and this has provided the motivation for several attempts to determine the crack tip stress intensity factors for such configurations. If the crack is open along its entire length, it is

possible to use classical methods to determine the local stress field, and early attempts to do this were based on analysing the crack in a full plane, and applying corrective tractions to restore equilibrium at the free surface. The corrective surface tractions induce more unsatisfied stresses on the crack face, which must themselves be annulled, thereby contributing to the stress intensity factor. This process is repeated until convergence occurs, which may be particularly slow in the case of oblique cracks or loading near the mouth (Hills, Sackfield, and Uzel (1984)). A small improvement to the method, equivalent to the generation of integral equations along the crack and at the surface, and their approximate solution was proposed by Uzel, Hills, and Sackfield (1985). This too, worked well if the 'corrective' term was small in comparison with the contribution from the applied loading, but is unwieldy, and gives poor accuracy for the size of matrices involved.

An alternative is to employ a very powerful method which may be used for the calculation of stress intensity factors for plane cracks at or near the free surface, with arbitrary far-field conditions. This method is based on the modelling of the crack by distributions of displacement discontinuities or dislocations and has been used by several researchers in the U.S.A., principally for the analysis of problems where cracks are closed (e.g. Schmueser, Comninou, and Dundurs (1981)) or partially closed (e.g. Schmueser, Comninou, and Dundurs (1980)). However, the technique is equally effective for open cracks.

8.2. Formulation

The principal difficulty encountered in any method which relies on the cancelling of unsatisfied tractions along the crack faces is that

non-zero stresses arise on the free surface. If the crack is deeply buried, these stresses may be insignificant compared with the primary stress field, and hence an approximate answer is found, equivalent to assuming that the crack exists in a full-plane. However, in most practical applications this condition is not satisfied, leading to an iterative sequence being set up between two solutions, viz. the cracked full-plane and the arbitrarily loaded half-plane, sometimes called the alternating method (Hartranft and Sih (1973)).

These difficulties are avoided completely by modelling the crack as a continuous distribution of displacement discontinuities, or dislocations. It must be emphasised that these are not real dislocations, in the sense of being lattice flaws, but rather are a mathematical convenience. One might imagine that the discontinuity arises by making a slit in the continuum which terminates at the dislocation core, inserting or removing material on one side, and re-joining the cut faces, so that a state of residual stress exists. This operation has been likened to the process of inserting 'darts' in dress making. Solutions in closed form are available for an arbitrarily orientated and located edge dislocation in a half plane (Dundurs and Mura (1964)), so that any number of such dislocations may be superposed, without in any way affecting the traction-free surface.

Figure 8.1 shows a half plane, free of externally imposed loads, but containing a dislocation, located at $(0,-y_d)$. Thin slabs of material of thicknesses b_x and b_y have been inserted along $x = 0$, $-y_d < y < \infty$ and $y = -y_d$, $0 < x < \infty$ respectively. Thus b_x and b_y denote the contributions to the Burger's vector resolved in x and y directions. Dundurs and Mura (1964) have found the stress field induced by an arbitrarily orientated edge dislocation in the neighbourhood of an

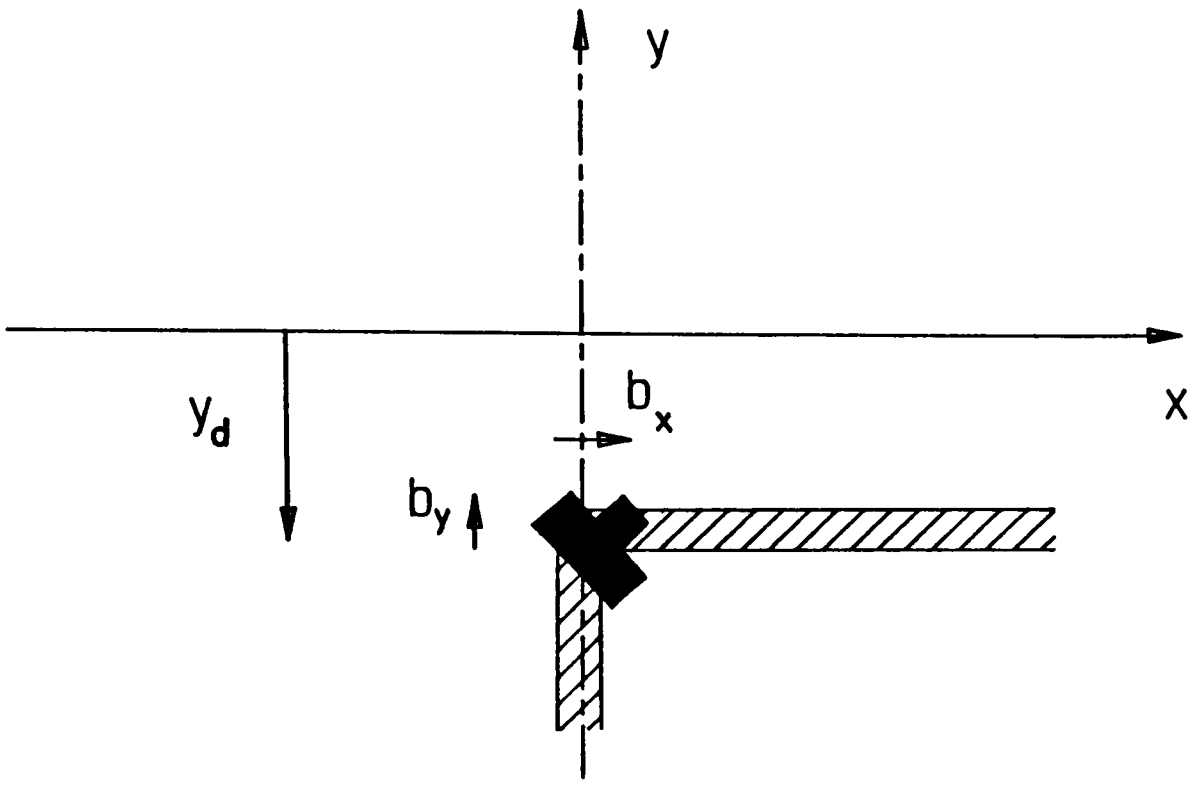

Fig. 8.1 An arbitrarily orientated dislocation near the free surface of a half-plane.

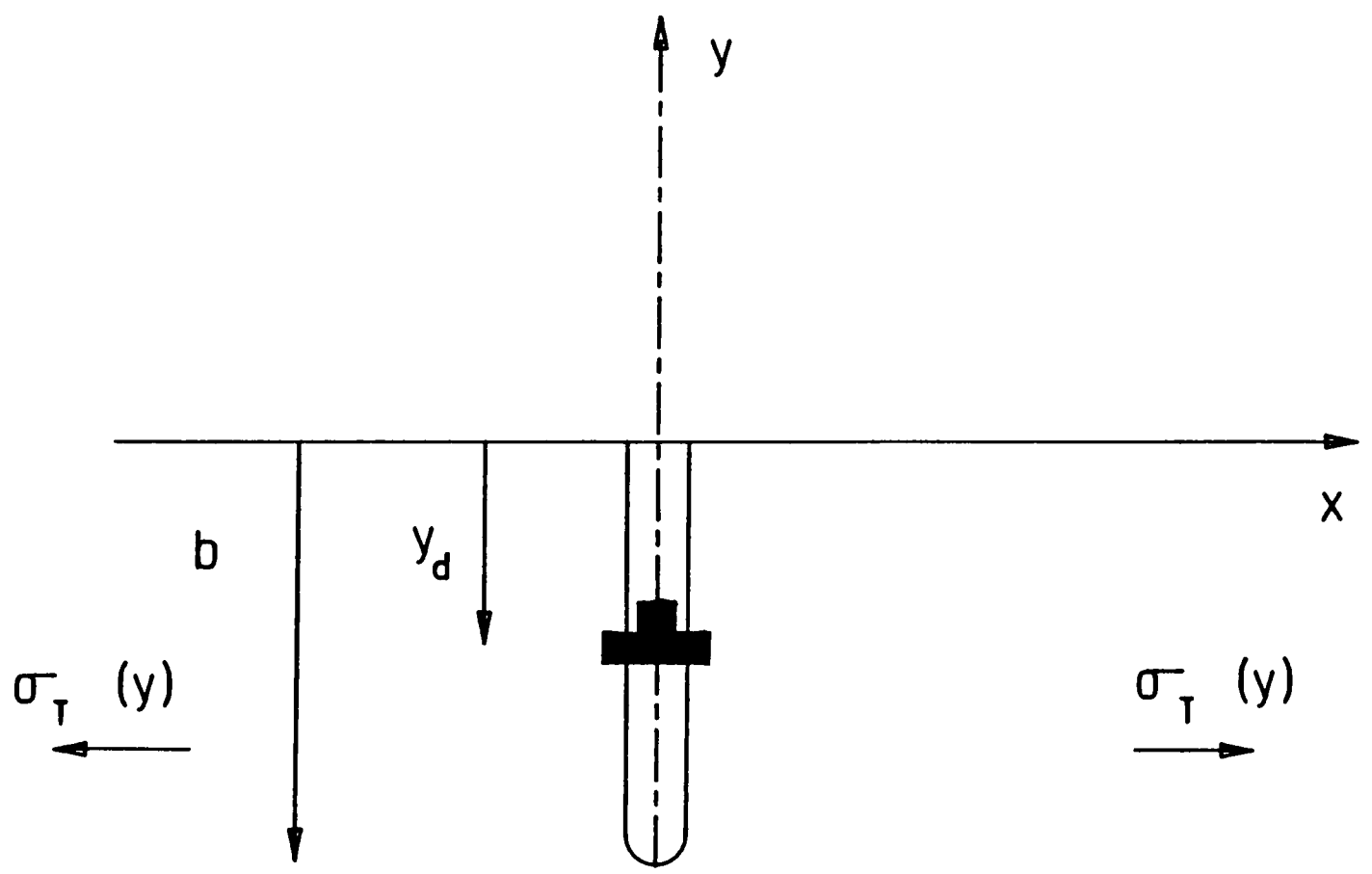

Fig. 8.2 A surface breaking crack perpendicular to the free edge

elastic inclusion having different elastic constants from the matrix. This geometry may be specialized to that shown in Fig. 8.1 and the stress field readily deduced using stress function-stress relations given by Dundurs and Sendeckyj (1965). The results are:

$$\tilde{\sigma}_{xx} = \frac{\mu}{\pi(\chi + 1)} \{b_x G_{xxx}(x,y,y_d) + b_y G_{yxx}(x,y,y_d)\} \qquad (8.1a)$$

$$\tilde{\sigma}_{yy} = \frac{\mu}{\pi(\chi + 1)} \{b_x G_{xyy}(x,y,y_d) + b_y G_{yyy}(x,y,y_d)\} \qquad (8.1b)$$

$$\tilde{\sigma}_{xy} = \frac{\mu}{\pi(\chi + 1)} \{b_x G_{xxy}(x,y,y_d) + b_y G_{yxy}(x,y,y_d)\} \qquad (8.1c)$$

where μ is the modulus of rigidity, $\chi = 3 - 4\upsilon$ in plane strain, υ being Poisson's ratio, and the functions G_{ijk} are given in Appendix D. These complete expressions for the stress field, though lengthy, are needed if an analysis of slanting cracks is contemplated. To demonstrate the method more clearly a crack normal to the free surface will be analysed first.

8.3 Normal Cracks

Figure 8.2 shows a surface-breaking crack of length b, normal to the free surface, and loaded by distant arbitrary tensile stress of magnitude $\sigma_T(y)$. Also shown is an edge dislocation, with Burgers' vector b_x located at some general point $(0,-y_d)$ along the line of the crack. It will be recognised that this configuration will induce no mode II stress intensity, so that no tangential mismatch of the crack faces is anticipated, and hence no glide dislocations (with Burgers' vectors b_y) are required. The method requires an array of climb dislocations (b_x),

such as the one shown, to be distributed along the crack so that the crack opening at any point ($-b < y < 0$) is correctly modelled. This will be done by ensuring that, along the crack faces, the total direct stress, σ_{xx} due to both the external loading and the influence of the dislocations, is zero, i.e. so that the crack faces remain traction free. It should be noted at this point that the far field stress can be any known function of y. The power of the method is that it may cope readily with any imposed loading, although the formulation in the present section is restricted to cases where (a) the crack remains open at all points, and (b) there is no shear component of loading. An expression for the tractions $\sigma_{xx}(0,y)$ due to a climb dislocation of magnitude b_x located at point $(0,-y_d)$ is required. From (8.1b):

$$\tilde{\sigma}_{xx}(0,y) = \frac{\mu\, b_x}{\pi(\chi + 1)} K(y,y_d) \qquad (8.2)$$

where $K(y,y_d) = 2\left[\frac{1}{(y + y_d)} + \frac{1}{(y - y_d)} - \frac{2y_d}{(y - y_d)^2} - \frac{4y_d^2}{(y - y_d)^3} \right]$

and, from (8.1c), $\tilde{\sigma}_{xy}(0,y) = 0$ so that no shearing effect is introduced. Instead of discrete dislocations a continuous distribution of density $B_x(y_d)$ is employed, so that the total direct traction is;

$$N(y) = \sigma_T(y) + \frac{\mu}{\pi(\chi + 1)} \int_0^b B_x(y_d) K(y,y_d)\, dy_d = 0 \qquad (8.3)$$

$$-b < y < 0$$

This is an integral equation in the unknown function $B_x(y_d)$, with a Cauchy kernel, ie. $K \to \infty$ as $y \to -y_d$. It is not possible to solve the equation analytically, but the numerical quadratures employed in previous

chapters may also be used here. The interval of integration is normalised by setting;

$$s = 2y_d/b - 1$$

$$t = -2y/b - 1 \qquad (8.4)$$

giving

$$N(t) = \sigma_T(t) + \frac{\mu}{\pi(\chi + 1)} \int_{-1}^{1} B_x(s)K(s,t)ds = 0 \qquad (8.5)$$

$$-1 < t < 1$$

Discretisation again follows the method of Erdogan Gupta and Cook (1973). A singularity in the σ_{xx} stress component occurs at y = -b, but regular behaviour near y = 0 is anticipated (the effect of the sharp corners at the mouth does not produce a stress intensification there). This singularity is abstracted by writing the solution for $B_x(s)$ in terms of a bounded function $\phi(s)$ and a fundamental function:

$$B_x(s) = \phi(s)(1 - s)^{-1/2} (1 + s)^{1/2} \qquad (8.6)$$

This permits the use of Gauss-Chebyshev quadrature, and the discretized form of (8.5) becomes:

$$\frac{\mu}{\pi(\chi + 1)} \sum_{i=1}^{n} \frac{2\pi(1 + s_i)}{2n + 1} K(t_k, s_i)\phi(s_i) = -\sigma_T(t_k) \qquad (8.7)$$

where $s_i = \cos\left[\frac{2i - 1}{2n + 1}\pi\right]$ $\qquad i = 1.....n$

$$v_k = \cos\left[\frac{2k}{2n + 1}\pi\right] \qquad k = 1.....n$$

This gives n simultaneous equations in the n unknowns $\phi(s_i)$ which may readily be solved by a computer library routine. Stress intensity factors remove the $r^{-1/2}$ singularity in the stress at the crack tip, since $K_I = \lim_{r\to 0} \sqrt{2\pi r}\, \sigma_{\theta\theta}$ and $K_{II} = \lim_{r\to 0} \sqrt{2\pi r}\, \tau_{r\theta}$. An equivalent fundamental function has already been chosen , so that the stress intensity factor may be seen to be proportional to $\phi(1)$. A detailed

proof of this is given by Erdogan, Gupta and Cook (1973). Since ϕ is only known at certain points (viz ϕ_i) extrapolation is required to find $\phi(1)$. This has been examined by Krenk (1975) who gives:

$$\phi(1) = \frac{2}{2n+1} \sum_{i=1}^{n} \cot\left[\frac{(2i-1)\,\pi}{(2n+1)\,2}\right] \sin\left[\frac{n}{(2n+1)}\,(2i-1)\pi\right] \phi(s_i) \tag{8.8}$$

K_I is then given by:

$$K_I = 2\sqrt{2\pi b}\,\frac{\mu}{(\chi+1)}\,\phi(1) \tag{8.9}$$

Buried normal cracks may be analysed by following an essentially similar formulation to that developed above and choosing a different fundamental function. Since such analysis is not directly relevant to fretting fatigue it is not included here and the reader is referred to Nowell and Hills (1987). Crack tip stress intensity factors may be found by the above method for both buried and surface breaking cracks normal to the free surface under an arbitrary far field stress, provided that the cracks remain open. In order to compare results of this method with known solutions results for an illustrative case of uniform far-field tension (σ_T = constant) are given.

Under this stress state a stress intensity factor of $K_I = 1.12148\,\sigma\sqrt{\pi b}$ is found, which corresponds with the usually accepted value (Hartranft and Sih (1973)). Convergence to 5 significant figures occurred with n set to 30.

8.4 Slant cracks

Figure 8.3 depicts a slant surface-breaking crack of length b, being loaded by an arbitrary external stress $\sigma(x,y)$ which may have both direct and shear components. In the most general case the crack will suffer both direct and shear loading, and therefore both climb ($b_{x''}$) and glide ($b_{y''}$) dislocations will be needed. The stress induced by an edge dislocation having these Burger's components may be found as follows. First b_x and b_y are found by resolution:

$$\begin{bmatrix} b_x \\ b_y \end{bmatrix} = \begin{bmatrix} \cos\theta & \sin\theta \\ -\sin\theta & \cos\theta \end{bmatrix} \begin{bmatrix} b_{x''} \\ b_{y''} \end{bmatrix} \tag{8.10}$$

Substitution in (8.1) gives $\tilde{\sigma}_{xx}$, $\tilde{\sigma}_{xy}$, $\tilde{\sigma}_{yy}$ at any point in terms of $b_{x''}$, $b_{y''}$, and y''_d. Stress transformations are then employed to find the corresponding stress components in the x", y" coordinate system yielding expressions for $\tilde{\sigma}_{x''x''}$ and $\tilde{\sigma}_{x''y''}$ as functions of $b_{x''}$, $b_{y''}$:

$$\tilde{\sigma}_{x''x''} = \frac{\mu}{\pi(\chi + 1)} \{b_{x''}(y''_d)\, K^N_{x''}(y'', y''_d) + b_{y''}(y''_d)\, K^N_{y''}(y'', y''_d)\}$$

$$\tilde{\sigma}_{x''y''} = \frac{\mu}{\pi(\chi + 1)} \{b_{x''}(y''_d)\, K^S_{x''}(y'', y''_d) + b_{y''}(y''_d)\, K^S_{y''}(y'', y''_d)\} \tag{8.11}$$

where $K^S_{x''}$, $K^N_{x''}$, $K^S_{y''}$, $K^N_{y''}$ are the kernels established by the above method. The expressions are lengthy and will not be reproduced here. It will now be recognized that, in contrast to the normal crack example, each component of the dislocation induces both shear and direct tractions, so that the solutions for the modes I and II stress intensities are coupled. The integral equations expressing the requirement that the crack faces be

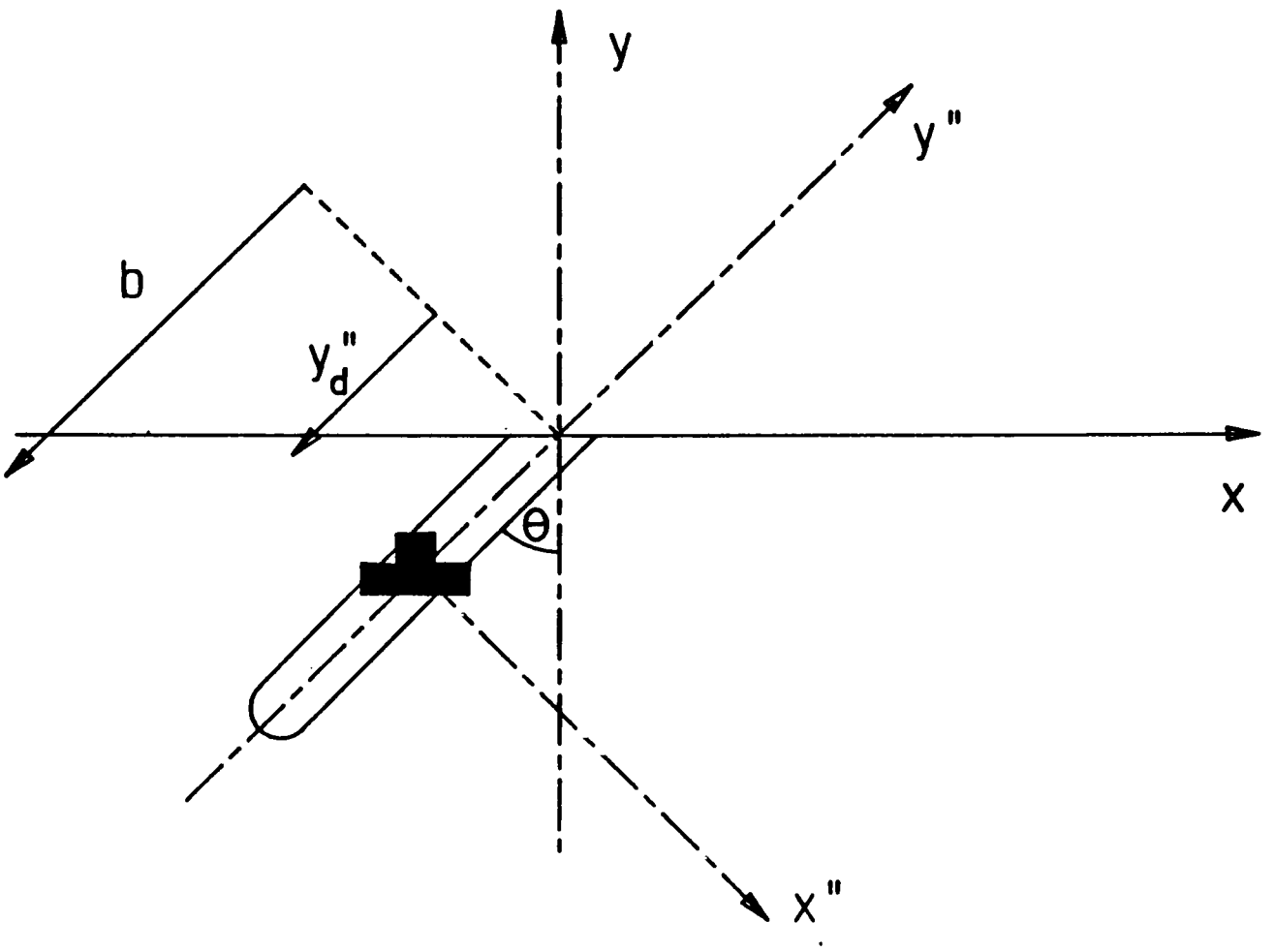

Fig. 8.3 A slant edge crack in a half-plane

traction-free are;

$$S(y'') = \sigma_s(y'') + \frac{\mu}{\pi(\chi + 1)} \left[\int_0^b B_{x''}(y_d)\, K^S_{x''}(y,y_d)\, dy_d + \int_0^b B_{y''}(y_d)\, K^S_{y''}(y,y_d)\, dy_d \right] = 0 \quad (8.12a)$$

$$N(y'') = \sigma_n(y'') + \frac{\mu}{\pi(\chi + 1)} \left[\int_0^b B_{x''}(y_d)\, K^N_{x''}(y,y_d)\, dy_d + \int_0^b B_{y''}(y_d)\, K^N_{y''}(y,y_d)\, dy_d \right] = 0 \quad (8.12b)$$

where $\sigma_s(y'')$, $\sigma_n(y'')$ are the resolved shear and normal components of the stress tensor $\sigma(x,y)$ in the (x'',y'') co-ordinate system. eg. for uniform tensile stress in the x direction $\sigma(x,y) = \sigma_T$

$$\sigma_s(x'',y'') = \sigma_T \sin\theta \cos\theta$$

$$\sigma_n(x'',y'') = \sigma_T \cos 2\theta$$

These equations are normalised in the same way as for a normal crack, and after discretisation give:

$$\frac{\mu}{(\chi + 1)} \sum_{i=1}^{n} \frac{2\pi(1 + s_i)}{(2n + 1)} \left[K^S_{x''}(t_k,s_i)\, \phi_{x''}(s_i) + K^S_{y''}(t_k,s_i)\, \phi_{y''}(s_i) \right] = -\sigma_s(t_k) \quad (8.13a)$$

$$\frac{\mu}{(\chi + 1)} \sum_{i=1}^{n} \frac{2\pi(1 + s_i)}{(2n + 1)} \left[K^N_{x''}(t_k,s_i)\, \phi_{x''}(s_i) + K^N_{y''}(t_k,s_i)\, \phi_{y''}(s_i) \right] = -\sigma_n(t_k) \quad (8.13b)$$

where $\phi_{x''}$, $\phi_{y''}$ denote the bounded functions modelling $B_{x''}$, $B_{y''}$ respectively and s_i, t_k are given in (8.7). The 2n simultaneous equations in the 2n unknowns $\phi_{x''}(s_i)$, $\phi_{y''}(s_i)$ may be readily solved, and the corresponding stress intensity factors (cf. equation 8.8) found as

before. A slant, buried crack may be treated using a combination of the techniques previously described (Nowell and Hills (1987)).

Once again, illustrative results are provided for stress intensity factors under a uniform tension parallel to the free surface. Figure 8.4 shows the stress intensity factors for a slant edge crack under such uniform tensile stress. As expected, the mode I contribution falls from a maximum at $\theta = 0^{o}$ to zero at $\theta = 90^{o}$, whilst the mode II contribution reaches a peak near $\theta = 45^{o}$, where the resolved shear stress is a maximum. The value of n used in these solutions varied between 40 and 60 with the larger number of points being required for cracks at shallow angles to the surface. Solutions for other loading conditions have been calculated by Nowell and Hills (1987) and compare well with established solutions. This suggests that the accuracy of the technique is good, certainly sufficiently so for application to fretting fatigue, where some of the salient parameters (e.g. the coefficient of friction) are subject to a significant degree of experimental uncertainty.

8.5 Application to fretting fatigue

The power of the technique described above is that stress intensity factors for open cracks may be calculated under an arbitrary stress field. Once the kernels have been established, solutions for different loading conditions may be obtained simply by changing σ_s and σ_n in (8.13). The stress field in the specimen has already been calculated in chapter 4 and may be substituted into equation (8.13) to obtain stress intensity factors for cracks growing under the experimental conditions. An implicit assumption is that the distribution of surface tractions remains unaltered in the presence of a crack (i.e. that the compliance of

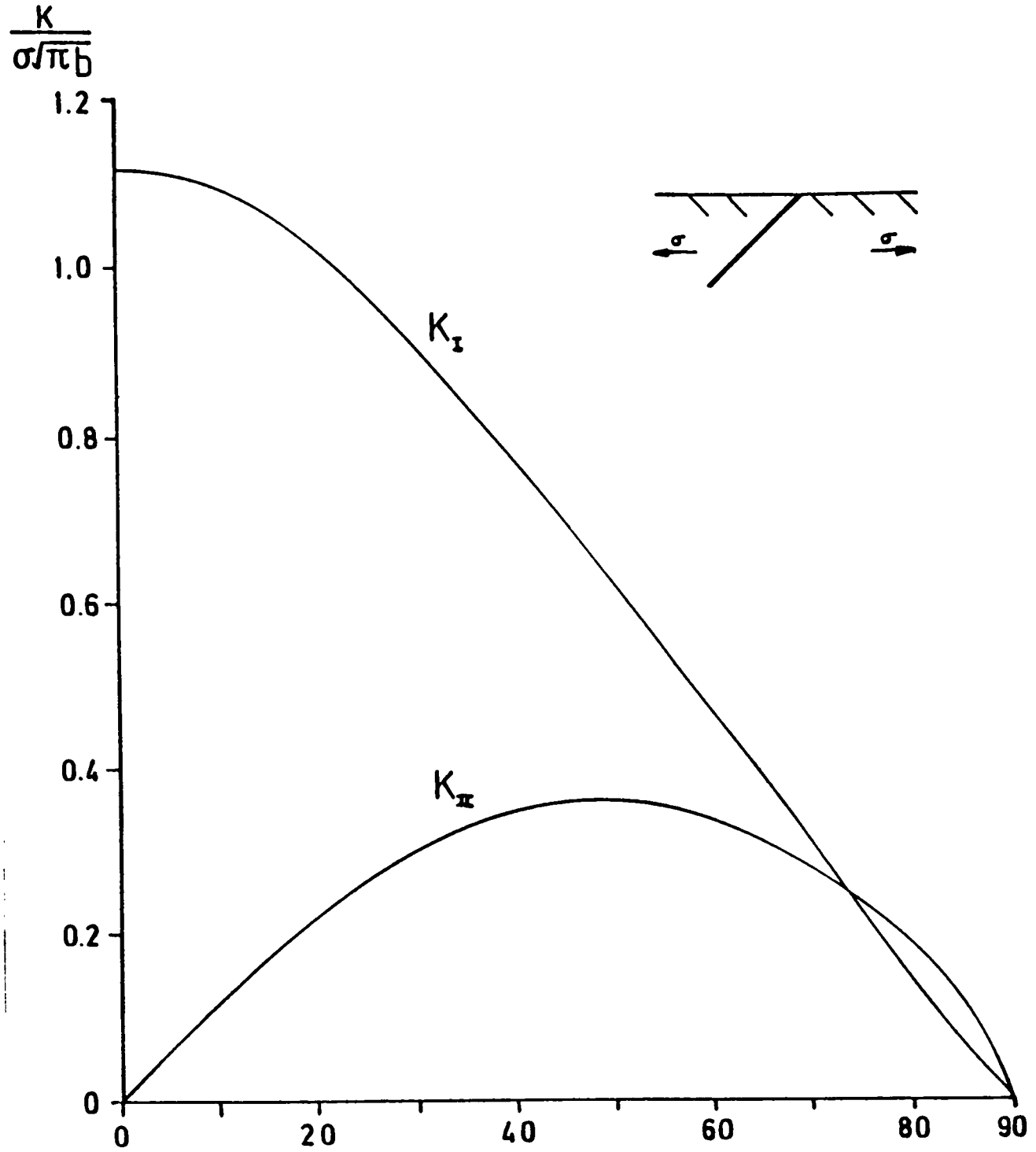

Fig. 8.4 Stress intensity factors for a slant edge crack under uniform tensile stress

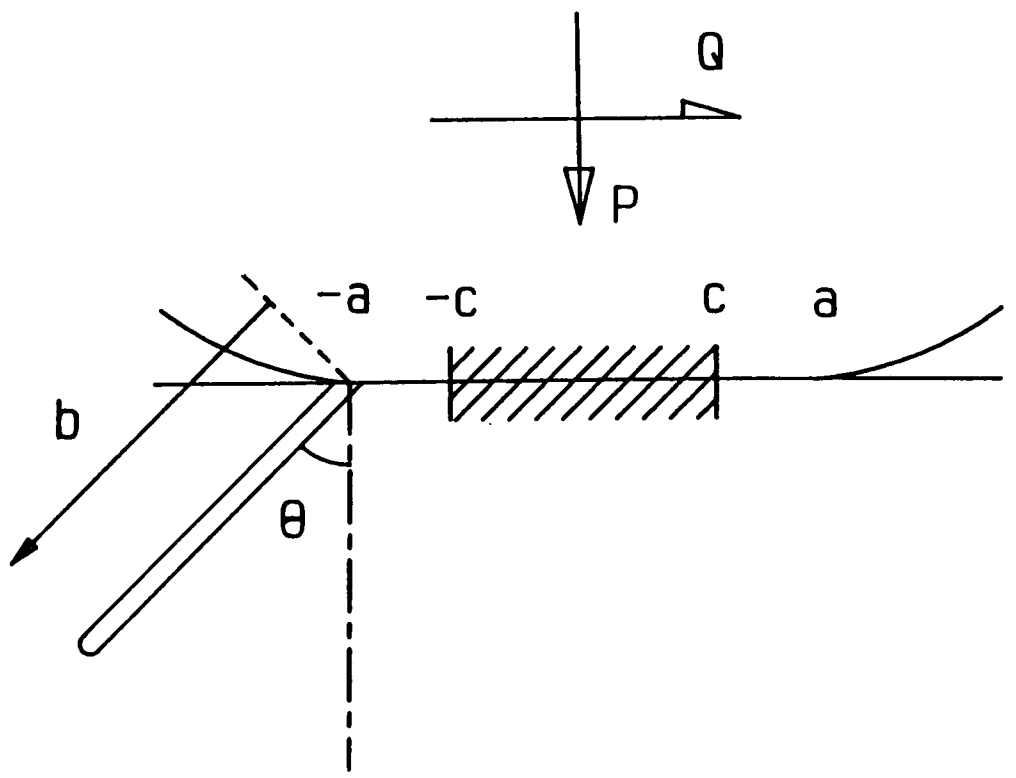

Fig. 8.5 Model of fretting fatigue crack

the specimen does not change). The validity of this assumption has been tested by Bryant, Miller, and Keer (1984) who conclude that the effect of the crack on the surface tractions is small.

As with the determination of surface tractions, the specimen is modelled as a half-plane for the purposes of calculating stress intensity factors. Benthem and Koiter (1973) have shown that a perpendicular edge crack in a strip under uniform tension has to grow to at least 15% of the strip width before the stress intensity factor varies by more than 10% from the half-plane value. In the current experiments cracks of this length will be propagating largely under the influence of the bulk stress σ rather than the stresses associated with the contact. Thus the effect of finite strip width will only become significant once the effect of the contact stresses has ceased to be so. The retention of the half-plane assumption is therefore justified for the present analysis. The dislocation method of calculating stress intensity factors can be used for cracks in strips of finite width (Tsamasphyros and Theotokoglou (1986)) but the influence functions contain infinite integrals which render the method far more cumbersome.

It is important to check that the crack remains open under the applied loading for the results to remain valid. The Burgers vector densities $B_{x''}$ and $B_{y''}$ are equivalent to the differentials of crack opening and relative axial displacement of the crack faces respectively (Erdogan, Gupta, and Cook (1973)). Hence the relevant check may be performed by ensuring:

$$\int_{-b}^{y_1} B_{x''}(y'')\, dy'' > 0 \qquad -b < y_1 < 0 \qquad (8.14)$$

In practice, however, under the type of stress fields present in fretting

fatigue closure at the crack-tip occurs first and the condition that $K_I > 0$ is sufficient to determine the validity of the method. If a crack tip is closed, no growth can take place in mode I and growth in mode II is unlikely in practice (O'Connor and Hills (1986)) because the crack faces are usually sufficiently rough to prevent relative slip. The additional complexity involved in calculating K_{II} values for closed cracks was not therefore thought worthwhile for the current investigation.

Experimentally, cracks were found to initiate at or near the trailing edge of the contact ($x/a = -1$) and this is also the location of both the most positive principal stress and the maximum shear stress in the specimen. Stress intensity factors were therefore evaluated for the configuration shown in Fig. 8.5 where a crack of length b has propagated at an angle θ to the surface normal from a point at the trailing edge of the contact. Crack growth will be governed by the severest stress state encountered during the fretting cycle, i.e. when Q and σ take their most positive values. The maximum values of Q and σ were therefore used in the analysis. Results are presented here for the experimental configuration of series 3 ($Q/fP = 0.6$, $\sigma/p_o = 0.648$, $f = 0.75$) and are typical of those for the other experiments. Figure 8.6 is in the form of a polar plot of stress intensity factors against crack angle for three different crack lengths ($b/a = 0.1$, 0.5, and 1.0). Both K_I and K_{II} are normalised with respect to the contact semi-width a rather than the more usual crack length b. This allows the variation of K with crack length to be presented more clearly. Values of mode II stress intensity factor change sign at $\theta \approx 10^o$ and, since the magnitude of K_{II} rather than its sign quantifies the shear-mode stress intensity, $|K_{II}|$ is plotted.

For all three crack lengths, K_I reaches a maximum for cracks within

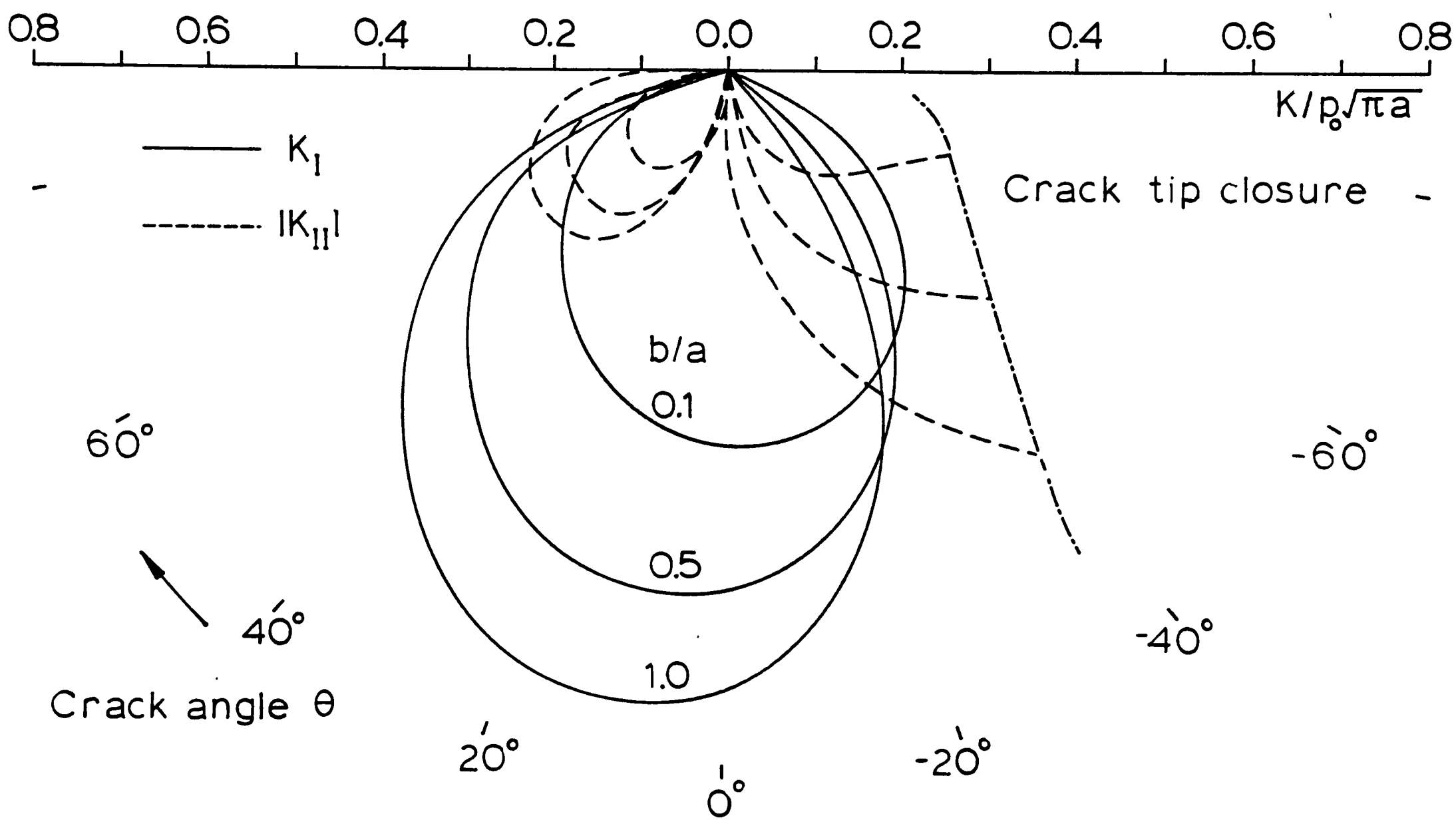

Fig. 8.6 Polar plot of stress intensity factors for fretting fatigue cracks propagating from the trailing edge of contact Series 3 experiments

10^{o} of the surface normal. This is as expected, since this plane is perpendicular to the most positive principal stress (chapter 4). K_{II} values are very small for cracks at these orientations. The magnitude of the shear-mode stress intensity factor, $|K_{II}|$, reaches maxima for cracks at $\pm$ 45^{o} to the surface normal. Values for cracks orientated under the contact are much higher than those on the perpendicular plane, reflecting the higher shear stresses present. An extensive zone of crack tip closure is present directly under the contact where K_{I} falls to zero. As discussed above, the present formulation cannot calculate K_{II} in this region without introducing additional complexity and this was not attempted since cracks are unlikely to continue propagating once the crack tip has closed.

Experimentally cracks were observed to propagate obliquely under the contact at between 30^{o} and 50^{o} to the surface normal and this is precisely the orientation which gives rise to the maximum values of $|K_{II}|$. It seems likely, therefore, that this phase of oblique propagation is controlled by a shear mechanism. Propagation cannot continue at this orientation indefinitely since the zone of crack-tip closure is entered. In the experiments cracks were found to change direction after some distance and to continue to grow normal to the free surface. This takes them away from the zone of crack tip closure. The requirement for this direction change to take place before the closure zone is encountered by the crack tip provides one possible explanation for the size effect which will be discussed at greater length in chapter 9.

Chapter 9

Interpretation of results

9.1 Introduction

The existence of a size effect observed by Bramhall (1973) has been confirmed by the present series of experiments. A similar effect has also been discovered by Waterhouse (1968) for different materials (α-Brass, and an Al-Mg-Zn alloy). The techniques of contact stress analysis and evaluation of stress intensity factors developed in previous chapters may now be used to develop possible explanations of this phenomenon.

9.2 Statistical effects

One possible cause of the size effect, which must be examined first, arises as a consequence of the random distribution of defects present in any material. The initiation of a failure may be taken to occur when a defect is stressed above a particular critical value. Clearly, for any given material with a constant density of defects, the larger the volume which is stressed above the critical level, the larger the probability that a defect will be present within that volume. In the experiments carried out in this investigation, the stressed volume increases with contact size and thus the larger contacts would have a greater probability of failure. This effect would manifest itself in the experimental results by an increase in mean life to failure with decreasing contact size, since the probability of a defect initiating a

failure would also decrease.

This type of statistical model has been successfully employed by Ioannides and Harris (1984) to predict the mean fatigue life of rolling element bearings under varying stress levels. An immediate difficulty arises in applying the technique to the current results in that only one experiment has been carried out at each stress state and contact size so that a good estimate for the mean life is not available. However, the lack of scatter in the experimental results suggests that the fatigue life recorded for each test may be taken as an estimate for the mean fatigue life under those conditions.

The analysis of Ioannides and Harris is based on the Weibull (1949) weakest link theory of fatigue failure. Its application to the analysis of the current size effect may be summarised briefly as follows. The entire fatigue life of the specimen is assumed to be taken up by initiation. The probability of survival Δs_i of a volume element ΔV_i may be expressed as:

$$\ln(1/\Delta s_i) = F(N, \sigma_i - \sigma_{ui})\ \Delta V_i \qquad (9.1)$$

where N represents the number of cycles to failure, σ_i a stress-related fatigue parameter such as the maximum shear stress amplitude, and σ_{ui} is the fatigue limit of this parameter (i.e. no failure takes place if $\sigma_i < \sigma_{ui}$). The function F may be approximated by a product of power functions such that:

$$\ln(1/\Delta s_i) = A\ N^e\ H(\sigma_i - \sigma_{ui})\ (\sigma_i - \sigma_{ui})^c\ \Delta V_i \qquad (9.2)$$

where e and c are material constants and H is the Heaviside function.

The probability of survival, s, of the entire body is given by:

$$s = \Delta s_1 . \Delta s_2 . \Delta s_3 ..... \Delta s_n \tag{9.3}$$

so that in the limit $\Delta V \rightarrow 0$

$$\ln(1/s) = \int_V A\ N^e\ (\sigma_i - \sigma_{ui})\ dv \tag{9.4}$$

where the integration is carried out over the whole volume for which $\sigma_i > \sigma_{ui}$. To account for the observation that flaws near the surface are more likely to initiate a failure a depth term y is added. Hence, for the two-dimensional case of interest here:

$$\ln(1/s) = B\ N^e \int_A \frac{(\sigma_i - \sigma_{ui})}{y^h}\ dA \tag{9.5}$$

which, when non-dimensionalised with respect to the contact semi width, a, becomes:

$$\ln(1/s) = B\ N^e\ a^{2-h} \int_A \frac{(\sigma_i - \sigma_{ui})}{(y/a)^h}\ \frac{dA}{a^2} \tag{9.6}$$

The integral is now constant for the experiments within a particular series, since the non-dimensional stress field is constant. Hence:

$$\ln(1/s) = C\ N^e\ a^{2-h} \tag{9.7}$$

and for a given probability of failure

$$N_s = k\, a^{((h-2)/e)} \qquad (9.8)$$

where k is a constant depending on the stress state and h and e are material constants. Thus, if the statistical argument provides an explanation of the size effect, the mean specimen lives might be expected to follow the above power-law relationship. The exponent would be a material constant and thus the same for all series.

The variation of specimen lives with contact semi-width is plotted on logarithmic scales in Fig. 9.1. It can be seen that there is little evidence of any such power-law relationship, although it is recognised that the specimen life from a single experiment provides a poor estimate of the mean life. The statistical analysis does not therefore seem capable of explaining the rapid increase in fatigue life that takes place at the critical contact size. For a more tenable explanation a more detailed consideration of the fretting process is neccessary.

9.3 Crack arrest

Bramhall (1973) suggests that the size effect is due to the increase in stressed volume at the larger contact sizes. He argued that the stress field due to the contact must be sufficiently extensive to propagate cracks to a length from which they could grow under the bulk tensile stress alone. This argument was formalised by O'Connor and Hills (1986). They calculated stress intensity factors for normal cracks growing from the trailing edge of a typical fretting contact and looked for conditions under which these cracks would self-arrest. Unfortunately, they discovered that K_I values for these cracks increased monotonically with crack length. Thus, if linear elastic fracture

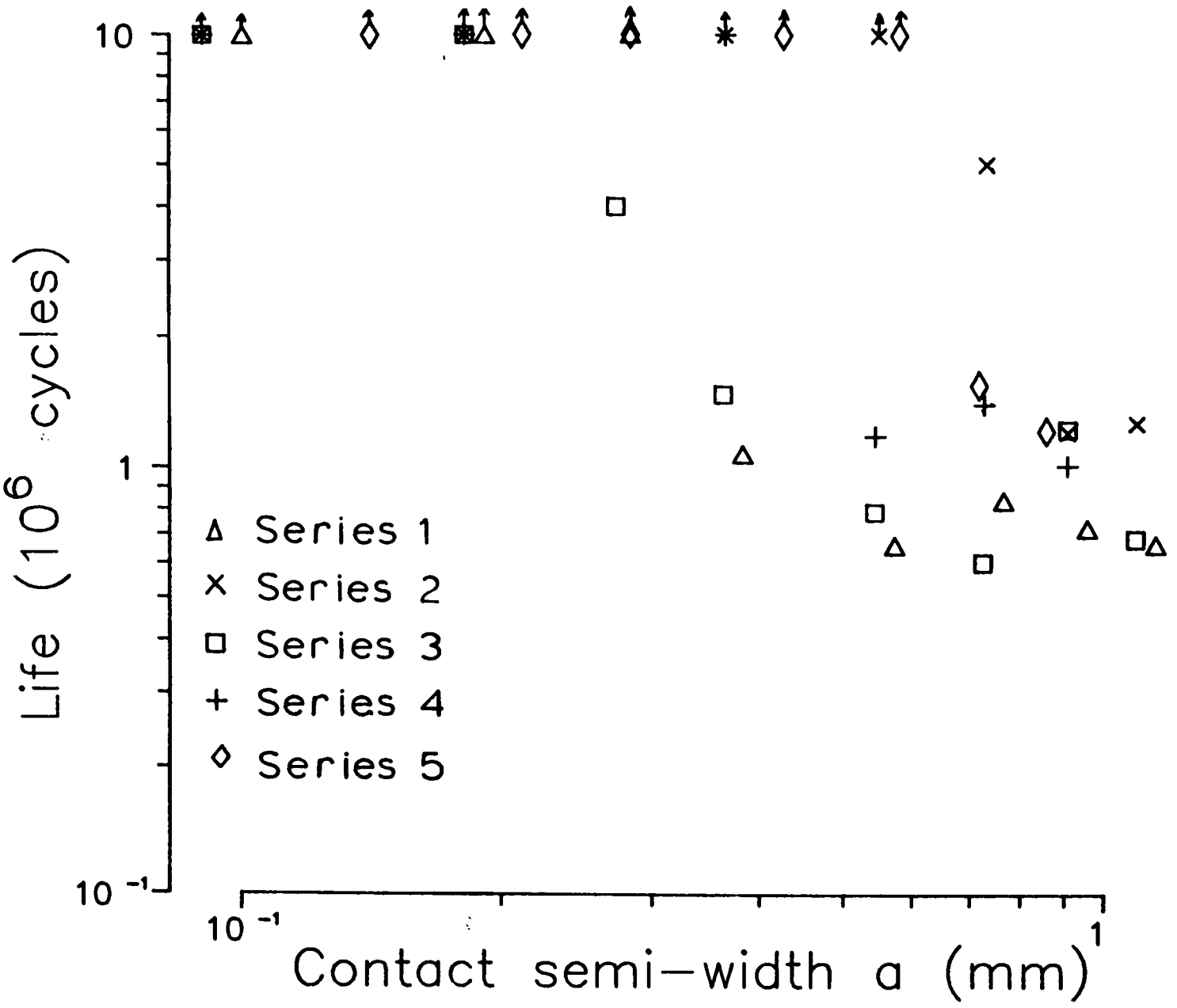

Fig. 9.1 Variation of fatigue lives with contact size (logarithmic plot)

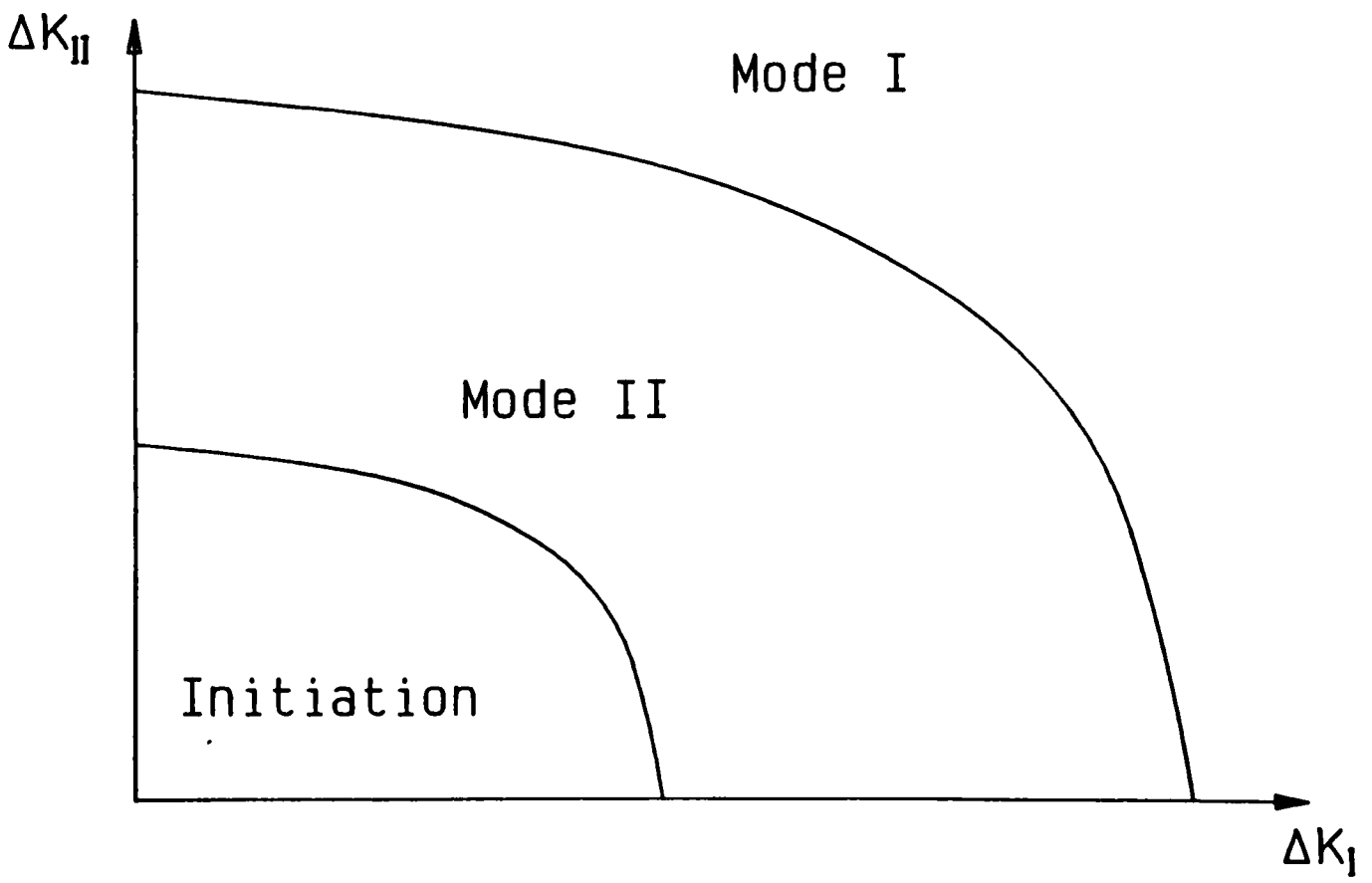

Fig. 9.2 Boundaries between different modes of crack propagation (Otsuka, Mori, and Miyata (1975))

mechanics predicted crack growth under the contact field, then this growth would always continue and no self-arrest would occur.

Experimental observations in this and other investigations reveal a characteristic phase of oblique crack growth before the direction of propagation changes to one normal to the free surface. This oblique phase is more closely aligned with the direction of maximum shear stress than with the perpendicular to the most positive principal stress (Fig. 4.10). This suggests that the oblique phase is controlled by a shear mechanism (Stage 1, as described by Forsythe (1961)). In contrast, the normal phase of crack propogation is nearly perpendicular to the most positive principal stress and is most likely to take place in the tensile mode (Stage 2, Forsythe (1961)).

Cracks growing obliquely from the trailing edge of the contact will eventually encounter the compressive region of crack tip closure shown in Fig. 8.6. This is likely to lead to crack self arrest, since the crack faces will be held together in this zone and the high coefficient of friction between the rough surfaces will reduce the shear-mode stress intensity factor ΔK_{II}. The existence of this possible mode of self-arrest allows an explanation of the size effect to be formulated as follows: Any crack growing in stage 1 (mode II) obliquely under the contact must change to stage 2 (mode I) propagation normal to the free surface before the region of crack tip closure is reached, otherwise self-arrest will occur. For large contacts, cracks will be long enough to attain the threshold for mode I growth before the compressive zone is reached and failure will result. For small contact widths the compressive zone will be closer to the point of crack initiation and so any oblique cracks will not be long enough to start growing in mode I before the crack tip closes and consequently self-arrest will occur.

The results of chapter 8 allow stress intensity factors to be calculated for oblique cracks growing under the contact from the trailing edge. In general such cracks will experience both shear and tensile loading and, in order to calculate the length at which transition to mode I growth takes place a relationship between the calculated values of ΔK_I and ΔK_{II} and the mode of propagation is required. Otsuka, Mori, and Miyata (1975) have proposed lower bounds for the onset of both shear (mode II) and tensile (mode I) growth. An outline of their derivation is as follows: the tangential and shear stresses near the crack tip are:

$$\sigma_{\theta\theta} = \frac{1}{\sqrt{2\pi r}} \cos\frac{\theta}{2} \left[K_I \cos^2\frac{\theta}{2} - \frac{3}{2} K_{II} \sin\theta\right]$$

$$\tau_{r\theta} = \frac{1}{2\sqrt{2\pi r}} \cos\frac{\theta}{2} \left[K_I \sin\theta + K_{II} (3\cos\theta - 1)\right] \qquad (9.9)$$

where r,θ are polar co-ordinates relative to the crack tip. From these, parameters K_σ and K_τ which represent the intensity of these stresses are defined:

$$K_\sigma = \sigma_{\theta\theta}\sqrt{2\pi r} = \cos\frac{\theta}{2} \left[K_I \cos^2\frac{\theta}{2} - \frac{3}{2} K_{II} \sin\theta\right]$$

$$K_\tau = \tau_{r\theta}\sqrt{2\pi r} = \frac{1}{2}\cos\frac{\theta}{2} \left[K_I \sin\theta + K_{II} (3\cos\theta - 1)\right] \qquad (9.10)$$

For any given crack, these quantities are maximised with respect to θ. The boundary between initiation and shear growth is then found to be:

$$K_\tau(\theta)_{max} = \text{material constant} \qquad (9.11)$$

and the corresponding boundary between shear and tensile mode growth is:

$$K_{\sigma}(\theta)_{max} = \text{material constant} \qquad (9.12)$$

These boundaries are shown diagramatically in Fig. 9.2. Pook (1985) supports these criteria by analysing the results of many experimental investigations with different alloys of both steel and aluminium and produces empirical equations for the boundary curves. The boundary between initiation and mode II growth is given by:

$$\frac{\Delta K_{II}}{\Delta K_{th}} = 0.25 \left[1 - 2.6(\Delta K_I/\Delta K_{th})^2\right]^{0.5} \qquad (9.13)$$

That between mode II and mode I growth is similarly given by:

$$\frac{\Delta K_{II}}{\Delta K_{th}} = \left[0.75 - 0.83\ (\Delta K_I/\Delta K_{th}) - 0.08\ (\Delta K_I/\Delta K_{th})^2\right]^{0.5} \qquad (9.14)$$

where ΔK_{th} is the threshold mode I stress intensity factor range in fatigue.

Both mode I and mode II stress intensity factors can be calculated for the experimental configurations as outlined in chapter 8. These can then be plotted on the propagation mode map developed above to determine if crack closure occurs before transition to mode I growth. Figure 9.3 shows the different results obtained. For large contact widths the variation of ΔK_I and ΔK_{II} with crack length produces the locus A. Transition to mode I growth (with a corresponding change in the direction of propagation) occurs before the crack has reached the closure zone and hence the crack will continue to grow to failure. For smaller contacts,

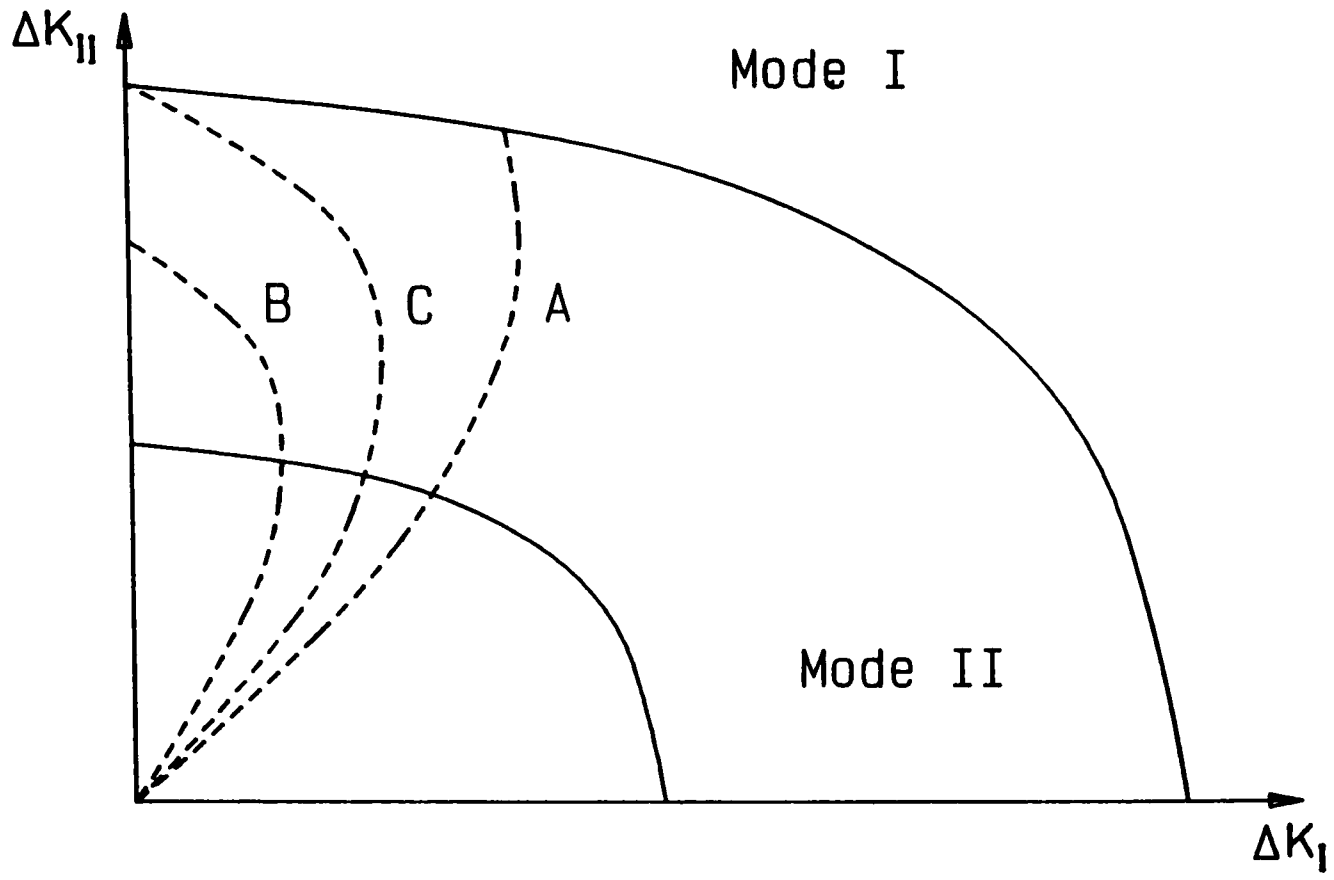

Fig. 9.3 Possible histories of crack growth plotted on propagation mode map

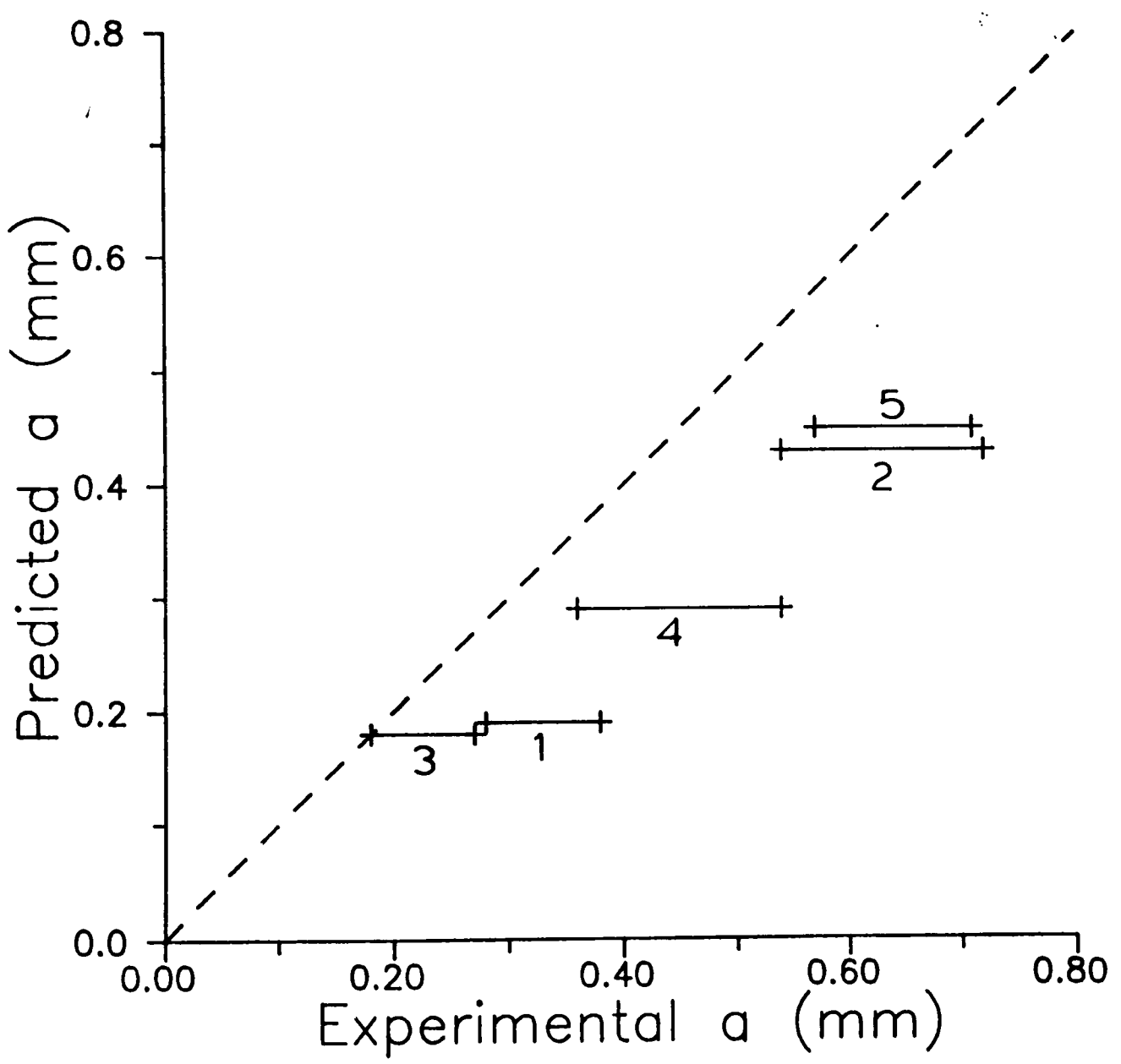

Fig. 9.4 Comparison of experimental and predicted critical contact sizes (crack arrest criterion)

locus B results, where crack closure ($K_I \rightarrow 0$) occurs first and self arrest takes place. The locus at the critical contact width is given by C where transition takes place just as the closure zone is reached. Hence an estimate of the critical contact width for failure can be found by finding the value of a for which a curve of form C is obtained.

The experiments of all 5 main series were analysed in this way and predictions of critical contact size made. A crack angle of 45^o to the surface normal was chosen, since this is the plane of maximum resolved shear stress in the uncracked body and therefore the most likely plane on which cracks will initiate. A value of $\Delta K_{th} = 2.1\ MN/m^{3/2}$ was employed (Pook (1978), R = -1.0). A comparison of predicted and actual critical contact semi-widths is presented in Fig. 9.4

The agreement between experimental and predicted values is quite reasonable, although all the predicted values are less than those recorded in the experiments. Designing on the basis of this criterion would therefore appear to result in a safe component. However accurate values of ΔK_{th} are difficult to obtain and the discrepancy may well be due to an incorrect value being employed in the analysis. Equally, values of K_{II} for cracks at these oblique angles vary significantly with crack angle (Fig. 8.6) and consequently predicted values of critical contact width are sensitive to the choice of crack angle. Indeed, if a crack angle of 40^o is chosen (i.e. 5^o closer to the surface normal) analysis of series 1 shows that cracks will miss the closure zone altogether and no self arrest will occur. Hence, although the results presented here seem reasonable, they are extremely sensitive to the choice of initial propagation angle.

If crack self-arrest does take place at the smaller contact widths, arrested cracks would be present in the intact specimens. The fracture

mechanics analysis carried out predicts that these would have lengths of the order of the contact semi-width and so would be relatively easy to detect. As reported in Chapter 3, several intact specimens were sectioned and examined under the scanning electron microscope yet no cracks were visible. This may have been because the sectioning process itself destroyed all evidence of the cracks, although the fact that many subsidiary cracks were observed in the sections of failed specimens suggests that this was not the case.

In order to save machining time, several intact specimens were re-used in subsequent experiments by fretting at a different point. If arrested micro-cracks had been present from the original fretting, these might have been expected to start propagating since the compressive region was no longer present. Thus, one might have expected that failure would occur at the original fretting scar, where micro-cracks were already present, rather than at the site of the new scar, where they would have first to be initiated. However, no such failures took place, adding further to the argument that there are no arrested cracks in the intact specimens.

If the controlling mechanism was crack arrest as described above, the specimen's life might be expected to be independent of slip amplitude, provided that the stress intensity factor amplitudes ΔK_I, ΔK_{II} remained constant. However, the results of series 6 show that specimen life is highly dependent on the degree of load reversal and consequently on the amplitude of micro-slip. It would seem, therefore, that the mechanism of crack self-arrest described above cannot account for all the experimental observations and an alternative hypothesis linking the amplitude of micro-slip to the probability of crack initiation must be developed.

9.4 Crack initiation

Several authors (e.g. Nishioka and Hirakawa (1969d)) have reported the variation of fretting fatigue life with amplitude of slip at identical stress conditions. In each series of the current experiments the geometric size of the contact is increased whilst keeping the magnitude of the stress state constant. This increase in size will automatically increase the amplitude of micro-slip taking place in the slip zones, since the contacts are geometrically similar. Calculated maximum slip amplitudes for the current experiments lie between 0.4 and 4.0 μm (peak - peak). There could well be a critical amount of slip necessary to initiate fretting fatigue cracks and, if so, this might be responsible for the size effect reported. The main effect of micro-slip is to cause surface damage and so it is perhaps better to consider the amount of such damage rather than slip amplitude alone.

In order to investigate further the possibility that a critical amount of damage is neccesary to initiate fretting fatigue cracks a damage parameter must be defined. It should be recognised first that the initiation process takes place on the surface and is therefore influenced by surface conditions such as roughness, residual stress, and degree of asperity interaction. These will vary with both position and time and it is not possible to define precisely the conditions at any particular point. The best approach available is to attempt to characterise the average surface conditions by use of the known bulk properties calculated from classical contact theory. There are, it is recognised, limitations to this approach, but it should be possible to compare mean amounts of fretting damage.

Sato, Shima, and Sugawara (1985) conducted a study of the fretting of glass and attempted to relate the amount of fretting damage to the values of several candidate damage parameters. One of those suggested was the amount of shear work per unit surface area in each fretting cycle. A measure of this quantity is given by the product $\tau.\delta$ where τ is the peak value of the cyclic shear traction at the surface and δ the amplitude of relative displacement between the two surfaces at that point in each fretting cycle. This parameter is attractive for several reasons: first it accords well with the experimentally observed location of fretting damage. Sato, Shima , and Sugawara found that fretting fatigue cracks initiated close to the point of maximum $\tau.\delta$. Secondly, the parameter falls to zero within the stick zone and outside the contact, where no damage takes place. More fundamentally, crack initiation is thought to take place by a shear process (Buckley (1975)) and so a parameter describing the amount of shear work available seems appropriate.

Ruiz, Boddington, and Chen (1984) carried out an investigation of the fretting of turbine blade dovetail joints. They calculated surface tractions and displacements by the finite element method and compared the values to the amount of fretting damage recorded and the initiation site of fatigue cracks. The damage parameter ($\tau.\delta$) was found to describe the amount of fretting damage well. However, in discussing the initiation of cracks they recognise that the tensile stress parallel to the surface is also a factor. Cracks are more likely to initiate if there is a high tensile stress in the surface and are less likely to do so in the presence of a compressive stress. The precise effect of the surface stress is difficult to quantify, but Ruiz, Boddington, and Chen suggest that by multiplying the damage parameter ($\tau.\delta$) by the peak value of the

cyclic tensile stress (σ) parallel to the surface, a simple initiation parameter ($\sigma.\tau.\delta$) may be obtained which describes the probability of crack initiation at any particular surface point under fretting conditions. The sites of crack initiation in their experiments agreed well with the maximum values of this parameter.

Some recent experimental work has been carried out by Kuno (1988) in which fretting of a steel ball on a plane surface was carried out under closely controlled conditions of partial slip, giving rise to an annular slip zone surrounding the central region of stick. The sites of crack initiation were recorded and compared with the positions of maxima of various candidate initiation parameters. Cracks initiated in the slip zones and were initially perpendicular to the axis of fretting. These locations correlated well with the point of maximum $\sigma.\tau.\delta$, whereas the $\tau.\delta$ parameter suggests initiation is equally likely for all points at a given radius.

The initiation parameter ($\sigma.\tau.\delta$) seems the best available candidate to describe crack initiation and it can easily be applied to the current experimental configuration. The stress analysis carried out in chapter 4 has already revealed values of the surface shear traction τ and the tensile stress in the surface σ. The amplitude of micro-slip can also be easily obtained. The results of Poritsky (1950) which give tangential displacements resulting from parabolic distributions of normal and shear traction may be employed together with the principle of superposition for all those configurations where the surface traction distribution is the sum of parabolic components. For other configurations (e.g. series 2 experiments, where reverse slip takes place at the leading edge) a numerical approach can be adopted. The relative surface strain $\left[\frac{\partial u_1}{\partial x} - \frac{\partial u_2}{\partial x} \right]$ may be calculated at any point outside the stick zone by

invoking (4.14) and expressing q(x) as the sum of the full slip solution together with a perturbation q'(x). Once this is known throughout the region of slip, the relative displacement is found by integration:

$$\delta(x) = \int_{c1}^{x} \left[\frac{\partial u_1}{\partial x} - \frac{\partial u_2}{\partial x} \right] dx \qquad (9.15)$$

Figure 9.5 shows the variation of the damage parameter ($\tau.\delta$) and the initiation parameter ($\sigma.\tau.\delta$) in the trailing slip zone (i.e. the one from which cracks are found to initiate) for series 3 experiments. The maxima of both parameters occurs very close to the edge of contact and are thus consistent with the experimental observation that fatigue cracks start at or near the trailing edge of the contact. Since the amount of micro-slip δ is proportional to contact size, the initiation parameter $\sigma.\tau.\delta$ will also vary proportionally with a. The maximum value of this parameter can now be calculated for the critical contact width of each series of experiments. Results are presented below.

Series	Critical contact semi-width a_{crit} (mm)	Maximum value of initiation parameter $\sigma.\tau.\delta$ (N^2/mm^3)
1	0.28 → 0.38	4.47 → 6.06
2	0.54 → 0.72	3.26 → 4.35
3	0.18 → 0.27	2.42 → 3.63
4	0.36 → 0.54	3.94 → 5.91
5	0.57 → 0.71	3.47 → 4.32

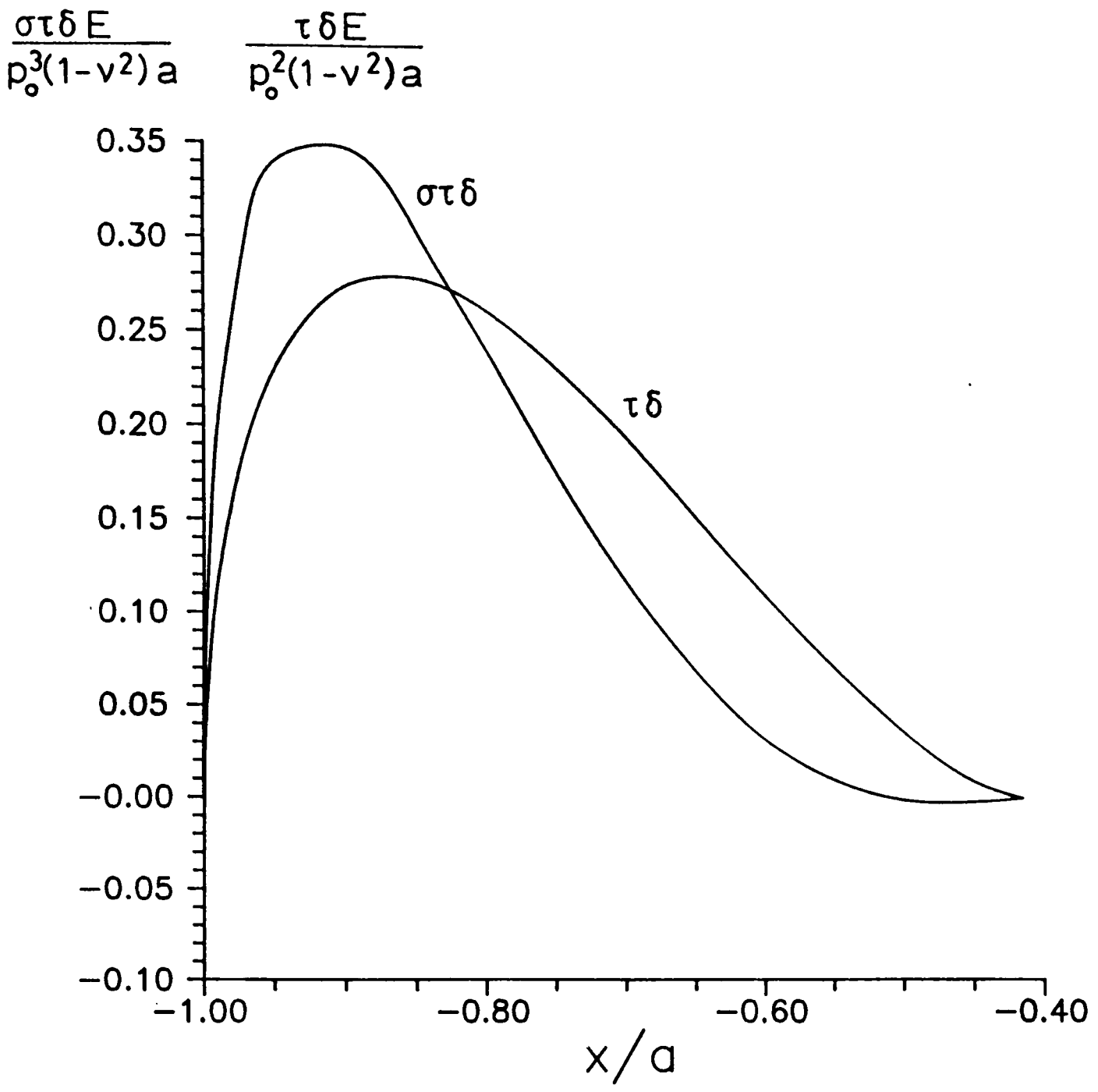

Fig. 9.5 Variation of damage parameter ($\tau.\delta$) and initiation parameter ($\sigma.\tau.\delta$) in trailing slip zone for series 3 experiments

The mean value of $(\sigma.\tau.\delta)|_{max}$ at the onset of failure is 4.18 N^2/mm^3. For the purposes of assessing the validity of the proposed initiation criterion this may be taken to be a material constant expressing the minimum conditions necessary to initiate a fretting fatigue crack. Expected critical contact semi-widths can now be calculated at which $\sigma.\tau.\delta$ would exceed this value and compared with the experimental values.

Figure 9.6 shows the relationship between actual and predicted contact semi-widths for the onset of fretting fatigue failure. The agreement is remarkably good, although it should be borne in mind that the critical value for $\sigma.\tau.\delta$ was itself obtained from the experimental results rather than being a material constant measured in some other way. Values of the $\sigma.\tau.\delta$ parameter may also be calculated in a similar way for the experiments in series 6, where the degree of load reversal and consequently the amplitude of micro-slip was varied. The critical value of minimum bulk stress was found to lie between -52.4 MN/m^2 and -39.9 MN/m^2 (Appendix A). These correspond to values of $\sigma.\tau.\delta$ in the range 3.04 → 4.17 N^2/mm^3. Thus the critical value of the initiation parameter in this series of experiments was very close to the mean value for the other 5 series (4.18 N^2/mm^3). Indeed, the specimen tested at a minimum bulk stress of -52.4 MN/m^2 ($\sigma.\tau.\delta$ = 4.17 N^2/mm^3) survived for 7.7 x 10^6 cycles (whereas most failures occurred in less than 2 x 10^6 cycles), indicating that initiation had taken much longer than usual and suggesting that conditions might be close to the critical values for initiation to take place.

The assumption of a critical amount of damage for crack initiation to take place also fits the observations found from examining the specimens much better than the criterion of self-arrest. If the amount

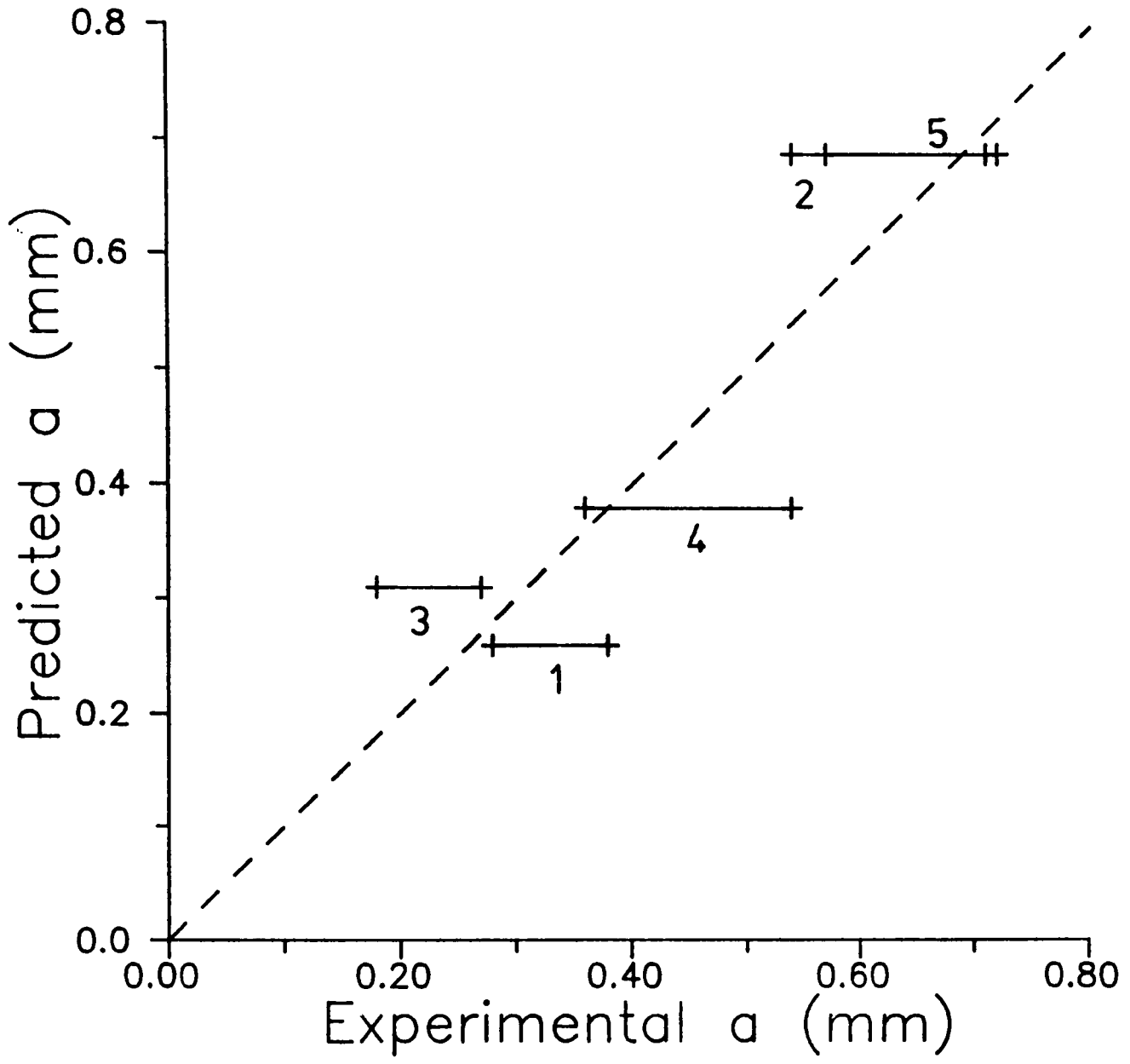

Fig. 9.6 Comparison of experimental and predicted critical contact sizes (crack initiation criterion)

of damage is less than the critical value, no initiation would occur and no cracks would be observed in the intact specimens. Examination of the intact specimens did not reveal any cracks and thus it is likely that initiation did not take place. The observed amount of fretting damage on intact specimens was much less than on those that failed. The damage and initiation parameters chosen have lower values for these contacts and thus the reduced fretting effect might have been predicted.

9.5 Discussion

Three possible explanations of the size effect have been postulated. First, the possibility of a statistical effect was investigated and it was shown that this could not account for the rapid transition in fatigue lives at the critical contact size. Second, a mechanism of crack-arrest was proposed and critical contact sizes calculated using the stress analysis and fracture mechanics techniques developed in previous chapters. This postulation led to reasonable predictions of critical contact size, but the results of the calculations are sensitive to the input parameters particularly the choice of initial crack angle. There was also little additional evidence in support of the arrest mechanism. No arrested cracks could be found in intact specimens and the theory cannot account for the variation of fatigue life with the amplitude of micro-slip between the contacting surfaces.

The third possibility investigated was that a critical amount of fretting damage was required to initiate cracks. This amount of damage can be characterised by the shear work per unit surface area ($\tau.\delta$) and, when combined with the tensile stress in the surface, a simple initiation parameter $\sigma.\tau.\delta$ first proposed by Ruiz, Boddington, and Chen (1984) can

be calculated. Although necessarily simplified this approach seems to provide a good explanation of the experimental results. The existence of a critical value of the initiation parameter, below which cracks will not form, can account for the size effect revealed in the main series of experiments in addition to the variation of fatigue life with the degree of load reversal discovered in series 6. A critical value for the initiation parameter would also explain the absence of cracks in the intact specimens, together with the reduced amount of fretting damage.

The concept of a critical amount of fretting for initiation of fatigue cracks seems to provide the best explanation of the size effect first noted by Bramhall (1973) and confirmed by the present series of experiments. It would also account for the variation of fatigue life with slip amplitude recorded by many previous authors.

The original aim of this project was to provide design guidelines for contacts subject to fretting fatigue. The results of the investigation suggest that a profitable approach would be to minimise the initiation parameter, $\sigma.\tau.\delta$, by varying the design parameters. If the maximum value of this parameter can be reduced below the levels found to initiate cracks for the chosen combination of materials and external conditions, then fretting fatigue might be avoided. Figure 9.7 shows how the maximum value of $\sigma.\tau.\delta$ varies with the coefficient of friction for two sample contacts of cylinders on a half-plane. The chosen parameters are $Q/P = 0.3$, $\nu = 0.3$, and $\sigma/p_o = 0.0$ or 0.5. In both cases the value of the initiation parameter falls with reducing coefficient of friction. It might therefore be possible to increase the fretting fatigue resistance of such a contact by introducing a surface coating with a lower coefficient of friction (provided that the contact is not allowed to enter the sliding regime). These predictions accord with the

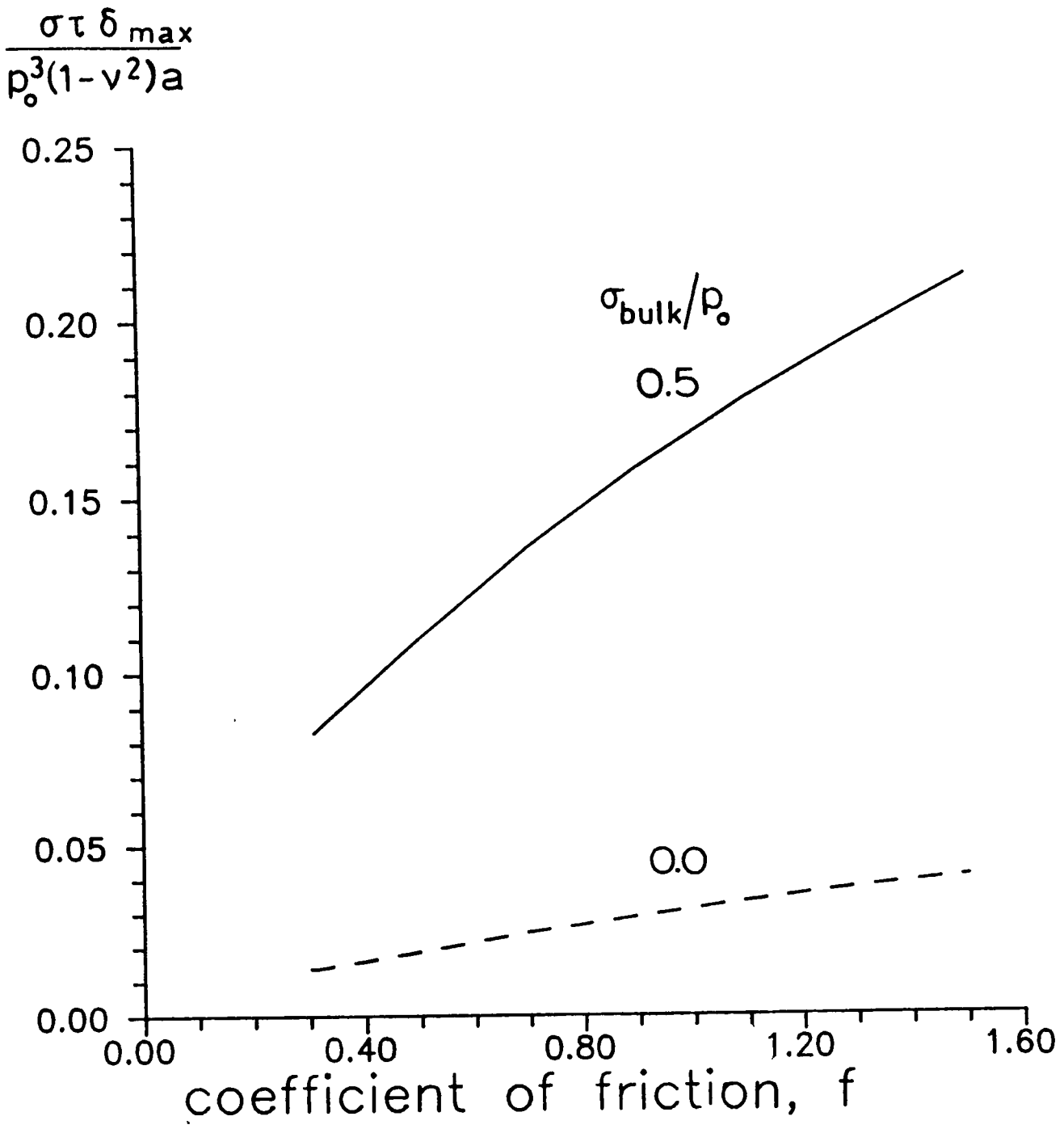

Fig. 9.7 Variation of initiation parameter with coefficient of friction for two sample contacts ($Q/P = 0.3$, $\nu = 0.3$, $\sigma/p_o = 0.0$ or 0.5)

experimental results of Ruiz and Chen (1986), who show that dovetail joints have a higher fretting fatigue strength at 600°C than at room temperature, principally because oxide formation reduced the interfacial coefficient of friction.

Chapter 10

Conclusions and suggestions for further work

10.1 Conclusions

The following main conclusions can be drawn from the work carried out in this investigation.

(i) The variation in fretting fatigue life with contact size reported by Bramhall (1973) for an Al/4% Cu alloy has been clearly demonstrated under closely controlled experimental conditions in which all the important parameters were monitored.

(ii) The chosen experimental contact configuration of cylinders acting on a plane specimen has been shown to be amenable to analysis using the techniques of elastic contact mechanics and linear elastic fracture mechanics. The effects of bulk stress in the specimen, finite specimen thickness, dissimilar material constants, and surface roughness have been considered. For the present configuration, only the bulk stress and surface roughness alter the stress field substantially from that of the classic Mindlin (1949) analysis. The effect of the specimen bulk stress can be analysed with little difficulty, but surface roughness effects are less predictable, owing to the random nature of the surface. A simple analysis predicts that the discrepancy between classical and exact analyses persists for only a small distance from the surface for most of the experimental configurations

studied here. Surface topography is more significant for the smaller contacts studied and may be important in many practical situations.

(iii) The size effect discovered appears to be caused by the variation in slip amplitude with contact size. Lower amplitudes prevalent in smaller contacts reduce the amount of fretting damage that takes place and this eventually falls below the critical value required for crack initiation to occur.

(iv) The initiation parameter proposed by Ruiz, Boddington, and Chen (1974) provides a reasonable means of characterising the probability of crack initiation and can be used to predict the critical contact sizes for the current experiments. More work is required to see if a critical value of $\sigma.\tau.\delta$ exists which may be regarded as a material constant and hence detailed design rules cannot yet be produced. The probability of failure will, however, be reduced by reducing the value of the initiation parameter $\sigma.\tau.\delta$ by varying, for example, the coefficient of friction or the contact size and geometry. It is not possible to provide general guidelines on how to achieve this since the most effective technique will depend on the exact contact configuration. It is also far from clear that the critical value of $\sigma.\tau.\delta$ is a material constant and geometry independent.

(v) Alternative hypotheses, viz. that the variation of fatigue life with contact size is due to a statistical effect or to crack self-arrest were examined. Statistical considerations were unable

to provide a satisfactory explanation for the behaviour of the alloy used in the experiments. Crack arrest could explain the size effect but experimental evidence does not support this suggestion. It is conceivable that such a mechanism could control growth once initiation has taken place in small contacts.

10.2 Suggestions for further work

The following suggestions for further work are made:

(i) More experiments might be carried out using a different material (e.g. steel) to determine if the same variation of fatigue life with contact size occurs. The initiation parameter ($\sigma.\tau.\delta$) could be employed in the analysis of the experiments to see if the predictions of critical contact size were as accurate as those obtained for aluminium alloy. The use of steel specimens would enable a better surface finish to be obtained, as would the adoption of a different method of surface finishing (e.g. longitudinal grinding or polishing). Decreasing the effects of surface roughness would produce clearer fretting scars and it should then be possible to detect the offset stick zone predicted by the analysis of chapter 4.

(ii) A series of experiments carried out with different geometries and conditions (e.g. fully sliding contact with an independently controlled slip amplitude) would allow critical conditions for fretting fatigue failure to be compared. The initiation parameter ($\sigma.\tau.\delta$) could be assessed to see if the

critical value for failure was similar under different fretting conditions. If so, it could be regarded as a material constant characterising the resistance to the initiation of fretting fatigue cracks. It is likely, however, that the critical value of $\sigma.\tau.\delta$, if it exists, will be highly dependent on factors such as temperature and environment.

(iii) A series of experiments carried out at a constant value of shear work density ($\tau.\delta$) but varying the tangential stress at the surface (σ) may allow a better initiation parameter to be devised. The multiplication of these two quantities to produce $\sigma.\tau.\delta$ is rather arbitrary and it should be possible to define a more satisfactory parameter based on a comprehensive series of experiments.

(iv) The techniques for calculating stress intensity factors for oblique cracks under fretting conditions have not been of direct use in explaining the size effect which was the main aim of the present study. However, several authors have (e.g. Sato, Fujii, and Kodama (1986)) have produced comprehensive data relating crack growth rate, $\frac{da}{dN}$, to crack length in fretting fatigue. In particular these studies have highlighted an accelerated propagation rate for short cracks, when compared to plain fatigue. Techniques used to analyse this data have so far been restricted to modelling normal cracks. The techniques now available to calculate stress intensity factors for oblique cracks under contact loads should enable the relationship between growth rate and stress intensity factors to be found. This can then be compared with

established empirical relationships such as the Paris Law. A greater understanding of the propagation phase of fretting fatigue should thus be obtained.

REFERENCES

Almen, J.O. (1937) 'Lubricants and the false brinelling of ball and roller bearings' Mech. Eng. 4 , 59, 415.

Antler, M. (1985) 'Electrical effects of fretting connector contact materials: A review' Wear, 106 , 357-368.

Bentall, R.H., and Johnson, K.L., (1967) 'Slip in the rolling contact of dissimilar elastic rollers' Int. Jnl. Mech. Sci., 9 , 389-404.

Bentall, R.H., and Johnson, K.L., (1968) 'An elastic strip in plane rolling contact' Int. Jnl. Mech. Sci., 10 , 636-663.

Benthem, J. P., and Koiter, W.J. (1973) 'Asymptotic approximations to crack problems' in " Methods of analysis and solutions of crack problems", Ed. G. C. Sih, Noordhoff, Leyden, pp 131-178.

Bramhall, R. (1973) 'Studies in fretting fatigue' DPhil thesis, Oxford University.

Bryant, M.D., Miller, G.R., and Keer, L.M., (1984) 'Line contact between a rigid indenter and a damaged elastic body' Q. Jnl. Mech. Appl. Math., 37 , 3, 467-478.

Bryggman, U., and Söderberg, S., (1986) 'Contact conditions in fretting' Wear, 110 , 1-17.

Buckley, D.H. (1975) 'The effect of various material properties on the adhesive phase of fretting' AGARD, CP161, paper 13.

Cattaneo, C.,(1938) 'Sul contatto di due corpi elastici: distribuzion locale degli sforzi' Reconditi dell Accademia nazionale dei Lincei, 27 , 342-348, 434-436,474-478.

Chivers, T.C., and Gordelier, S.C., (1984) 'Fretting fatigue palliatives; some comparative experiments' Wear, 96 , 153-175.

Conte, S.D., and DeBoor, C. (1972) 'Elementary numerical analysis (2nd edition)', McGraw-Hill, New York.

Doeser, B., (1981) 'The study of fretting fatigue using finite element analysis and electron microscopy' PhD Thesis, Nottingham University.

Dundurs, J. and Mura, T. (1964) 'Interaction between an edge dislocation and a circular inclusion', J. Mech. Phys. Solids, 12, 177-189.

Dundurs, J. and Sendeckyj, G. P. (1965) 'Behaviour of an edge dislocation near a bimetallic interface', J. Appl. Phys., 36, 3353-3354.

Eden, E.M., Rose, W.N., and Cunningham, F.L. (1911) 'The endurance of metals' Proc. I Mech E, 4 , 139.

Edwards, P.R., (1981) 'The application of fracture mechanics to predicting fretting fatigue' Ch 3, pp 67-98, of " Fretting Fatigue", ed R B Waterhouse, Applied Science.

Edwards, P.R., Ryman, R.J., and Cook, R., (1977) 'Fracture mechanics prediction of fretting fatigue under constant amplitude loading' RAE Technical report 77056,

Endo K., and Goto, H., (1976) 'Initiation and propagation of fretting fatigue cracks' Wear, 38 , 311-324.

Endo, K., Goto, H., and Fukunaga, T., (1974) 'Frictional force in fretting fatigue' Bull. JSME, 17, 108, 647-654.

Erdogan, F., Gupta, G. D. and Cook, T. S., (1973) 'Numerical solution of singular integral equations', In Methods of Analysis and Solutions of Crack Problems, (Ed. G. C. Sih). Noordhoff, Leyden, pp368-425.

Fenner, A.J., and Field, J.E., (1960) 'A study of the onset of fatigue damage due to fretting' Proc. N E Coast Institute of Engineers and Shipbuilders, 76 , 183.

Fenner, A.J., Wright, K.H.R., and Mann, J.Y. (1956) 'Fretting corrosion and its influence on fatigue failure' p386 of Proc. Int. Conf. on fatigue of metals, I Mech E, London.

Flamant (1892) Compt. Rendus, 114, 1465.

Fleming, J. R. and Suh, N. P. (1977) 'Mechanics of crack propagation in delamination wear' Wear, 44, 39-56.

Forsythe, P.J.E. (1961) 'A two-stage process of crack growth' Proc. Crack. Symp., Cranfield College of Aeronautics, pp 76-94.

Forsythe, P.J.E. (1981) 'Occurrence of fretting fatigue failures in practice' Ch4, pp 99-125 of "Fretting fatigue", ed R.B. Waterhouse, Applied Science, London.

Frost, N.E., Marsh, K.J., and Pook L.P. (1974) 'Metal fatigue' Clarendon Press, Oxford.

Fuchs, S., (1913) 'Haputspannungstrajektorie bei der Beruchreng einer Kugel mit einer Platter' Physikalische Zeitschrift, 14 , 1282.

Goodman, L.E. (1962) 'Contact stress analysis of normally loaded rough spheres' Jnl. Appl. Mech., 29, 3, 515-522.

Greenwood, J. A., and Tripp, J. H. (1967) 'The elastic contact of rough spheres' Jnl. App. Mech., 34 , 153-159.

Hartranft, R. J. and Sih, G. C. (1973)'Alternating methods applied to edge and surface crack problems', In Mechanics of Fracture (Ed. G. C. Sih), Noordhoff, Gronigen, pp179-238.

Hertz, H., (1882) 'Uber die Beruhrung fester elastischer Korper' Jnl. reine und angewandte Mathematik, 92 ,156-171.

Hills, D.A. and Sackfield, A. (1985) 'Sliding contact between dissimilar elastic cylinders', Jnl. Tribology, 107, 463-466.

Hills, D.A., Sackfield, A., and Uzel, A., (1984) 'The Greens function for a slant edge crack' Eng. Fracture Mech., 20 2, 245-253.

Hoeppner, D.W., and Gates, F.L., (1981) 'Fretting fatigue considerations in engineering design' Wear, 70 , 155-164.

Hoeppner, D.W., and Goss, A., (1974) 'A fretting fatigue damage threshold concept' 27 , 61.

Ioannides, E., and Harris, T.A. (1984) 'A new fatigue life model for rolling bearings' Proc. ASME/ASLE Lubrication Conference, San Diego, October 22-24, 1984.

Johnson, K.L. (1955) 'Surface interaction between elastically loaded bodies under tangential forces' Proc. Roy. Soc., Series A, 230, 531-548.

Johnson, K.L. (1985) 'Contact Mechanics' Cambridge University Press, p29

Kantimathi, A., and Alic, J.A., (1981) 'The effect of periodic high loads on fretting fatigue' Jnl. Eng. Mat., 103 ,3, 218-225.

Keer, L.M., and Farris, T. (1986), Private communication.

Krenk, S. (1975)' On the use of the interpolation polynomial for solutions of singular integral equations', Q. Appl. Maths., 32, 479-484.

Kuno, M. (1988) PhD. Thesis, Department of Metallurgy and Materials Science, University of Nottingham

Lo, C. C. (1969) 'Elastic contact of rough cylinders' Int. Jnl. Mech Sci., 11 , 105-115.

Maxwell, W.W., Dudley, B.R., Cleary, A.B., Richards, J., and Shaw, J.(1967) 'Measures to counter fatigue failures in railway axles' Proc. I Mech E, 182 , 1, 89-108.

Milestone, W.D., (1970) 'Fretting and fretting fatigue in metal to metal contacts' Proc. AIAA Structural dynamics and materials conf.,Denver, Colorado, 86.

Milestone, W.D., and Janeczko, J.J., (1981) 'Friction between steel surfaces during fretting' Wear, 18 , 219-240.

Mindlin, R.D., (1949) 'Compliance of elastic bodies in contact' Jnl. App. Mech., 16 , 259-268.

Mindlin, R.D., and Deresciewicz, H., (1953) 'Elastic spheres in contact under varying oblique forces' Jnl. App. Mech., 75 , 327-344.

Morton, W.P., and Close, L.J., (1922) 'Notes on Hertz' theory of contact problems' Philosophical Magazine, 43 ,320.

Muskhelishvili, N.I. (1953a) 'Some basic problems of the mathematical theory of elasticity', Translated by J.R.M. Radok, Noordhoff, Groningen.

Muskhelishvili, N.I. (1953b) 'Singular Integral Equations, boundary problems of function theory and their application to mathematical physics' Noordhoff, Gronigen.

Nishioka, K., and Hirakawa, K., (1968) 'Fundamental investigations of fretting fatigue (part 1)' Bull. JSME, 11 , 45, 437.

Nishioka, K., and Hirakawa, K.,(1969a) 'Fundamental investigations of fretting fatigue (part 2)' Bull. JSME, 12 , 50, 180-187.

Nishioka, K., and Hirakawa, K.,(1969b) 'Fundamental investigations of fretting fatigue (part 3)' Bull. JSME, 12 , 51, 397-407.

Nishioka, K., and Hirakawa, K.,(1969c) 'Fundamental investigations of fretting fatigue (part 4)' Bull. JSME, 12 , 52, 408-414.

Nishioka, K., and Hirakawa, K.,(1969d) 'Fundamental investigations of fretting fatigue (part 5)' Bull. JSME, 12 , 52, 692-697.

Nishioka, K., and Hirakawa, K.,(1972) 'Fundamental investigations of fretting fatigue (part 6)' Bull. JSME, 15 , 80, 135-144

Nix, K.T., and Lindley, T.C., (1984) 'The application of fracture mechanics to fretting fatigue' CEGB Report TPRD/L/2648/N84.

Noble, B. and Spence, D.A. (1971) University of Wisconsin Tech Summary, report No.1971, p.11.

Nowell, D. and Hills, D.A. (1987) 'Open cracks at or near free edges' Jnl. Strain Anal., 22, 3, 177-185.

Nowell, D., Hills, D.A., and Sackfield, A. (1988) 'Contact of dissimilar elastic cylinders under normal and tangential loading' Jnl. Mech. Phys. Solids, 36 , 1, 59-75.

O'Connor, J.J., and Hills, D.A. (1986) 'A fracture mechanics correlation of fretting fatihue experiments' pp 55-63 of "Mechanisms and surface distress", Proc. 12th Leeds-Lyon symposium on tribology, Ed D Dowson, Butterworths.

Otsuka, A., Mori, K., and Miyata, T., (1975) 'The condition of fatigue crack growth in mixed mode condition' Fracture Mech., 7 , 429-439.

Piessens, R., VanRoy-Branders, M., and Mertens, J., (1976) 'The automatic evaluation of Cauchy principal value integrals' Angew. Inf., 18, 31-33.

Pook, L.P. (1978) 'Analysis and application of fatigue crack growth data' in "A general introduction to fracture mechanics" I.Mech.E., London.

Pook, L.P. (1985) 'The significance of branch cracks for mixed-mode fatigue crack growth threshold behaviour' Proc. second conf. on biaxial/multiaxial fatigue, Sheffield University, December 1985

Poon, C.J., and Hoeppner, D.W., (1981) 'A statistically based investigation of the environmental and cyclic stress effects of fretting fatigue' Jnl. Eng. Mat., 103 ,3, 218-223.

Poritsky, H., (1950) 'Stresses and deformations of cylindrical bodies in contact with application to contact of gears and of locomotive wheels' Jnl. App. Mech., 72 ,191-201.

Rooke, D.D., and Jones, D.A., (1977) 'Stress intensity factors in fretting fatigue' RAE Technical report 71977.

Ruiz, C., Boddington, P.H.B., and Chen, K.C. (1984) 'An investigation of fatigue and fretting in a dovetail joint' Experimental Mechanics, 24 , 3, 208-217.

Ruiz, C., and Cheng, K.C., (1986) 'Life assessment of dovetail joints between blades and discs in aero-engines' Proc. Int. Conf. Fatigue, I Mech E, Sheffield,

Sackfield, A., and Hills, D.A., (1985) 'A note on the Hertz contact problem: a correlation of standard formulae' Jnl. Strain Analysis, 18 ,195.

Sato, J., Shima, M., and Sugawara, T. (1985) 'A fundamental study of fretting damage to glass using an improved apparatus' Wear, 106, 53-61.

Sato, K., Fujii, H., and Kodama, S., (1986) 'Crack propagation behaviour in fretting fatigue' Wear, 107 , 245-262.

Schmueser, D., Comninou, M. and Dundurs, J. (1980) 'Separation and slip between a layer and substrate caused by a tensile load', Int. Jnl. Eng. Sci, 18, 1149-1155.

Schmueser, D., Comninou, M. and Dundurs, J. (1981) 'Frictional slip between a layer and a substrate', Trans. ASCE, Jnl. Eng. Mech. E., 1103-1119.

Smith, J.O., and Liu, C.K., (1953) 'Stresses due to tangential and normal loads on an elastic solid with application to some contact stress problems' Jnl. App. Mech. 20, 157.

Sneddon, I.N. (1951) 'Fourier Transforms', McGraw-Hill.

Spence, D.A. (1968) 'Self-similar solutions to adhesive contact problems with incremental loading', Proc. Roy. Soc. Series A, 305, 55-80.

Spence, D.A. (1973) 'An eigenvalue problem for elastic contact with finite friction' Proc. Camb. Phil. Soc., 73, 249-268.

Spence, D.A. (1975) 'The Hertz contact problem with finite friction', Jnl. Elasticity, 5, 3-4, 297-319.

Spence, D.A. (1986) 'Frictional contact with transverse shear' Q. Jnl. App. Math., 39, 2, 233-253.

Tomlinson, G. A., (1927) 'The rusting of steel surfaces in contact' Proc. Roy. Soc., Ser. A, 115 ,472-483.

Tomlinson, G.A., Thorpe P.L., and Gough, H.J., (1939) 'An investigation of the fretting corrosion of closely fitting surfaces' Proc. I Mech E , 141 , 223-249.

Tsamasphyros, G. J., and Theotokoglou, E. N. (1986) 'Integral equation solution of the infinite strip with cracks and holes' Mech. Res. Comms., 13 , 3, 133-140

Uhlig, H.H., (1954) 'A mechanism of fretting corrosion' Jnl. App. Mech., 21 , 401-407.

Uhlig, H.H., and Ming-Feng, I., (1954) 'Fretting corrosion of mild steel in Air and Nitrogen' Jnl. App. Mech., 21 , 395-400.

Uzel, A. R., Hills, D. A. and Sackfield, A. (1985) 'Stress intensity factors for a cracked half-plane', Jnl. Strain Anal. 20, 4, 209-216.

Warlow-Davies, E.J., (1941) 'Fretting corrosion and fatigue strength: brief results of preliminary experiments' Proc. I Mech E, 146 , 33-38.

Waterhouse, R.B. (1968) 'The effect of clamping stress distribution on the fretting fatigue of α-brass and Al-Mg-Zn alloy' Trans. ASLE, 11 ,1-5.

Waterhouse, R.B., and Lamb, M. (1980) 'Fretting corrosion of orthopaedic implant materials by bone cement' Wear, 60 , 357-368.

Way, S. (1935) 'Pitting due to rolling contact' Jnl. App. Mech., 2, 49- 58.

Weibull, W. (1949) 'A statistical representation of fatigue failures in solids' Acta Polytechnica, Mechanical Engineering Series, Royal Swedish Academy of Engineering Sciences, 9.49

Wright, G.P., (1970) 'Studies in fretting fatigue' DPhil thesis, Oxford University.

APPENDIX A

EXPERIMENTAL RESULTS

(i) Series 1, p_o = 157 MN/m^2, σ = 92.7 MN/m^2, Q/P = 0.45, f = 0.75

Test No.	Pad radius, R (mm)	a (mm)	life (10^6 cycles)
25	12.5	0.10	10→
5	25	0.19	10→
26	37.5	0.28	10→
53	50	0.38	1.29
4	75	0.57	0.67
7	100	0.76	0.85
54	125	0.95	0.73
30	150	1.14	0.67

(ii) Series 2, p_o = 143 MN/m^2, σ = 92.7 MN/m^2, Q/P = 0.24, f = 0.75

Test No.	Pad radius, R (mm)	a (mm)	life (10^6 cycles)
24	12.5	0.09	10→
13	25	0.18	10→
28	50	0.36	10→
41	75	0.54	10→
10	100	0.72	5.06
9	125	0.90	1.22
8	150	1.08	1.28

(iii) Series 3, p_o = 143 MN/m^2, σ = 92.7 MN/m^2, Q/P = 0.45, f = 0.75

Test No.	Pad radius, R (mm)	a (mm)	life (10^6 cycles)
20	12.5	0.09	10→
17	25	0.18	10→
37	37.5	0.27	4.04
42	50	0.36	1.50
21	75	0.54	0.80
22	100	0.72	0.61
18	125	0.90	1.24
16	150	1.08	0.69

(iv) Series 4, p_o = 143 MN/m^2, σ = 77.2 MN/m^2, Q/P = 0.45, f = 0.75

Test No.	Pad radius, R (mm)	a (mm)	life (10^6 cycles)
36	12.5	0.09	10→
35	25	0.18	10→
31	50	0.36	10→
33	75	0.54	1.20
32	100	0.72	1.42
34	125	0.90	1.02

(v) Series 5, p_o = 120 MN/m^2, σ = 61.8 MN/m^2, Q/P = 0.45, f = 0.75

Test No.	Pad radius, R (mm)	a (mm)	life (10^6 cycles)
39	25	0.14	10→
43	37.5	0.21	10→
44	50	0.28	10→
45	75	0.42	10→
47	100	0.57	10→
46	125	0.71	1.57
49	150	0.85	1.23

(vi) Series 6. p_o = 120 MN/m^2, σ_{max} = 61.8 MN/m^2, Q_{max}/P = 0.45, f = 0.75, R = 150mm, a = 0.85mm

Test No.	σ_{min} (MN/m^2)	Q_{min}/P	life (10^6 cycles)
49	-61.8	-0.45	1.23
52	-52.4	-0.38	7.77
50	-39.9	-0.29	10→
51	-20.6	-0.15	10→
48	0.0	0.00	10→

APPENDIX B

INFLUENCE FUNCTIONS (CHAPTER 5)

$$I_{AO} = \frac{2}{z} \int_o^\infty \left[\frac{1 - \cosh \beta}{\beta + \sinh \beta} \right] \sin^2 z\beta \ \frac{d\beta}{\beta^3}$$

$$I_A[n] = \frac{-4}{z} \int_o^\infty \left[1 + \frac{1 - \cosh \beta}{\beta + \sinh \beta} \right] \sin^2 z\beta \ \sin^2 nz\beta \ \frac{d\beta}{\beta^3}$$

$$I_B[n] = \frac{-2}{z} \int_o^\infty \left[\frac{\beta}{\beta + \sinh \beta} \right] \sin^2 z\beta \ \sin 2nz\beta \ \frac{d\beta}{\beta^3}$$

$$I_{AR}[n] = \int_o^\infty \sin^2 \beta \ \sin^2 n\beta \ \frac{d\beta}{\beta^3}$$

$$I_{BR}[n] = \int_o^\infty \sin^2 \beta \ \sin 2n\beta \ \frac{d\beta}{\beta^3}$$

$$I_D[n] = \frac{-4}{z} \int_o^\infty \left[1 - \frac{1 + \cosh \beta}{\beta + \sinh \beta} \right] \sin^2 z\beta \ \sin^2 nz\beta \ \frac{d\beta}{\beta^3}$$

Where $z = \frac{a}{4sb}$

APPENDIX C

TRACTIVE ROLLING OF DISSIMILAR ELASTIC CYLINDERS

The problem of tractive rolling of two elastically dissimilar cylinders, whose contacting surfaces suffer coulomb friction, may be treated by a technique similar to that developed in chapter 6. The relevant calculations are included here as an appendix since it may be useful to study them in the light of arguments introduced in the analysis contained in chapter 6. The work is not, however, directly relevant to the analysis of fretting fatigue.

Notation

A	$(1 - \nu_1)/\mu_1 + (1 - \nu_2)/\mu_2$
a	- Contact half-width
b, b_1, b_2, b_3	- Stick zone boundaries, normatised with respect to a.
c	- Stick zone semi-width, normalised with respect to a.
f	- Coefficient of friction
h(x)	$(\partial u_1/\partial x) - (\partial u_2/\partial x)$
P	- Normal force per unit length
p(x)	- Normal traction under contact
p_0	- Peak normal traction
$\bar{p}(x)$	$p(x)/p_0$
Q	- Tangential force per unit length
q(x)	- Shear traction under contact
$\bar{q}(x)$	$q(x)/fp_0$
q'(x)	- Perturbation on $\bar{q}(x)$ in stick zone
R	- Relative radii of curvature of cylinders
r,s,t,w	- Normalised integration variables
u	- Displacement in x direction
V	- Mean peripheral velocity of cylinders
v	- Instantaneous velocity of a point
v_s	- Slip velocity
W	- Power loss per unit length
x	- Tangential coordinate
β	- Dundurs' constant $((1 - 2\nu_1)/\mu_1 - (1 - 2\nu_2)/\mu_2)/2A$
δv	- Creep velocity
ζ	- Creep ratio
μ	- Modulus of rigidity
ν	- Poisson's ratio
ξ	- Integration variable
$\phi(x)$	- Bounded component of shear traction
χ	$3 - 4\nu$ in plane strain

1. Introduction

Twenty years ago, Bentall and Johnson [1] published their classic paper on the behaviour of frictional and adhesive contact of two cylinders, concentrating mainly on 'free' rolling, but including some discussion of the case where a nett shear force Q is transmitted. Their method was based on a piecewise-linear discretization of the shear traction distribution, and used the solution for a triangle of traction as the basic influence function. Later, Kalker [2] formulated a minimum principle which established the stick and slip regions automatically, but his implementation again approximated the shear traction in a piecewise-linear fashion. It is the intention of the present paper to formulate the problem in terms of a singular integral equation, and then to solve the equation numerically, using a powerful quadrature which enables a very accurate solution to be found at the expense of little computing effort. This enables several outstanding points from the Bentall and Johnson paper to be resolved, and permits a wider range of the independent variables to be treated.

2. Formulation

At the outset, we shall make the assumption that the effect of shear traction on vertical displacements of the contacting bodies is negligible. This is the so-called Goodman approximation [3] and is certainly valid if Poisson's ratio is large, although it is less satisfactory if there is little Poisson effect [4]. Further, if the contact patch is small compared with the radii of curvature of the contacting cylinders, they may be approximated by half-planes, and the pressure distribution becomes the classical Hertzian one, ie.

$$p(x) = -p_0 \sqrt{1 - (x/a)^2} \qquad |x| \le a \qquad (1)$$

$$= 0 \qquad |x| > a$$

where p_0 is the peak contact pressure, and a is the semi-width of contact, Fig. 1. The peak pressure is related to the relative radius of curvature R and the applied load per unit length P by [5]

$$p_0 = \frac{2P}{\pi a} \qquad (2)$$

and

$$a^2 = \frac{2PRA}{\pi}$$

where

$$A = \frac{1 - \nu_1}{\mu_1} + \frac{1 - \nu_2}{\mu_2} \quad .$$

Here, ν is Poisson's ratio and μ is the modulus of rigidity, and we have added the subscript 1 to denote the upper cylinder and 2 to denote the lower cylinder, Fig. 1.

The tangential displacement of surface particles on the cylinder is given by [6]

$$\frac{\partial u_1}{\partial x} = \frac{\chi_1 + 1}{4\mu_1 \pi} \int_{-a}^{a} \frac{q(\xi)d\xi}{x - \xi} + \frac{\chi_1 - 1}{4\mu_1} p(x) \qquad (3a)$$

$$\frac{\partial u_2}{\partial x} = - \frac{\chi_2 + 1}{4\mu_2 \pi} \int_{-a}^{a} \frac{q(\xi)d\xi}{x - \xi} + \frac{\chi_2 - 1}{4\mu_2} p(x) \qquad (3b)$$

where $\chi_i = 3 - 4\nu_i$ in plane strain.

We shall need to ensure that in slip regions the slip velocity of corresponding particles on the cylinders is consistent with the slip direction, and therefore introduce the quantity h(x), given by

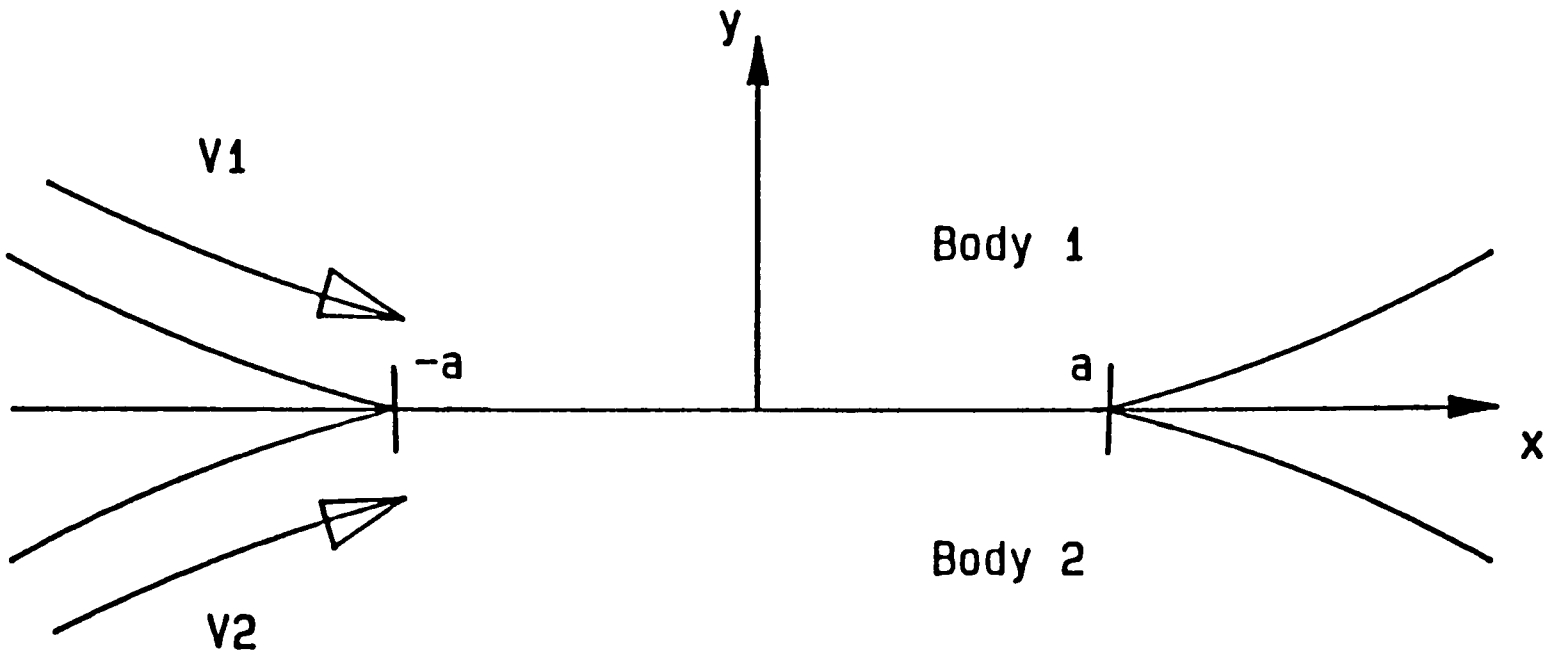

Fig. 1. Tractive rolling (configuration of problem)

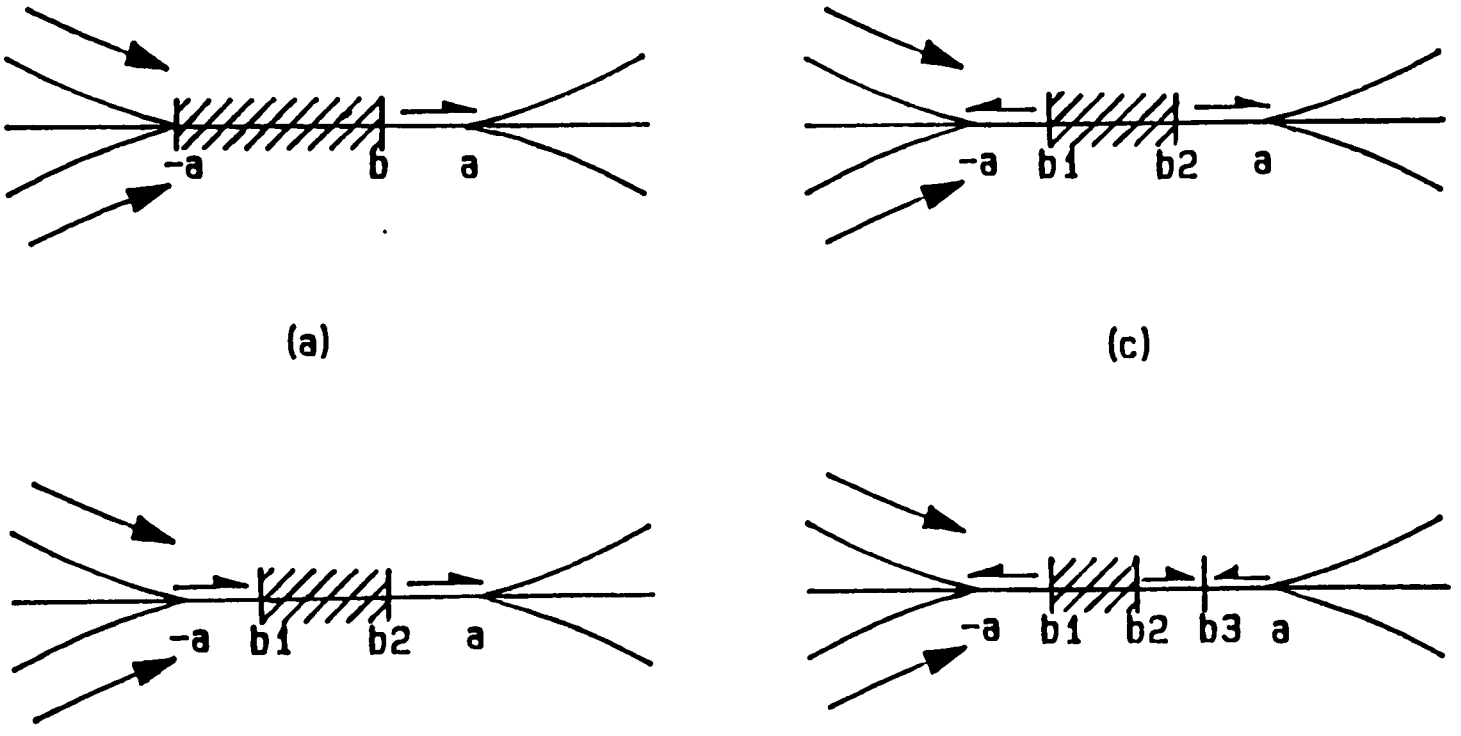

Fig. 2 (a) Single slip zone regime (Carter)
(b) Two slip zones of the same sign
(c) Two slip zones of opposite sign
(d) Three slip zones

$$h(x) = \frac{\partial u_1}{\partial x} - \frac{\partial u_2}{\partial x} \tag{4}$$

Substituting (3) into (4), and introducing Dundurs' constant* defined by

$$\beta = \left[\frac{1 - 2\nu_1}{\mu_1} - \frac{1 - 2\nu_2}{\mu_2}\right] /2A \tag{5}$$

we arrive at the following equation:

$$\frac{h(x)}{A} = \frac{1}{\pi} \int_{-a}^{a} \frac{q(\xi)d\xi}{x - \xi} + \beta p(x) \tag{6}$$

It is convenient to normalise the coordinate over the contact zone by writing

$$x = as$$

$$\xi = ar$$

and to normalise the tractions by letting

$$\tilde{p}(s) = \frac{p(s)}{p_0}$$

$$\tilde{q}(s) = \frac{q(s)}{fp_0}$$

By using these relations together with Hertz' contact law (2) we arrive at

$$\frac{1}{\pi} \int_{-1}^{+1} \frac{\tilde{q}(r)dr}{s - r} + \frac{\beta}{f} \tilde{p}(s) = \frac{Rh(s)}{fa} \qquad -1 < s < +1 \tag{7}$$

---

* Note that apart from a constant of proportionality this is the same quantity used by Goodman and subsequently denoted by Bentall and Johnson as χ, and by Spence as $\tilde{\gamma}$.

We expect the contact patch to consist of a combination of stick and slip zones, whose locations are unknown at this stage, but we may write down the following general requirements:

(i) Stick zones

Within a stick zone, the relative velocity of corresponding surface particles must be zero. The velocity v_i of any surface point is given by Johnson [7] as

$$v_i = V + \delta v_i + V \frac{\partial u_i}{\partial x}$$

where V is the mean peripheral velocity of the cylinders and δv_i the creep velocity of cylinder i. Hence the slip velocity at any point v_s is given by

$$v_s = v_1 - v_2 = \delta v_1 - \delta v_2 + V\left(\frac{\partial u_1}{\partial x} - \frac{\partial u_2}{\partial x}\right)$$

giving

$$\frac{v_s}{V} = \zeta + h(x) \qquad (8)$$

where the creep ratio is given by

$$\zeta = \frac{\delta v_1 - \delta v_2}{V}$$

In a stick zone, $v_s = 0$ so that $h(x) = \text{constant} = -\zeta$.

Moreover, if there is more than one stick zone, it must be true that in the steady state the amount of material leaving the first stick zone must be the same as the amount entering the second. We may express this continuity condition by requiring that h(x) takes the same value in <u>all</u> stick zones.

Also, the magnitude of the shear traction must be less than the limiting friction value, ie.

$$|q(x)| < - fp(x) \tag{9}$$

(ii) Slip zones

Within the slip zones the magnitude of the shear traction is limited by friction, and hence

$$q(x) = \pm fp(x) \tag{10}$$

whilst the direction of shear must be consistent with the relative slip velocity of surface particles. This is ensured by demanding that

$$\mathrm{sgn}(v_s) = \mathrm{sgn}(q(x))$$

ie

$$\mathrm{sgn}(h(x) + \zeta) = \mathrm{sgn}(q(x)) \tag{11}$$

Conditions expressed by equations (8-11) are necessary, but insufficient to determine the location of stick and slip zones. It would have been possible at this stage to use a variational approach to locate stick and slip zones [2], but we have instead been guided by the results of [1], and expect one of the four regimes given in Fig. 2 to obtain.

The first configuration shown (Fig. 2a) exists only when the bodies are elastically similar, and was first solved by Carter [8]. His solution may be obtained by writing down the shear tractions as the limiting sliding value together with a correction term in the stick zone (q'(x)). Conditions (8-11) may be fulfilled by letting q'(x) also be parabolic in form and setting

$$q(x) = \pm fp_0 \sqrt{1 - (x/a)^2} + q'(x)$$

where

$$\begin{aligned} q'(x) &= 0 && b < x/a < 1 \\ q'(x) &= \mp \sqrt{1 - ((x/a + 1 - c)/c)^2} && -1 < x/a < b \end{aligned} \tag{12}$$

and

$$c = \sqrt{1 - |Q/fP|}$$

$$b = -1 + 2c$$

We assume that v_1, $v_2 > 0$, and choose the upper sign if body 1 is driving, body 2 being driven and vice versa.

3. Analysis (Two Slip Zones)

As soon as β is changed from zero, ie. there is any elastic mismatch , a small slip zone starts to develop at the leading edge of contact. This may be of either the same or opposite sign to the main slip zone (Fig. 2b,c) depending on whether the more compliant roller is driving or braking. We discuss the appropriateness of each in a later section. We shall consider first the case where both slip zones have the same sign.

Following the same strategy outlined above for the Carter solution, we write the shear traction distribution as a perturbation of the sliding solution, fig. 3a:

$$\bar{q}(r) = \sqrt{1 - r^2} + q'(r) \tag{13}$$

where

$$q'(r) = 0 \qquad r \le b_1 \text{ and } r \ge b_2$$

We then combine (7) and (8) to enforce the no slip condition in the stick zone;

$$\frac{1}{\pi}\int_{-1}^{+1} \frac{\sqrt{1 - r^2}\,dr}{s - r} + \frac{1}{\pi}\int_{b_1}^{b_2} \frac{q'(r)dr}{s - r} - \frac{\beta}{f}\sqrt{1 - s^2} = -\frac{R\zeta}{fa} \qquad b_1 \le s \le b_2 \tag{14}$$

The first integral may be evaluated and the equation re-cast as a Cauchy integral equation in $q'(r)$, thus

$$\frac{1}{\pi}\int_{b_1}^{b_2} \frac{q'(r)dr}{s - r} = -\frac{R\zeta}{fa} - s + \frac{\beta}{f}\sqrt{1 - s^2} \qquad b_1 \le s \le b_2 \tag{15}$$

A satisfactory solution to this equation may be found by discretization of $q'(r)$ as a truncated series of Chebyshev polynomials and inversion of the resulting set of linear algebraic equations. The quadrature is described by Erdogan, Gupta and Cook [9]. First we transform the coordinates s, r in (15) to a new pair t, w, defined over the interval ±1.

$$t = \frac{2r - (b_1 + b_2)}{b_2 - b_1}$$

$$w = \frac{2s - (b_1 + b_2)}{b_2 - b_1} \qquad (16)$$

Therefore (15) becomes

$$\frac{1}{\pi} \int_{-1}^{+1} \frac{q'(t)dt}{w - t} = -\frac{R\zeta}{fa} - s + \frac{\beta}{f}\sqrt{1 - s^2} \qquad -1 \le w \le +1 \qquad (17)$$

Since we require $q'(t)$ to be bounded at $t = \pm 1$ (Fig. 3a) we choose to represent it as the product of a fundamental solution $U(t) = \sqrt{(1 - t^2)}$ and an unknown function $\phi(t)$. The discretized version of (17) is then

$$\sum_{i=1}^{n} \frac{(1 - t_i^2)\phi(t_i)}{(n + 1)(w_k - t_i)} = -\frac{R\zeta}{fa} - s_k + \frac{\beta}{f}\sqrt{1 - s_k^2} \qquad (18)$$

where

$$t_i = \cos\left(\frac{\pi i}{n+1}\right) \qquad i = 1\ldots n$$

$$w_k = \cos\left(\frac{\pi(k - (1/2))}{n+1}\right) \quad k = 1\ldots n+1$$

and s_k is given by (16).

Although it is physically an independent variable, the normalized nett shear force Q/fP appears in the present formulation as a dependent quantity, since b_1 and b_2 are chosen, whereas in reality they are dependent. Thus, for overall horizontal equilibrium

$$Q = \int_{-a}^{+a} q(\xi)d\xi \tag{19}$$

Using (2)

$$\frac{Q}{fP} = \frac{2}{\pi}\int_{-1}^{+1} \tilde{q}(r)dr$$

and invoking (13) we find

$$\frac{Q}{fP} = 1 + \frac{2}{\pi}\int_{b_1}^{b_2} q'(r)dr \tag{20}$$

Transforming the interval of integration to ±1 and using the quadrature utilised to solve (17) gives

$$\frac{Q}{fP} = 1 + (b_2 - b_1) \sum_{i=1}^{n} \frac{(1 - t_i^2)\phi(t_i)}{n + 1} \tag{21}$$

Lastly, in order to verify that (11) holds, we need to determine h(x) external to the stick zone. From (7) (cf (14))

$$\frac{Rh(s)}{fa} = s - \frac{\beta}{f}\sqrt{1 - s^2} + \frac{1}{\pi}\int_{b_1}^{b_2} \frac{q'(r)dr}{s - r} \tag{22}$$

or, in discretized form

$$\frac{Rh(s)}{fa} = s - \frac{\beta}{f}\sqrt{1 - s^2} + \sum_{i=1}^{n} \frac{(1 - t_i^2)\phi(t_i)}{(n + 1)(w - t_i)} \tag{23}$$

where w and s are related by (16), and, since (22) is not Cauchy for $s < b_1$ or $s > b_2$, (23) may be evaluated at any location outside the stick zone.

Referring again to equations (18), we note that a pair of values b_1, b_2 must first be chosen. The n + 1 equations are then used to find the n values of $\phi(t_i)$ together with a consistent creep ratio $R\zeta/fa$. However, the choice of b_1 and b_2 is not arbitrary: in practice, a pair of values is chosen and a solution found. A check is then carried out to see if the consistency conditions (9) and (11) are satisfied. If violations occur, b_2 is adjusted and another solution found until a wholly consistent set of tractions is obtained. For certain values of b_1 it is not possible to find such a solution, indicating that a different stick/slip configuration must be postulated.

A satisfactory solution is not, therefore, always found using the above scheme and an alternative arrangement of two slip zones of opposite sign is

postulated (Fig. 2c). Since, as in the above solution, we shall use a quadrature which falls to zero at the ends of the stick interval, we replace equation (13) by an alternative form, so that the function on which the perturbation is imposed assumes correct values at $r = b_1, b_2$, viz.

$$\begin{aligned}\tilde{q}(r) &= +\sqrt{1 - r^2} && -1 < r < b_1 \\ &= -\sqrt{1 - r^2} && b_2 < r < 1 \\ &= q'(r) + \frac{\sqrt{1 - b_1^2}(b_2 - r) - \sqrt{1 - b_2^2}(r - b_1)}{b_2 - b_1} && b_1 < r < b_2 \end{aligned} \tag{24}$$

This function is shown by the dotted line in Fig.3b. Substituting into (7) gives, in lieu of (14):

$$\begin{aligned}\frac{1}{\pi}\int_{b_1}^{b_2} \frac{q'(r)dr}{s - r} &= -\frac{R\zeta}{fa} + \frac{\beta}{f}\sqrt{1 - s^2} - \frac{1}{\pi}\int_{-1}^{b_1} \frac{\sqrt{1 - r^2}\,dr}{s - r} + \frac{1}{\pi}\int_{b_2}^{1} \frac{\sqrt{1 - r^2}}{s - r}\,dr \\ &- \frac{1}{\pi}\int_{b_1}^{b_2} \frac{\sqrt{1 - b_1^2}(b_2 - r) - \sqrt{1 - b_2^2}(r - b_1)dr}{(b_2 - b_1)(s - r)} \qquad b_1 \le s \le b_2 \end{aligned} \tag{25}$$

As before, we normalize the interval of integration by making substitution (16) and discretize by the same quadrature. The resulting family of equations is similar to (18), except that the right hand side is given by the right hand side of (25). The evaluation of h(x) and Q/fP follows a similar strategy to that described above, mutatis mutandis. In each case the integrals on the right hand side of (25) were evaluated numerically using a computer library routine [10].

4. Analysis - Three Slip Zones

In their original article, Bentall and Johnson obtain a solution (under free rolling conditions) which contains a total of five contact regions. This corresponded to Fig. 2d, except that there was a small stick zone (less than one of their discretization steps, even when refined), between the adjacent slip zones of opposite sign. Tentatively, we shall assume that this stick zone is vanishingly small, and that the shear traction distribution is as sketched in Fig. 3(c). Following the same general strategy as in the previous cases, we now seek a function q'(r) to enable us to satisfy the inequalities, which is again a perturbation on a simple shear traction distribution. Thus

$$\begin{aligned}
\bar{q}(r) &= +\sqrt{1 - r^2} && -1 < r < b_1 \\
&= -\sqrt{1 - r^2} && b_2 < r < b_3 \\
&= +\sqrt{1 - r^2} && b_3 < r < 1 \\
&= q'(r) + \frac{\sqrt{1 - b_1^2}\,(b_2 - r) - \sqrt{1 - b_2^2}\,(r - b_1)}{b_2 - b_1} && b_1 < r < b_2
\end{aligned} \qquad (26)$$

Since the corresponding integral equation is analogous to (14) and (25), but with a more complicated right hand side, we shall refrain from writing it explicitly, but note that again numerical integration is utilised to find the right hand side. Precisely the same techniques are used to establish Q/fP and h(x). It should be carefully noted that we must now invoke the continuity condition cited earlier, viz. that

$$h(b_3) = h(r_0) \qquad r_o \in b_1, b_2$$

At this point it might be appropriate to recall that the driving (or braked!) cylinder is the one where the shear force sustained and the tangential velocity

are in the opposite sense, ie. cylinder 1 drives cylinder 2 if (in our co-ordinate system) $Q/fP > 0$, and vice versa. Of course $|Q/fP| \leq 1$, and the equality occurs only when the bodies are sliding. Also, if $\beta > 0$ this means (5) that body 1 is more compliant than body 2, and vice versa.

5. Results

In Fig. 3 we show three typical sets of shear traction and relative slip results, one corresponding to each of the regimes described above. By themselves they do not serve to illustrate trends clearly, and therefore in Fig. 4 a sequence of tractions and slip velocities is shown for $\beta/f = -2.88$ (eg. roller 1 steel and roller 2 aluminium). Starting from $Q/fP = -1.0$, ie. sliding contact with roller 2 driving, we see (Fig. 4a) that upon reducing the magnitude of Q slightly, a stick zone starts at about $x/a = -0.25$ (towards the entry side). As Q/fP is reduced, the stick zone expands and the shear traction within it becomes increasingly positive (Fig. 4b). By the time Q/fP has been reduced to -0.06 (very little nett work being input by roller 2), the shear traction within the stick zone is on the point of reverse, ie. forward slip, Fig. 4c. Forward slip progresses quickly, and by the time $Q/fP = -0.04$, Fig. 4d, there is a significant forward slip zone, so that the three slip zone model is appropriate. Making Q/fP more positive (> 0) implies that roller 1 is nov providing the energy input, and the forward slip zone grows at the expense of both reverse slip regions. At about $Q/fP = 0.74$ the trailing forward slip zone has almost completely vanished, Fig. 4e. For larger values of Q/fP the case of two slip zones of opposite sign applies (Fig. 4f). This general scheme persists until the onset of sliding, with cylinder 1 driving. Figs. 4b, 4d and 4e may be compared with Figs. 9b, 6, and 9a of [1].

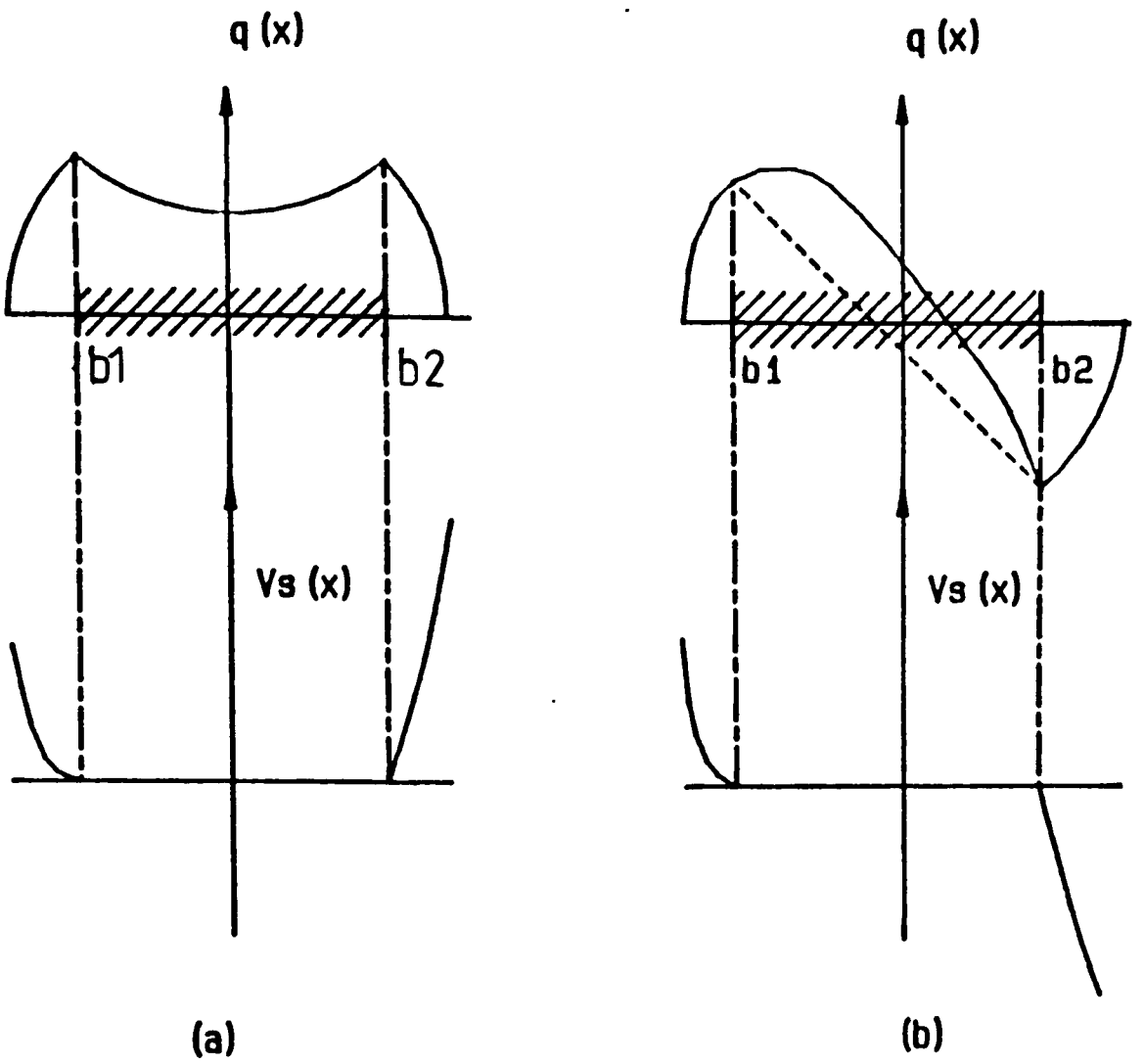

Fig. 3 Variation of shear traction and slip velocity
(a) Two slip zones of the same sign
(b) Two slip zones of opposite sign
(c) Three slip zones

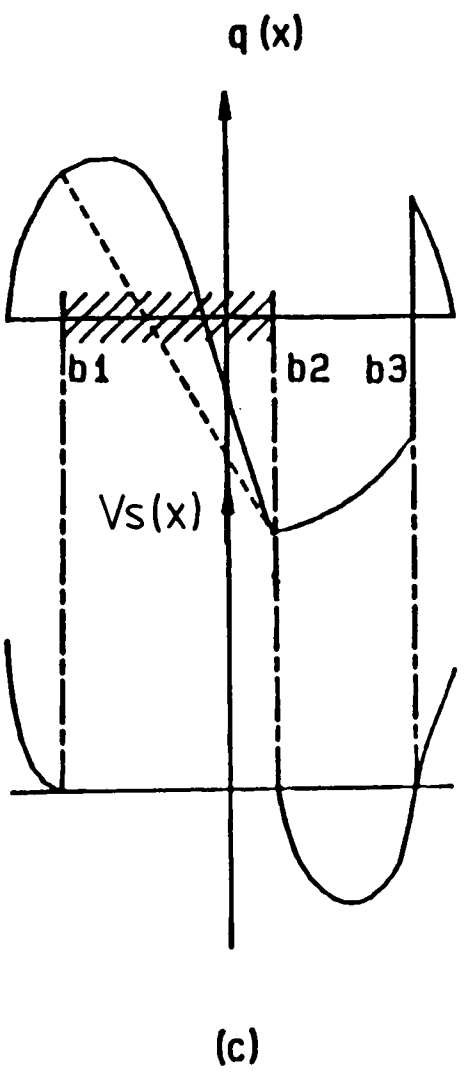

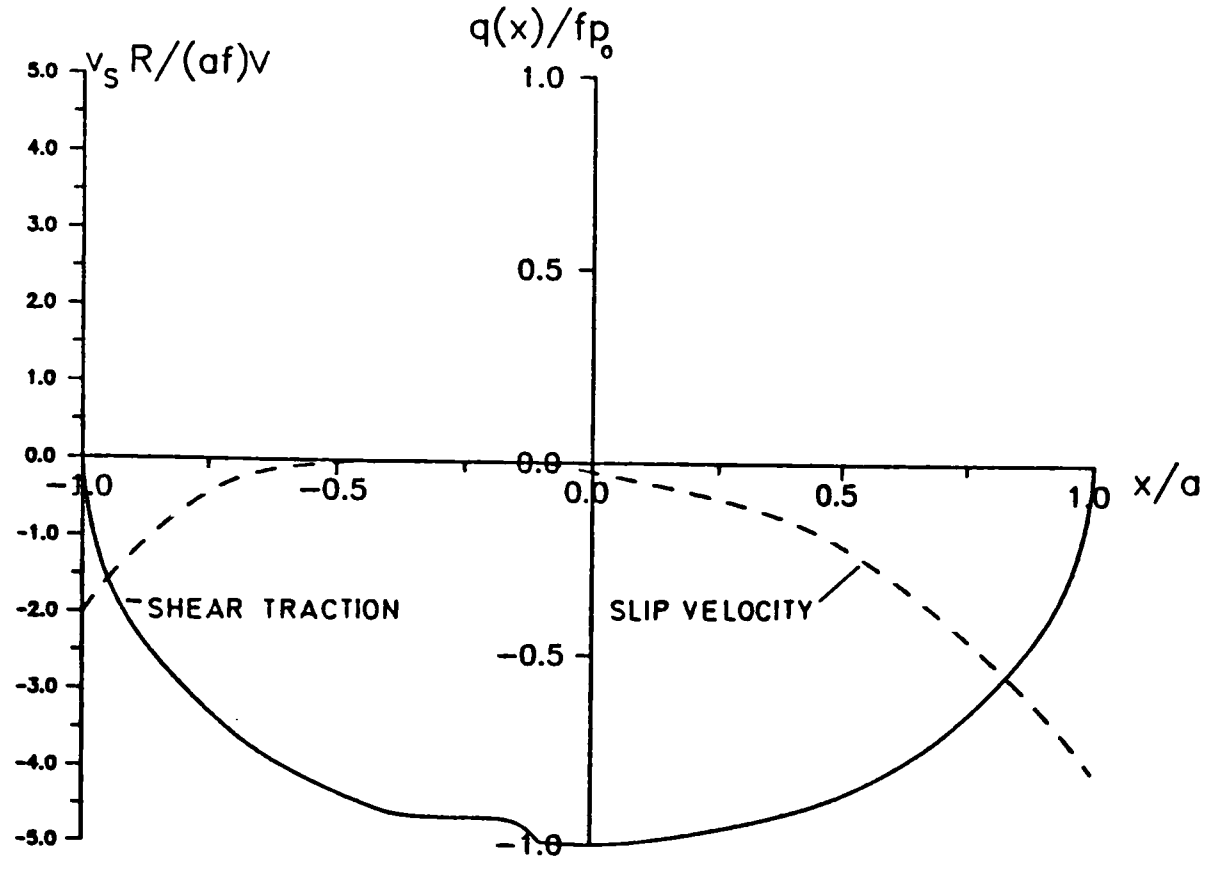

Fig.4 Variation of shear traction and slip velocity, $\beta/f = -2.88$
(a) Roller 2 driving, $Q/fP = -0.99$
(b) Roller 2 driving, $Q/fP = -0.75$

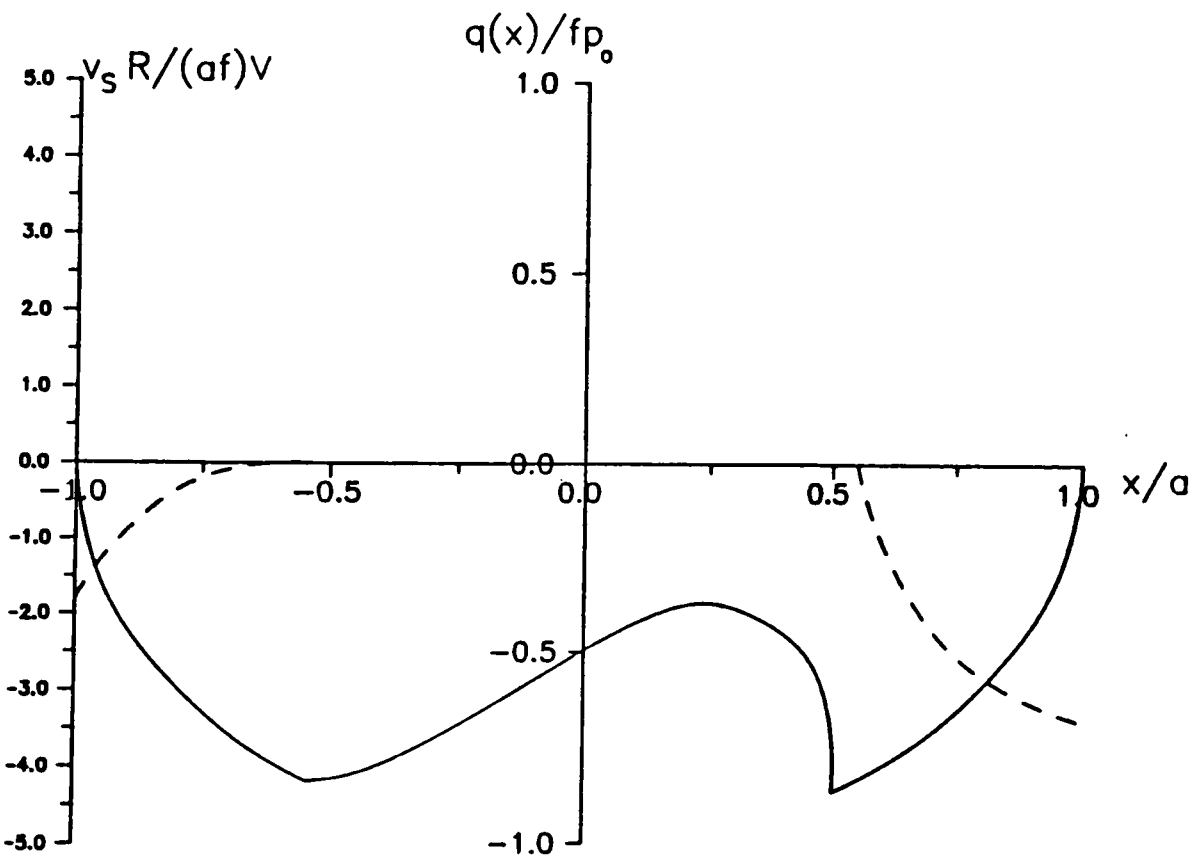

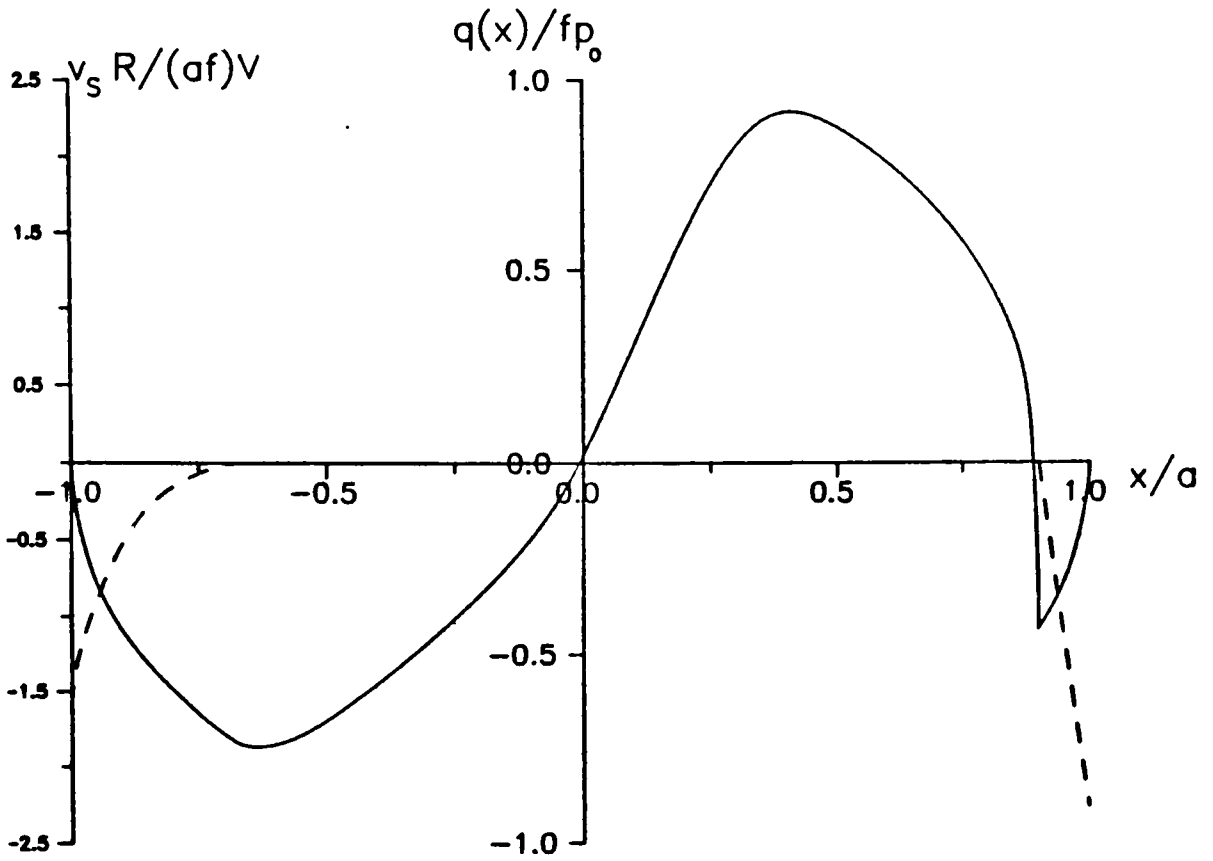

Fig. 4 Variation of shear tractions and slip velocity, $\beta/f = -2.88$
(c) Roller 2 driving, $Q/fP = -0.06$
(d) Roller 2 driving, $Q/fP = -0.04$

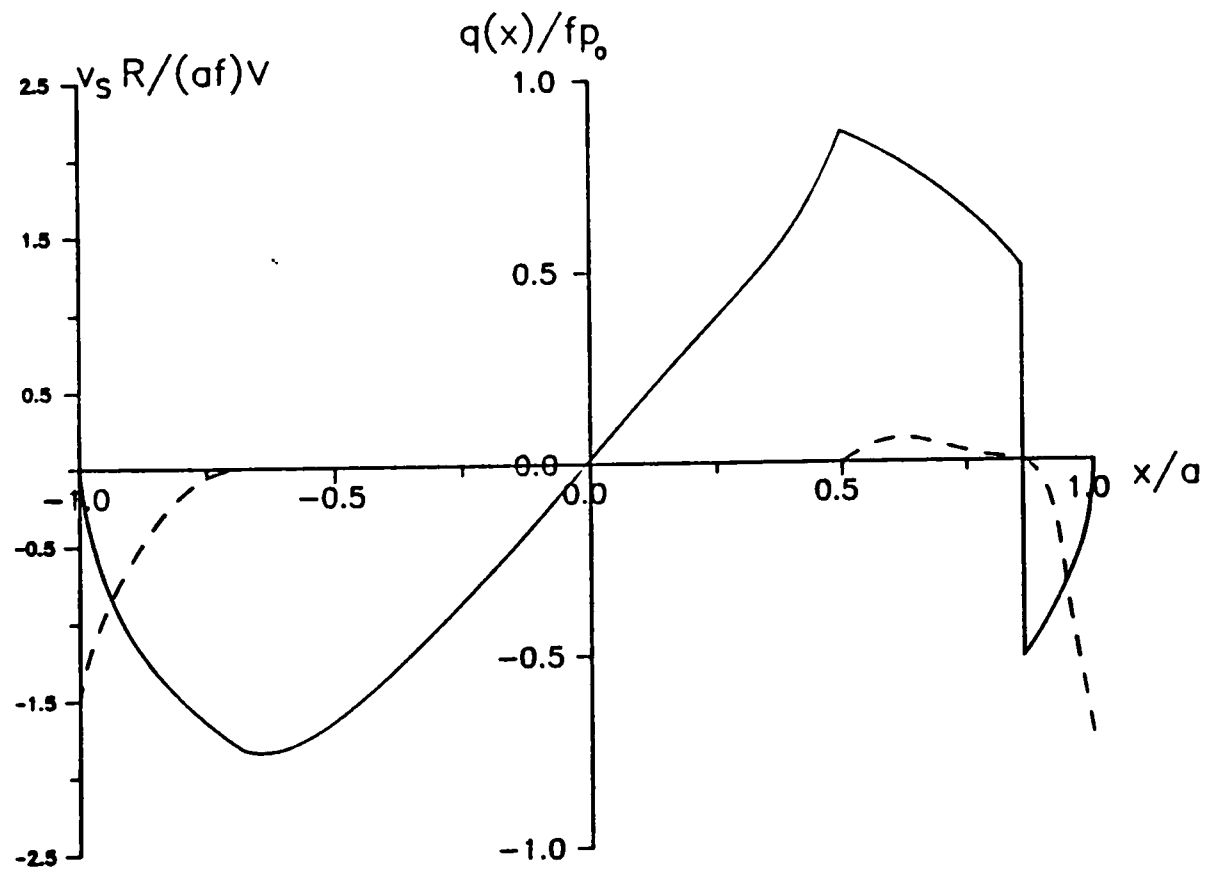

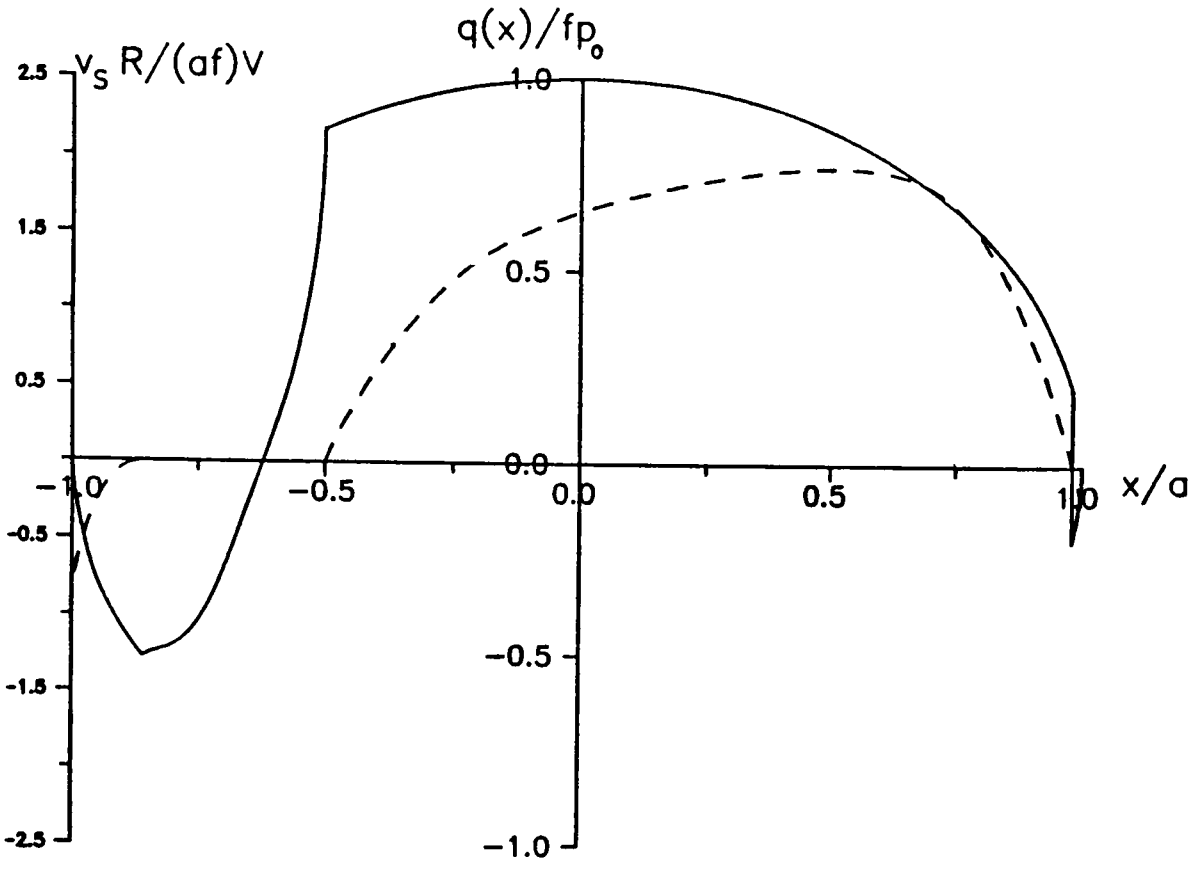

Fig. 4 Variation of shear tractions and slip velocity, $\beta/f = -2.88$
(e) Roller 1 driving, $Q/fP = 0.74$
(f) Roller 1 driving, $Q/fP = 0.83$

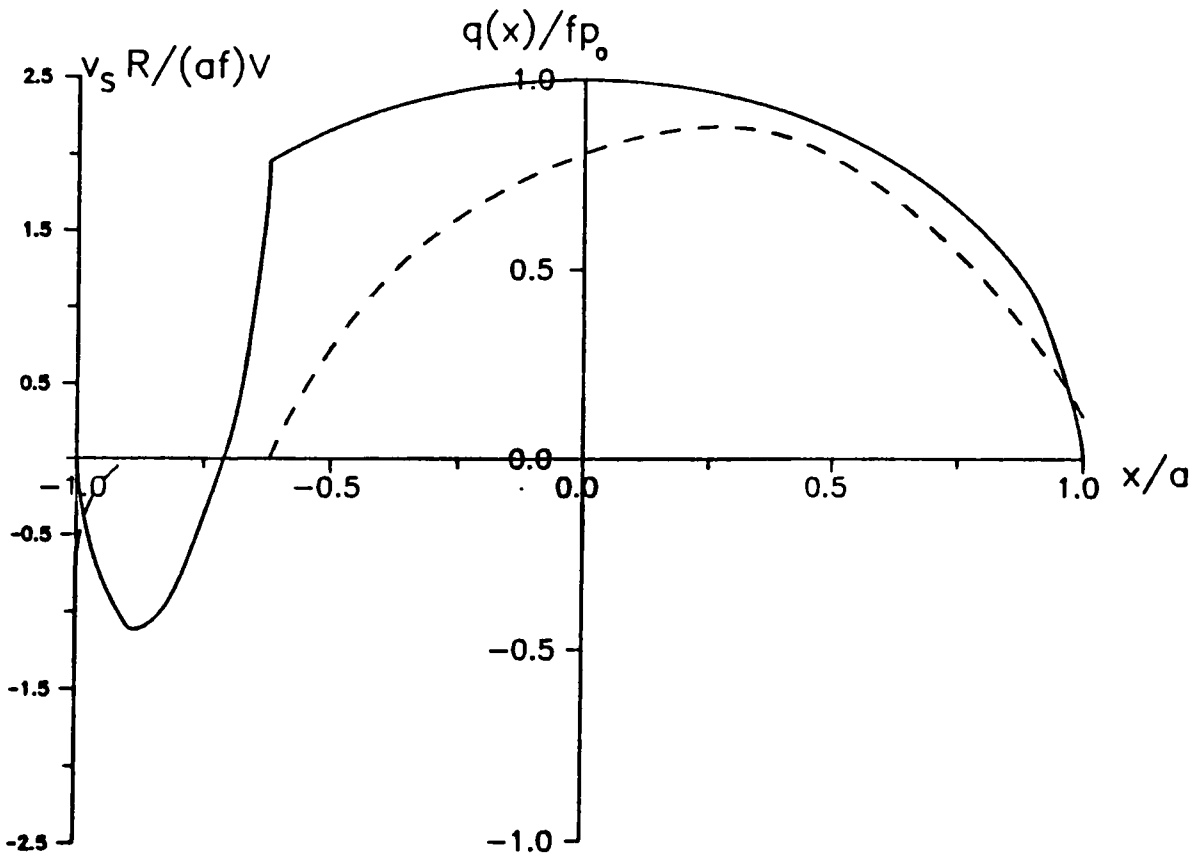

It is impractical to provide families of such curves, and so in Fig. 5 a summary is shown of the size and nature of interfacial stick and slip zones for β/f = -1.0, -2.0 and -2.88. Results for positive β/f may be found be reversing the vertical axis. It should be noted that over the majority of range where the three slip zone model is appropriate we found no violations of the consistency conditions (9) and (11) and therefore conclude that there is an abrupt change of slip direction. The remaining difficulty is in describing behaviour near the triple point bounding (stick/forward slip/backward slip) where we were unable to find a consistent solution using our model for a small range of values of Q/fP. This area of uncertainty is very small and diminishes as $\beta/f \to 0$. We conclude that a 5 zone regime is likely in this area (ie. backslip/stick/forward slip/stick/backslip). The trailing stick zone would have finite width and thus our model is not able to provide a good representation of the shear traction in this region. A much more complicated model would be required and has not been pursued.

Figure 6 summarises the general scheme of interface response as a function of β/f. The single stick zone (Carter) solution is valid only if the materials are identical, and any discrepancy between elastic constants will immediately introduce a second slip zone.

6. Further Observations

It may be noted that the slip-to-stick transitions are invariably accompanied by a smooth change in the shear traction. This is apparent if we require a continuity of the surface strain ε_{xx} as particles pass into the stick zone; this implies $\partial u^2/\partial x^2 = 0$.

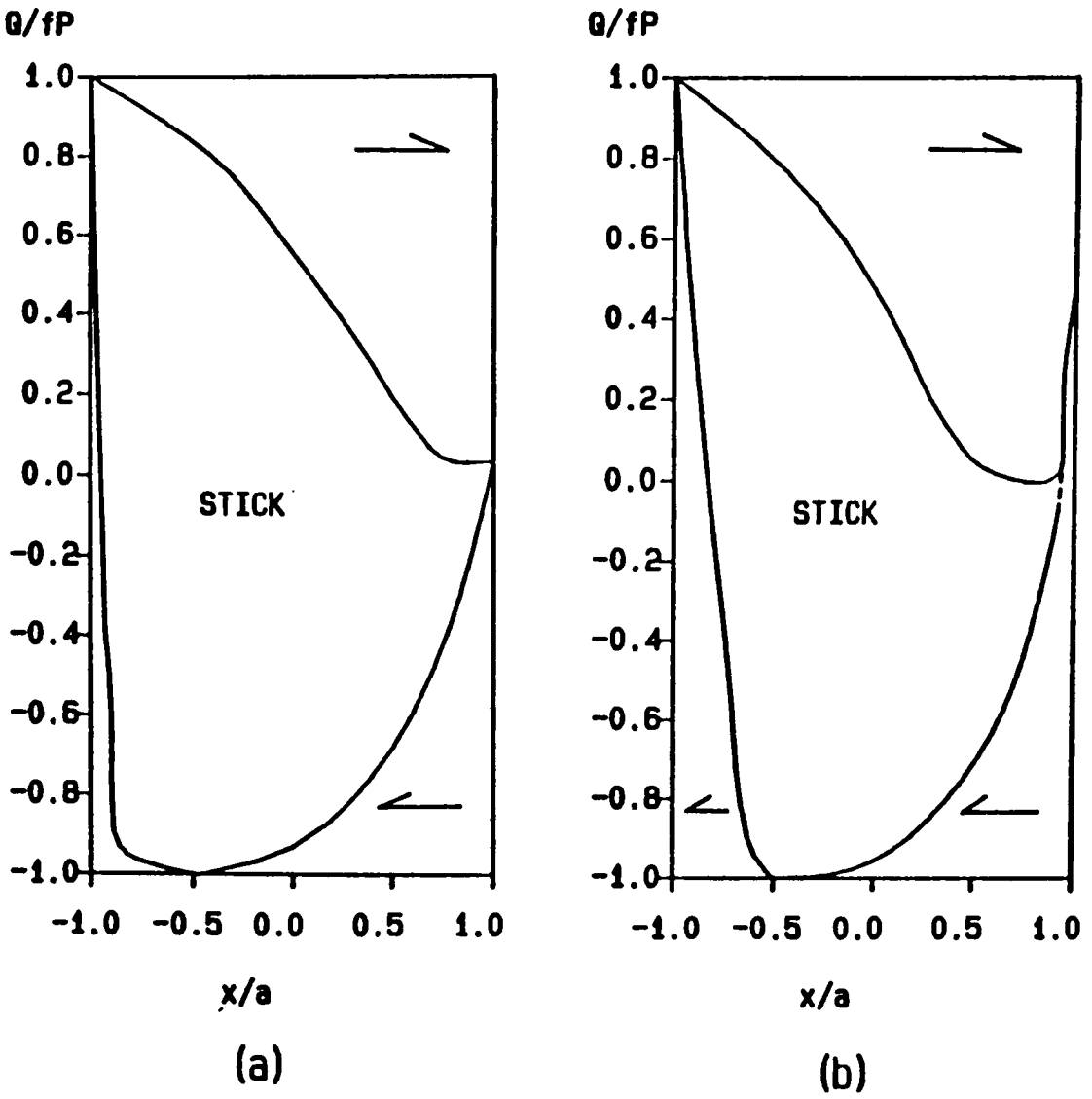

Fig. 5 Stick/slip maps, (a) $\beta/f = -1.0$
(b) $\beta/f = -2.0$
(c) $\beta/f = -2.88$

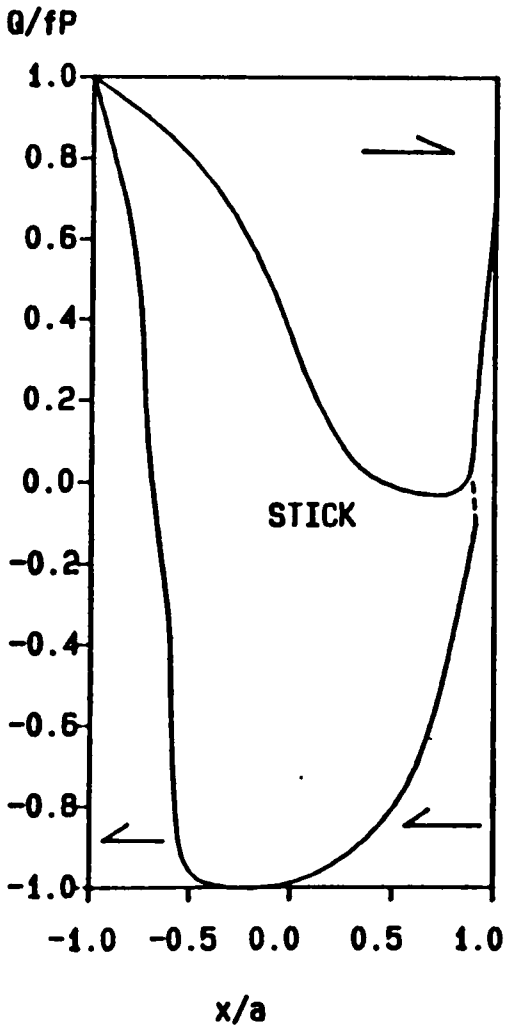

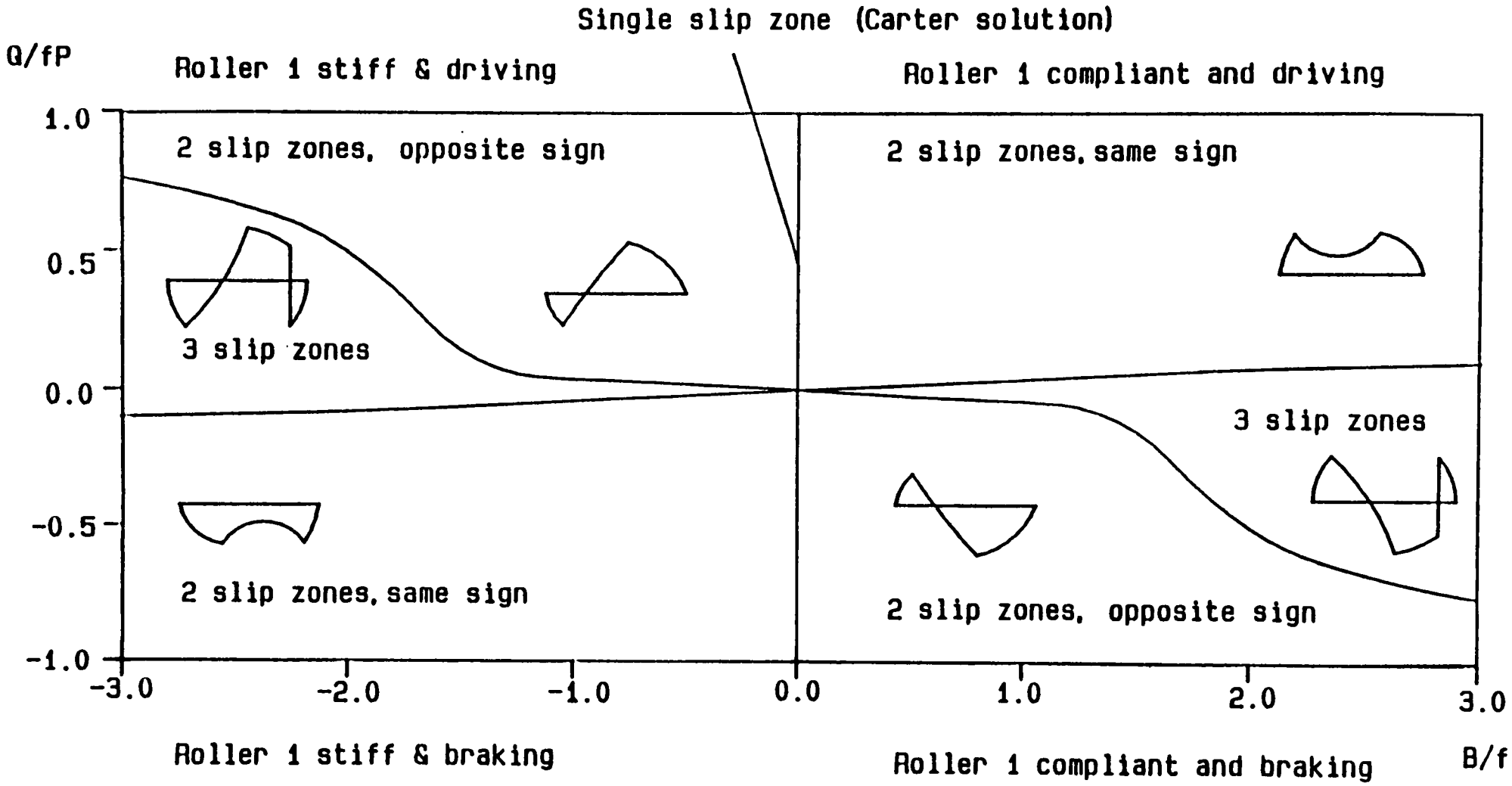

Fig. 6. Interface response regime map for tractive rolling

Since the shear traction q(x) is proportional to γ_{xy}, a smooth change in shear traction requires $\partial^2\gamma_{xy}/\partial x^2$ to vanish.

Now

$$\frac{\partial^2\gamma_{xy}}{\partial x^2} = \frac{\partial^3 u}{\partial x^2 \partial y} + \frac{\partial^3 v}{\partial x^3} \tag{27}$$

and the first term on the right hand side is certainly zero. Since for Hertzian contact the surface vertical displacement varies quadratically, ie. $v \propto x^2$ the second term must vanish too. This same phenomenon of a smooth change in shear passing from slip to stick, but a discontinuity in slope in passing from stick to slip has been observed by Sheppard et al [12] for closed crack problems.

The formulation allows the creep velocity to be abstracted immediately from the relative tangential strain in the stick zone equation (8). Results are summarised in Fig. 7, and are in agreement with Kalker [2]. Curves for $\beta/f > 0$ may be obtained from those plotted by rotating the axes through 180°. A remarkable feature is that, except for similar materials, the creep ratio does not change sign at the same point as Q/fP. There is therefore a range of values of shear force where, when the more rigid body is driving, the driven wheel has a greater peripheral velocity!

Lastly, we calculated the frictional losses occurring. The power loss (W) per unit length of cylinders is given by:

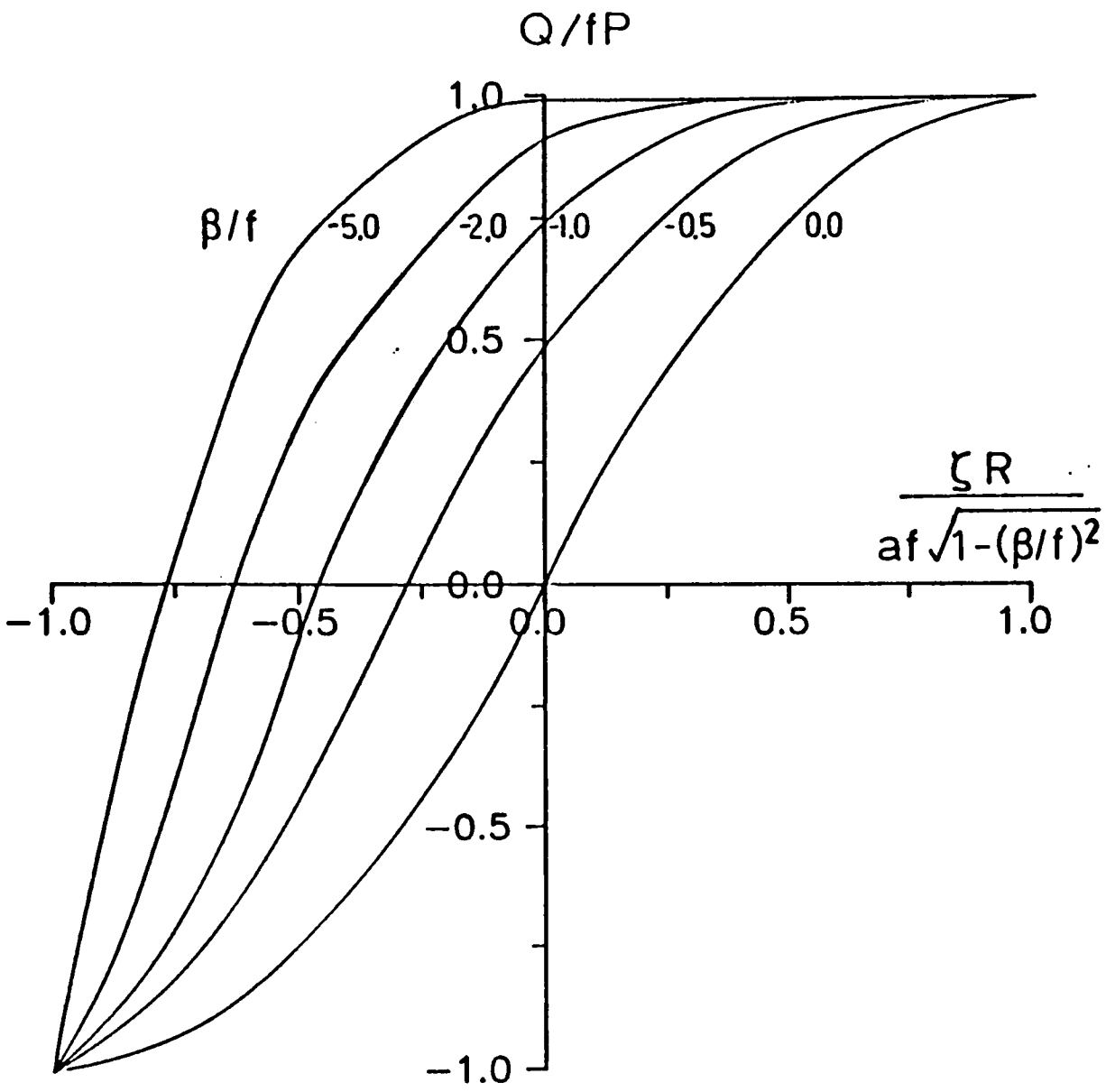

Fig. 7 Variation of creep ratio with β/f

$$W = \int_{-a}^{a} q(x)v_s(x)dx$$

$$= V \int_{-a}^{a} q(x)[h(x) + \zeta]\, dx \qquad (28)$$

It will be recognised that the term in square brackets vanishes in the stick zone, and the requirement that slip direction and shear traction be consistent demands that the integrand is positive in all slip zones. Results are shown in Fig. 8. Good agreement is found with Bentall and Johnson [2] for the sample results given by them. Results for positive β may be deduced by reversing the horizontal axis. It may be noted that even when the nett shear force is small (or zero) there are finite losses for $\beta \neq 0$, and that these increase dramatically with $|Q/fP|$. An interesting comparison may be made between the pover losses evaluated according to (28), and a "bulk" approach given by Johnson [11] for the case of $\beta = 0$.

The latter gives the losses as

Pover loss $= Q\zeta$

$$= \zeta \int_{-a}^{a} q(x)\, dx \qquad (29)$$

which may be compared with (28). It can be shown that, for the Carter case ($\beta = 0$)

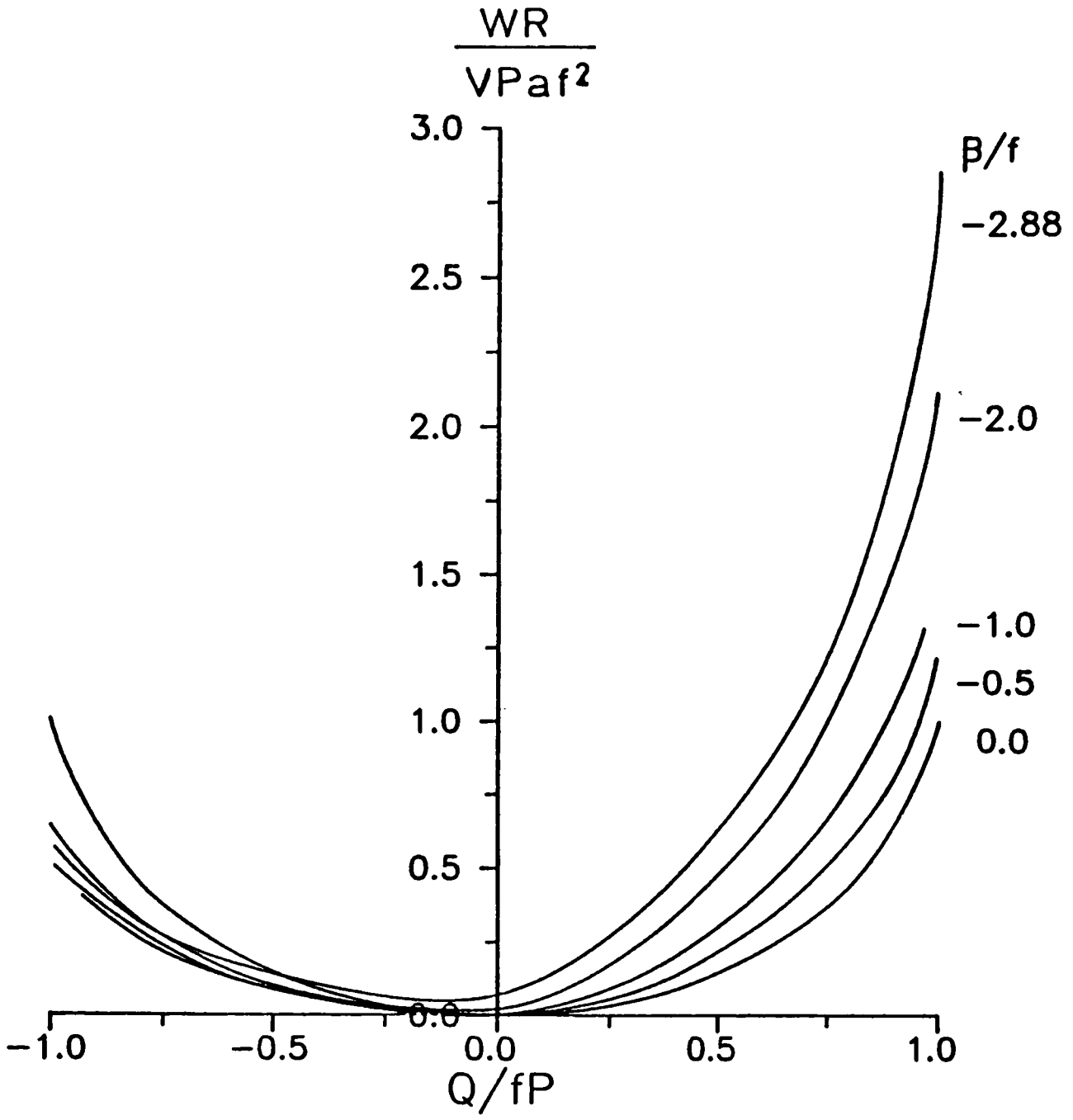

Fig. 8 Variation of frictional losses with β/f

$$\int_{-a}^{a} q(x)h(x)dx = 0$$

and thus the two expressions are equivalent. For $\beta \neq 0$, however, significant discrepancies arise. Indeed, it may be seen from Fig. 7 that application of equation (29) would lead to a negative answer for power loss when Q/fP and ζ have opposite sign.

Conclusions

The rolling contact of two dissimilar elastic cylinders has been studied and solutions obtained by representing the shear tractions as a series of Chebyshev polynomials. Consistent solutions have been found for the shear traction distribution under a wide range of elastic constants and nett tangential force. These enable the prevailing stick/slip regime to be deduced and the stick boundaries determined.

Comprehensive results for the creep ratio between the rollers and the frictional losses produced by the contact are given. The results are compared with the piece-wise linear solutions of Bentall and Johnson [1], and Kalker [2]. Good agreement is found in all cases.

Acknowledgements

David Novell would like to acknowledge the support of the SERC under Contract Number GR/D55610.

References

1. R. H. Bentall, and K. L. Johnson, Slip in the rolling contact of two dissimilar elastic rollers, Int. J. Mech. Sci, 9, 389-404, (1967).

2. J. J. Kalker, A minimum principle for the law of dry friction with application to elastic cylinders in rolling contact, (Part 1), J. Appl. Mech. 38, 875-880, (1971).

3. L. E. Goodman, Contact stress analysis of rough spheres, J. Appl. Mech., 84, 515-522, (1962).

4. D. A. Spence, The Hertz contact problem with finite friction, Journal of Elasticity, 5, 297-319 (1975).

5. S. P. Timoshenko and J. N. Goodier, Theory of elasticity, p. 381, McGrav-Hill, New York, (1951).

6. N. I. Muskhelishvili, Some basic problems of the mathematical theory of elasticity, Noordhoff, Groningen, (1953).

7. K. L. Johnson, Contact mechanics, p.224, C.U.P., (1985).

8. F. W. Carter, On the action of a locomotive driving wheel, Proc. Roy. Soc., Ser. A, 112, 151-157, (1926).

9. F. Erdogan, G. D. Gupta, and T. S. Cook, Numerical solution of singular integral equations. Methods and analysis and solutions of crack problems, (edited by G. C. Sih), Chap. 7, pp. 368-425, Noordhoff Groningen, (1973).

10. R. Piessens, M. Van Roy-Branders and I. Mertens, The automatic evaluation of Cauchy principal valve integrals, Angev. Inf. 18, 31-33, (1976).

11. K. L. Johnson, Contact mechanics, p. 308, C.U.P., (1985).

12. S. D. Sheppard, D. A. Hills and J. R. Barber, An analysis of fretting cracks - II, unloading and reloading phases, Int. J. Solids Structures, 22, 4, 387-396, (1986).

APPENDIX D

INFLUENCE FUNCTIONS (CHAPTER 8)

$$G_{xxx} = \left[\frac{-6(y + y_d)}{r_1^2} + \frac{4(y + y_d)^3}{r_1^4} + \frac{6(y - y_d)}{r_2^2} - \frac{4(y - y_d)^3}{r_2^4} - \frac{4y_d}{r_2^2} + \frac{32y_d(y - y_d)^2}{r_2^4} - \frac{32y_d(y - y_d)^4}{r_2^6} - \frac{24y_d^2(y - y_d)}{r_2^4} - \frac{32y_d^2(y - y_d)^3}{r_2^6} \right]$$

$$G_{xyy} = \left[\frac{2(y + y_d)}{r_1^2} - \frac{4(y + y_d)^3}{r_1^4} - \frac{2(y - y_d)}{r_2^2} + \frac{4(y - y_d)^3}{r_2^4} - \frac{4y_d}{r_2^2} - \frac{16y_d(y - y_d)^2}{r_2^4} + \frac{32y_d(y - y_d)^4}{r_2^6} - \frac{24y_d^2(y - y_d)}{r_2^4} + \frac{32y_d^2(y - y_d)^3}{r_2^6} \right]$$

$$G_{xxy} = -x \left[\frac{-2}{r_1^2} + \frac{4(y + y_d)^2}{r_1^4} + \frac{2}{r_2^2} - \frac{4(y - y_d)^2}{r_2^4} + \frac{8y_d(y - y_d)}{r_2^2} - \frac{32y_d(y - y_d)^3}{r_2^6} + \frac{8y_d^2}{r_2^4} - \frac{32y_d^2(y - y_d)^2}{r_2^6} \right]$$

$$G_{yxx} = x \left[\frac{-2}{r_1^2} + \frac{4(y + y_d)^2}{r_1^4} + \frac{2}{r_2^2} - \frac{4(y - y_d)^2}{r_2^4} - \frac{24y_d(y - y_d)}{r_2^2} + \frac{32y_d(y - y_d)^3}{r_2^6} - \frac{8y_d^2}{r_2^4} + \frac{32y_d^2(y - y_d)^2}{r_2^6} \right]$$

$$G_{yyy} = x \left[\frac{-2}{r_1^2} - \frac{4(y + y_d)^2}{r_1^4} + \frac{2}{r_2^2} + \frac{4(y - y_d)^2}{r_2^4} + \frac{8y_d(y - y_d)^3}{r_2^4} - \frac{32y_d(y - y_d)^3}{r_2^6} + \frac{8y_d^2}{r_2^4} - \frac{32y_d^2(y - y_d)^2}{r_2^6} \right]$$

$$G_{yxy} = \left[\frac{2(y + y_d)}{r_1^2} - \frac{4(y + y_d)^3}{r_1^4} - \frac{2(y - y_d)}{r_2^2} + \frac{4(y - y_d)^3}{r_2^4} - \frac{4y_d}{r_2^2} + \frac{32y_d(y - y_d)^2}{r_2^4} - \frac{32y_d(y - y_d)^4}{r_2^6} + \frac{24y_d^2(y - y_d)}{r_2^4} - \frac{32y_d^2(y - y_d)^3}{r_2^6} \right]$$

Where: $r_1^2 = x^2 + (y + y_d)^2$

$r_2^2 = x^2 + (y - y_d)^2$